Evolution and genetic architecture of resistance in a natural population of *Daphnia magna* undergoing strong epidemics of the bacteria *Pasteuria ramosa*

Inauguraldissertation

zur

Erlangung der Würde eines Doktors der Philosophie

vorgelegt der

Philosophisch-Naturwissenschaftlichen Fakultät

der Universität Basel

von

Camille Ameline

Aus La Madeleine de Nonancourt, Frankreich

Basel, 2022

Genehmigt von der Philosophisch-Naturwissenschaftlichen Fakultät

auf Antrag von

Fakultätsverantwortlicher:	Prof. Dr. Dieter Ebert, Basel
Korreferent:	Prof. Dr. Luís Teixeira, Oeiras

Basel, den 23. Juni 2020

Prof. Dr. Martin Spiess

Dekan

Acknowledgments

This thesis results from the work, help and support of many people, which I would like to warmly thank. First of all, my supervisor, Dieter Ebert, gave me the opportunity to come to Basel to study evolutionary biology, even though I had an ecology background. Not only did I learn a lot about evolution and many of its fascinating (and often complex) aspects, but I also got the chance to discover beautiful Switzerland, I made friends, and I learned a lot about myself. Dieter gave me the freedom to organize my projects but was always here to share his knowledge, give advice, and remind me of the important things. He taught me how to write papers more efficiently and conduct good scientific research in general, so for all of this thank you very much. Thank you as well to Luís Teixeira, for taking the time to be my external referee and for his valuable comments.

My work in the lab was made possible by Jürgen, Urs, Kristina, Michelle, Dita and Nicolas who patiently shared with me their experience and helped me on numerous occasions with my data collection. For your support and all the good moments, thank you. Thank you to Yasmin and Brigitte for dealing with the administrative part of things and often bringing delicious desserts; and thank you to Lukas for trying to explain informatics to me. Being part of the Ebert group was a treat, as I got to work and interact with people from so many different horizons. For all the help, discussions, beers and fun, thank you to Tobi, Marjut, Marinela, Elena, Roberto, Nicola, Sabrina, Gilberto, Mariko, Meret, Sasha, Leonie, Kathrin, Eevi, Vitor, Luca, Yann, Jason, David, Pepijn, Pascal, Eric, Georgia, Peter, Louis, Fabienne & Fabian (thank you for the giant fondue and Älplermagronen in Emmeten guys…), Vital, Marlon, Benjamin and Moena. To collegues and office mates who became friends: Maridel, Lilla, Joana, Cheng Choon (we'll go karaoking again guys), Pragya, Andrea and Jeremias, thank you for the good moments and the support in the difficult times.

Thank you to Yan Galimov in Moscow who took Maridel and I to a very intense and beautiful daphnia hunting trip through the desert in Russia. Thank you to friends in Bern and elsewhere, who listened to my complaints and provided the much-needed distractions and warmth: Simona, Aude, Matina, Karen, Andrea, Pierre and Robin. To my parents Marco et Titi, and brother Guigui, thank you for the skype sessions with guitar playing and garden tour during the quarantine.

Working at the institute was always very stimulating, rich with seminars, aperos and cakes. For organizing all of this and being part of it, thank you to everyone I crossed path with at Zoology in Basel.

TABLE OF CONTENTS

Summary ..... p. 1

Introduction ..... p. 3

Chapter 1 A two-locus system with strong epistasis underlies rapid parasite-mediated evolution of host resistance ..... p. 9

Chapter 2 Genetic slippage after sex maintains diversity for parasite resistance in a natural host population ..... p. 37

Chapter 3 Inheritance of resistance to two *Pasteuria ramosa* isolates in a *Daphnia* population ..... p. 59

Chapter 4 New attachment sites and patterns of *Pasteuria ramosa* spores on the cuticle of *Daphnia magna* ..... p. 81

Supplementary Material

Chapter 1 ..... p. 103

Chapter 2 ..... p. 121

Chapter 3 ..... p. 139

Chapter 4 ..... p. 153

Concluding remarks ..... p. 157

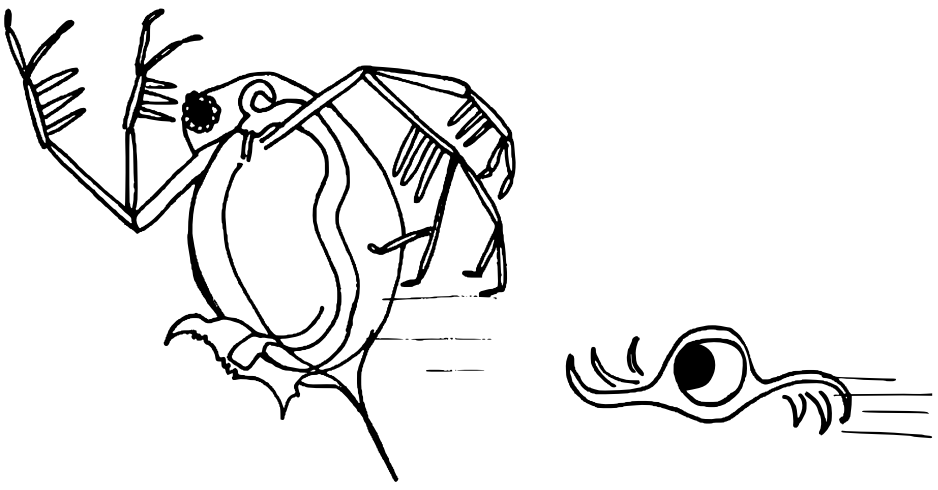

Summary

Host–parasite coevolution is believed to be a major force driving phenotypic and genotypic diversity, notably, through the maintenance of sexual reproduction, as proposed in the Red Queen theory. To understand how resistance evolves in the host, a large body of theory about the dynamics of resistance and its underlying genetics has been proposed. However, empirical data about the long-term evolution of resistance and its underlying genetics is still scarce. In this thesis, I monitor the evolution of resistance in a natural population of the freshwater crustacean *Daphnia magna* undergoing strong epidemics of the bacterial parasite *Pasteuria ramosa*, and I investigate the associated underlying genetics of resistance.

The focal population of this thesis occurs in the Aegelsee in Frauenfeld, Switzerland. In this population, *D. magna* resistance to *P. ramosa* increases during the planktonic season of the host, and I show that these phenotypic changes are caused by parasite-mediated selection (Chapter 1). In this first chapter, I further investigate the genetic architecture of resistance in the host using a genome-wide association approach combined with genetic crosses and find that resistance is determined by two loci strongly linked with epistasis. In Chapter 2, the evolution of resistance in the host population over eight consecutive planktonic seasons is revealed. Every season, selection increases resistance in the host population, and sexual reproduction causes genetic slippage to reset resistance diversity in the first host cohort of the following season. Sampling of the sexual eggs, and the genetic model of resistance described in Chapter 1, allows me to partially predict the observed resistance diversity resulting from recombination. In Chapter 3, I further expand the genetic model of resistance to *P. ramosa* in *D. magna* using genetic crosses coupled with a PoolSeq association approach and find that epistasis plays a major role linking the different resistance loci found in the host. The first step of the infection process in the *D. magna–P. ramosa* system is the attachment of the bacterial endospores to the host cuticle. Attachment has been shown to be highly specific and is thus crucial for the study of host-parasite interactions. The resistance phenotype in the host can be easily scored in the laboratory with an attachment test, where fluorescent spores are fed to the host and attachment is observed under the microscope. Until recently, clear attachment patterns had been observed in two sites of the gut cuticle. In Chapter 4, I use new isolates of *P. ramosa* and describe a much higher diversity of attachment sites and patterns than previously described.

Background

The evolution of resistance is of major interest in a variety of fields, such as epidemiology (Galvani 2003), conservation (Kilpatrick 2006), agronomy (Mithila et al. 2011), and medicine (Woolhouse et al. 2002). The evolution of resistance has the potential to be rapid in the face of parasite-mediated selection (Kurtz et al. 2016; Morgan and Koskella 2017; Koskella 2018) and is suggested to be associated with changes in allele frequency at the underlying resistance genes (Schmid-Hempel 2011). Indeed, dynamics of resistance genes are central in host-parasite coevolution theory (Bergelson et al. 2001; Tellier et al. 2014; Gibson et al. 2018). Two main models of allele frequency dynamics have been proposed to ensue from host-parasite interactions: oscillations caused by negative indirect frequency-dependent selection (NFDS) (Hamilton et al. 1990; Lively 2010), and selective sweeps caused by directional selection (Gómez et al. 2015; Retel et al. 2019). In contrast with the large body of theory investigating the dynamics of resistance in the host, the observation of resistance evolution is rarely associated to its underlying genetics (Turko et al. 2018).

To link the evolution of resistance to dynamics of allele frequency, understanding the genetic architecture of resistance is necessary. Host-parasite coevolution theory proposes many genetic models that try to make sense of the evolution and maintenance of diversity and sexual reproduction through interaction with parasites (Agrawal and Lively 2002; Otto and Nuismer 2004; de Visser and Elena 2007; Thrall et al. 2016). Resistance is suggested to be coded by a few loci with strong effect (Sasaki 2000; Tellier and Brown 2007), presenting dominance patterns and linked with epistasis (Howard and Lively 1998; Salathé et al. 2008; Kouyos et al. 2009). In a few plant and animal model systems, this has been corroborated (Li and Cowling 2003; Carton et al. 2005; Bangham et al. 2008; Wilfert and Schmid-Hempel 2008; Magwire et al. 2012). In the era of genomics, investigating the genetic architecture of resistance often involves whole-genome association studies (Cerqueira et al. 2017), while Mendelian genetics still provide a powerful functional validation of the revealed statistical associations.

Knowledge of the genetics of resistance also provides the opportunity to investigate the impact of sexual reproduction on the evolution of resistance. Indeed, sexual reproduction might be advantageous through the creation of rare variants (Hamilton et al. 1990; Lively 2010), but it might also reduce fitness by breaking up advantageous allele combinations.

Aims of the thesis

This thesis aims to bridge the gap between the dynamics of resistance and the evolution of underlying genetics—in other words—to link selection to genetics by resolving the genetic architecture of resistance in a host population that undergoes strong parasite-mediated selection. The second aim

of this thesis is to use the developed genetic model of resistance to predict the impact of recombination on the evolution of resistance.

A host …

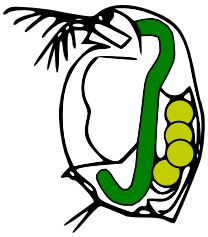

To achieve this, I use a cyclical parthenogen host, as this mode of reproduction will allow to distinguish the impact of selection from the impact of sexual reproduction on resistance evolution. Indeed, cyclical parthenogens reproduce clonally throughout their active phase to colonize their environment and undergo seasonal episodes of sexual reproduction, producing resting stages that can withstand harsh environmental conditions (Decaestecker et al. 2009). If directional selection acts on a population of cyclical parthenogens, and if the active season of the population is long enough, selection should increase the mean fitness of the population and decrease its variance. When recombination occurs through sexual reproduction, diversity increases, and the mean performance of the population decreases. This is known as genetic slippage in response to sex (Lynch and Deng 1994). In this thesis I use the cyclical parthenogen *Daphnia magna*, a freshwater cladoceran that has become a model species in the study of host-parasite coevolution.

… and a parasite …

D. magna has been observed to be infected by various parasites, showing various coevolutionary patterns (Ebert 2008). *Pasteuria ramosa* is a gram-positive, endospore-forming bacteria that infects *Daphnia* with a high fitness cost. Interactions with *D. magna* have been shown to be highly specific (Luijckx et al. 2011), and a matching-allele model has been shown to determine infections (Luijckx et al. 2013), which is in compliance with negative-frequency-dependent selection (Agrawal and Lively 2002).

… who stick together

Specificity in the *P. ramosa–D. magna* system is evaluated at the first step of infection: the attachment step (Duneau et al. 2011). *Daphnia* filter-feed the sediment and the water column, thereby ingesting resting spores of the bacteria, which get activated, and adhere to the cuticle of the host only in compatible host genotype–parasite genotype combinations (Ebert et al. 2016). Attached spores then penetrate the body cavity of the host, where they complete their development cycle and produce millions of copies of themselves (Duneau et al. 2011). As specificity is a key assumption in host–parasite coevolution theory, notably in the Red Queen theory for the evolution of sex (Auld et al. 2012; Auld et al. 2016), a clear and reliable assay of the attachment in the system is essential. However, recent observations reveal that attachment might be more complex and variable than initially thought.

Outline of the thesis

In this thesis, I monitor the evolution of resistance in a natural population of *D. magna* undergoing strong epidemics of *P. ramosa* and link the observed phenotypic patterns of resistance dynamics to the underlying genetics of

resistance in this population.

Chapter 1

In the first chapter, I observe a rapid increase of resistance in the host population and use an infection experiment and field measurement to demonstrate the role of selection by the local parasite. Using a combination of genome-wide association approach and genetic crosses in the host, I further resolve the genetic architecture of resistance to the local parasite, thereby completing the previously established genetic model of resistance in the system. Variation in the resistance phenotype is mainly determined by variation at two loci showing different dominance patterns and strongly linked with epistasis.

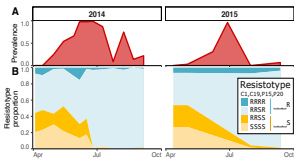

Chapter 2

In the second chapter, I characterize the evolution of resistance in the study host population across eight consecutive planktonic seasons. I further describe the role of sexual reproduction in the observed dynamics by regularly collecting and hatching the overwintering resting eggs. The rapid evolution of resistance is consistently observed throughout each season, but sexual reproduction reduces the mean resistance of the population and increases its variance, thereby creating genetic slippage. I further use the genetic model to predict the resistance phenotypes composition of the sexually produced hatchlings and find that our model only partially explains the observed resistance phenotype diversity in the hatchling population.

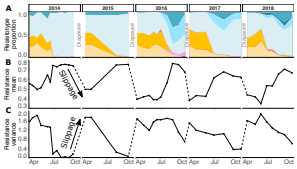

Chapter 3

As Chapter 2 revealed a missing piece in the current genetic model of resistance in the *D. magna–P. ramosa* system, I investigate additional complexity in the model using genetic crosses in the host and new parasite isolates. I find that complex epistatic interactions between several loci—presenting distinct dominance patterns—shape most of the observed resistance diversity, thereby emphasizing the importance of these interactions in shaping host-parasite coevolution.

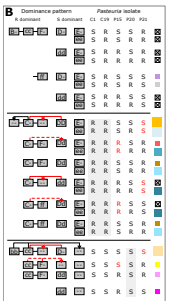

Chapter 4

Most of the research I have led in the previous chapters has made use of the attachment test to characterize resistance phenotypes in the host. The reliability of this test is thus indispensable for the investigation of the evolution of resistance and its underlying genetic architecture. In an attempt to get more diversity from the parasite population, I isolated new *P. ramosa* genotypes from the study population and found new diversity and patterns of attachment of the bacterial spores on the host cuticle. In this chapter, I describe these new attachment sites on the host cuticle and discuss their implication in the specificity of the *D. magna–P. ramosa* system.

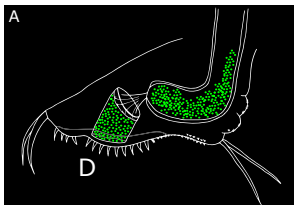

References

Agrawal A, Lively CM. 2002. Infection genetics: gene-for-gene versus matching-alleles models and all points in between. *Evolutionary Ecology Research* **4**:79–90.

Auld SKJR, Hall SR, Duffy MA. 2012. Epidemiology of a *Daphnia*–multiparasite system and its implications for the Red Queen. *PLoS ONE* **7**:e39564.

Auld SKJR, Tinkler SK, Tinsley MC. 2016. Sex as a strategy against rapidly evolving parasites. *Proceedings of the Royal Society B: Biological Sciences* **283**:20162226.

Bangham J, Knott SA, Kim K-W, Young RS, Jiggins FM. 2008. Genetic variation affecting host–parasite interactions: major-effect quantitative trait loci affect the transmission of sigma virus in *Drosophila melanogaster*. *Molecular Ecology* **17**:3800–3807.

Bergelson J, Kreitman M, Stahl EA, Tian D. 2001. Evolutionary dynamics of plant R-genes. *Science* **292**:2281–2285.

Carton Y, Nappi AJ, Poirie M. 2005. Genetics of anti-parasite resistance in invertebrates. *Developmental & Comparative Immunology* **29**:9–32.

Cerqueira GC, Cheeseman IH, Schaffner SF, Nair S, McDew-White M, Phyo AP, Ashley EA, Melnikov A, Rogov P, Birren BW, et al. 2017. Longitudinal genomic surveillance of *Plasmodium falciparum* malaria parasites reveals complex genomic architecture of emerging artemisinin resistance. *Genome Biology* **18**:1–13.

Decaestecker E, De Meester L, Mergeay J. 2009. Cyclical parthenogenesis in *Daphnia*: sexual versus asexual reproduction. In: Schön I, Martens K, Dijk P, editors. Lost Sex. Dordrecht: Springer Netherlands. p. 295–316.

Duneau D, Luijckx P, Ben-Ami F, Laforsch C, Ebert D. 2011. Resolving the infection process reveals striking differences in the contribution of environment, genetics and phylogeny to host–parasite interactions. *BMC biology* **9**:1–11.

Ebert D. 2008. Host–parasite coevolution: Insights from the *Daphnia*–parasite model system. *Current Opinion in Microbiology* **11**:290–301.

Ebert D, Duneau D, Hall MD, Luijckx P, Andras JP, Du Pasquier L, Ben-Ami F. 2016. A population biology perspective on the stepwise infection process of the bacterial pathogen *Pasteuria ramosa* in *Daphnia*. *Advances in Parasitology* **91**:265–310.

Galvani AP. 2003. Epidemiology meets evolutionary ecology. *Trends in Ecology & Evolution* **18**:132–139.

Gibson AK, Delph LF, Vergara D, Lively CM. 2018. Periodic, parasite-mediated selection for and against sex. *The American Naturalist* **192**:537–551.

Gómez P, Ashby B, Buckling A. 2015. Population mixing promotes arms race host–parasite coevolution. *Proceedings of the Royal Society B: Biological Sciences* **282**:20142297.

Hamilton WD, Axelrod R, Tanese R. 1990. Sexual reproduction as an adaptation to resist parasites (a review). *Proceedings of the National Academy of Sciences* **87**:3566–3573.

Howard RS, Lively CM. 1998. The maintenance of sex by parasitism and mutation accumulation under epistatic fitness functions. *Evolution* **52**:604–610.

Kilpatrick AM. 2006. Facilitating the evolution of resistance to avian malaria in Hawaiian birds. *Biological Conservation* **128**:475–485.

Koskella B. 2018. Resistance gained, resistance lost: an explanation for host–parasite coexistence. *PLOS Biology* **16**:e3000013.

Kouyos RD, Salathé M, Otto SP, Bonhoeffer S. 2009. The role of epistasis on the evolution of recombination in host–parasite coevolution. *Theoretical Population Biology* **75**:1–13.

Kurtz J, Schulenburg H, Reusch TBH. 2016. Host–parasite coevolution—rapid reciprocal adaptation and its genetic basis. *Zoology* **119**:241–243.

Li C, Cowling W. 2003. Identification of a single dominant allele for resistance to blackleg in *Brassica napus* "Surpass 400." *Plant Breeding* **122**:485–488.

Lively CM. 2010. A review of Red Queen models for the persistence of obligate sexual reproduction. *Journal of Heredity* **101**:S13–S20.

Luijckx P, Ben-Ami F, Mouton L, Du Pasquier L, Ebert D. 2011. Cloning of the unculturable parasite *Pasteuria ramosa* and its *Daphnia* host reveals extreme genotype–genotype interactions. *Ecology Letters* **14**:125–131.

Luijckx P, Fienberg H, Duneau D, Ebert D. 2013. A matching-allele model explains host resistance to parasites. *Current Biology* **23**:1085–1088.

Lynch M, Deng H-W. 1994. Genetic slippage in response to sex. *The American Naturalist* **144**:242–261.

Magwire MM, Fabian DK, Schweyen H, Cao C, Longdon B, Bayer F, Jiggins FM. 2012. Genome-wide association studies reveal a simple genetic basis of resistance to naturally coevolving viruses in *Drosophila melanogaster*. *PLoS Genetics* **8**:e1003057.

Mithila J, Hall JC, Johnson WG, Kelley KB, Riechers DE. 2011. Evolution of resistance to auxinic herbicides: historical perspectives, mechanisms of resistance, and implications for broadleaf weed management in agronomic crops. *Weed Science* **59**:445–457.

Morgan AD, Koskella B. 2017. Coevolution of host and pathogen. In: Tibayrenc M, editor. Genetics and evolution of infectious diseases (Second edition). Elsevier. Sara Tenney. p. 115–140.

Otto SP, Nuismer SL. 2004. Species interactions and the evolution of sex. *Science* **304**:1018–1020.

Retel C, Kowallik V, Huang W, Werner B, Künzel S, Becks L, Feulner PGD. 2019. The feedback between selection and demography shapes genomic diversity during coevolution. *Science Advances* **5**:eaax0530.

Salathé M, Kouyos R, Bonhoeffer S. 2008. The state of affairs in the kingdom of the Red Queen. *Trends in Ecology & Evolution* **23**:439–445.

Sasaki A. 2000. Host–parasite coevolution in a multilocus gene-for-gene system. *Proceedings of the Royal Society B: Biological Sciences* **267**:2183–2188.

Schmid-Hempel P. 2011. Evolutionary parasitology. The integrated study of infections, immunology, ecology, and genetics. New York: Oxford University Press

Tellier A, Brown JKM. 2007. Polymorphism in multilocus host–parasite coevolutionary interactions. *Genetics* **177**:1777–1790.

Tellier A, Moreno-Gamez S, Stephan W. 2014. Speed of adaptation and genomic signatures in arms race and trench warfare models of host–parasite coevolution. *Evolution* **68**:2211–2224.

Thrall PH, Barrett LG, Dodds PN, Burdon JJ. 2016. Epidemiological and evolutionary outcomes in gene-for-gene and matching allele models. *Frontiers in Plant Science* **6**:1–12.

Turko P, Tellenbach C, Keller E, Tardent N, Keller B, Spaak P, Wolinska J. 2018. Parasites driving host diversity: incidence of disease correlated with *Daphnia* clonal turnover. *Evolution* **72**:619–629.

de Visser JAGM, Elena SF. 2007. The evolution of sex: empirical insights into the roles of epistasis and drift. *Nature Reviews Genetics* **8**:139–149.

Wilfert L, Schmid-Hempel P. 2008. The genetic architecture of susceptibility to parasites. *BMC Evolutionary Biology* **8**:187.

Woolhouse MEJ, Webster JP, Domingo E, Charlesworth B, Levin BR. 2002. Biological and biomedical implications of the co-evolution of pathogens and their hosts. *Nature Genetics* **32**:569–577.

CHAPTER 1

A two-locus system with strong epistasis underlies rapid parasite-mediated evolution of host resistance

Ameline C, Bourgeois Y, Vögtli F, Savola E, Andras J, Engelstädter J, Ebert D. 2021. A two-locus system with strong epistasis underlies rapid parasite-mediated evolution of host resistance. *Molecular Biology and Evolution* **38**:1512–1528.

The data underlying this article and analysis scripts are available in the Figshare Repository https://doi.org/10.6084/m9.figshare.13259828.v2. Raw sequence data from the GWAS analysis is deposited in the NCBI Bioproject PRJNA680821.

Abstract Parasites are a major evolutionary force, driving adaptive responses in host populations. Although the link between phenotypic response to parasite-mediated natural selection and the underlying genetic architecture often remains obscure, this link is crucial for understanding the evolution of resistance and predicting associated allele frequency changes in the population. To close this gap, we monitored the response to selection during epidemics of a virulent bacterial pathogen, *Pasteuria ramosa*, in a natural host population of *Daphnia magna*. Across two epidemics, we observed a strong increase in the proportion of resistant phenotypes as the epidemics progressed. Field and laboratory experiments confirmed that this increase in resistance was caused by selection from the local parasite. Using a genome wide association study (GWAS), we built a genetic model in which two genomic regions with dominance and epistasis control resistance polymorphism in the host. We verified this model by selfing host genotypes with different resistance phenotypes and scoring their F1 for segregation of resistance and associated genetic markers. Such epistatic effects with strong fitness consequences in host–parasite coevolution are believed to be crucial in the Red Queen model for the evolution of genetic recombination.

Keywords parasite-mediated selection, zooplankton, resistance, genetic architecture, epistasis, dominance, multi-locus genetics, *Daphnia magna*, *Pasteuria ramosa*

Introduction

Darwinian evolution is a process in which the phenotypes that are best adapted to the current environment produce more offspring for the next generation. Genetic variants that code for these phenotypes are thus expected to increase in frequency in the population. Although this concept is fundamental in evolutionary biology, it remains difficult to connect the phenotype under selection with the underlying changes in the gene pool of natural populations (Ellegren and Sheldon 2008; Whitlock and Lotterhos 2015; Hoban et al. 2016). While single gene effects have been shown to explain the phenotype–genotype interplay in some naturally evolving populations (Daborn 2002; Cao et al. 2016; van't Hof et al. 2016), the genetic architecture underlying a phenotype is often complex. In addition, the way the environment influences the expression of a trait, and genotype x environment interactions may further obscure the link between phenotype and genotype. It is, thus, often impossible to predict genetic changes in a population that result from selection on specific phenotypes. Among the most potent drivers of evolutionary change in host populations are parasites; parasite-mediated selection can raise the frequency of resistant phenotypes rapidly (Schmid-Hempel 2011, Morgan and Koskella 2017, Koskella 2018, Kurtz et al. 2016) and is thought to contribute to many biological phenomena, such as biodiversity (Laine 2009), speciation (Schlesinger et al. 2014) and the maintenance of sexual recombination in the host (Lively 2010; Gibson et al. 2018).

To link patterns produced by parasite-mediated selection with evolutionary theory, we need to know the genetic architecture that underlies resistance; this includes the number of loci, their relative contribution to the phenotype, and the interaction between loci (epistasis) and alleles (dominance). In this way, we may be able to predict the outcome of selection, test theoretical models, and understand epidemiological dynamics (Hamilton 1980; Galvani 2003; Schmid-Hempel 2011). In a few cases, resistance to parasites has been found to be determined by single loci with strong effects, e.g. in plants (Gómez-Gómez et al. 1999; Li and Cowling 2003; Li et al. 2017), invertebrates (Juneja et al. 2015; Xiao et al. 2017), and vertebrates (Samson et al. 1996). However, the genetic architecture is often obscured by intrinsic complexity and confounding factors that may influence the phenotype. Resistance might be determined by multiple loci with qualitative or quantitative effects, present distinct dominance patterns, and display interactions with other genes or the environment. Indeed, multi-locus genetic architecture of resistance can create more diversity, and is thus thought to be more common than single loci (Sasaki 2000; Tellier and Brown 2007; Wilfert and Schmid-Hempel 2008). Multi-locus architecture was described in *Drosophila melanogaster*, for example, where resistance was found to be determined mostly by a few large-effect loci (Bangham et al. 2008; Magwire et al. 2012) and some additional small-effect loci (Cogni et al. 2016; Magalhães and Sucena 2016). Quantitative resistance has also been found in crops where it may be used as a pathogen control strategy (Pilet-Nayel et al. 2017). In the water flea *Daphnia magna*, resistance has been found to be quantitative to a microsporidian parasite, but qualitative to a bacterial

pathogen (Routtu and Ebert 2015). Although resistance tends to be dominant (Hooker and Saxena 1971; Carton et al. 2005), resistant alleles have been found to be both dominant and recessive in plants (Gómez-Gómez et al. 1999; Li and Cowling 2003; Li et al. 2017) and invertebrates (Luijckx et al. 2012; Juneja et al. 2015; Xiao et al. 2017). Epistasis between resistance loci has also been found in diverse plants and animals (Kover and Caicedo 2001; Wilfert and Schmid-Hempel 2008; Jones et al. 2014; González et al. 2015; Metzger et al. 2016), emphasizing its crucial role in the evolution of resistance. The link between genetic architecture and natural selection for resistance remains weak, however, mainly limited to the theoretical extrapolation of results from laboratory experiments.

Dominance and epistasis describe the non-additive interaction among alleles of the same or different loci, respectively, making them crucial for the evolutionary response to selection. Epistasis among resistance genes could contribute to the maintenance of genetic diversity by reducing fixation rates at individual loci, and is thus thought to be pervasive (Tellier and Brown 2007). In the Red Queen model for the evolution of sex, thus, epistasis among resistance loci helps maintain genetic diversity and recombination in the host (Hamilton 1980; Hamilton et al. 1990; Howard and Lively 1998; Salathé et al. 2008; Engelstädter and Bonhoeffer 2009; Kouyos et al. 2009). Important with regard to the role of epistasis for the evolution of host–parasite interactions is furthermore, that the interacting loci must be polymorphic within the same natural populations. However, the importance of genetic architecture for understanding the evolution of resistance stands in stark contrast to the limited amount of available data on natural populations (Alves et al. 2019). In this study, we investigate the evolution of resistance in a natural population of the planktonic crustacean *Daphnia magna* as it experiences epidemics of the virulent bacterial pathogen *Pasteuria ramosa*. We link parasite-mediated selection to its associated allele frequency change by resolving the underlying genetic architecture of host resistance.

In recent years, water fleas of the genus *Daphnia* (Crustacea, Cladocera) and their microparasites have become one of the best understood systems for studying the evolution and ecology of host–parasite interactions (Ebert 2005, Vale et al. 2011, Izhar and Ben-Ami 2015, González-Tortuero et al. 2016, Strauss et al. 2017, Turko et al. 2018, Shocket et al. 2018, Rogalski and Duffy 2020). Parasite selection in natural *Daphnia* populations has been shown to alter the phenotypic distribution of resistance (Little and Ebert 1999; Decaestecker et al. 2007; Duffy and Sivars-Becker 2007; Duncan and Little 2007), and genetic mapping studies identified loci involved in host resistance (Luijckx et al. 2012; Luijckx et al. 2013; Routtu and Ebert 2015; Metzger et al. 2016; Bento et al. 2017; Bento et al. 2020) and parasite infectivity (Andras et al. 2020); however, because studies on host resistance largely involved crosses among populations, the results may not reflect genetic variation within populations. Genetic changes in natural host populations have been observed but so far it was not possible to link this change to parasite resistance loci (Mitchell et al. 2004; Duncan and Little 2007). Understanding the link between parasite-mediated selection on

host resistance and the underlying genetic architecture would enable us to determine and predict the tempo and mode of evolution in natural populations and to link observed phenotypic changes to frequency changes of alleles under selection. This study provides such a phenotype–genotype link. We quantified the change in frequency of resistance phenotypes over time in a natural *D. magna* population and, through experiments, showed that the locally dominant, virulent parasite genotype of *P. ramosa* played a major role in the observed phenotypic changes. A genome-wide association study (GWAS) and genetic crosses revealed the underlying genetic architecture of resistance in our study population and provided a genetic model for inheritance of resistance. This genetic model comprises two resistance loci presenting distinct dominance patterns and strongly linked with epistasis. These results strongly support the Red Queen model of host–parasite coevolution and the maintenance of genetic recombination.

Results

Parasite-mediated selection explains phenotypic dynamics

Monitoring

We monitored the Aegelsee *Daphnia magna* population from fall 2010 to fall 2015, while the present study focuses on the 2014 and 2015 planktonic seasons. In this population, *D. magna* diapauses during winter as resting eggs, while the active season spans from early April to early October. Each summer, we observed a *Pasteuria ramosa* epidemic that typically started in early May, about a month after *Daphnia* emerged from diapause, and lasted throughout the summer (Fig. 1.1A) with peak prevalence of 70% to 95%. *P. ramosa* infection in the host is characterized by gigantism, a reddish-brownish opaque coloration, and castration, i.e. an empty brood pouch. *P. ramosa* is a virulent parasite, stripping the host of 80% to 90% of its residual reproductive success and killing it after six to ten weeks, at which point it releases millions of long-lasting spores into the environment (Ebert et al. 1996, 2016).

Animals sampled from the field were cloned, and their resistance phenotypes (resistotypes) were scored. *Daphnia magna* produces asexual clonal eggs which are used in the laboratory to produce clonal lines, a.k.a. genotypes. Individuals castrated by the parasite received an antibiotic treatment to allow clonal reproduction. Resistance to the bacteria is indicated when parasite spores are unable to attach to the gut wall of the host (Duneau et al. 2011; Luijckx et al. 2011). We thus defined host clone resistotypes according to the ability of parasite spores of given isolates to attach to the host gut wall or not. The host's overall resistotype is its combined resistotypes for the four *P. ramosa* isolates in the following order: C1, C19, P15 and P20, e.g. a clone susceptible to all four isolates will have the SSSS resistotype. P20 had been isolated from our study population in May 2011; isolates C1, C19 and P15 had previously been established in the laboratory from other *D. magna* European populations. Overall, we found three predominant resistotypes: RRSR, RRSS and SSSS, which together accounted for 95.1±1.0% of all tested animals over the active season in 2014 (n = 995) and 2015 (n

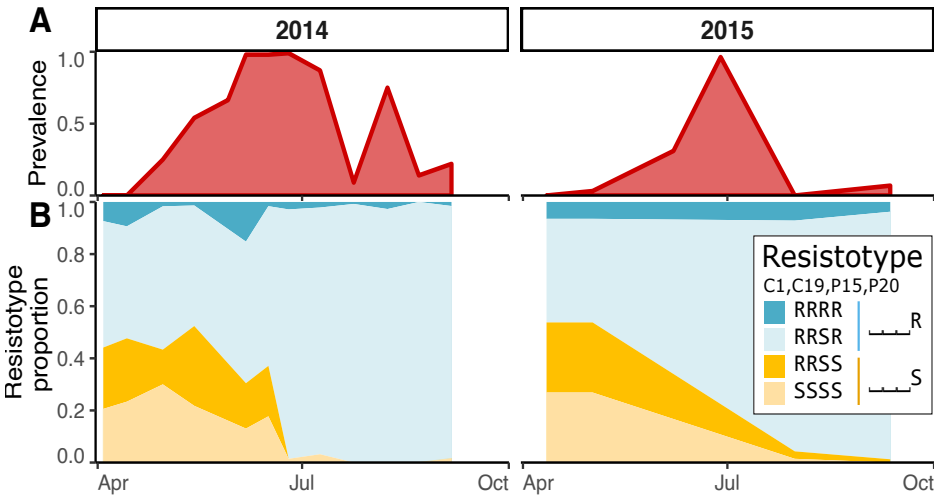

Figure 1.1

Prevalence and resistotype dynamics observed in the Aegelsee *Daphnia magna* population. **A**: *Pasteuria ramosa* prevalence across two summer epidemics. **B**: Resistotype (resistance phenotype) frequencies across time (n = 60–100 *D. magna* clones from each sampling date in two- to three-week intervals). Resistotypes = resistance to *P. ramosa* C1, C19, P15 and P20, consecutively).

= 260). RRRR represented a much smaller proportion of the resistotypes (4.9±1.0%) (Fig. 1.1B). Excluding the resistotype data for *P. ramosa* isolate P15, for which over 95% of the hosts were susceptible, the study population was mainly composed of the three resistotypes: RR␣R, RR␣S and SS␣S. When one isolate was not considered, we used the placeholder "␣" for that resistotype: e.g. "RR␣R resistotype". A few other resistotypes that were absent in the 2014 and 2015 samples were observed in other samples. Notably, the SR␣S resistotype was found in 0.3% of hatched animals from *D. magna* resting eggs sampled during the winter 2014 diapause. The SR␣R resistotype has never been found in the field samples but was found in the selfed offspring of the rare resistotype SR␣S. Resistotypes RS␣␣ and SS␣R were not observed in this population.

In 2011, we sampled a subset of infected animals (n = 113) to characterize *P. ramosa* diversity among infected hosts throughout the active season and found that the P20 genotype represented about 50% of the parasite diversity among infected hosts when the epidemics began. This proportion decreased to zero during the epidemic, as other *P. ramosa* genotypes took over (Supplementary Fig. S1.1).

The temporal dynamics revealed an increase in animals resistant to P20 (RRSR and RRRR, in short: RR␣R, or ␣␣␣R) soon after the onset of the epidemics, while animals susceptible to P20 (RRSS and SSSS, or ␣␣␣S) declined accordingly (Fig. 1.1B) in both study years. Resistance to C1, C19 and P15 did not seem to play a strong role in the selection process during the epidemics. In the result described next, we tested the hypothesis that selection by *P. ramosa* isolate P20 is the main driver of natural resistotype dynamics in our study population during the early planktonic season. As a reminder, P20 has been isolated from a spring sample of the here-studied population.

Experimental and field infections

First, we tested the impact of the parasite on the different resistotypes to associate disease phenotype with resistotype. To do this, we obtained a sample of the spring cohort of the *D. magna* population by hatching resting eggs collected in February 2014. These animals represented, in total, 70 clones

Figure 1.2

Experimental infections of *Daphnia magna* with different resistotypes (resistance phenotype). Resistotypes RRSR, RRSS, SSSS (n = 20 clones for each) and RRRR (n = 10 clones) were infected with parasite spores from the early phase of the epidemic. Five repeats were performed for each clone (total n = 334). Controls (n = 210) remained uninfected and are not shown here. **A**: Proportion of infected *D. magna* among the four resistotypes. **B**: Number of clutches produced before parasitic castration in the infected P20-resistant (___R) and susceptible (___S) animals (n = 115). **C**: Time before visible infection in P20-resistant and P20-susceptible individuals (n = 115).

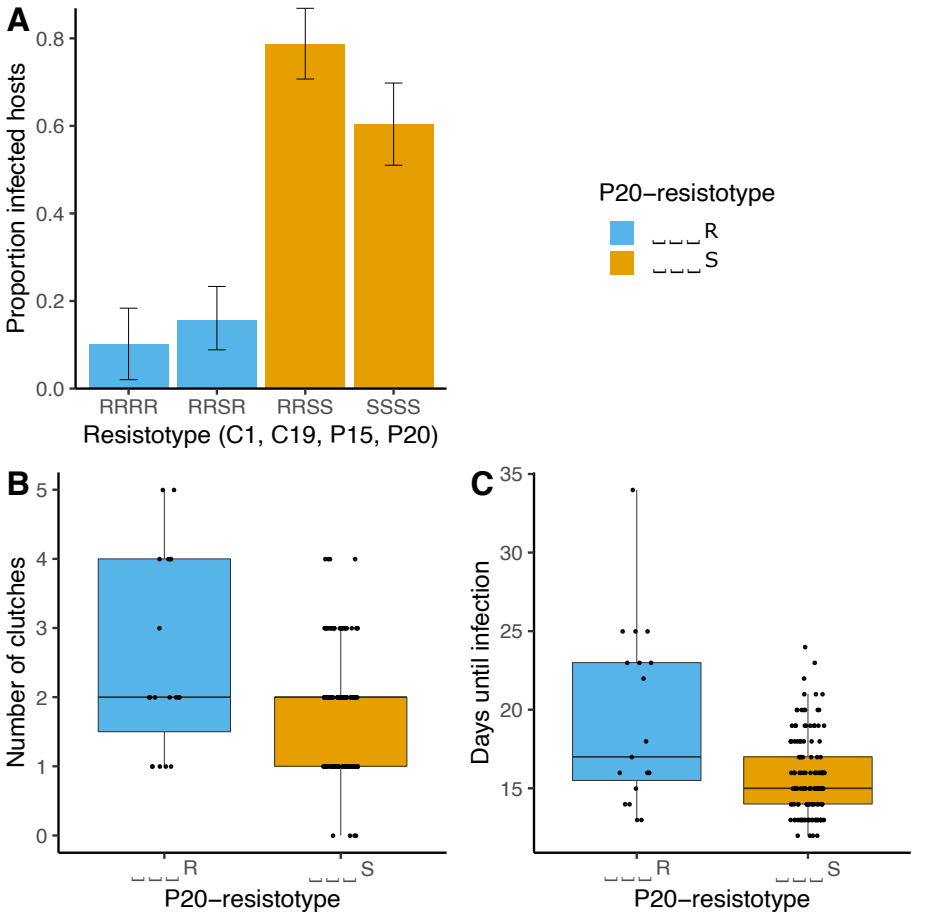

of the four most common resistotypes (RRSR, RRSS, SSSS, RRRR), with each clone replicated five times (n = 350). We exposed these clonal offspring to a mixture of *P. ramosa* spores that represented the diversity of the parasite population during the early phase of the epidemic. We then monitored the hosts for infection (looking for visible signs) and fecundity (counting the number of produced clutches). Sixteen animals died before we could test their infection status, resulting in a total sample size of n = 334. Individuals with resistotypes RRSS and SSSS (susceptible to P20) were infected far more frequently than RRSR and RRRR (resistant to P20) individuals (Fig. 1.2A; Null deviance = 461.3 on 333 df, Residual deviance = 358.4 on 329 df, $p < 0.001$). The analysis also compared P20-susceptible and P20-resistant resistotypes, confirming the high susceptibility of the P20-susceptible animals (Fig. 1.2A; Null deviance = 461.3 on 333 df, Residual deviance = 360.7 on 331 df, $p < 0.001$). Infected P20-susceptible individuals produced on average about one less clutch before parasitic castration (n = 136, 1.83 ± 0.07 clutches) than did infected P20-resistant individuals (n = 19, 2.53 ± 0.3 clutches) (Fig. 1.2B; Null deviance = 76.9 on 154 df, Residual deviance = 74.0 on 152 df, $p = 0.023$). Accordingly, the average time period until visible infection was shorter in P20-susceptible clones (15.7 ± 0.2 days) than in P20-resistant clones (19.4 ± 1 days) (Fig. 1.2C; Null deviance = 94.4 on 154 df, Residual deviance = 85.1 on 152 df, $p = 0.0018$). These results clearly support the hypothesis that early season *P. ramosa* strains from the field select on the P20 resistotype.

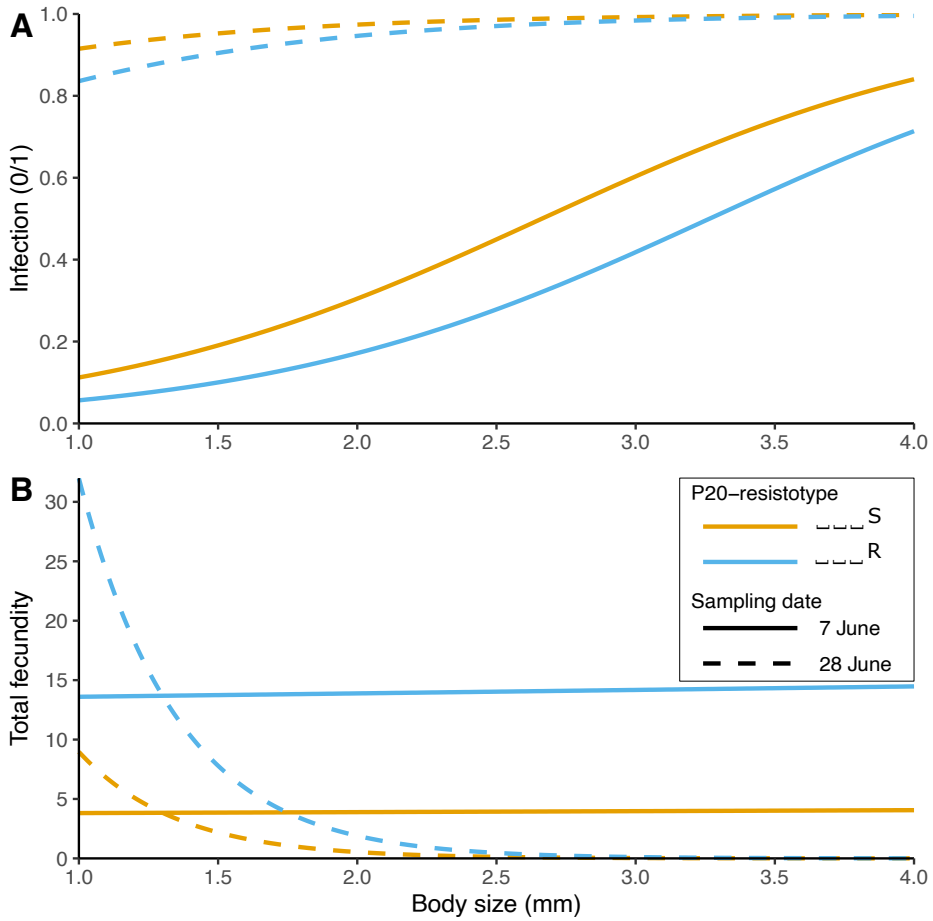

Figure 1.3

Fitted models of infection phenotypes in field-collected *Daphnia magna* relative to their body size at capture (x-axis) and their resistance to P20 for two sampling dates in June 2015. **A**: P20-susceptible (orange) animals have a higher likelihood to be infected than P20-resistant (blue) ones for any body size. **B**: Infected P20-susceptible animals have a lower total fecundity than P20-resistant ones for any body size. Differences between the data are partially due to the difference in parasite prevalence on the two sampling dates (31% on 7 June and 96% on 28 June).

In the following year, we looked at the relationship of disease phenotype and P20 resistotype only in the field by measuring the parasite's impact on P20-resistant and P20-susceptible hosts. We collected animals in the field during the early half of the *P. ramosa* epidemic and raised them individually in the laboratory, recording their disease symptoms. We then cured infected animals with antibiotics, allowed them to produce clonal offspring, and determined their P20 resistotype. Our analysis revealed higher infection rates (size corrected) for P20-susceptible than for P20-resistant individuals in these natural conditions (Fig. 1.3A; Fitted model: glm (Infected (1/0) ~ P20 resistotype + Body_size + Sampling_date, family = quasibinomial(), n = 331; Null deviance = 415.1 on 330 df, Residual deviance = 209.1 on 327 df, p = 0.025). Field-caught infected P20-susceptible individuals also produced, on average, fewer offspring before parasitic castration than infected P20-resistant ones (Fig. 1.3B; Fitted model: glm.nb (Fecundity ~ P20 resistotype + Body_size * Sampling_date), n = 224; Null deviance = 127.9 on 223 df, Residual deviance = 92.9 on 219 df, p = 0.014). In both models, the sampling date also had a significant effect. Parasite prevalence on the two sampling dates differed strongly (31% on 7 June and 96% on 28 June 2015). We observed on the first sampling date that larger individuals were more infected and consequently produced less offspring. This size difference is not visible anymore on the second sampling date, where almost all individuals were infected. The overall pattern in relation to the P20 resistotype remained the same, even though the difference in infection and fecundity between field collected P20 resistotypes was less pronounced than

in the controlled infection experiment (compare Fig. 1.2 and Fig. 1.3). In summary, the results of the two experiments clearly support the hypothesis that early season *P. ramosa* from the field select on the P20 resistotype.

Linking resistance phenotypes to genotypes

Excluding the P15 resistotype, which has very low variability because most animals are P15-susceptible, the study population was composed mainly of three resistotypes: RR_R, RR_S and SS_S. A supergene for resistance to C1 and C19 has been described in *D. magna* using QTL mapping (Routtu and Ebert 2015; Bento et al. 2017), and the genetic architecture of resistance at this so-called ABC-cluster, or *P. ramosa* resistance (PR) locus, has been further resolved using genetic crosses among host genotypes (Metzger et al. 2016). According to this genetic model, an SS_ _ resistotype (susceptible to C1 and C19) has an "aabbcc" genotype (lower case letters indicate recessive alleles), while RS_ _ individuals (resistant to C1 and susceptible to C19) are "A---cc" (upper case letters indicate dominant alleles and a dash "-" indicates alleles that do not influence the phenotype); SR_ _ individuals are "aaB-cc", and RR_ _ individuals are "----C-". In other words, allele A epistatically nullifies variation at the B locus, and allele C nullifies variation at the A and B loci (Metzger et al. 2016; Bento et al. 2017). See also Supplementary Fig. S1.2. Considering this genetic model, we assume that the recessive allele at the A locus is fixed in our study population ("aa" genotype) and that the dominant allele at the B locus is very rare, as we never observed RS_ _ individuals and only found SR_ _ in very low proportions. In our study population, the SS_ _ /RR_ _ polymorphism can therefore be best described by the C-locus polymorphism, i.e. genotypes "aabbcc" and "aabbC-", respectively, with C being the dominant allele for resistance. Given this, we assume, in the following sections, that variation at the C locus underlies the resistance polymorphism for C1 and C19.

Genomic regions of resistance to the parasite

We sequenced the genomes of 16, 10 and 11 clones with resistotypes RR_R, RR_S and SS_S, respectively and conducted a GWAS comparing five pairs of these resistotypes to identify candidates for resistance to C1, C19 and P20: (i) SS_ _ vs. RR_ _, (ii) SS_S vs. RR_S, (iii) _ _ _S vs. _ _ _R, (iv) RR_S vs. RR_R and (v) SS_S vs. RR_R. Comparisons (i) and (ii) (variation at C1 and C19 resistotypes) revealed a strong signal on linkage group (LG) 3 (Fig. 1.4A and B). This region encompasses the super gene described earlier by Routtu and Ebert (2015) and Bento et al. (2017), the so-called ABC-cluster, or *P. ramosa* resistance (PR) locus. Comparisons (iii) and (iv) (variation at P20 resistotype) revealed a strong signal on LG 5 (Fig. 1.4C and D), hereafter called the E-locus region. In the present host-parasite system, the D locus determines resistance to P15 and is not considered here (Bento et al. 2020). The E-locus region has not yet been associated with resistance, and no *P. ramosa* resistance gene has been described on the same linkage group in *D. magna*. Finally, comparison (v) (variation at C1, C19 and P20 resistotypes) indicated a strong signal at both the ABC cluster and the E-locus region (Fig. 1.4E). The genomic regions associated with resistotypes in our GWAS were not sharp peaks, but rather table-like blocks of associ-

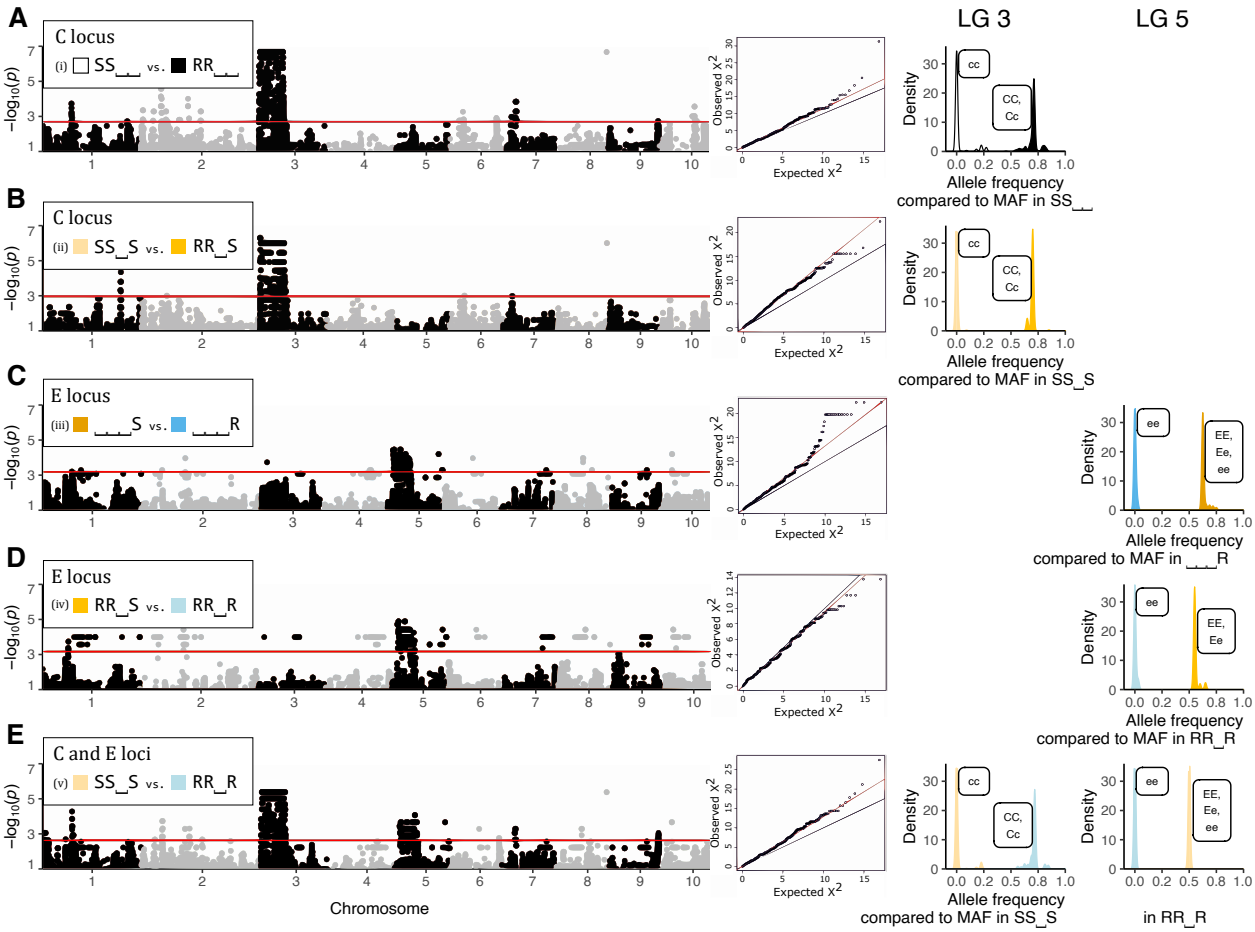

Figure 1.4

GWAS analysis comparing the most common resistance phenotypes (resistotypes) in the Aegelsee *Daphnia magna* population. The resistotype depicts resistance (R) or susceptibility (S) to *Pasteuria ramosa* isolates C1, C19, P15 and P20. (i) SS_ _ vs. RR_ _; (ii) SS_S vs. RR_S; (iii) _ _ _S vs. _ _ _R; (iv) RR_S vs. RR_R, and (v) SS_S vs. RR_R. Comparisons (i) and (ii) (variation at C1 and C19 resistotypes) revealed a strong signal on linkage group (LG) 3 corresponding to the C locus. Comparisons (iii) and (iv) (variation at P20 resistotype) revealed a strong signal on LG 5 corresponding to the E locus. Comparison (v) (variation at C1 and C19, and P20 resistotypes) revealed a strong signal on both regions. **Left panel**: Manhattan plots of relationships between different resistotype groups (showing only SNPs with $P_{corrected} < 0.01$). The x-axis corresponds to SNP data mapped on the 2.4 *D. magna* reference genome (Routtu et al. 2014), representing only SNPs, not physical distance on the genome. **Middle panel**: Quantile-quantile plots of non-corrected p-values excluding SNPs from linkage groups 3 and 5, since these scaffolds displayed an excess of strongly associated markers. **Right panel**: Comparison of allele frequencies between resistotype groups at the C and the E loci. Significant SNPs on LG 3 or LG 5 were used (SNPs with $p < P_{lim}/100$, with P_{lim} as defined in the Methods section, Eq. 1.1. For each SNP, the allele with the minor allele frequency (MAF) within resistotype groups that presented only one allele at the C or the E locus (all homozygous individuals) was used for comparisons. Hence, the x-axis represents allele frequency of the dominant allele within resistotype groups (considering total allele number, or chromosome number: 2n). Labels attached to peaks describe the inferred possible genotypes at the C or the E locus within resistotype groups. In comparisons at the C locus on LG 3, resistotype groups susceptible to C1 and C19 presented only one allele, i.e. they contained only homozygous recessive individuals at the C locus (dominant allele frequency of zero). Resistotype groups resistant to C1 and C19 did contain the dominant allele (frequency between 0.5 and 1), showing that resistance is dominant at the C locus, as the resistant group contains heterozygous individuals. Similarly, in comparisons at the E locus on LG 5, resistotype groups resistant to P20 do not present the dominant allele (frequency of zero), while resistotype groups susceptible to P20 do, i.e. contain heterozygous individuals (dominant allele frequency between 0.5 and 1). This shows that, in contrast with the C locus, susceptibility is dominant at the E locus. Screening individual genomes revealed that some SS_S individuals (susceptible to C1 and C19, and P20) presented the "ee" genotype at the E locus (resistance to P20), although susceptibility is dominant at the E locus. This was not observed in RR_S individuals (resistant to C1 and C19 but susceptible to P20) (Supplementary Table S1.3). This observation can be explained by an epistatic relationship linking the C and the E loci. This epistasis confers susceptibility to P20 to individuals susceptible to C1 and C19, i.e. presenting the "cc" genotype regardless of the genotype at the E locus. In contrast, with groups containing SS_S individuals, i.e. comparisons (iii) and (iv), some SS_S individuals present the "ee" genotype at the E locus. In these groups, the frequency of the dominant allele can be lower than 0.5.

ated SNPs (Fig. 1.4). This structure was expected for the C locus, which is a known supergene—a large block of genome space with apparently little or no recombination that contains many genes (Bento et al. 2017). Figure 1.4 indicates that the same may be the case for the E-locus region, where the block of associated SNPs makes up nearly half of the linkage group. A few single SNPs also showed significant association in all the comparisons (Fig. 1.4), but because of the strength of the observed pattern and because we expected a large region to be associated with resistance, we do not consider these single SNPs further.

The E-locus region encompassed 22 scaffolds and one contig on version 2.4 of the *D. magna* reference genome, with a cumulative length of more than 3 Mb (3101076 bp) (Supplementary Table S1.1). We found 485 genes on all associated scaffolds. The strongest signals of association were found on scaffolds 2167 and 2560, which harboured 82 genes. Some of these genes were similar to genes identified in a previous study of the ABC cluster on LG 3 (Bento et al. 2017), with a glucosyltransferase found on scaffold 2167. Three other sugar transferases (galactosyltransferases) were identified, two of them on scaffold 2560 (Supplementary Table S1.2).

Genetic model of resistance inheritance

Mean allele frequencies at associated SNPs showed that SS_._ individuals (susceptible to C1 and C19) display a single allele at the C locus, while RR_._ individuals display two distinct alleles at the C locus. This suggests that SS_._ individuals are homozygous at the C locus, while RR_._ individuals comprise homo- and heterozygotes. At the E locus, _._._R individuals (resistant to P20) are presumably homozygous, while _._._S individuals (susceptible to P20) comprise homo- and heterozygous individuals (Fig. 1.4, right panel). These results indicate that resistance to C1 and C19 is governed by a dominant allele ("C-" genotype), as shown before (Metzger et al. 2016). In contrast, resistance to P20 is determined by a recessive allele ("ee" genotype), as was shown before for a different resistance locus (D locus, (Bento et al. 2020). Screening individual genomes revealed that some SS_S individuals (susceptible to C1 and C19, and P20) present the "ee" genotype at the E locus (underlying P20 resistotype), although this genotype should confer resistance to P20. This was not observed in RR_S individuals (resistant to C1 and C19, but susceptible to P20) (Supplementary Table S1.3), which we hypothesize to be explained by an epistatic relationship linking the C and the E loci. This epistasis confers P20 susceptibility to individuals susceptible to C1 and C19, i.e. presenting the "cc" genotype, regardless of their genotype at the E locus. This genetic model is presented in Figure 1.5 (without variation at the B locus, see below). In the present study, we mostly considered variation at the C and E loci, as they seem to play a major role in the diversity of resistotypes in our study population.

To test the genetic model derived from the GWAS, we investigated segregation of resistotypes among selfed offspring of *D. magna* genotypes with diverse resistotypes. *Daphnia magna* reproduces by cyclical parthenogenesis, in which asexual eggs produce clonal lines and sexual reproduction allows to perform genetic crosses. Our genetic model allowed us to predict

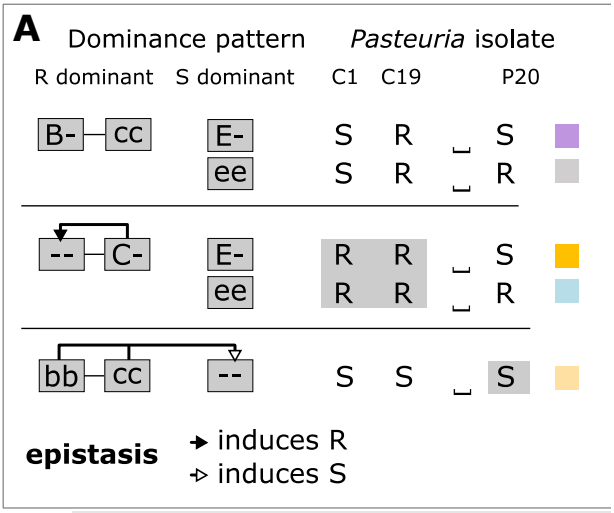

B

	CC	Cc	bbcc	Bbcc
EE	CCEE RR_S	CcEE RR_S	bbccEE SS_S	BbccEE SR_S
Ee	CCEe RR_S	CcEe RR_S	bbccEe SS_S	BbccEe SR_S
ee	CCee RR_R	Ccee RR_R	bbccee SS_S	Bbccee SR_R

Figure 1.5

Model for the genetic architecture of resistance to C1, C19 and P20 *Pasteuria ramosa* isolates in the Aegelsee *Daphnia magna* population as inferred from the GWAS analysis (Fig. 1.4) and the genetic crosses (Tables 1.1 and 1.2). **A**: Schematic representation of the genetic model. Resistance to C1 and C19 is determined by the ABC cluster as described in Metzger et al. (2016), and the model is extended to include the newly discovered E locus. The dominant allele at the B locus induces resistance (R) to C19 and susceptibility (S) to C1. The dominant allele at the C locus confers resistance to both C1 and C19, regardless of the genotype at the B locus (epistasis). The newly discovered E locus contributes to determining resistance to P20. Resistance is dominant at the C locus (resistance to C1 and C19) but recessive at the E locus (resistance to P20). Homozygosity for the recessive allele at the B and C loci induces susceptibility to P20, regardless of the genotype at the E locus (epistasis). Hence epistasis can only be observed phenotypically in the "bbccee" genotype, which has the resistotype SS_S. Without epistasis, the "bbccee" genotype is expected to have the phenotype SS_R, a phenotype we never observed in the population or in our genetic crosses. **B**: Multi-locus genotypes and resistotypes at the B, C and E loci. Resistotypes are grouped by background color. As the C allele epistatically nullifies the effect of the B locus, only combinations of the B and E loci are shown where the C locus is homozygous for the c allele. This model does not consider variation at the A locus, as the recessive allele at this locus is believed to be fixed in the Aegelsee *D. magna* population.

the segregation of genotypes and phenotypes, which can then be compared to the observed segregation patterns among selfed offspring. From 24 host genotypes (F0 parent clones), we produced 24 groups of selfed F1 offspring. Twenty-two F0 clones included animals with all possible combinations of alleles at the C and E loci, while two F0s showed the rare variation at the B locus and variation at the E locus. Expected and observed resistotype frequencies are presented in Tables 1.1 and 1.2 and detailed for each F1 group in Supplementary Tables S1.4 to S1.15. In the 22 F1 groups showing variation at the C and E loci, segregation of offspring followed the predictions of our genetic model (Fig. 1.5), i.e. we observed all expected resistotypes and saw no significant deviations from the expected frequencies based on the model. These data clearly support the genetic model for resistance at the C and E loci.

As described above, earlier research (Metzger et al. 2016; Bento et al. 2017) has shown that the dominant allele at the C locus interacts epistatically with the A and B loci (all are part of the ABC cluster), such that variation at the A and B loci becomes neutral when a C allele is present. We assume that the a allele is fixed in the Aegelsee *D. magna* population, so that only variation at the B locus influences the C1 and C19 resistotypes in individuals with the "cc" genotype (see above). As variation at the B locus is very rare in our *D. magna* study population and could not be included in the GWAS

Table 1.1

Genetic crosses of resistance phenotypes (resistotypes) from the Aegelsee *Daphnia magna* population, where only the C and the E loci are considered.

A

RR_S CcEe	CE	Ce	cE	ce
CE	RR_S	RR_S	RR_S	RR_S
Ce	RR_S	RR_R	RR_S	RR_R
cE	RR_S	RR_S	SS_S	SS_S
ce	RR_S	RR_R	SS_S	SS_S

B

F0 parent		Selfed F1 offspring							
				Proportion					
					Observed				
				Expected	Repeat (F1 groups from different parent clones)				C-M-H test on counts
Inferred genotype	Resistotype	Inferred genotype	Resistotype		a	b	c	d	
CCEE	RR_S	CCEE	RR_S	1	*n* = 43 1	*n* = 37 1			NA
CCEe	RR_S	CCE- CCee	RR_S RR_R	0,75 0,25	*n* = 89 0,79 0,21	*n* = 31 0,74 0,26	*n* = 79 0,84 0,16		X^2=0.85, *df*=1, *p*=0.36
CCee	RR_R	CCee	RR_R	1	*n* = 39 1	*n* = 42 1	*n* = 70 1	*n* = 79 1	NA
CcEE	RR_S	C-EE ccEE	RR_S SS_S	0,75 0,25	*n* = 19 0,74 0,26				*Fisher test on counts* *p*=1
CcEe	RR_S	C-E- cc-- C-ee	RR_S SS_S RR_R	0,56 0,25 0,19	*n* = 48 0,47 0,30 0,23	*n* = 34 0,56 0,06 0,38	*n* = 64 0,65 0,13 0,22	*n* = 65 0,51 0,21 0,28	M^2=4.61, *df*=2, *p*=0.10
Ccee	RR_R	C-ee ccee	RR_R SS_S	0,75 0,25	*n* = 36 0,75 0,25	*n* = 49 0,80 0,20	*n*= 22 0,62 0,38		X^2=0.0062, *df*=1, *p*=0.94
ccEE	SS_S	ccEE	SS_S	1	*n* = 87 1				NA
ccEe	SS_S	ccE-	SS_S	1	*n* = 84 1	*n* = 65 1			NA
ccee	SS_S	ccee	SS_S	1	*n* = 74 1	*n* = 35 1			NA

A: Punnett square for all possible gamete combinations according to our genetic model of resistance inheritance. The table shows the resistotypes (grouped by background colour) from the 16 combinations of gametes from a double heterozygote for the C and the E loci. The bottom right cell (red font, bold) represents offspring individuals where the epistatic interaction between the C and the E loci is revealed (Fig. 1.5). **B**: Results from selfing of *D. magna* clones. Resistotypes of F0 mothers and F1 offspring groups were obtained using the attachment test, and resistance genotypes of F0 parents at the C and E loci were inferred from their resistotypes and the segregation patterns of resistotypes in their F1 offspring. Expected resistotype proportions within F1 groups were calculated using the genetic model presented in the Punnett square and the R package "peas" (Fig. 1.5; Supplementary Document S1.1. Detailed results and statistical analyses for each cross are presented in Supplementary Tables S1.4 to S1.12 and Table S1.15. Segregation of offspring is presented as proportions, although statistical tests were run on counts. One to four crosses using distinct mother clonal lines (repeats a to d) were conducted for each F0 mother resistance genotype at the C and E loci. No variation at the B locus was observed (all F0 mothers are inferred to have the "bb" genotype according to F1 resistotype segregation).

analysis, we selfed two *D. magna* genotypes that presented the very rare SR_S resistotype, whose underlying genotype at the ABC cluster we expect to be "B-cc" (probably "Bbcc", considering the B allele is rare in the population). In the F1 offspring of the two F0 parents with the SR_S resistotype and the "Bbcc--" genotype, we observed SR_R individuals. We speculate that SR_R animals have the genotype "B-ccee", indicating that the epistatic relationship previously described between the C and the E loci ("cc" acts epistatically on the E locus) should also include the B locus. If this is the case, "bbcc" acts epistatically on the E locus (Fig. 1.5). The two groups of selfed F1 offspring involving "Bb" heterozygotes showed a good fit between

Table 1.2

Genetic crosses of resistance phenotypes (resistotypes) from the Aegelsee *Daphnia magna* population considering the B and the E loci, with the C locus fixed for genotype "cc".

A

SR_S BbccEe	BcE	Bce	bcE	bce
BcE	SR_S	SR_S	SR_S	SR_S
Bce	SR_S	SR_R	SR_S	SR_R
bcE	SR_S	SR_S	SS_S	SS_S
bce	SR_S	SR_R	SS_S	**SS_S**

B

F0 parent		Selfed F1 offspring				
				Proportion		
Inferred genotype	Resistotype	Inferred genotype	Resistotype	Expected	Observed	Fisher test on counts
					n = 37	
BbccEE	SR_S	B-ccEE	SR_S	0,75	0,74	
		bbccEE	SS_S	0,25	0,23	*p*=1
		B-ccee	SR_R	0,00	0,03	
					n = 38	
BbccEe	SR_S	B-ccE-	SR_S	0,56	0,56	
		bbccE-	SS_S	0,25	0,33	*p*=0.58
		B-ccee	SR_R	0,19	0,11	

A: Punnett square for all possible gamete combinations according to our genetic model of resistance inheritance. The table shows the resistotypes (grouped by background colour) resulting from the 16 combinations of gametes from a double heterozygote for the B and the E loci. The bottom right cell (red font, bold) represents offspring individuals where the epistatic interaction between the B, the C, and the E loci is revealed (Fig. 1.5). **B**: Results from selfing of *D. magna* clones. Resistotypes of F0 parents and F1 offspring were obtained using the attachment test, and resistance genotypes of F0 parents at the B, C and E loci were inferred from their resistotypes and the segregation patterns of resistotypes in their F1 offspring. Expected resistotype proportions of F1 were calculated following the genetic model outlined in the Punnett square and using the R package "peas" (Fig. 1.5; Supplementary Document S1.2). The detailed results and statistical analyses for each cross are presented in Supplementary Tables S1.13 to S1.15. Segregation of offspring is presented as proportions, although the statistical tests were run on counts.

this expectation in the expanded model and the observed phenotypic segregation. We observed one SR_R offspring produced from a SR_S parent with the inferred "aaB-ccEE" genotype, which is not expected in our model (Table 1.2B, lower panel), but typing mistakes cannot be fully ruled out.

Linking the genomic regions and the genetic model of resistance

To test whether the segregation of the genomic regions we discovered in the GWAS and the segregation of resistotypes in our crosses agreed with each other, we designed size-polymorphic markers in the genomic regions of the C and the E loci (two for each locus). We tested whether these markers co-segregated with the resistotypes as predicted by our genetic model. Of the four markers, DMPR1 (C locus) and DMPR3 (E locus) showed better linkage with their respective resistance loci (99.6% and 94.8% match, respectively) compared to DMPR2 (C locus) and DMPR4 (E locus) (91.4% and 69.4% match, respectively) (Supplementary Tables S1.16 to S1.18). These numbers reflect that our markers are close to the actual resistance loci, but that recombination between them is possible, leading to non-perfect association. We further based our scoring of resistance genotypes on the more predictive marker genotypes of DMPR1 and DMPR3. In 20 of 22 F1 groups representing all possible combinations of alleles at the C and E loci (Table 1.1), the segregation of marker genotypes in the F1 offspring followed

our genetic model predictions, i.e. all expected genotypes were observed, with no statistically significant deviations from the expected frequencies. In two F1 groups from "CCEe" and "CcEe" F0 parents, the E-locus markers appeared not to be linked to the E locus (Supplementary Tables S1.5 and S1.8). Based on the genotype markers results we had assigned the "EE" genotype to the F0 parent and F1 offspring, but phenotypic segregation in the F1 offspring indicated the parent would have the "Ee" genotype. We speculate that recombination had uncoupled the genetic marker and the resistance loci in these two parent genotypes. Together, these results show that the genomic regions found in the GWAS are indeed associated with the segregation of resistotype in the F1 selfed offspring, supporting our genetic model for the segregation of resistance (Fig. 1.5).

Discussion

This present study aims to assess how annual epidemics by a parasitic bacterium, *Pasteuria ramosa*, influence resistance and the frequencies of the underlying genes in a natural host population of the crustacean *Daphnia magna*. Over the course of epidemics in two consecutive years, we observed drastic changes in resistance phenotype (resistotype). Using experimental infections and fitness measurements on wild-caught individuals, we showed that these changes in resistotype frequency were caused by a local parasite type common during the early phases of the epidemics. A genome-wide association study (GWAS) and laboratory crosses enabled us to locate the resistance genes that responded to this selection and to uncover their mode of inheritance. We pinpointed the genetic architecture of resistance to two genomic regions with dominance and epistasis, thus bridging the gap between natural selection on phenotypes and the underlying genetics.

Parasite-mediated selection

Over the two consecutive years of this study, resistotype frequencies in the host population changed drastically during the parasite epidemics, but remained stable outside of the epidemics (Fig. 1.1)—a pattern consistent with the host population being under strong selection for resistance to *P. ramosa.* The P20 *P. ramosa* isolate, collected during the early epidemic, turned out to be representative of the parasite population during the early part of the two epidemics studied here: Host genotypes characterized by their susceptibility to *P. ramosa* P20 drastically decreased in proportion during the epidemics and were much more susceptible to the local parasite than P20-resistant individuals in experimental infections (Fig. 1.2A). Infected P20-susceptible genotypes also became infected earlier and produced fewer offspring than P20-resistant individuals (Fig. 1.2B and C), revealing a stronger fitness impact of infection by the local parasite. Field data confirmed this result, as wild-caught P20-susceptible individuals were infected more frequently and produced fewer offspring than infected P20-resistant individuals (Fig. 1.3), again showing the higher virulence of the parasite in these P20-susceptible individuals. This effect of the parasite seemed less strong in field collected animals than for those infected in the laboratory. Multiple factors may contribute to this, including differences

among field and laboratory, and differences in the host and parasite populations from the two study years (2014 and 2015). Our findings reveal nevertheless a strong and rapid response to parasite-mediated selection on host resistotypes, that are characterized by their interaction with the P20 *P. ramosa* isolate, in the natural Aegelsee *D. magna* population.

In field samples, smaller individuals were found to be less infected than larger ones. This is not surprising, as older—hence bigger—animals have longer exposure to the parasite than younger animals. For a chronic disease like *P. ramosa* infections, it is expected that, with increasing size and age, prevalence will increase. These results are thus not in conflict with reports showing that younger—hence smaller—*Daphnia* were more susceptible to parasitic infections (Garbutt et al. 2014; Izhar and Ben-Ami 2015, 2019). Differences in age-related susceptibility might, however, influence the shape of the body size–prevalence relationship observed in the field.

Although the parasite P20 was isolated during the early phase of the yearly epidemics, previous research also shows other parasite genotypes in the Aegelsee population (Andras and Ebert 2013) that, as we observed in an earlier year, become more common in infected hosts later in the epidemics (Supplementary Fig. S1.1). We speculate that these later-season isolates may represent different parasite infectotypes (infection phenotypes). Consistent with this, we observed that animals resistant to P20 did, in fact, become infected, both in the field and in the laboratory (Figs. 1.1, 1.2 and 1.3), which cannot be explained with P20-infectotype parasites alone. The present study focuses on natural selection during the early part of the epidemics, which, as our data and data from other years shows, has a fairly consistent selection pattern (Chapter 2), being mainly defined by a drastic increase in P20-resistant individuals from around 50% to almost 100% within a period of two to three months (Fig. 1.1).

The composition of the resistotypes at the beginning of the two seasons (2014 and 2015) in which we monitored this system was strikingly similar, which is surprising given that selection increased resistance over the course of the summer 2014. While answering this question is not part of the current study, there are a few tentative explanations for this observation. First, part of the yearly resting eggs yield, which form the basis of the new population in the following spring, are produced as early as mid-June before selection has diminished some of the resistotypes. Second, epistasis and dominance can protect alleles from natural selection, thus slowing down the response to selection (Feldman et al. 1975; Otto 2009). Our study, as well as earlier studies on this system (Luijckx et al. 2012; Luijckx et al. 2013; Metzger et al. 2016), all indicate strong epistasis and dominance for resistance loci. Further studies are needed to understand how much resting egg production and the genetic architecture of resistance explain the slow response to selection observed across seasons in the Aegelsee *D. magna* population.

Genetic architecture of resistance

To understand the genetic architecture of resistance loci under selection in our study population, we combined a GWAS using *D. magna* genotypes with different resistotypes together with a series of genetic crosses. We found that the most diversity in host resistance to the bacteria is determined by variation at the C locus, situated in a previously described supergene, the PR locus containing the ABC cluster (Bento et al. 2017), and at a newly discovered locus on a different chromosome, the E locus (Fig. 1.4). Taken alone and in the right genetic background, i.e. when there is no epistatic relationship, each of these two loci show Mendelian segregation with resistance being dominant (C locus) or recessive (E locus) (Fig. 1.4, right panel). The two loci interact epistatically with each other, resulting in a complex pattern of inheritance (Fig. 1.5). Balancing selection is hypothesized to maintain diversity at resistance genes (Llaurens et al. 2017; Wittmann et al. 2017; Connallon and Chenoweth 2019), and these genes are often found to have different dominance patterns and epistatic interactions (Saavedra-Rodriguez et al. 2008; González et al. 2015; Conlon et al. 2018).

The E locus is situated on linkage group (LG) 5 (genome version 2.4: Routtu et al. 2014) and appears as a large region of 3.1 Mb (Fig. 1.4). In this regard, the E locus is similar to the ABC cluster, a well-characterized, non-recombining and extremely divergent region on LG 3 (Bento et al. 2017). Non-recombining genomic structures, i.e. supergenes, are suggested to facilitate adaptation via association of advantageous alleles in host–parasite coevolution (Joron et al. 2011; Llaurens et al. 2017). Such large, diverse genomic regions are difficult to study because the absence of recombination hampers fine mapping (Bento et al. 2017). Therefore, we do not know where the actual resistance loci lie within the ABC- and E-loci regions. This may also explain why our genetic markers are not perfectly linked to the resistance loci (Supplementary Tables S1.17 and S1.18). Supergenes may also harbor several resistance loci, thus variation at the C or the E locus could actually represent variation at several loci physically very close to each other. Within the E-locus region, we find four sugar transferases. Glycosylation genes are candidates to explain variation of resistance in this system (Bento et al. 2017; Bourgeois et al. 2017).

In the *D. magna–P. ramosa* system, the ABC cluster has been shown to play a major role in host resistance and the evolutionary dynamics of resistance (Routtu and Ebert 2015; Bento et al. 2017; Bourgeois et al. 2017). Our results confirm the role of this cluster in a natural population and describe a new resistance region in the *D. magna* genome that is polymorphic in the Aegelsee population. Multi-locus polymorphisms have been shown to underlie parasite resistance in hostparasite coevolution (Sasaki 2000; Tellier and Brown 2007; Cerqueira et al. 2017). In the Aegelsee *D. magna* population, there seems to be no variation at the A locus and little variation at the B locus. The observed variation at the B and C loci is consistent with the genetic model of resistance at the ABC cluster described in Metzger et al. (2016). Also, resistance to *P. ramosa* isolate P15 (influenced by the D locus, (Bento et al. 2020) remains fairly consistent, with the vast majority

of animals being susceptible to P15 (Fig. 1.1). Resistance to *P. ramosa* P21, also isolated from our study population, varies only towards the end of the summer epidemic (Chapter 2). In summary, the ability to resist P20 plays a major role in the early epidemics and most resistotype diversity we measured in the Aegelsee *D. magna* population is well explained by genotypic variation at these loci. As we use more parasite isolates in further research, we might find other resistance regions in the *D. magna* genome. This is likely to be of importance in the later phase of the epidemics in the Aegelsee population.

Resistance segregation in *D. magna* is currently best explained by a genetic model where each locus contains just two alleles. This model was compiled by studies that used either mapping panels created from a few *D. magna* genotypes or, as here, host genotypes from one focal population. Additional resistance alleles may be revealed instead of new resistance regions if we test the genetic model on a larger panel of host and parasite genotypes.

We created 22 F1 offspring groups from the three common resistotypes in our study population. Segregation of resistance phenotypes and genotypes among the selfed F1 strongly supported the genetic model of resistance, consisting of the C and E loci, each with two alleles, and their epistatic interaction, produced by the GWAS (Tables 1.1 and 1.2; Supplementary Tables S1.4 to S1.15). Two F1 offspring groups showed rare variation at the B locus, suggesting yet an additional epistatic interaction in this model besides the previously described role of the B locus for the *P. ramosa* C1 and C19 resistotypes. This consisted of the "bbcc" genotype that causes susceptibility to P20, irrespective of the genotype at the E locus (Fig. 1.5). However, this modified model needs to be further investigated and verified with more genetic crosses.

Conclusion

In this study, we demonstrate rapid parasite-mediated selection in a natural plankton population. We find the genomic regions associated with resistance under selection and describe their mode of inheritance. This knowledge will allow us to conduct direct measurements of resistance allele frequency changes over time and to test theories on the dynamics of host and parasite coevolution, for example by tracing genetic changes in the resting stages of *Daphnia magna* derived from the layered sediments in ponds and lakes (Decaestecker et al. 2007). Pinpointing resistance loci can also be used to infer mechanisms of selection in the host with the molecular evolution tool box (Charlesworth 2006; Fijarczyk and Babik 2015; Hahn 2018). Our model of resistance consists of a few loci linked with epistasis and different dominance patterns, characteristics that have been shown to be relevant in coevolution, in particular when balancing selection maintains diversity at resistance genes (Tellier and Brown 2007; Engelstädter 2015; Conlon et al. 2018). The genomic regions we pinpoint can now be further studied, e.g. by testing for genomic signatures for balancing selection (Charlesworth 2006; Ebert and Fields 2020). Hence, a precise knowledge of the genetic architecture of resistance opens the door to addressing

wider evolutionary questions. For example, the Red Queen theory states that host–parasite interactions may explain the ubiquity of sex and recombination (Salathé et al. 2008).

Materials and methods

Study site

Our study site is the Aegelsee, a pond near Frauenfeld, Switzerland (code: CH-H for Hohliberg; coordinates: 47.557769 N, 8.862783 E, about 30000 m^2 surface area) where *D. magna* is estimated to have a census population size over ten million individuals and an overwintering resting egg bank of about the same size. Every year from early October, the pond is used as a waste repository by a sugar factory: they progressively lower the water level from May to September and from October, warm ammoniacal condensation water is released into the pond, warming the water temporarily to 40–60 °C (Seefeldt and Ebert 2019) and killing all zooplankton, but not the resting eggs. In winter the pond usually freezes over, and in April, *Daphnia* and other invertebrates hatch from resting eggs. We sampled the pond in February 2014 and March 2015 and did not find *D. magna*, suggesting little or no overwintering. Besides *D. magna*, the plankton community includes *D. pulex*, *D. curvirostis* and a diverse array of other invertebrates, among them copepods, ostracods, rotifers and corixids. The waste water treatment prevents fish from invading the pond. The *D. magna* population experiences strong yearly epidemics of *P. ramosa*, reaching prevalence of 70–95%. Infections by other parasites were only rarely observed. The other *Daphnia* species in the pond were never observed to be infected by *P. ramosa*.

Temporal monitoring

In 2014 and 2015, we sampled the host population every two to three weeks from early April to early October to study the impact of the pathogen epidemics. For each sampling date, we aimed to obtain about 100 cloned host lines (produced as iso-female lines). To achieve this, we randomly took about 200–300 female *D. magna* from the sample, placed them in 80-mL jars filled with ADaM (Artificial *Daphnia* Medium, Klüttgen et al. 1994, as modified by Ebert 1998) and let them reproduce asexually. Oversampling was necessary during the hot summer months, as many animals would die for unknown reasons within 48 hours under laboratory conditions. This mortality was, to the best of our knowledge, not disease related. Over the following three weeks, we screened animals for *P. ramosa* infections by checking for the typical signs of disease: gigantism, reddish-brownish opaque body coloration and empty brood pouch. Infected animals that had not yet reproduced asexually were treated with tetracycline (50 $mg.L^{-1}$) (an antibiotic which kills Gram-positive bacteria) until an asexual clutch was observed, usually after about two weeks. They were fed 25 million cells of the unicellular green algae *Scenedesmus* sp. three times a week, and the medium was renewed every two weeks. Feeding and fresh medium protocols were adapted according to the size and number of animals in a jar when necessary.

Resistotype assessment: the attachment test

We assessed resistance phenotype (resistotype) for all cloned hosts using four *P. ramosa* isolates (C1, C19, P15 and P20). We isolated the parasite, P20, from our study population at the start of the epidemic on 13 May 2011 and subsequently passaged it three times through a susceptible *D. magna* host clone from the same population. The three other *P. ramosa* clones or isolates had been previously established in the laboratory: C1 (clone), originated from a *D. magna* population in Russia (Moscow), C19 (clone) from Germany (Gaarzerfeld) and P15 (isolate) from Belgium (Heverlee) (Luijckx et al. 2011; Bento et al. 2020). We used these three *P. ramosa* allopatric isolates in the present study to implement our working genetic model for resistance (Luijckx et al. 2012; Luijckx et al. 2013; Metzger et al. 2016). Parasite transmission stage (= spore) production in the laboratory followed the protocol by Luijckx et al. (2011).

The resistotypes of *D. magna* clones were assessed using a spore attachment test (Duneau et al. 2011). Bacterial spores attach to the foregut or the hindgut of susceptible host clones. Attachment is a prerequisite for subsequent infection. We call these genotypes susceptible, otherwise they are considered resistant. A genotype allowing attachment and penetration of the parasite into the host, may sometimes still resist infection, based on subsequent immune defence (Hall et al. 2019). To test for attachment, we exposed each individual *Daphnia* to 8000 (C1, C19) or 10000 (P15, P20) fluorescently labelled spores following the protocol of Duneau et al. (2011). We used higher spore doses for P15 and P20 because previous observations had shown that fewer of these isolate spores attach to the host oesophagus, resulting in a weaker fluorescent signal. Three repeats were used for C1, C19 and P15, whereas six to nine repeats were used for P20. A clone was considered susceptible to the bacterial isolate when more than half of its replicates showed clear attachment. Its overall resistotype is the combination of its resistotypes to the four individual *P. ramosa* isolates in the following order: C1, C19, P15 and P20, e.g. a clone susceptible to all four isolates would have resistotype SSSS. Since resistance to P15 had low variability in our study population, this isolate was only considered in the first experiment presented here and was otherwise represented with the placeholder "_", e.g. "RR_R resistotype".

Experimental infections of resistotypes

As an initial assessment of the parasite's fitness impact on the host population, we conducted experimental infections on a representative sample of the spring 2014 host population. We collected surface sediment from five different points in the pond in February 2014, before onset of the natural hatching season and placed one hundred *D. magna* ephippia from each replicate in 80-L containers with 30 L ADaM. The five containers were placed outdoors under direct sunlight and checked for hatchlings every two days. We recorded hatching dates and cloned hatchlings in the laboratory where we then scored their resistotypes. For the infection experiment, we used parasites collected from the ongoing epidemic in the pond. We collected three pools of 20 randomly chosen infected individuals during the first

phase of the epidemic in early June 2014. These field-infected animals were kept in the laboratory under ad libitum feeding conditions. Shortly before their expected death, we pooled all 60 animals, homogenized them to produce a spore suspension and froze it at -20 °C. A placebo suspension was produced from 60 homogenized uninfected *D. magna*. The parasite spore mixture was not passaged before we used it, so, in contrast to the isolates used for the attachment test, it represents a population sample of the parasite.

Among the four predominant resistotypes we observed in the cloned cohort of spring hatchlings (SSSS, RRSS, RRSR and RRRR), we used 20 clones each from the more common resistotypes SSSS, RRSS and RRSR and ten of the less common resistotype RRRR for an infection experiment, due to limited availability. From each of these 70 clones, we produced five replicate lines, and these 350 lines were maintained individually in 80-mL jars. To reduce maternal effects before the experiment, we kept all lines for three generations in the same experimental conditions: 20 °C, 16:8 light:dark cycle, ADaM medium and daily ad libitum feeding of 8 million *Scenedesmus* sp. cells per jar. The three generations were produced as follows: as soon as a female produced a clutch, she was discarded and the offspring were kept. When these offspring were mature, a single female was kept in the jar until she in turn produced a clutch. The medium was changed every four days or when the females released offspring. We exposed two- to three-day old juveniles from all replicates to the parasite spore suspension by placing individual *D. magna* in 10 mL of medium with 10000 spores. Additionally, three controls from the third-generation offspring were randomly taken from among the five replicates for each clone (n = 210) and were exposed to the equivalent volume of placebo suspension. Three days after exposure, the jars were filled to 80 mL. Medium was changed after ten days, and then every four days until the end of the experiment. Jars were monitored daily for 35 days. We recorded infection occurrence, clutch number, and time when visible signs of infection were observed. Controls did not get infected and produced offspring at regular intervals.

We tested both the effect of the full resistotype and of the P20 resistotype only on the three dependent variables: infection (binary: 1/0), clutch number (integer) and time of infection (continuous). Replicates were nested within clones, which were nested within resistotypes. We fitted general linear models using binomial data family type for infection and quasi-Poisson for clutch number and time to infection. For clutch size and time to infection, only data on infected individuals was used.

Infection phenotypes of field-collected hosts

As a second assessment of the impact of the local parasite on the host population, we measured fitness traits of animals caught during the epidemics. Because the infection experiment described above (carried out in the previous year) indicated that P20 played a strong role, we focused on this parasite isolate. On June 7 and 28, 2015, we collected large *D. magna* samples from our study site and measured body length, from the top of the head through the eye to the base of the tail spine. We kept all females (n =

331) individually under ad libitum feeding conditions, each in about 80 mL medium. We recorded clutches (time and size) and the onset time of disease symptoms over the following three weeks. After parasitic castration was evident, we cured animals with tetracycline. These data have also been reported in a paper describing the disease phenotype under natural conditions (Savola and Ebert 2019). The current dataset is however smaller than the published data, as we report here only those animals for which we were able to score the resistotypes.

Using generalized linear models, we tested the effect of the P20 resistotype on infection and fecundity, taking body size into account. Sampling date was included as a fixed effect since there are only two sampling dates. Interaction terms were excluded from the model when not significant ($p > 0.1$). We fitted a general linear model using quasibinomial data family type for infection, and a negative binomial generalized linear model for total fecundity (R packages used: MASS: Venables and Ripley 2002, lme4: Bates et al. 2015).

Genome-wide association study

Because our experiments revealed that resistance to P20 plays a major role in the disease dynamics in both laboratory experiments and the field, we used a genome-wide association approach to investigate the genetic architecture of resistance with 37 clones that presented the three most common resistotypes in our study population, excluding P15 resistotype (n = 16 RR_R, 10 RR_S and 11 SS_S). All 37 clones were derived directly from our study population (Supplementary Table S1.3).

Whole-genome DNA extraction, sequencing and bioinformatics

To remove microbial DNA, individuals were treated for 72 h with three antibiotics (streptomycin, tetracycline, ampicillin at a concentration of 50 $mg.L^{-1}$ each in filtered water) and fed twice daily with 200 µL of a dextran bead solution (Sephadex G-25 Superfine by Sigma Aldrich: 20–50 µm diameter at a concentration of 5 $g.L^{-1}$) to remove algae from the gut. DNA was extracted from 15-20 adult animals using an isopropanol precipitation protocol (QIAGEN DNeasy Blood & Tissue Kit). Paired-end 125-cycle sequencing was performed on an Illumina HiSeq 2000.

Raw reads were aligned using BWA MEM (Li and Durbin 2009) on the *Daphnia magna* draft genome (v. 2.4) and a genetic map (Routtu et al. 2014). BAM alignment files were then filtered for quality, and PCR duplicates were removed using PICARD tools (http://broadinstitute.github.io/picard/). Variant calling was performed using freebayes (v. 0.9.15-1). VCF files were then filtered using VCFTOOLS v. 0.1.12b (Danecek et al. 2011) to include SNPs with a minimum quality of 20, a minimum genotype quality of 30, and a mean sequencing depth between 10X and 50X. Only SNPs that passed filters in every clone sample were included in subsequent analyses, resulting in a dataset of 510,087 SNPs. Association analyses were performed using the command "-assoc" in PLINK (Purcell et al. 2007), which compares allele counts between cases and controls and outputs a p-value from a chi-square test with one degree of freedom. Five pairwise compar-

isons were performed to identify possible candidates for resistance to C1, C19 and P20: (i) SS_ _ vs. RR_ _, (ii) SS_S vs. RR_S, (iii) _ _ _S vs. _ _ _R, (iv) RR_S vs. RR_R and (v) SS_S vs. RR_R. We corrected for the genomic inflation of p-values (λ) that may have resulted from relatedness between samples using the R package GenABEL (Aulchenko et al. 2007). Lambda was calculated excluding SNPs from linkage groups 3 and 5, since these scaffolds displayed an excess of strongly associated markers. We divided raw chi-square scores by λ to obtain corrected p-values using R commands "pchisq" and "estlambda". For each SNP:

$$P_{corrected} = P_{\chi 2}\left(\frac{\chi 2}{\lambda(\chi 2_{LG\neq 3\&5})}\right) \qquad \text{(Eq. 1.1)}$$

Histograms of corrected p-values were examined to confirm their uniform distribution. We estimated the minimum false discovery rate incurred when a given p-value was identified as significant (so-called q-value) from the set of corrected p-values using the R package "qvalue" (Storey et al. 2015).

$$Q = qvalue(P_{corrected}) \qquad \text{(Eq. 1.2)}$$

The minimum significant threshold for a given association was then calculated as the maximum corrected p-value with a q-value less than 5%.

$$P_{lim} = \max(P_{Q<0.05}) \qquad \text{(Eq. 1.3)}$$

The "gg.manhattan" function in R was used to display manhattan plots of the comparisons between different resistotypes (https://github.com/timknut/gg.manhattan/). We used BEDTOOLS (v 2.25.0) to extract genes found in the associated candidate regions, using the 2011 annotation of the genome (available at: wfleabase.org).

Assessment of resistotype segregation

The genetic model that resulted from the GWAS analysis allowed us to make predictions about the segregation of resistotypes in sexually reproducing *D. magna* lines. To test these predictions, we selfed *D. magna* clones with different resistotypes. Selfing is possible with *D. magna* because the same clonal line can produce sons (asexual production) as well as eggs by sexual production. The latter need fertilization by males. The resulting sexual eggs must undergo an obligatory resting phase before they can hatch (Ślusarczyk et al. 2019). The resistotypes of the selfed offspring (F1) were examined to assess whether their segregation matched expectations from the genetic model derived from the GWAS.

All clones used for the genetic crosses derived from the study population. We selfed five to ten *D. magna* clones of the three common resistotypes (RR_R, RR_S and SS_S) and two clones of a rare resistotype (SR_S), fol-

lowing the protocol from (Luijckx et al. 2012). Hatching of selfed offspring is not always successful, resulting in uneven sample sizes. We obtained between 19 to 89 selfed offspring from each of 22 parent clones (Supplementary Table S1.19). Their resistotypes were assessed with the attachment test. Samples from each clonal line were stored at -20 °C for future DNA extraction and genotyping.

Predictions of segregation patterns

We compared the resistotype segregation patterns in the selfed offspring to predictions in our genetic model. To calculate proportions of expected phenotypes, we developed an R package called "peas" (https://github.com/JanEngelstaedter/peas) that enables the user to predict distributions of offspring genotypes and phenotypes in complex genetic models with Mendelian inheritance (Supplementary Documents S1.1 and S1.2). We compared these predictions to the segregation patterns from our selfed offspring using the Cochran-Mantel-Haenszel (C-M-H) test for repeated tests of independence. The C-M-H test is applied either to 2x2 tables and outputs a Chi-square statistic (χ^2) or to larger tables (generalized C-M-H test), where it outputs a M^2 statistic. When there was only one repeat per parent genotype, we used the Fisher test. When there was only one category of expected and observed phenotype (i.e. no segregation), no test was possible, and expectation and observation showed a perfect match. Following each C-M-H test, assumption of homogeneity of the odds ratio across repeats was confirmed using a Breslow-Day test (R package DescTools: Signorell et al. 2018). However, this test can only be used with 2x2 tables. We ran a Fisher test of independence on each comparison (expected vs. observed for each repeat, Bonferroni corrected) to detect differences in opposite directions across repeats, which would have resulted in a non-significant C-M-H test, but no such differences in direction were detected (see Supplementary Table S1.15 for detailed results of statistical analyses). Tests were run on counts, but for better illustration we present here segregation of offspring as proportions.

Linking the phenotype to the genotype

We designed PCR-based diagnostic markers physically linked to the resistance loci that the GWAS identified (DMPR1 to 4 for "*Daphnia magna–Pasteuria ramosa*" markers, Supplementary Table S1.20) and tested if these markers (and their corresponding resistance regions) are indeed associated with the resistotypes, by comparing expected and observed association between marker genotypes and resistotypes (Supplementary Tables S1.16 to S1.18). We then used these markers to confirm genotyping of the selfed parents.

DNA extraction and PCR-based markers analysis

DNA of parents and selfed offspring was extracted on 96-well PCR plates using a 10-% Chelex bead solution (Bio-Rad) adapted from Walsh et al. (1991). First, individuals were crushed in the wells with 20 µL of deionized water using a customized rack of metallic pestles. We added 150 µL of 10-% Chelex solution and 10 µL of proteinase K and incubated samples

for two hours at 55 °C followed by 10 min at 99 °C. Fragment amplification, genotyping and allele scoring was done following the protocol described in Cabalzar et al. (2019) (see Supplementary Table S1.21, for PCR reaction details).

Statistical software

Unless otherwise stated, all statistical analyses and graphics were performed using R software version 3.6.1 (R Core Team 2021). Graphics were edited in Inkscape v. 1.0.1 (https://inkscape.org/). Mean values are presented with standard error: mean ± se (Package RVAideMemoire v. 09-45-2, Hervé 2015). Packages used in R for package installation, data manipulation and graphics are the following: package development, documentation and installation: devtools v. 2.2.1 (Wickham, Hester, et al. 2019) and roxygen2 v. 6.1.1 (Wickham et al. 2018), data manipulation: dplyr v. 0.8.3 (Wickham, François, et al. 2019), tidyr v. 1.0.0 (Wickham and Henry 2019), tidyquant v. 0.5.8 (Dancho and Vaughan 2019), tidyverse v. 1.2.1 (Wickham 2017), xlsx v. 0.6.1 (Dragulescu and Arendt 2018), graphics: ggplot2 v. 3.3.0 (Wickham 2016), extrafont v. 0.17 (Chang 2014), scales v. 1.0.0 (Wickham 2018), cowplot v. 1.0.0 (Wilke 2019), gridExtra v. 2.3 (Auguie 2017), ggpubr v. 0.2.3 (Kassambara 2019), ggplotify v. 0.0.4 (Yu 2019), magick v. 2.2 (Ooms 2019), egg v. 0.4.5 (Auguie 2019), ggsci v. 2.9 (Xiao 2018) and png v. 0.1-7 (Urbanek 2013).

Acknowledgments

We thank Jürgen Hottinger, Urs Stiefel, Kristina Müller, Michelle Krebs, Samuel Pichon, Dita Vizoso and Jelena Rakov for help in the field and laboratory. Sequencing for the GWAS analysis was performed at the Genomics Facility at the Department of Biosystem Science and Engineering (D-BSSE, ETH) in Basel. The AB3130xl sequencer used for the markers analysis was operated by Nicolas Boileau. Members of the Ebert group, Jonathon Stillman and Luís Teixeira provided valuable feedback on the study and the manuscript. Suzanne Zweizig improved the language of the manuscript. This work was supported by the Swiss National Science Foundation (SNSF) (grant number 310030B_166677 to DE); the Freiwillige Akademische Gesellschaft Basel (FAG) to CA; the University of Basel to DE and CA and the Australian Research Council through a Future Fellowship (FT140100907 to JE).

Authors contribution

DE and JA designed the overall study. FV and DE designed the infection experiment. FV conducted the infection experiment and analyzed the data. ES and DE designed the fitness measurements. ES conducted the fitness measurements and analyzed the data. YB and DE designed the GWAS analysis. YB conducted the GWAS analysis. CA and DE designed the crossings. CA conducted the crossings and analyzed the data. JE developed the “peas” R package. CA analyzed the data, wrote the manuscript and designed the figures. All authors reviewed the manuscript.

References

Alves JM, Carneiro M, Cheng JY, Lemos de Matos A, Rahman MM, Loog L, Campos PF, Wales N, Eriksson A, Manica A, et al. 2019. Parallel adaptation of rabbit populations to myxoma virus. *Science* **363**:1319–1326.

Andras JP, Ebert D. 2013. A novel approach to parasite population genetics: Experimental infection reveals geographic differentiation, recombination and host-mediated population structure in *Pasteuria ramosa*, a bacterial parasite of *Daphnia*. *Molecular Ecology* **22**:972–986.

Andras JP, Fields PD, Du Pasquier L, Fredericksen M, Ebert D. 2020. Genome-wide association analysis identifies a genetic basis of infectivity in a model bacterial pathogen. *Molecular Biology and Evolution* **37**:3439–3452.

Auguie B. 2017. gridExtra: Miscellaneous functions for "Grid" graphics. Available from: https://CRAN.R-project.org/package=gridExtra

Auguie B. 2019. egg: Extensions for "ggplot2": Custom geom, custom themes, plot alignment, labelled panels, symmetric scales, and fixed panel size. Available from: https://CRAN.R-project.org/package=egg

Aulchenko YS, Ripke S, Isaacs A, van Duijn CM. 2007. GenABEL: an R library for genome-wide association analysis. *Bioinformatics* **23**:1294–1296.

Bangham J, Knott SA, Kim K-W, Young RS, Jiggins FM. 2008. Genetic variation affecting host–parasite interactions: major-effect quantitative trait loci affect the transmission of sigma virus in *Drosophila melanogaster*. *Molecular Ecology* **17**:3800–3807.

Bates D, Maechler M, Bolker B, Walker S. 2015. Fitting linear mixed-effects models using lme4. *Journal of statistical software* **67**:1–48.

Ben-Ami F. 2019. Host age effects in invertebrates: epidemiological, ecological, and evolutionary implications. *Trends in Parasitology* **35**:466–480.

Bento G, Fields PD, Duneau D, Ebert D. 2020. An alternative route of bacterial infection associated with a novel resistance locus in the *Daphnia–Pasteuria* host–parasite system. *Heredity* **125**:173–183.

Bento G, Routtu J, Fields PD, Bourgeois Y, Du Pasquier L, Ebert D. 2017. The genetic basis of resistance and matching-allele interactions of a host–parasite system: The *Daphnia magna–Pasteuria ramosa* model. *PLOS Genetics* **13**:e1006596.

Bourgeois Y, Roulin AC, Müller K, Ebert D. 2017. Parasitism drives host genome evolution: Insights from the *Pasteuria ramosa–Daphnia magna* system. *Evolution* **71**:1106–1113.

Cabalzar AP, Fields PD, Kato Y, Watanabe H, Ebert D. 2019. Parasite□mediated selection in a natural metapopulation of *Daphnia magna*. *Molecular Ecology* **28**:4770–4785.

Cao C, Magwire MM, Bayer F, Jiggins FM. 2016. A polymorphism in the processing body component Ge-1 controls resistance to a naturally occurring Rhabdovirus in *Drosophila*.Schneider DS, editor. *PLOS Pathogens* **12**:e1005387.

Carton Y, Nappi AJ, Poirie M. 2005. Genetics of anti-parasite resistance in invertebrates. *Developmental & Comparative Immunology* **29**:9–32.

Cerqueira GC, Cheeseman IH, Schaffner SF, Nair S, McDew-White M, Phyo AP, Ashley EA, Melnikov A, Rogov P, Birren BW, et al. 2017. Longitudinal genomic surveillance of *Plasmodium falciparum* malaria parasites reveals complex genomic architecture of emerging artemisinin resistance. *Genome Biology* **18**:1–13.

Chang W. 2014. extrafont: Tools for using fonts. Available from: https://CRAN.R-project.org/package=extrafont

Charlesworth D. 2006. Balancing selection and its effects on sequences in nearby genome regions. *PLoS Genetics* **2**:e64.

Cogni R, Cao C, Day JP, Bridson C, Jiggins FM. 2016. The genetic architecture of resistance to virus infection in *Drosophila*. *Molecular Ecology* **25**:5228–5241.

Conlon BH, Frey E, Rosenkranz P, Locke B, Moritz RFA, Routtu J. 2018. The role of epistatic interactions underpinning resistance to parasitic *Varroa* mites in haploid honey bee (*Apis mellifera*) drones. *Journal of Evolutionary Biology* **31**:801–809.

Connallon T, Chenoweth SF. 2019. Dominance reversals and the maintenance of genetic variation for fitness. *PLOS Biology* **17**:e3000118.

Daborn PJ. 2002. A single P450 allele associated with insecticide resistance in *Drosophila*. *Science* **297**:2253–2256.

Dancho M, Vaughan D. 2019. tidyquant: Tidy quantitative financial analysis. Available from: https://CRAN.R-project.org/package=tidyquant

Danecek P, Auton A, Abecasis G, Albers CA, Banks E, DePristo MA, Handsaker RE, Lunter G, Marth GT, Sherry ST, et al. 2011. The variant call format and VCFtools. *Bioinformatics* **27**:2156–2158.

Decaestecker E, Gaba S, Raeymaekers JAM, Stoks R, Van Kerckhoven L, Ebert D, De Meester L. 2007. Host–parasite 'Red Queen' dynamics archived in pond sediment. *Nature* **450**:870–873.

Dragulescu AA, Arendt C. 2018. xlsx: Read, write, format Excel 2007 and Excel 97/2000/XP/2003 files. Available from: https://CRAN.R-project.org/package=xlsx

Duffy MA, Sivars-Becker L. 2007. Rapid evolution and ecological host–parasite dynamics. *Ecology Letters* **10**:44–53.

Duncan AB, Little TJ. 2007. Parasite-driven genetic change in a natural population of *Daphnia*. *Evolution* **61**:796–803.

Duneau D, Luijckx P, Ben-Ami F, Laforsch C, Ebert D. 2011. Resolving the infection process reveals striking differences in the contribution of environment, genetics and phylogeny to host–parasite interactions. *BMC biology* **9**:1–11.

Ebert D. 1998. Experimental evolution of parasites. *Science* **282**:1432–1436.

Ebert D. 2005. Ecology, epidemiology, and evolution of parasitism in *Daphnia*. Bethesda, MD: National Library of Medicine (US), National Center for Biotechnology Information

Ebert D, Duneau D, Hall MD, Luijckx P, Andras JP, Du Pasquier L, Ben-Ami F. 2016. A population biology perspective on the stepwise infection process of the bacterial pathogen *Pasteuria ramosa* in *Daphnia*. *Advances in Parasitology* **91**:265–310.

Ebert D, Fields PD. 2020. Host–parasite co-evolution and its genomic signature. *Nature Reviews Genetics* **21**:754–768.

Ebert D, Rainey P, Embley TM, Scholz D. 1996. Development, life cycle, ultrastructure and phylogenetic position of *Pasteuria ramosa* Metchnikoff 1888: rediscovery of an obligate endoparasite of *Daphnia magna* Straus. *Philosophical Transactions of the Royal Society B: Biological Sciences* **351**:1689–1701.

Ellegren H, Sheldon BC. 2008. Genetic basis of fitness differences in natural populations. *Nature* **452**:169–175.

Engelstädter J. 2015. Host–parasite coevolutionary dynamics with generalized success/failure infection genetics. *The American Naturalist* **185**:E117–E129.

Engelstädter J, Bonhoeffer S. 2009. Red Queen dynamics with non-standard fitness interactions.Stormo GD, editor. *PLoS Computational Biology* **5**:e1000469.

Feldman MW, Lewontin RC, Franklin IR, Christiansen FB. 1975. Selection in complex genetic systems III. An effect of allele multiplicity with two loci. *Genetics* **79**:333–347.

Fijarczyk A, Babik W. 2015. Detecting balancing selection in genomes: limits and prospects. *Molecular Ecology* **24**:3529–3545.

Galvani AP. 2003. Epidemiology meets evolutionary ecology. *Trends in Ecology*

& Evolution **18**:132–139.

Garbutt JS, O'Donoghue AJP, McTaggart SJ, Wilson PJ, Little TJ. 2014. The development of pathogen resistance in *Daphnia magna*: implications for disease spread in age-structured populations. *Journal of Experimental Biology* **217**:3929–3934.

Gibson AK, Delph LF, Vergara D, Lively CM. 2018. Periodic, parasite-mediated selection for and against sex. *The American Naturalist* **192**:537–551.

Gómez-Gómez L, Felix G, Boller T. 1999. A single locus determines sensitivity to bacterial flagellin in *Arabidopsis thaliana*. *The Plant Journal* **18**:277–284.

González AM, Yuste-Lisbona FJ, Rodiño AP, De Ron AM, Capel C, García-Alcázar M, Lozano R, Santalla M. 2015. Uncovering the genetic architecture of *Colletotrichum lindemuthianum* resistance through QTL mapping and epistatic interaction analysis in common bean. *Frontiers in Plant Science* **6**:1–13.

González-Tortuero E, Rusek J, Turko P, Petrusek A, Maayan I, Piálek L, Tellenbach C, Giessler S, Spaak P, Wolinska J. 2016. *Daphnia* parasite dynamics across multiple *Caullerya* epidemics indicate selection against common parasite genotypes. *Zoology* **119**:314–321.

Hahn MW. 2018. Molecular population genetics. Sinauer Associates. New York: Oxford University Press

Hall MD, Routtu J, Ebert D. 2019. Dissecting the genetic architecture of a stepwise infection process. *Molecular Ecology* **28**:1–16.

Hamilton WD. 1980. Sex versus non-sex versus parasite. *Oikos* **35**:282.

Hamilton WD, Axelrod R, Tanese R. 1990. Sexual reproduction as an adaptation to resist parasites (a review). *Proceedings of the National Academy of Sciences* **87**:3566–3573.

Hervé M. 2015. RVAideMemoire: Diverse basic statistical and graphical functions. Available from: http://CRAN.R-project.org/package=RVAideMemoire

Hoban S, Kelley JL, Lotterhos KE, Antolin MF, Bradburd G, Lowry DB, Poss ML, Reed LK, Storfer A, Whitlock MC. 2016. Finding the genomic basis of local adaptation: Pitfalls, practical solutions, and future directions. *The American Naturalist* **188**:379–397.

van't Hof AE, Campagne P, Rigden DJ, Yung CJ, Lingley J, Quail MA, Hall N, Darby AC, Saccheri IJ. 2016. The industrial melanism mutation in British peppered moths is a transposable element. *Nature* **534**:102–105.

Hooker AL, Saxena KMS. 1971. Genetics of disease resistance in plants. *Annual Review of Genetics* **5**:407–424.

Howard RS, Lively CM. 1998. The maintenance of sex by parasitism and mutation accumulation under epistatic fitness functions. *Evolution* **52**:604–610.

Izhar R, Ben-Ami F. 2015. Host age modulates parasite infectivity, virulence and reproduction.Plaistow S, editor. *Journal of Animal Ecology* **84**:1018–1028.

Jones AG, Bürger R, Arnold SJ. 2014. Epistasis and natural selection shape the mutational architecture of complex traits. *Nature Communications* **5**:1–10.

Joron M, Frezal L, Jones RT, Chamberlain NL, Lee SF, Haag CR, Whibley A, Becuwe M, Baxter SW, Ferguson L, et al. 2011. Chromosomal rearrangements maintain a polymorphic supergene controlling butterfly mimicry. *Nature* **477**:203–206.

Juneja P, Ariani CV, Ho YS, Akorli J, Palmer WJ, Pain A, Jiggins FM. 2015. Exome and transcriptome sequencing of *Aedes aegypti* identifies a locus that confers resistance to *Brugia malayi* and alters the immune response. Besansky NJ, editor. *PLOS Pathogens* **11**:e1004765.

Kassambara A. 2019. ggpubr: "ggplot2" based publication ready plots. Available from: https://CRAN.R-project.org/package=ggpubr

Klüttgen B, Dülmer U, Engels M, Ratte HT. 1994. ADaM, an artificial freshwater for the culture of zooplankton. *Water Research* **28**:743–746.

Koskella B. 2018. Resistance gained, resistance lost: an explanation for host–parasite coexistence. *PLOS Biology* **16**:e3000013.

Kouyos RD, Salathé M, Otto SP, Bonhoeffer S. 2009. The role of epistasis on the evolution of recombination in host–parasite coevolution. *Theoretical Population Biology* **75**:1–13.

Kover PX, Caicedo AL. 2001. The genetic architecture of disease resistance in plants and the maintenance of recombination by parasites. *Molecular Ecology* **10**:1–16.

Kurtz J, Schulenburg H, Reusch TBH. 2016. Host–parasite coevolution—rapid reciprocal adaptation and its genetic basis. *Zoology* **119**:241–243.

Laine A-L. 2009. Role of coevolution in generating biological diversity: spatially divergent selection trajectories. *Journal of Experimental Botany* **60**:2957–2970.

Li C, Cowling W. 2003. Identification of a single dominant allele for resistance to blackleg in *Brassica napus* "Surpass 400." *Plant Breeding* **122**:485–488.

Li H, Durbin R. 2009. Fast and accurate short read alignment with Burrows–Wheeler transform. *Bioinformatics* **25**:1754–1760.

Li W, Zhu Z, Chern M, Yin J, Yang C, Ran L, Cheng M, He M, Wang K, Wang Jing, et al. 2017. A natural allele of a transcription factor in rice confers broad-spectrum blast resistance. *Cell* **170**:114-126.e15.

Little TJ, Ebert D. 1999. Associations between parasitism and host genotype in natural populations of *Daphnia* (Crustacea:Cladocera). *Journal of Animal Ecology* **68**:134–149.

Lively CM. 2010. A review of Red Queen models for the persistence of obligate sexual reproduction. *Journal of Heredity* **101**:S13–S20.

Llaurens V, Whibley A, Joron M. 2017. Genetic architecture and balancing selection: the life and death of differentiated variants. *Molecular Ecology* **26**:2430–2448.

Luijckx P, Ben-Ami F, Mouton L, Du Pasquier L, Ebert D. 2011. Cloning of the unculturable parasite *Pasteuria ramosa* and its *Daphnia* host reveals extreme genotype–genotype interactions. *Ecology Letters* **14**:125–131.

Luijckx P, Fienberg H, Duneau D, Ebert D. 2012. Resistance to a bacterial parasite in the crustacean *Daphnia magna* shows Mendelian segregation with dominance. *Heredity* **108**:547–551.

Luijckx P, Fienberg H, Duneau D, Ebert D. 2013. A matching-allele model explains host resistance to parasites. *Current Biology* **23**:1085–1088.

Magalhães S, Sucena É. 2016. Genetics of host–parasite interactions: towards a comprehensive dissection of *Drosophila* resistance to viral infection. *Molecular Ecology* **25**:4981–4983.

Magwire MM, Fabian DK, Schweyen H, Cao C, Longdon B, Bayer F, Jiggins FM. 2012. Genome-wide association studies reveal a simple genetic basis of resistance to naturally coevolving viruses in *Drosophila melanogaster*. *PLoS Genetics* **8**:e1003057.

Metzger CMJA, Luijckx P, Bento G, Mariadassou M, Ebert D. 2016. The Red Queen lives: Epistasis between linked resistance loci. *Evolution* **70**:480–487.

Mitchell SE, Read AF, Little TJ. 2004. The effect of a pathogen epidemic on the genetic structure and reproductive strategy of the crustacean *Daphnia magna*. *Ecology Letters* **7**:848–858.

Morgan AD, Koskella B. 2017. Coevolution of host and pathogen. In: Tibayrenc M, editor. Genetics and evolution of infectious diseases (Second edition). Elsevier. Sara Tenney. p. 115–140.

Ooms J. 2019. magick: Advanced graphics and image-processing in R. Available from: https://CRAN.R-project.org/package=magick

Otto SP. 2009. The evolutionary enigma of sex. *The American Naturalist* **174**:S1–S14.

Pilet-Nayel M-L, Moury B, Caffier V, Montarry J, Kerlan M-C, Fournet S, Durel

C-E, Delourme R. 2017. Quantitative resistance to plant pathogens in pyramiding strategies for durable crop protection. *Frontiers in Plant Science* **8**:1838.

Purcell S, Neale B, Todd-Brown K, Thomas L, Ferreira MAR, Bender D, Maller J, Sklar P, de Bakker PIW, Daly MJ, et al. 2007. PLINK: A tool set for whole-genome association and population-based linkage analyses. *The American Journal of Human Genetics* **81**:559–575.

R Core Team. 2021. R: A language and environment for statistical computing. R Foundation for Statistical Computing, Vienna, Austria. Available from: http://www.R-project.org

Rogalski MA, Duffy MA. 2020. Local adaptation of a parasite to solar radiation impacts disease transmission potential, spore yield, and host fecundity. *Evolution* **74**:1856–1864.

Routtu J, Ebert D. 2015. Genetic architecture of resistance in *Daphnia* hosts against two species of host-specific parasites. *Heredity* **114**:241–248.

Routtu J, Hall MD, Albere B, Beisel C, Bergeron RD, Chaturvedi A, Choi J-H, Colbourne J, De Meester L, Stephens MT, et al. 2014. An SNP-based second-generation genetic map of *Daphnia magna* and its application to QTL analysis of phenotypic traits. *BMC genomics* **15**:1–15.

Saavedra-Rodriguez K, Strode C, Flores Suarez A, Fernandez Salas I, Ranson H, Hemingway J, Black WC. 2008. Quantitative trait loci mapping of genome regions controlling permethrin resistance in the mosquito *Aedes aegypti*. *Genetics* **180**:1137–1152.

Salathé M, Kouyos R, Bonhoeffer S. 2008. The state of affairs in the kingdom of the Red Queen. *Trends in Ecology & Evolution* **23**:439–445.

Samson M, Libert F, Doranz BJ, Rucker J, Liesnard C, Farber C-M, Saragosti S, Lapouméroulie C, Cognaux J, Forceille C, et al. 1996. Resistance to HIV-1 infection in Caucasian individuals bearing mutant alleles of the CCR-5 chemokine receptor gene. *Nature* **382**:722–725.

Sasaki A. 2000. Host–parasite coevolution in a multilocus gene-for-gene system. *Proceedings of the Royal Society B: Biological Sciences* **267**:2183–2188.

Savola E, Ebert D. 2019. Assessment of parasite virulence in a natural population of a planktonic crustacean. *BMC Ecology* **19**:14.

Schlesinger KJ, Stromberg SP, Carlson JM. 2014. Coevolutionary immune system dynamics driving pathogen speciation.Whitaker RJ, editor. *PLoS ONE* **9**:e102821.

Schmid-Hempel P. 2011. Evolutionary parasitology. The integrated study of infections, immunology, ecology, and genetics. New York: Oxford University Press

Seefeldt L, Ebert D. 2019. Temperature- versus precipitation-limitation shape local temperature tolerance in a Holarctic freshwater crustacean. *Proceedings of the Royal Society B: Biological Sciences* **286**:20190929.

Shocket MS, Vergara D, Sickbert AJ, Walsman JM, Strauss AT, Hite JL, Duffy MA, Cáceres CE, Hall SR. 2018. Parasite rearing and infection temperatures jointly influence disease transmission and shape seasonality of epidemics. *Ecology* **99**:1975–1987.

Signorell A et al. 2018. DescTools: Tools for descriptive statistics. R package version 0.99.26.

Ślusarczyk M, Chlebicki W, Pijanowska J, Radzikowski J. 2019. The role of the refractory period in diapause length determination in a freshwater crustacean. *Scientific Reports* **9**:11905.

Storey J, Bass A, Dabney A, Robinson D. 2015. qvalue: Q-value estimation for false discovery rate control. Available from: http://github.com/jdstorey/qvalue

Strauss AT, Hite JL, Shocket MS, Cáceres CE, Duffy MA, Hall SR. 2017. Rapid evolution rescues hosts from competition and disease but—despite a dilution effect—increases the density of infected hosts. *Proceedings of the Royal Society B: Biological Sciences* **284**:20171970.

Tellier A, Brown JKM. 2007. Polymorphism in multilocus host–parasite coevolutionary interactions. *Genetics* **177**:1777–1790.

Turko P, Tellenbach C, Keller E, Tardent N, Keller B, Spaak P, Wolinska J. 2018. Parasites driving host diversity: incidence of disease correlated with *Daphnia* clonal turnover. *Evolution* **72**:619–629.

Urbanek S. 2013. png: Read and write PNG images. Available from: https://CRAN.R-project.org/package=png

Vale PF, Wilson AJ, Best A, Boots M, Little TJ. 2011. Epidemiological, evolutionary, and coevolutionary implications of context-dependent parasitism. *The American Naturalist* **177**:510–521.

Venables WN, Ripley BD. 2002. Modern applied statistics with S. Fourth edition. New York: Springer

Walsh PS, Metzger DA, Higuchi R. 1991. Chelex 100 as a medium for simple extraction of DNA for PCR-based typing from forensic material. *Biotechniques* **10**:506–513.

Whitlock MC, Lotterhos KE. 2015. Reliable detection of loci responsible for local adaptation: Inference of a null model through trimming the distribution of F_{ST}. *The American Naturalist* **186**:S24–S36.

Wickham H. 2016. ggplot2: Elegant graphics for data analysis. New York: Springer-Verlag

Wickham H. 2017. tidyverse: Easily install and load the "Tidyverse." Available from: https://CRAN.R-project.org/package=tidyverse

Wickham H. 2018. scales: Scale functions for visualization. Available from: https://CRAN.R-project.org/package=scales

Wickham H, Danenberg P, Eugster D. 2018. roxygen2: In-line documentation for R. Available from: https://CRAN.R-project.org/package=roxygen2

Wickham H, François R, Henry L, Müller K. 2019. dplyr: A grammar of data manipulation. Available from: https://CRAN.R-project.org/package=dplyr

Wickham H, Henry L. 2019. tidyr: Tidy messy data. Available from: https://CRAN.R-project.org/package=tidyr

Wickham H, Hester J, Chang W. 2019. devtools: Tools to make developing R packages easier. Available from: https://CRAN.R-project.org/package=devtools

Wilfert L, Schmid-Hempel P. 2008. The genetic architecture of susceptibility to parasites. *BMC Evolutionary Biology* **8**:187.

Wilke CO. 2019. cowplot: Streamlined plot theme and plot annotations for "ggplot2." Available from: https://CRAN.R-project.org/package=cowplot

Wittmann MJ, Bergland AO, Feldman MW, Schmidt PS, Petrov DA. 2017. Seasonally fluctuating selection can maintain polymorphism at many loci via segregation lift. *Proceedings of the National Academy of Sciences* **114**:E9932–E9941.

Xiao N. 2018. ggsci: Scientific journal and sci-fi themed color palettes for "ggplot2." Available from: https://CRAN.R-project.org/package=ggsci

Xiao Y, Dai Q, Hu R, Pacheco S, Yang Y, Liang G, Soberón M, Bravo A, Liu K, Wu K. 2017. A single point mutation resulting in cadherin mislocalization underpins resistance against *Bacillus thuringiensis* toxin in cotton bollworm. *Journal of Biological Chemistry* **292**:2933–2943.

Yu G. 2019. ggplotify: Convert plot to "grob" or "ggplot" object. Available from: https://CRAN.R-project.org/package=ggplotify

CHAPTER 2

Genetic slippage after sex maintains diversity for parasite resistance in a natural host population

AMELINE C, VÖGTLI F, ANDRAS JP, DEXTER E, ENGELSTÄDTER J, EBERT D. 2021. Genetic slippage after sex maintains diversity for parasite resistance in a natural host population. *bioRxiv*. https://doi.org/10.1101/2021.07.11.451958

Abstract Although parasite-mediated selection is a major driver of host evolution, its influence on genetic variation for parasite resistance is not yet well understood. To gain insight into the temporal dynamics of genetic variation, we monitored resistance in a large population of the planktonic crustacean *Daphnia magna* over eight years, as it underwent yearly epidemics of the bacterial pathogen *Pasteuria ramosa*. We observed cyclic dynamics of resistance: resistance increased throughout the epidemics, but susceptibility was restored each spring when hosts hatched from sexual resting stages. We interpreted this phenomenon to be a result of genetic slippage in response to sex. Host resting stages collected across the year showed that largely resistant host populations can produce susceptible sexual offspring. Resting stages produced throughout the planktonic season accurately represent the hatching population cohort of the following spring. A genetic model of resistance developed for this host–parasite system, based on multiple loci and strong epistasis, is in partial agreement with our findings. Our results reveal that, despite strong selection for resistance in a natural host population, genetic slippage after sexual reproduction can be a strong factor for the maintenance of genetic diversity of host resistance.

Keywords parasite-mediated selection, zooplankton, resistance, resting egg, resting stage, sex, dormancy, genetic model of resistance, *Daphnia magna*, *Pasteuria ramosa*

Introduction

The origin and maintenance of diversity is a major question in evolutionary biology, with the respective roles of selection, mutation, and drift in maintaining genetic diversity in nature still being disputed (Fisher 1930; Fisher 1958; Frank 2013; Kern and Hahn 2018). Parasites, including pathogens, have been suggested as a causal factor for some highly diverse regions in plant and animal genomes. Indeed, the role of selection by parasites is well established for the major histocompatibility (MHC) gene complex in jawed vertebrates and resistance (R) genes in plants (Jeffery and Bangham 2000; Hughes 2002; Radwan et al. 2020), both of which have remarkably high genetic diversity (Sommer 2005; Baggs et al. 2017). In particular, coevolution with parasites is linked to increased host diversity (Wang et al. 2017; Duxbury et al. 2019), and high diversity at resistance genes has been shown to be advantageous against parasites (Sommer 2005; Zhao et al. 2016; Gösser et al. 2019; Peters et al. 2019; White et al. 2020).

As a key mechanism for creating diversity via novel allele combinations, sexual reproduction is a central component of host-parasite coevolution theory (Lively 2010; Morran et al. 2011; Auld et al. 2016). Recombination may allow a host population to create new genotypes to which the common parasites are not yet adapted to, thereby reducing the damage caused by parasites adapted to specific host genotypes. Based on this reasoning, it has been suggested that parasites select for the maintenance of host sexual reproduction as a mechanism to create and maintain beneficial genetic diversity—the Red Queen theory (Jaenike 1978; Bell and Smith 1987; Hamilton et al. 1990; MacPherson and Otto 2018). Coevolution with parasites has indeed been shown to promote sex and outbreeding (Morran et al. 2011; Gibson et al. 2016), and there is empirical evidence of the advantage of sexual over asexual reproduction in natural systems and associated experiments (Tobler and Schlupp 2008; Auld et al. 2016; Gibson et al. 2018). The Red Queen theory posits that parasite interactions make sexual recombination advantageous for hosts as they can produce and benefit from rare allele combinations. Selection should then have the form of time-lagged negative frequency-dependent selection (NFDS) (Hamilton et al. 1990; Salathé et al. 2008; Lively 2010). On the other hand, sexual reproduction may represent a cost for a population that has evolved adaptive resistance to a parasite because it may destroy advantageous allele combinations (Otto and Nuismer 2004; Otto 2009). Models have shown that recombination could indeed be selected against under certain conditions of genetic architecture and selection strength (Engelstädter and Bonhoeffer 2009; Kouyos et al. 2009; Engelstädter 2015).

Coevolution by NFDS was suggested to maintain genetic diversity through balancing selection within and among populations (reviewed in Ebert and Fields 2020). Red Queen dynamics assume specific forms of host–parasite interactions without which polymorphisms at loci under selection would soon disappear (Agrawal and Lively 2002; Otto and Nuismer 2004; Thrall et al. 2016). A major assumption of the specific genetic interaction matrices of Red Queen models is epistasis (i.e. nonadditive gene action) and—for

diploid organisms—dominance. For most host-parasite systems, however, we know little about the link between the genetic architecture of resistance, the effect of selection on resistance, and the role of genetic recombination for the evolution of the system. Empirical work determining resistance to parasites in natural systems has suggested a genetic architecture with few loci, with dominance and epistasis, for most systems (Sasaki 2000; Li and Cowling 2003; Tellier and Brown 2007; Wilfert and Schmid-Hempel 2008; Metzger et al. 2016). Dominance and epistasis are particularly important because they determine the degree to which the mean and variance of phenotypes change after genetic recombination (Otto and Nuismer 2004; Otto 2009). Depending on the form and strength of natural selection and the mode of gene action determining the trait under selection, recombination may impede or enhance the response to selection (Lynch and Deng 1994; Otto 2009). To understand the role of sexual recombination in shaping the evolutionary dynamics of resistance, knowledge of the genetic architecture of resistance is necessary. Here we aim to fill this gap for a cyclic parthenogenetic crustacean that undergoes seasonal epidemics of a virulent bacterial pathogen.

Many organisms in diverse taxa, such as cladocerans, monogonont rotifers, bryozoan, and aphids, reproduce by cyclical parthenogenesis. They produce parthenogenetic eggs directly throughout most of the season, with occasional periods of sexual reproduction that result in resting stages that usually hatch at the beginning of the following season (Decaestecker et al. 2009). In such a reproductive system, selection is expected to increase the mean fitness of the population. After a round of sexual recombination, the mean fitness of the population presumably decreases, a phenomenon known as regression to the mean before selection (Falconer 1981), or genetic slippage in response to sex (Lynch and Deng 1994; Decaestecker et al. 2009). The variance of the trait under selection is also expected to change, although the direction of the change cannot be easily predicted as it depends on the signs of the covariances between genetic effects in the parental generation (Lynch and Deng 1994; Decaestecker et al. 2009). In rotifer populations, variance has been observed to both increase and decrease after sexual reproduction (Becks and Agrawal 2011; Becks and Agrawal 2012). Due to their extended period of asexual reproduction, cyclic parthenogens are good systems to study genetic slippage (Becks and Agrawal 2011). During the asexual phase, selection over time can build up stronger linkage disequilibria among loci and deviations from Hardy-Weinberg equilibrium (Lynch and Deng 1994), making the effect of both selection and recombination on the trait under selection more evident.

We monitored resistance phenotypic changes over eight consecutive years in a large natural population of the crustacean *Daphnia magna*, whose yearly population cycle includes strong summer epidemics of the bacterial parasite *Pasteuria ramosa,* sexual reproduction to survive the winter, and the hatching of sexual resting stages in spring. In a previous study, we documented parasite-mediated selection and resolved parts of the underlying genetic architecture of resistance to the local parasite (Chapter 1, Ameline et al. 2021). Here we reveal genetic slippage created by sexual reproduc-

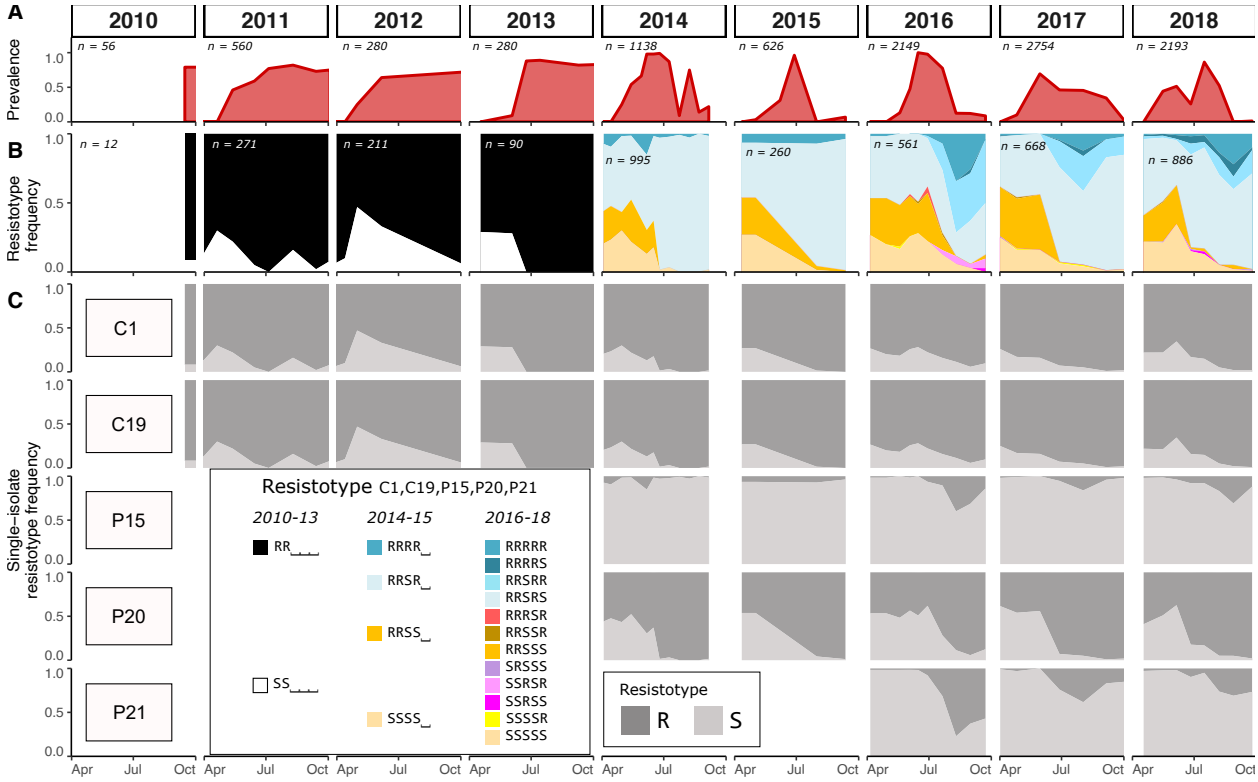

Figure 2.1

Cyclic resistotype dynamics across eight years in the Aegelsee. From 2010 to 2018, samples of *Daphnia magna* were collected from early April to early October every two to four weeks. Parasite prevalence was recorded and about 60 to 100 animals were cloned and their resistotypes (resistance phenotypes) assessed. **A**: *Pasteuria ramosa* prevalence (= proportion of infected females) in the *D. magna* population. **B**: Resistotype frequency in the *D. magna* population. Resistance and susceptibility to individual *P. ramosa* isolates are denoted as R and S, respectively. The combined resistotype shows resistance for up to five *P. ramosa* isolates: C1, C19, P15, P20 and P21. Until 2013 only C1 and C19 were tested; in 2014 and 2015 isolates C1, C19, P15 and P20 were tested; and all five isolates were tested after 2015. We use the placeholder "␣" when an isolate was not tested. Resistance to P20 is pinpointed because of its importance in the evolution of the host population (Chapter 1, Ameline et al. 2021). The "n" denotes the total number of genotypes tested in a given year. **C**: Resistotype frequency to each of the five *P. ramosa* isolates. Note the strong increase in resistance to P20 every year.

tion in this cyclical parthenogen, showing that resistance increases during the yearly parasite epidemics, but that recombination reestablishes the initial resistance diversity in the following planktonic season. We link this long-term monitoring to a system-specific genetic model of resistance that predicts the impact of sexual reproduction on the temporal dynamics of the evolution of resistance. Our data suggest that dominance and epistasis are crucial for explaining the maintenance of genetic diversity for resistance in this host population.

Results

Seasonal epidemics

We monitored a large *Daphnia magna* population in the fishless Lake Aegelsee, Switzerland (Chapter 1, Ameline et al. 2021) from 09.10.2010 to 24.09.2018, observing strong annual epidemics of *Pasteuria ramosa* that typically started in early May, about a month after the host emerged from diapause and lasted through most of the summer (Fig. 2.1A). Epidemics reached peak prevalence of 70% to nearly 100%; no epidemic of any other known *D. magna* parasite was observed in this population. The population overwinters exclusively in the form of sexually produced resting stages,

with an estimated overwintering population size of several millions. We also monitored environmental and ecological variables over the course of our study and present those results in Supplementary Fig. S2.1 and Discussion S2.1.

Resistotype dynamics

Using five isolates of the pathogen *Pasteuria ramosa*, we quantified the proportion of resistant (R) and susceptible (S) host phenotypes in the population with an attachment test that measures the parasite's ability to attach to the host cuticle; failure to attach indicates resistant hosts (Duneau et al. 2011). Because we can clone females using the host's parthenogenetic eggs (iso-female lines), we can perform this test on several individuals with the same genotype. Resistotypes—i.e. resistance phenotypes—are here presented as a sequence of R and S letters, each letter representing resistance or susceptibility to one of the five tested parasite isolates in the following order: C1, C19, P15, P20 and P21. We used the placeholder "␣" for isolates that we did not test or consider.

For eight successive years we observed similar resistotype frequencies in spring (Fig. 2.1B). From 2011 to 2013, when data resolution was lower due to less frequent sampling and smaller sample sizes, the spring cohort was composed of about 25% of the SS␣␣␣ resistotype and 75% of the RR␣␣␣ resistotype (Fig. 2.1B). Two additional *P. ramosa* isolates were added from 2014 and one more from 2016 onwards, allowing for a more refined picture that was dominated by four phenotypes: resistotypes SSSS␣ and RRSS␣ each represented about 25% of the population, RRSR␣ about 45%, and RRRR␣ about 5% (Fig. 2.1B). Overall, R resistotypes were more common for C1, C19 and P20, while S resistotypes were more common for the P15 and P21 parasites (Fig. 2.1C).

Each year, these resistotype frequencies were relatively stable at the beginning of the season, but changed dramatically after the start of the *P. ramosa* epidemic in May. Two resistant phenotypes, namely RRSR␣ and RRRR␣ (blue in Fig. 2.1B, 2014–2018), increased in proportion, while the resistotypes susceptible to P15 and P20—RRSS␣ and SSSS␣—decreased in proportion (orange and yellow in Fig. 2.1B). Overall, resistance to all individual *P. ramosa* strains increased over the season (dark gray in Fig. 2.1C): resistance to C1 and C19 increased every year from 79±2% to 97±1% during the entire six months of the *D. magna* planktonic phase. The biggest change was resistance to P20, which increased from 49±4% to 96±2% within two months during the main peak of the epidemics. Resistance to P15 and P21 showed a more complex pattern, with a tendency to increase during the second half of the summer and decrease again towards the end of the season (Fig. 2.1C).

The stable spring frequencies across years, together with the strong dynamics across the summer season, resulted in a strong pattern of cyclic resistotype frequencies changes. Among about four thousand tested genotypes across eight years, some resistotypes were never observed in our samples, e.g. SS␣R␣ and RS␣␣␣, possibly indicating genetically impossible

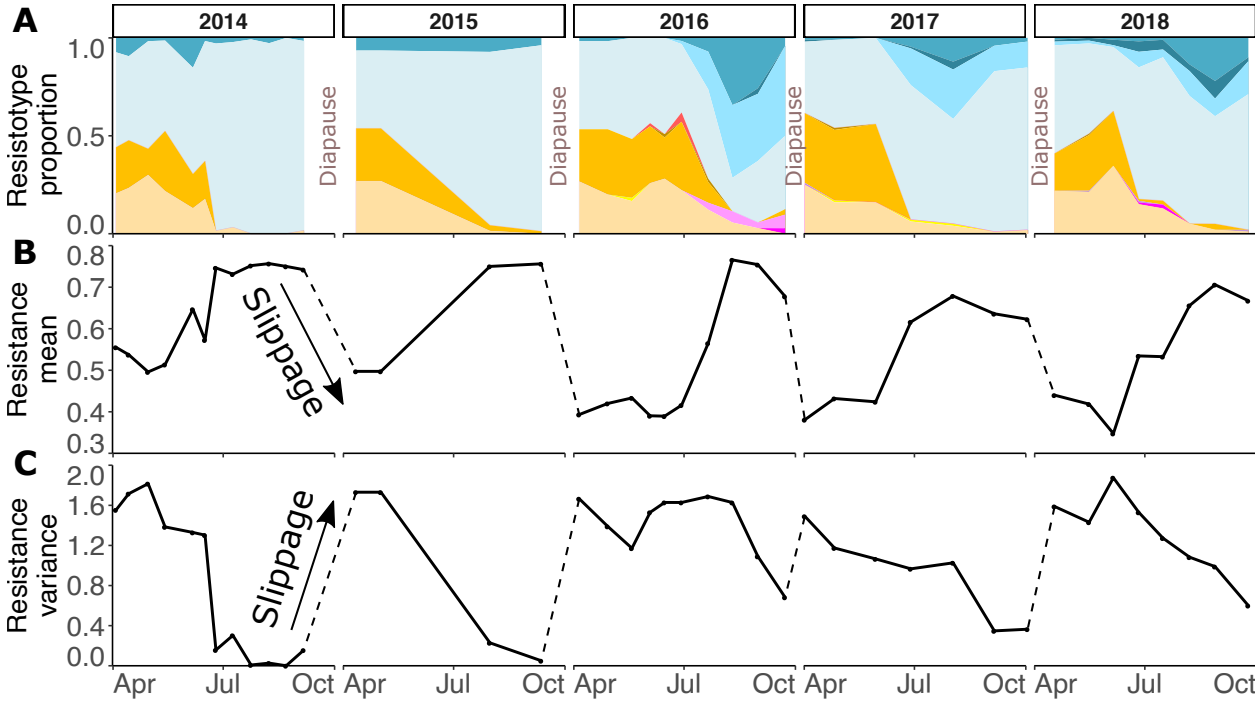

Figure 2.2

Genetic slippage resulting from sexual reproduction in the Aegelsee *Daphnia magna* population. **A**: Observed resistotype (resistance phenotype) frequencies in the *D. magna* population from 2014 to 2018 (same as Fig. 2.1B for 2014 to 2018; repeated here for better comparison). **B**: Mean resistance to *Pasteuria ramosa* across time. Mean resistance increases across every summer planktonic phase. We attributed to each resistotype a resistance score ranging from zero to the number of isolates tested, and weighted the mean per sampling point by the number of tested isolates, resulting in a score between zero and one (e.g. RRRRR would have an overall resistance score of 1 and SSSSS would be 0). The dashed lines span the time windows during which sexual offspring overwinter and hatch the following spring. **C**: Variance of resistance across time, calculated along with the mean in panel B. Note that in 2014 and 2015, four bacterial isolates were tested, while we used five from 2016 to 2018. Therefore, mean and variance cannot be directly compared between years when different number of parasite isolates are used.

phenotypes combinations or absence of polymorphisms at the underlying resistance loci in this population.

Response to selection for resistance

As a cyclic parthenogen, *D. magna* reproduces asexually during most of the active season and produces sexual resting stages (embryos) in a protective case (ephippium) that overwinter and hatch in the spring. Because the planktonic animals do not overwinter in our population, the spring cohort is exclusively the result of sexual reproduction. To look at the impact of selection and recombination on resistance diversity during and between seasons, respectively, we calculated the mean and variance of resistance phenotypes of the planktonic population for each sample through time, assigning resistance (R) and susceptibility (S) a value of 1 and 0, respectively. If directional selection acts on resistance, we expect mean resistance to increase, as selection removes susceptible phenotypes. As hardly any susceptible resistotypes are left at the end of the summer, we further expected variance in resistance to decrease during the summer, as resistance reaches high values. Furthermore, a round of sexual reproduction is expected to restore, or partly restore, the variance and the mean is expected to relapse to some degree because genetic recombination leads (under most conditions) to a regress to the mean before selection (Falconer 1981)—also discussed as genetic slippage (Lynch and Deng 1994; Decaestecker et al. 2009). Our results align with these predictions: every year, mean resistance increased,

and variance declined over the planktonic season (Fig. 2.2). After sexual reproduction, variance was restored, and the mean regressed towards the mean of the previous year before selection. What was surprising, however, was that the relapse of the mean was nearly perfect over the entire study period, showing that there was no overall response to selection across seasons. Note that the apparent drop in the mean between 2015 and 2016 in Figure 2.2 is caused by the addition of one more *P. ramosa* isolate (P21) in the test panel.

Selection and sexual reproduction

To understand these pronounced dynamics in mean resistance and its variance, we collected and hatched sexually produced resting stages across three seasons, using sediment traps that we emptied at about monthly intervals. Sediment traps allow us to decouple the current resting egg production from resting eggs produced earlier (forming a seed bank-like reservoir), as these traps only collect resting stages that are dropped from the current planktonic population. This allowed us to estimate when sexual reproduction occurred and—by subsequent hatching of resting stages from each sampling date—to estimate the hatchlings resistotype frequencies.

We observed that resting stages were produced throughout most of *D. magna*'s planktonic phase and tended to show multiple peaks before and after the main change in resistotype frequencies in June-July (Fig. 2.3B). The number of resting stages per ephippium (zero, one or two) produced over the planktonic phase of *D. magna* remained approximately stable (Supplementary Fig. S2.2B and C, linear regression, all years pooled: R^2 = 0.14, F = 3.2 on 1 and 13 DF, p = 0.095). After diapausing the resting stages in the dark at 4 °C, the overall hatching success in outdoor containers in the following spring was 74.4±3.9%, which was independent of the date when the resting stages were collected (linear regression, pooled for all years: R^2 = 0.042, F = 1.75 on 1 and 16 DF, p = 0.20). The hatching pattern after induction was also consistent, with most resting stages hatching within a few days after induction (Supplementary Fig. S2.2). The few resting stages that hatched later did not differ in their resistotype proportions from the earlier hatchlings (measured only in 2014, Fisher's test, p = 0.32, Supplementary Fig. S2.3).

All hatchlings were cloned and tested for resistotypes. Surprisingly, in all years, the observed resistotype frequencies of the hatchlings remained rather stable over the season, both for the combined and for the individual bacterial isolates (Fig. 2.3C and D), independent of the strongly changing resistotype composition of the planktonic animals at the time of resting egg production (Fig. 2.3A). This created a substantial difference between the resistotype distribution of the parent population and their sexual offspring, especially in late summer, when we observed that susceptible offspring resistotypes (RRSS␣ and SSSS␣, orange and yellow in Fig. 2.3C) were created from a parental population that consisted almost solely of resistant resistotypes (RRSR␣ and RRRR␣, blue in Fig. 2.3A). Remarkably, the most resistant resistotypes in the planktonic population were hardly seen in the offspring populations (RRRR␣ in 2014 and 2015 (dark blue), RRRRR, RR-

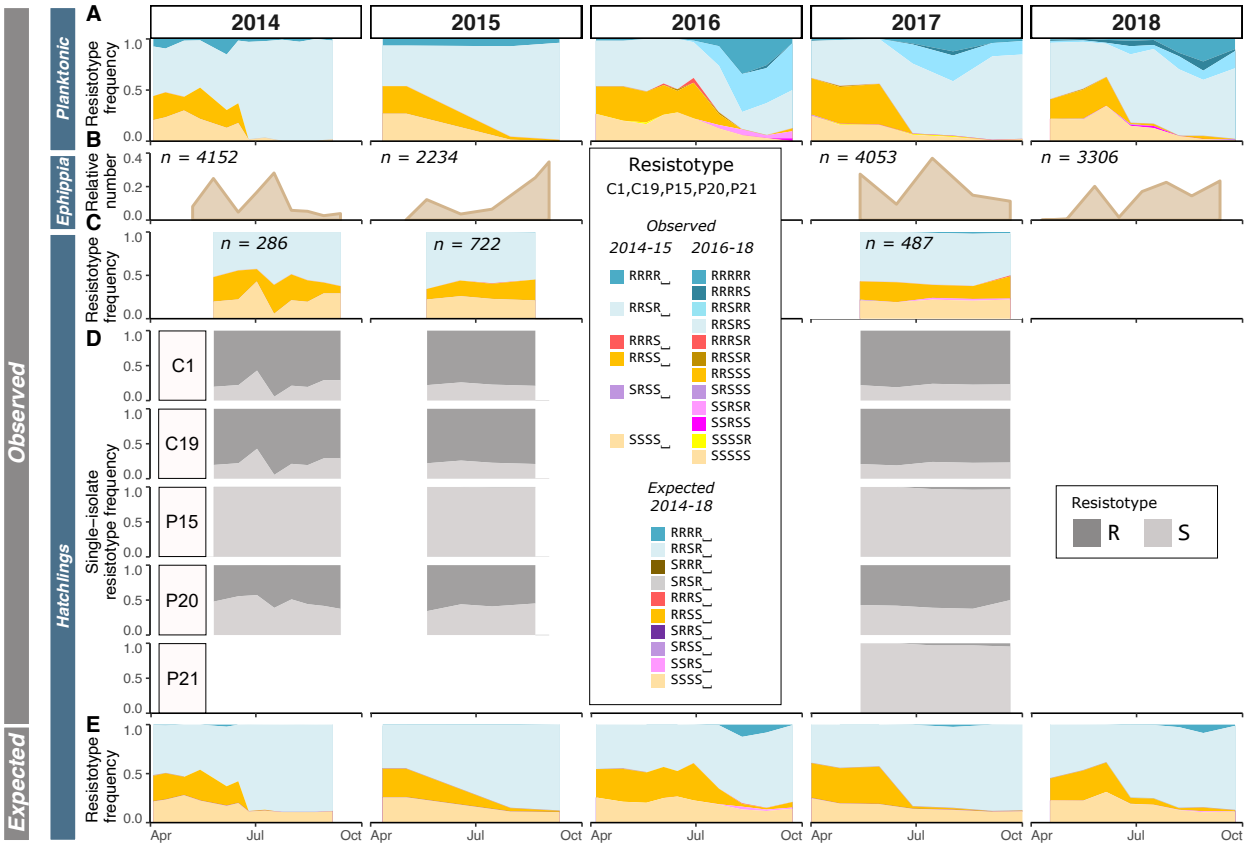

Figure 2.3

Longitudinal resting stage hatching of *Daphnia magna* from the Aegelsee. **A**: Observed resistotype (resistance phenotype) frequencies in the *D. magna* population from 2014 to 2018 (same as Fig. 2.1B, repeated here for better comparison). **B**: Observed relative number of *D. magna* resting stage cases (ephippia) produced in the pond and recovered from five to nine sediment traps, in two−four-week intervals from early April to early October in 2014, 2015, 2017 and 2018. Time on the x-axis represents the mid-point between two consecutive emptying of the traps. The "n" indicates the total number of ephippia for a given year. **C**: Resistotype frequencies of the hatchlings from the sediment traps plotted against the collection time (only for 2014, 2015 and 2017). Resting stages from 2018 were collected but not hatched. Note that in 2014, the first resting stage sample was lost. In 2015, no hatchlings emerged from the last sample. We represent the four-letter resistotype (C1, C19, P15, P20) to be comparable with the E panel. **D**: As in C but for each of the five *Pasteuria ramosa* isolates separately. **E**: Expected resistotype frequencies of hatchlings from sexually produced eggs (resting stages) by the planktonic population across the entire planktonic season (also for parts of the season where no resting stages were produced). Expected resistotype frequencies were calculated using the genetic model of resistance in the *D. magna–P. ramosa* system assuming random mating of the parent population at the time of resting stage production. Detailed methods and results of these calculations are given in the text and in Supplementary Figs. S2.5 and S2.6 and Tables S2.1 and S2.2.

RRS and RRSRR in 2017 (dark and bright blue), Fig. 2.3A and C).

Resting stages produced during the planktonic phase accumulate over the planktonic season, overwinter and hatch in the following spring. Pooling the resistotype data of the hatchlings from the sediment traps across the entire season and weighting resistotype frequencies by the abundance of resting stages in each sample is therefore a predictor of the expected resistotype composition for the following spring cohort. These predictions match the resistotype composition of the planktonic population in spring very well for all three years (Fig. 2.4, Supplementary Figs. S2.3 and S2.4), indicating that the populations of hatchlings from the cumulative sediment trap samples are representative of these spring cohorts.

Calculation of expected resistotype frequencies in resting stages

From previous genetic studies we know that dominance and epistasis are defining features of the inheritance of resistance to *P. ramosa* (Luijckx et al. 2013; Metzger et al. 2016; Bento et al. 2017; Bento et al. 2020; Chapter 1,

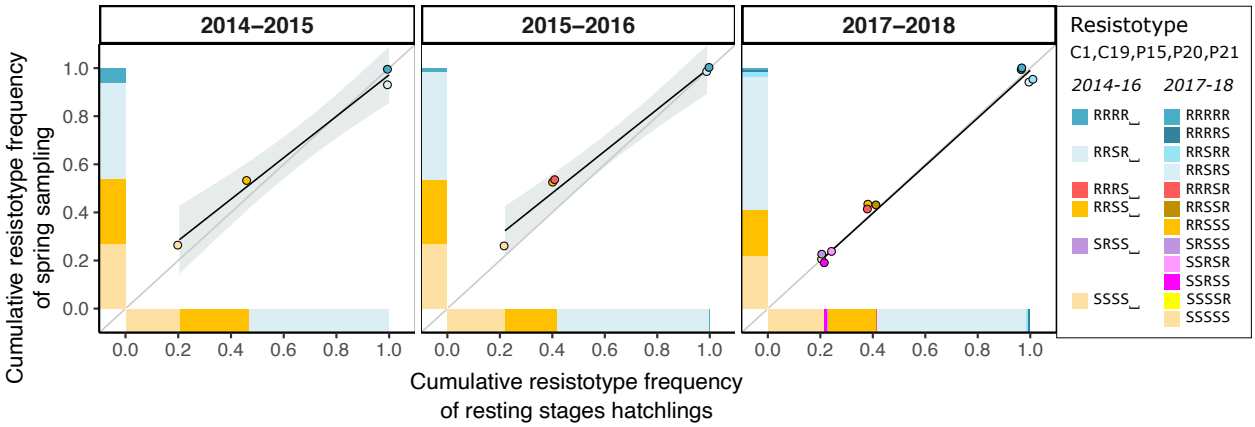

Figure 2.4

Scatter plot of resistotype frequencies of the hatchlings from the overwintering resting stages (collected in the sediment traps) against those of the *Daphnia magna* collected the following spring in the Aegelsee. The x-axis represents cumulated resistotype frequencies in the hatchlings from the sediment traps. These frequencies were calculated by weighing resistotype frequencies in the hatchling population by the relative number of resting stages produced at each sampling point. The y-axis represents cumulated resistotype frequencies in the first sample collected the following spring after the resting stages. Dots are plotted using jitter to reduce overlap. The grey line represents the y = x function and depicts an expected perfect match between both resistotype frequencies. The black line represents the fitted linear regression with 95% error as the grey area (not visible in the 2017–2018 panel because it is too small).

Ameline et al. 2021). To predict the role of sexual recombination in shaping resistance dynamics, we used an existing genetic model for resistance in our study population to calculate the expected resistotype frequencies in the offspring population at the time of resting stage production (sexual reproduction). These calculations require knowledge of allele frequencies at the resistance loci, which are unknown, but which we estimated using known resistotype distributions and assumptions. Although the published genetic model for resistance includes six loci (A to F), here we considered variation only at the B, C, D and E loci (Supplementary Fig. S2.5). The A and the F loci, known from other *D. magna* populations, seem to be monomorphic in the Aegelsee population. Alleles B and d are expected to be rare: resistotypes determined by the "B-" and the "dd" genotypes, regardless of the genotype at other loci, were only observed rarely (Fig. 2.1 and Chapter 1, Ameline et al. 2021). Allele frequency at the C and E loci have been previously determined in a spring sample from the Aegelsee *D. magna* population (Chapter 1, Ameline et al. 2021). Using these C- and E-loci allele frequencies within each resistotype and fixing the B and D loci to be "bbDD" genotype, we found that expected and observed resistotype frequencies match better than do several other scenarios, e.g. equally distributed allele frequency at the C and E loci (Fig. 2.3C and E, Supplementary Figs. S2.6 and S2.7, Tables S2.1 and S2.2). Expected and observed resistotype frequency in the hatchling population match especially well in the first half of the season (Fig. 2.3C and E). In the second half of the season, however, we see a marked difference, with the presence of the abundant RRSS_ resistotype (about 25%) not predicted by the model (orange in Fig. 2.3C and E).

This discrepancy between predicted and observed resistotype frequencies in the second half of the season may have been due to a non-representative distribution of animals producing the sexual eggs (resting stages) at this time of the year. We tested this by collecting, in August 2020, *D. magna* samples and quantifying the resistotype distribution of females carrying

resting stages, of males, and of a random sample of females. We found good correspondence between the random population samples, the sexual females, and the males (Supplementary Fig. S2.8), indicating that the animals reproducing sexually are a representative sample of the population with regards to resistotypes. Additionally, we quantified the resistotype distribution of a random sample of females in April 2021 and found a similar distribution than in the previous spring samples (Supplementary Fig. S2.8), indicating that the strong genetic slippage has been shaping the resistance profile of this population for ten years.

Discussion

Genetic variation for parasite resistance in natural populations is known to be very high, but the mechanisms maintaining this variation are not well understood. Here we address this topic by monitoring the long-term impact of seasonal epidemics of a bacterial pathogen (*Pasteuria ramosa*) on the genetic variation in parasite resistance in a natural zooplankton population (*Daphnia magna*). We observed an increase in mean resistance every summer coinciding with the epidemics, which have been shown to be driven by parasite mediated selection on two well-defined genomic regions (Chapter 1, Ameline et al. 2021). Surprisingly, despite the strong selection against susceptible hosts, the sexually produced hatchling population in spring showed again high frequencies of susceptible host resistotypes. These frequencies remained stable over the eight-year observation period, indicating an apparent absence of response to selection across years. These cyclical dynamics were also seen in the variance for resistance, which declined every summer, but increased again from Fall to Spring after overwintering. Despite the strong selection, these cycles maintain genetic variation for resistance in the host population. We show that the resistance cycles are shaped by the seasonality in production and hatching of sexual resting stages in combination with the underlying genetics for the inheritance of resistance involving dominance and epistasis.

Repeated strong parasite-mediated selection in a natural population

The seasonal change in resistotype proportions in the *D. magna* Aegelsee population that we observed followed a consistent pattern across our eight-year study period: resistant phenotypes increase during the planktonic phase of the host, coinciding with the *P. ramosa* epidemics (Fig. 2.1). Using material collected in the Aegelsee in 2014 and 2015, we previously confirmed experimentally that these resistotype frequency changes resulted from parasite-mediated selection (Chapter 1, Ameline et al. 2021). Parasite mediate selection has been shown to rapidly raise the frequency of resistance in *Daphnia* (Little and Ebert 1999; Decaestecker et al. 2007; Duffy and Sivars-Becker 2007; Duncan and Little 2007) and in other host–parasite systems (Schmid-Hempel 2011; Morgan and Koskella 2017; Koskella 2018), although long-term monitoring of natural populations remains scarce (Laine 2009; González-Tortuero et al. 2016; Gibson et al. 2018).

We observed that this increase in resistance occurred in the host population with some temporal variation in magnitude and speed (see season-

al increase in dark grey in Fig. 2.1C). Most notably, over five consecutive years, resistance to the sympatric *P. ramosa* isolate P20, which has been shown to play a major role in epidemics in our population (Chapter 1, Ameline et al. 2021), increased from about 50% to 100% each year within two months around the peak of the epidemics. Resistance to *P. ramosa* isolates C1 and C19 consistently increased throughout the planktonic phase each year (from about 75% to nearly 100%), showing that resistance to these infectotypes may also be selected for in the host population. From 2016 to 2018, resistance to P15 and P21 increased as well, but decreased somewhat when parasite prevalence declined towards the end of the season, which was not the case for resistance to P20. This result might be explained by a cost of resistance, as resistant genotypes lose their selective advantage once parasite prevalence declines below some level, making susceptible genotypes increase in frequency. We can safely exclude genetic drift as an explanation for these cyclic changes, because the *D. magna* census population size in the Aegelsee is estimated at over ten million individuals with an overwintering resting egg bank of about the same size. In summary, we observed a highly repeatable, adaptive increase in resistance to all tested parasite infectotypes every year. Despite this increase in resistance, however, susceptibility to the parasite was created anew after a round of sexual reproduction in the spring cohort, resulting in a stable long-term genetic diversity for resistance across years (Fig. 2.1B).

The effects of genetic recombination on resistotype composition

Decrease of population mean resistance

Because sexual reproduction is a prerequisite for resting stage formation in *D. magna*, we could decouple the effects of selection and genetic recombination on resistance in our host population. Overwintering happens only in the form of sexually produced resting stages, as planktonic individuals die off in early October due to the artificial warming of this sewage pond (Supplementary Fig. S2.1). Every spring, we observed that the mean resistance of the hatchlings was much below the mean resistance from the previous fall (Fig. 2.2B). While the strength of this effect was surprising to us, the observation that population regress back to the mean of the parental population before selection is well known (Falconer 1981; Lynch and Deng 1994; Otto 2009). Prolonged periods of asexual reproduction amplify this effect, which might explain the strength of genetic slippage observed in the studied population (Lynch and Deng 1994). However, despite regression back to the mean of the parental generation, it is usually expected that, under selection, the offspring mean will move away from the parents (long-term response to selection). This did not happen in our population, or it is so weak that we did not pick up the signal. We suggest that the combination of timing of sexual reproduction and genetic architecture of resistance causes these cycles in mean resistance.

We found that resting stages are not only produced at the end of the planktonic season, but already starting in somewhat irregular patterns during the season, with roughly two seasonal peaks, one early in the epidemic and one towards the end of the season (Fig. 2.3B). Resting stages produced at

different times did not vary in fitness-related aspects (hatching rate, resting stages per ephippium, hatching time, Supplementary Fig. S2.2), suggesting that their contribution to the next year spring cohort is approximately even. Thus, some of the sexual eggs (resting stages) that hatched in the spring were produced before selection acted on the parental generation, dampening the overall effect of selection on the spring cohort the following year. However, as typically more than 50% of the resting stages were produced after selection had increased resistance, this alone cannot explain the strong regression to mean resistance. We speculate that the genetic architecture underlying resistance may also contribute to this discrepancy.

Sex reestablishes resistance diversity

We phenotyped the hatchlings of the sexually produced resting stages collected in the sediment traps throughout the season. Early in the season, sexual offspring present approximately the same resistotype distribution as their planktonic parent population. Strikingly, however, resting stages collected late in the season show a markedly different resistotype from the planktonic host population at this time of the year. Namely, the parent population in the late season is composed of mainly resistant animals but produces about 50% susceptible offspring resistotypes (Fig. 2.3). Sexual recombination, coupled with a genetic architecture with epistasis and dominance, could create susceptible genotypes out of resistant ones.

To investigate how resistotype diversity is reestablished through sexual reproduction, or how resistant phenotypes can produce susceptible ones, we used a previously published genetic model for the inheritance of resistance in *D. magna* against *P. ramosa* infections (described in Supplementary Fig. S2.5, Metzger et al. 2016; Bento et al. 2020; Chapter 1, Ameline et al. 2021). This model allowed us to predict the resistotype frequencies of sexual offspring given a pool of parent resistotypes and their underlying genotypes. We then compared these predicted resistotype frequencies to those we observed among the resting stage hatchlings we collected throughout the season. In the early half of the season, our model worked rather well, with a slight discrepancy between the proportions of the RRSR␣ resistotype (the model predicted more than we observed; light blue in Fig. 2.3C and E) and RRSS␣ (the model predicted less than we observed, orange in Fig. 2.3C and E). In the second half of the season, we observed a stronger discrepancy between expected and observed resistotype distributions: P20-susceptible resistotypes (RRSS␣, orange in Fig. 2.3C and E) are very common (about 25%) among the sexual offspring resistotypes, although according to our model, they should not be produced by a parent population where P20-resistant resistotypes dominate, because resistance to P20 is recessive (Fig. 2.3, Supplementary Fig. S2.5). The genetic model of resistance displays strong epistasis and dominance, also influencing resistance to P20 (Bento et al. 2020; Chapter 1, Ameline et al. 2021). Two loci, the C and the B loci, epistatically influence resistance to P20, but in the present case, this cannot explain the emergence of RRSS␣ offspring from a parent population lacking RRSS␣ individuals. Taken together, genetic recombination in this multi-locus system with epistasis and dominance seems likely to be the main con-

tributor to the maintenance of genetic diversity for resistance. Our genetic model is not complete and seems to miss further epistatic interactions between the known loci or additional unknown loci. With multiple loci, dominance and epistasis, it is difficult to interpret the outcome of genetic crosses, because the number of possibilities increases rapidly.

Finally, the genetic model alone does not allow us to predict the frequencies of resistotypes after recombination without making assumptions about allele frequencies at these loci. We assumed allele frequencies derived from the overall observed resistotype diversity in the population and from previous estimates using genetic markers (see methods section and Chapter 1, Ameline et al. 2021). We also assumed that allele frequencies underlying each resistotype did not change across the planktonic phase because we have no reason to expect changes in the frequencies of genotypes coding for the same resistotype. With more knowledge about the actual loci underlying the resistotypes, we may be able to predict resistotype frequencies better in the future. However, changing the assumptions for the allele frequencies to predict resistotype frequencies in sexual offspring did not produce enough of an effect to explain the mismatch between the fall parent generation and their sexual offspring.

No evidence for pre-hatching or pre-zygotic selection related to resistotype

Pre-zygotic and/or pre-hatching selection could also contribute to the observed discrepancies between parent and offspring resistotypes. This could occur if different resistotypes in the planktonic population contributed unequally to sexual reproduction, producing males or resting stages differentially, or copulating at different rates. However, Orsini et al. (2016) suggest that the produced resting stages in *D. magna* population accurately represent the planktonic population, which agrees with an assessment in our study population indicating that the males and females that participate in sexual reproduction represent the resistotype distribution of the entire population well (Supplementary Fig. S2.8).

Another form of pre-zygotic selection could result from negative assortative mating that favors rare susceptible resistotypes. We cannot rule out an effect of assortative mating contributing to the resistotype distribution in the offspring population. Assortative mating describes non-random mating between male and female genotypes or phenotypes. Positive assortative mating linked to body size and other traits has been found in a variety of animals, while negative assortative mating linked to immune genes (MHC) has been found in mice and humans (Wedekind et al. 1995; Chaix et al. 2008; Jiang et al. 2013). However, assortative mating in relation to immunity or resistance remains to be investigated in invertebrates, and as most population genetics models—including the present study—assume random mating, this is an important aspect for further study. Resistotype-dependent selection during diapause or hatching could also distort resistotype frequencies.

Finally, one may imagine that our ephippia sediment traps collected late in the season contained resting stages that had been produced earlier in

the season and were re-suspended in the water column. However, several arguments speak against this. First, the pond does not contain fish, that may cause bioturbation. Second, the lake has no inflow, but only a very slow outflow, causing no detectable water movement. Third, at times when the *D. magna* population does not produce resting stages (the spring cohort in April), we find no resting stages in the sediment traps. Fourth, the same redistribution (in quantity and quality) would have needed to occur every year, as we observed the same patterns over three years. We thus conclude that water turbation is an unlikely explanation for the observed mismatch between resistotype distributions in the fall planktonic phase and the sexual stages it produced.

The Red Queen theory for the maintenance of sex

Genetic recombination is a double-edged sword. On one side, it creates novel genotypes and phenotypes on which selection can act; on the other side, it may destroy coadapted gene complexes. At first sight, the latter seems to be the case on our study population because the recombinant offspring are less resistant than their parents. This seems to contradict the Red Queen hypothesis for the maintenance of sex (Jaenike 1978; Hamilton et al. 1990; Otto and Nuismer 2004; Salathé et al. 2008), which postulates that genetic recombination is advantageous for hosts because, by creating previously lost genotypes, it overcomes the rapid adaptation of parasites to common host genotypes (Lively 2010; Gibson et al. 2018). Under this hypothesis, common hosts are expected to become over-infected, and rare hosts gain an advantage because at least some of them may be resistant to the common parasites. Indeed, in our population, recombination recreates genotypes and results in a more even distribution of genotypes and phenotypes, including the recreation of P20-susceptible phenotypes that were previously lost by selection. However, this seems to be disadvantageous, because the recreated phenotypes are susceptible to the common parasite.

In our study population, we have no good information about the parasite infectotypes spreading throughout the year. However, we saw that prevalence was still high after mid-season, when the P20-susceptible hosts became rare and presumably also the parasites of the P20 type. We speculate that parasites of the P21 type then become more common, which is consistent with the decline in P21-susceptible hosts late in the season. With better knowledge of the parasite population, we may be able to track yearly shifts in the frequency of parasite infectotypes and relate it to the changing host resistotype frequencies. In this scenario, genetic recombination in the host in the second half of the season may alter the host resistotypes that become the target of late-season parasites.

Conclusion

In this study, we demonstrate parasite-mediated selection in a natural host population and elucidate the role of sexual reproduction for diversity in resistance phenotypes. Our work stresses (i) the cyclical nature of host–parasite interactions, (ii) the very fast pace of parasite-driven changes in the host population and (iii) the fact that sexual recombination plays an

important role in reshuffling allele combinations. Due to dominance and epistasis in the genetic architecture of resistance, this reshuffling resets the clock to the time before selection acted, rendering the response to selection zero. Although this is an extreme case of genetic slippage in response to sex, it is a powerful agent to maintain genetic diversity, which is a hallmark of resistance in natural populations of *Daphnia* and other animals, plants and bacteria (Altermatt and Ebert 2008; Desai and Currie 2015; Zhao et al. 2016; Cabalzar et al. 2019; Broniewski et al. 2020; Sallinen et al. 2020; White et al. 2020). As climatic seasonality seems to determine the dynamics of parasite resistance in our host population, and given the known impact of climate change on epidemics in the *D. magna–P. ramosa* system (Auld and Brand 2017), one may speculate that the dynamics in our study population may change in response to the predicted changes in climatic conditions and seasonality.

However, for the maintenance of the genetic variation in resistance, the genetic mechanism underlying resistance is sufficient. The strong cycles observed every year are caused by the combination of this mechanism with the synchronous hatching of sexual eggs produced in the previous season. The seasonal production and hatching of the sexual stages make the effect of genetic slippage particularly strong, because the effect of selection on the asexual planktonic phase of the host becomes more apparent, but seems not necessary for the maintenance of genetic variation for resistance.

Materials and methods

The *Daphnia magna–Pasteuria ramosa* system

Daphnia magna Straus (Cladocera) is a freshwater planktonic crustacean that reproduces by cyclical parthenogenesis. Asexual females produce genetically identical (clones) diploid daughters or sons throughout the season. These females may switch to become sexual, and their haploid eggs need fertilization by males. Sexual eggs, which we call resting stages (precisely: embryos in developmental arrest) are produced, singly or in pairs, in a protective case (= ephippium) and require a resting period prior to hatching. All hatchlings from resting stages are asexually reproducing females. *Daphnia* filter-feed on planktonic algae and from the sediment surface, which is also how they ingest the transmission stages (= spores) of the bacterial parasite *Pasteuria ramosa* (Firmicutes: Bacillales). When infected by *P. ramosa, D. magna* take on a reddish coloration and increase in size (gigantism). Infection results in castration, reducing host reproductive success by 80% to 90%. Infected hosts die after six to ten weeks, releasing millions of long-lasting spores into the environment (Ebert et al. 1996, 2016; Ben-Ami 2017).

Temporal monitoring

Our study site was the Aegelsee pond near Frauenfeld, Switzerland, a fishless pond previously described in detail in Chapter 1 (Ameline et al. 2021), which contains a very large population of *D. magna*. To study the impact of the *P. ramosa* epidemics on the host, we sampled the *D. magna* population throughout its planktonic season (April to early October) for eight consec-

utive years, monitoring the frequencies of different resistance phenotypes (resistotypes) in the planktonic population. We also used traps to collect *D. magna* resting stages for three seasons and hatched them under semi-natural conditions the following spring. From 2011, a temperature logger was placed in the pond at a water depth of 0.5 m suspended from a buoy near the sampling spot. Water level was recorded at each sampling event.

Field work

Our first sample was collected in early October 2010. From 2011 to 2013, we collected approximately once a month, often a small sample size and without a standardized sampling protocol. From 2014 to 2018, we sampled the *D. magna* population using a standardized protocol every two to four weeks from early April to early October (more samples during the epidemic). Unless mentioned otherwise, all measurements were done at the deepest location close to the southern bank of the pond.

To monitor prevalence and the evolution of resistance, we sampled planktonic *D. magna* females at each collection date. We scooped the whole depth of the water column with a net (20-cm width and 1-mm mesh opening) to obtain several hundred animals. Samples were kept at 15 to 20 °C and transported to the laboratory and processed within four hours.

To sample the overwintering resting stages of the population, we collected surface sediment from five locations in the pond once in February 2014, before onset of the natural hatching season. This sample represents the overwintering resting population produced during the active season in 2013. To longitudinally sample the resting stages produced by the *D. magna* population across the season, we used five to nine sediment traps (vertically standing cylinders with 18-cm diameter and 0.4-mm mesh opening) placed on the lake bottom near the deepest part of the lake, and retrieved their content at each collection date during the planktonic season in 2014, 2015, 2017 and 2018. Collected *D. magna* resting stages were hatched in outside containers the following spring after overwintering at 4 °C in the dark. Each container contained a hundred ephippia per trap per timepoint and were monitored for several weeks. We collected hatchlings and cloned them in the laboratory. We measured the resistotype of 20 clonal lines (clones) per trap per timepoint, resulting in 100 clones per timepoint.

To obtain an estimate of *Daphnia* density, we used bottles to directly scoop the water from different depths three to five times (from 2011 to 2013). From 2014 we used a plankton net, performing ten vertical hauls from the bottom of the pond at the deepest point of the lake.

Analysis of field samples

The Aegelsee contains three *Daphnia* species: *D. magna*, *D. pulex* and *D. curvirostis*. The relative abundance of these species was measured in the laboratory by sorting and counting the density samples using a stereomicroscope. Because *D. pulex* and *D. curvirostis* have similar morphologies, we counted them together and inferred their relative proportions by determining the species in a random subset of 100 animals. We counted the

number of males in a subset of 100 *D. magna*.

From each sample, we established clonal (iso-female) lines of about 100 *D. magna* to be used later for resistotype assessment. We estimated the prevalence of infection as described in Chapter 1 (Ameline et al. 2021), and cured *P. ramosa* infections when they were observed, as otherwise cloning is not possible. *Pasteuria ramosa* is the only significant parasite in this population and was never observed to infect any species other than *D. magna* in this population.

We counted the *D. magna* ephippia retrieved from the traps and overwintered them at 4 °C in the dark. In the spring following the collection year (2014, 2015 and 2017), 20 to 100 ephippia (depending on how many were collected at a given sampling time point) from each sampling date were placed in 80-L containers filled with 30 L ADaM medium (Klüttgen et al. 1994, as modified in Ebert 1998). Containers were placed outdoors under direct sunlight and checked for hatchlings every second day. We recorded hatching dates and cloned hatchlings in the laboratory. We randomly chose 100 *D. magna* clones equally distributed among replicate traps at each sampling date to assess the resistotypes. To estimate hatching rate, we counted the number of resting stages per ephippium (zero, one or two) in a subset of ten to 20 ephippia that were not used for the hatching experiment, in at least two replicates for each collection date.

Pasteuria ramosa isolates

In addition to the four *P. ramosa* isolates used previously (C1, C19, P15 and P20, see Chapter 1, Ameline et al. 2021), we isolated another strain of *P. ramosa,* P21, from our study population by exposing *D. magna* clones to suspended pond sediment. We took one infected female and serially passaged the bacteria from this female three times by infecting females of the same host clone. Spore production in the laboratory followed the protocol described by Luijckx et al. (2011).

Resistotype assessment: the attachment test

We determined the resistance phenotype (resistotype) for each *D. magna* clone using the attachment test of Duneau et al. (2011). In short, early in the infection process, bacterial spores will attach to the foregut or the hindgut of susceptible host clones and penetrate the host's body cavity. Spore attachment indicates host susceptibility (S), while absence of attachment indicates host resistance (R). We exposed each individual host to 8,000 (C1, C19) or 10,000 (P15, P20, P21) fluorescent spores and assessed attachment microscopically. Attachment was judged in each individual as yes or no. At least three replicates of each clone were used for each parasite isolate. Replicates are highly consistent in their attachment (Bento et al. 2017; Bento et al. 2020). For each host–parasite combination we obtained a consensus resistotype (R or S), based on the majority of the individual attachment tests. Across parasite strains, we defined the overall resistotype as the combination of resistance phenotypes to the five individual *P. ramosa* isolates in the following order: C1, C19, P15, P20 and P21 (e.g. a clone susceptible to all isolates will have the SSSSS resistotype). When resistance to a strain is

not considered, we use the placeholder "␣", e.g. "RR␣RR resistotype". With time, we were able to include more parasite isolates: from 2010 to 2013, only the resistotypes to C1 and C19 were assessed. In 2014 and 2015, P15 and P20 were added, and all five *P. ramosa* isolates were tested from 2016.

To assess genetic slippage, we calculated the population mean resistance to *P. ramosa* for each sampling time. We assigned a resistance score to each resistotype ranging from zero to one to compare timepoints when we used different numbers of parasite isolates. For example, a host individual with a RRSRS resistotype was attributed a resistance score of 3/5 = 0.6.

Hatching modelling

To predict resistotype frequencies of sexual offspring of the planktonic *D. magna* population, we used the R-package "peas", which generates predictions about the distribution of offspring genotypes and phenotypes in genetic crosses, based on specified systems of Mendelian inheritance (https://github.com/JanEngelstaedter/peas). We implemented the genetic model of resistance described in Chapter 1 (Ameline et al. 2021) in the *D. magna–P. ramosa* system for our study population. This model includes the genetic architecture of three loci (the B, C and E loci) that govern host resistance in our study population. The dominant allele at the B locus confers resistance (R) to C19 and susceptibility (S) to C1. The dominant allele at the C locus confers resistance to both the C1 and C19 *P. ramosa* strains, regardless of the genotype at the B locus (epistasis). The E locus contributes to resistance to P20. Resistance is dominant at the C locus (resistance to C1 and C19), whereas resistance is recessive at the E locus (resistance to P20). Homozygosity for the recessive allele at the B and C loci induces susceptibility to P20, regardless of the genotype at the E locus (epistasis). In the present study, we add the genetic architecture of the D locus to the model, which determines resistance to the P15 *P. ramosa* isolate (Bento et al. 2020). Implementation of the model is described in Supplementary Fig. S2.5 and Doc. S2.1. Implementing this model in the "peas" package, we calculated the expected resistance genotypes and phenotypes of sexual offspring of each possible mating among parent resistotypes. We assumed different allele frequency scenarios because the known resistotypes of the parents are not sufficient to estimate their exact genotype- and allele-frequencies, as some alleles can be hidden by dominance and epistasis. We then calculated the expected offspring resistotype frequencies over time corresponding to each of resting stage sample. If the genetic model accurately represents the biology of the system, the expected resistotype frequencies will match those found in the hatchlings from the sediment traps corresponding to the same sampling time. Detailed calculations are described in Supplementary Doc. S2.2 and Fig. S2.9.

Statistical software

Software used for statistical analyses and graphics are described in Supplementary Doc. S2.3.

Acknowledgments

We thank Yann Bourgeois, Samuel Pichon, Sabrina Gattis, Georgia Rouseti, Jürgen Hottinger, Urs Stiefel, Kristina Müller, Michelle Krebs and Dita Vizoso for help in the field and in the laboratory. Members of the Ebert group; Jonathon Stillman and Luís Teixeira provided valuable feedback on the study and the manuscript. This work was supported by the Swiss National Science Foundation (SNSF) (grant numbers 310030B_166677 and 310030_188887 to DE); the Freiwillige Akademische Gesellschaft (FAG) Basel to CA and the University of Basel to DE and CA.

Author contributions

DE, JA and CA designed the study. JA conducted monitoring in 2010 to 2013, FV conducted monitoring and resting stage hatching in 2014, DE conducted monitoring in 2015 and CA conducted monitoring and resting stage hatching from 2016 to 2018. DE and ED monitored resistotype frequency and sexually reproducing animals in 2020 and 2021. JE developed the “peas” R package. CA analysed the data, designed figures and wrote the manuscript. All authors reviewed the manuscript.

References

Agrawal A, Lively CM. 2002. Infection genetics: gene-for-gene versus matching-alleles models and all points in between. *Evolutionary Ecology Research* **4**:79–90.

Altermatt F, Ebert D. 2008. Genetic diversity of *Daphnia magna* populations enhances resistance to parasites. *Ecology Letters* **11**:918–928.

Ameline C, Bourgeois Y, Vögtli F, Savola E, Andras J, Engelstädter J, Ebert D. 2021. A two-locus system with strong epistasis underlies rapid parasite-mediated evolution of host resistance. *Molecular Biology and Evolution* **38**:1512–1528.

Auld SKJR, Brand J. 2017. Simulated climate change, epidemic size, and host evolution across host-parasite populations. *Global Change Biology* **23**:5045–5053.

Auld SKJR, Tinkler SK, Tinsley MC. 2016. Sex as a strategy against rapidly evolving parasites. *Proceedings of the Royal Society B: Biological Sciences* **283**:20162226.

Baggs E, Dagdas G, Krasileva K. 2017. NLR diversity, helpers and integrated domains: making sense of the NLR IDentity. *Current Opinion in Plant Biology* **38**:59–67.

Becks L, Agrawal AF. 2011. The effect of sex on the mean and variance of fitness in facultatively sexual rotifers. *Journal of Evolutionary Biology* **24**:656–664.

Becks L, Agrawal AF. 2012. The evolution of sex is favoured during adaptation to new environments.Barton NH, editor. *PLoS Biology* **10**:e1001317.

Bell G, Smith JM. 1987. Short-term selection for recombination among mutually antagonistic species. *Nature* **328**:66–68.

Ben-Ami F. 2017. The virulence-transmission relationship in an obligate killer holds under diverse epidemiological and ecological conditions, but where is the tradeoff? *Ecology and Evolution* **7**:11157–11166.

Bento G, Fields PD, Duneau D, Ebert D. 2020. An alternative route of bacterial infection associated with a novel resistance locus in the *Daphnia–Pasteuria* host–parasite system. *Heredity* **125**:173–183.

Bento G, Routtu J, Fields PD, Bourgeois Y, Du Pasquier L, Ebert D. 2017. The genetic basis of resistance and matching-allele interactions of a host–parasite system: The *Daphnia magna–Pasteuria ramosa* model. *PLOS Genetics* **13**:e1006596.

Broniewski JM, Meaden S, Paterson S, Buckling A, Westra ER. 2020. The effect of phage genetic diversity on bacterial resistance evolution. *The ISME Journal* **14**:828–836.

Cabalzar AP, Fields PD, Kato Y, Watanabe H, Ebert D. 2019. Parasite□mediated selection in a natural metapopulation of *Daphnia magna*. *Molecular Ecology* **28**:4770–4785.

Chaix R, Cao C, Donnelly P. 2008. Is mate choice in humans MHC-dependent? *PLoS Genetics* **4**:e1000184.

Decaestecker E, De Meester L, Mergeay J. 2009. Cyclical parthenogenesis in *Daphnia*: sexual versus asexual reproduction. In: Schön I, Martens K, Dijk P, editors. Lost Sex. Dordrecht: Springer Netherlands. p. 295–316.

Decaestecker E, Gaba S, Raeymaekers JAM, Stoks R, Van Kerckhoven L, Ebert D, De Meester L. 2007. Host–parasite 'Red Queen' dynamics archived in pond sediment. *Nature* **450**:870–873.

Desai SD, Currie RW. 2015. Genetic diversity within honey bee colonies affects pathogen load and relative virus levels in honey bees, Apis mellifera L. *Behavioral Ecology and Sociobiology* **69**:1527–1541.

Duffy MA, Sivars-Becker L. 2007. Rapid evolution and ecological host–parasite dynamics. *Ecology Letters* **10**:44–53.

Duncan AB, Little TJ. 2007. Parasite-driven genetic change in a natural population of *Daphnia*. *Evolution* **61**:796–803.

Duneau D, Luijckx P, Ben-Ami F, Laforsch C, Ebert D. 2011. Resolving the infection process reveals striking differences in the contribution of environment, genetics and phylogeny to host–parasite interactions. *BMC biology* **9**:1–11.

Duxbury EM, Day JP, Maria Vespasiani D, Thüringer Y, Tolosana I, Smith SC, Tagliaferri L, Kamacioglu A, Lindsley I, Love L, et al. 2019. Host-pathogen coevolution increases genetic variation in susceptibility to infection. *eLife* **8**:e46440.

Ebert D. 1998. Experimental evolution of parasites. *Science* **282**:1432–1436.

Ebert D, Duneau D, Hall MD, Luijckx P, Andras JP, Du Pasquier L, Ben-Ami F. 2016. A population biology perspective on the stepwise infection process of the bacterial pathogen *Pasteuria ramosa* in *Daphnia*. *Advances in Parasitology* **91**:265–310.

Ebert D, Fields PD. 2020. Host–parasite co-evolution and its genomic signature. *Nature Reviews Genetics* **21**:754–768.

Ebert D, Rainey P, Embley TM, Scholz D. 1996. Development, life cycle, ultrastructure and phylogenetic position of *Pasteuria ramosa* Metchnikoff 1888: rediscovery of an obligate endoparasite of *Daphnia magna* Straus. *Philosophical Transactions of the Royal Society B: Biological Sciences* **351**:1689–1701.

Engelstädter J. 2015. Host–parasite coevolutionary dynamics with generalized success/failure infection genetics. *The American Naturalist* **185**:E117–E129.

Engelstädter J, Bonhoeffer S. 2009. Red Queen dynamics with non-standard fitness interactions.Stormo GD, editor. *PLoS Computational Biology* **5**:e1000469.

Falconer DS. 1981. Introduction to quantitative genetics, 2. ed. London: Longmans Green

Fisher RA. 1930. The genetical theory of natural selection. Oxford University Press

Fisher RA. 1958. Polymorphism and natural selection. *The Journal of Ecology* **46**:289–293.

Frank SA. 2013. Wright's adaptive landscape versus Fisher's fundamental theorem. In: Svensson E, Calsbeek R, editors. The Adaptive Landscape in Evolutionary Biology. Oxford University Press. p. 41–57.

Gibson AK, Delph LF, Vergara D, Lively CM. 2018. Periodic, parasite-mediated selection for and against sex. *The American Naturalist* **192**:537–551.

Gibson AK, Xu JY, Lively CM. 2016. Within-population covariation between sexual reproduction and susceptibility to local parasites. *Evolution* **70**:2049–2060.

González-Tortuero E, Rusek J, Turko P, Petrusek A, Maayan I, Piálek L, Tellenbach C, Giessler S, Spaak P, Wolinska J. 2016. *Daphnia* parasite dynamics across multiple *Caullerya* epidemics indicate selection against common parasite genotypes. *Zoology* **119**:314–321.

Gösser F, Schartl M, García-De León FJ, Tollrian R, Lampert KP. 2019. Red Queen revisited: Immune gene diversity and parasite load in the asexual *Poecilia formosa* versus its sexual host species *P. mexicana*. *PloS one* **14**:e0219000.

Hamilton WD, Axelrod R, Tanese R. 1990. Sexual reproduction as an adaptation to resist parasites (a review). *Proceedings of the National Academy of Sciences* **87**:3566–3573.

Hughes AL. 2002. Natural selection and the diversification of vertebrate immune effectors. *Immunological Reviews* **190**:161–168.

Jaenike J. 1978. An hypothesis to account for the maintenance of sex within populations. *Evolutionary Theory* **3**:191–194.

Jeffery KJM, Bangham CRM. 2000. Do infectious diseases drive MHC diversity? *Microbes and Infection* **2**:1335–1341.

Jiang Y, Bolnick DI, Kirkpatrick M. 2013. Assortative mating in animals. *The American Naturalist* **181**:E125–E138.

Kern AD, Hahn MW. 2018. The neutral theory in light of natural selection.Kumar S, editor. *Molecular Biology and Evolution* **35**:1366–1371.

Klüttgen B, Dülmer U, Engels M, Ratte HT. 1994. ADaM, an artificial freshwater for the culture of zooplankton. *Water Research* **28**:743–746.

Koskella B. 2018. Resistance gained, resistance lost: an explanation for host–parasite coexistence. *PLOS Biology* **16**:e3000013.

Kouyos RD, Salathé M, Otto SP, Bonhoeffer S. 2009. The role of epistasis on the evolution of recombination in host–parasite coevolution. *Theoretical Population Biology* **75**:1–13.

Laine A-L. 2009. Role of coevolution in generating biological diversity: spatially divergent selection trajectories. *Journal of Experimental Botany* **60**:2957–2970.

Li C, Cowling W. 2003. Identification of a single dominant allele for resistance to blackleg in *Brassica napus* "Surpass 400." *Plant Breeding* **122**:485–488.

Little TJ, Ebert D. 1999. Associations between parasitism and host genotype in natural populations of *Daphnia* (Crustacea:Cladocera). *Journal of Animal Ecology* **68**:134–149.

Lively CM. 2010. A review of Red Queen models for the persistence of obligate sexual reproduction. *Journal of Heredity* **101**:S13–S20.

Luijckx P, Ben-Ami F, Mouton L, Du Pasquier L, Ebert D. 2011. Cloning of the unculturable parasite *Pasteuria ramosa* and its *Daphnia* host reveals extreme genotype–genotype interactions. *Ecology Letters* **14**:125–131.

Luijckx P, Fienberg H, Duneau D, Ebert D. 2013. A matching-allele model explains host resistance to parasites. *Current Biology* **23**:1085–1088.

Lynch M, Deng H-W. 1994. Genetic slippage in response to sex. *The American Naturalist* **144**:242–261.

MacPherson A, Otto SP. 2018. Joint coevolutionary–epidemiological models dampen Red Queen cycles and alter conditions for epidemics. *Theoretical Population Biology* **122**:137–148.

Metzger CMJA, Luijckx P, Bento G, Mariadassou M, Ebert D. 2016. The Red Queen lives: Epistasis between linked resistance loci. *Evolution* **70**:480–487.

Morgan AD, Koskella B. 2017. Coevolution of host and pathogen. In: Tibayrenc M, editor. Genetics and evolution of infectious diseases (Second edition). Elsevier. Sara Tenney. p. 115–140.

Morran LT, Schmidt OG, Gelarden IA, Parrish RC, Lively CM. 2011. Running with the Red Queen: host-parasite coevolution selects for biparental sex. *Science* **333**:216–218.

Orsini L, Marshall H, Cuenca Cambronero M, Chaturvedi A, Thomas KW, Pfrender ME, Spanier KI, De Meester L. 2016. Temporal genetic stability in natural populations of the waterflea *Daphnia magna* in response to strong selection pressure. *Molecular Ecology* **25**:6024–6038.

Otto SP. 2009. The evolutionary enigma of sex. *The American Naturalist* **174**:S1–S14.

Otto SP, Nuismer SL. 2004. Species interactions and the evolution of sex. *Science* **304**:1018–1020.

Peters KJ, Evans C, Aguirre JD, Kleindorfer S. 2019. Genetic admixture predicts parasite intensity: evidence for increased hybrid performance in Darwin's tree finches. *Royal Society Open Science* **6**:181616.

Radwan J, Babik W, Kaufman J, Lenz TL, Winternitz J. 2020. Advances in the evolutionary understanding of MHC polymorphism. *Trends in Genetics* **36**:298–311.

Salathé M, Kouyos R, Bonhoeffer S. 2008. The state of affairs in the kingdom of the Red Queen. *Trends in Ecology & Evolution* **23**:439–445.

Sallinen S, Norberg A, Susi H, Laine A-L. 2020. Intraspecific host variation plays a key role in virus community assembly. *Nature Communications* **11**:5610.

Sasaki A. 2000. Host–parasite coevolution in a multilocus gene-for-gene system. *Proceedings of the Royal Society B: Biological Sciences* **267**:2183–2188.

Schmid-Hempel P. 2011. Evolutionary parasitology. The integrated study of infections, immunology, ecology, and genetics. New York: Oxford University Press

Sommer S. 2005. The importance of immune gene variability (MHC) in evolutionary ecology and conservation. *Frontiers in Zoology* **2**:16.

Tellier A, Brown JKM. 2007. Polymorphism in multilocus host–parasite coevolutionary interactions. *Genetics* **177**:1777–1790.

Thrall PH, Barrett LG, Dodds PN, Burdon JJ. 2016. Epidemiological and evolutionary outcomes in gene-for-gene and matching allele models. *Frontiers in Plant Science* **6**:1–12.

Tobler M, Schlupp I. 2008. Expanding the horizon: the Red Queen and potential alternatives. *Canadian Journal of Zoology* **86**:765–773.

Wang B, Ebbole DJ, Wang Z. 2017. The arms race between *Magnaporthe oryzae* and rice: Diversity and interaction of Avr and R genes. *Journal of Integrative Agriculture* **16**:2746–2760.

Wedekind C, Seebeck T, Bettens F, Paepke AJ. 1995. MHC-dependent mate preferences in humans. *Proceedings of the Royal Society B: Biological Sciences* **260**:245–249.

White PS, Choi A, Pandey R, Menezes A, Penley M, Gibson AK, de Roode J, Morran L. 2020. Host heterogeneity mitigates virulence evolution. *Biology Letters* **16**:20190744.

Wilfert L, Schmid-Hempel P. 2008. The genetic architecture of susceptibility to parasites. *BMC Evolutionary Biology* **8**:187.

Zhao Y, Huang J, Wang Z, Jing S, Wang Y, Ouyang Y, Cai B, Xin X-F, Liu X, Zhang C, et al. 2016. Allelic diversity in an NLR gene *BPH9* enables rice to combat planthopper variation. *Proceedings of the National Academy of Sciences* **113**:12850–12855.

CHAPTER 3

Inheritance of resistance to two *Pasteuria ramosa* isolates in a *Daphnia* population

CAMILLE AMELINE, CHENG CHOON ANG, MARIDEL FREDERICKSEN, MERET HALTER AND DIETER EBERT

Abstract Theory of host–parasite coevolution is based on diverse models of the genetic architecture of resistance and infectivity. However, the genetic architecture of resistance to parasites is only known in a few model systems, and rarely linked to evolutionary dynamics in natural populations. The *Daphnia magna–Pasteuria ramosa* host-parasite system has become a model system in coevolution research. Resistance to the parasite is highly specific, and many studies have addressed aspects of its genetic architecture. The genetic model grew more complex as studies discovered new resistance loci and mechanisms linking them. The present study provides a review of the genetic model of resistance in the system, and further investigates the inheritance mode of two *P. ramosa* isolates in a focal host population undergoing strong epidemics. We find complex epistatic interactions among resistance loci and distinct dominance patterns. This genetic model provides a powerful tool to further investigate the evolution of resistance in *D. magna*. We additionally provide empirical support to the importance of epistasis in host–parasite coevolution.

Keywords genetic model of resistance, zooplankton, resistance, loci, genetic architecture, epistasis, dominance, multi-locus genetics, *Daphnia magna*, *Pasteuria ramosa*

Introduction

In the middle of the nineteenth century, Gregor Mendel performed crossing experiments in pea plants and described how traits were inherited, seeding the yet-to-come field of genetics (Mendel 1865). In the era of genomics, the genetic architecture of a trait can be investigated through genomic association studies (Magwire et al. 2012), but genetic crosses still provide a powerful functional validation when combined with genomic data to understand the mode of inheritance of a given trait (Bangham et al. 2008).

In the context of host–parasite coevolution, understanding the genetic architecture of resistance and infectivity is crucial to test theories about the evolution of resistance and infectivity. Dynamics of allele frequencies are an essential part of the host-parasite coevolution theory and can be monitored in systems where coevolving genes are known. The Red Queen theory for the maintenance of sex predicts that resistance and infectivity alleles should be maintained at intermediate frequencies through the advantage of rare alleles, i.e. negative indirect frequency-dependent selection (Hamilton 1980; Hamilton et al. 1990; Lively 2010). Theoretical models propose diverse genetic models of infection, such as the gene-for-gene model and the matching-allele model (Agrawal and Lively 2002; Thrall et al. 2016). These models make assumptions about the number of genes involved, their dominance patterns and whether they are linked with epistatic interactions. For instance, in the Red Queen theory, epistasis among resistance loci is crucial for the maintenance of genetic diversity and recombination in the host (Howard and Lively 1998; Salathé et al. 2008; Engelstädter and Bonhoeffer 2009; Kouyos et al. 2009).

In a few plant and animal systems, the genetic architecture of resistance to specific parasites has been addressed (Bangham et al. 2008; Wilfert and Schmid-Hempel 2008; Magwire et al. 2012; Routtu and Ebert 2015; Cao et al. 2016; Cogni et al. 2016; Magalhães and Sucena 2016; Metzger et al. 2016; Li et al. 2017). Typically, few strong effect loci with patterns of dominance, and linked with epistasis are found (Hooker and Saxena 1971; Samson et al. 1996; Kover and Caicedo 2001; Wilfert and Schmid-Hempel 2008; Jones et al. 2014; Juneja et al. 2015; Li et al. 2017; Xiao et al. 2017).

In the *Daphnia magna–Pasteuria ramosa* host–parasite system, infections are highly specific and generate a high fitness cost in the host, making this system ideal to study the evolution of resistance (Ebert 2005). Additionally, resistance phenotype in the host can be easily scored (Duneau et al. 2011) and genetic crosses among host genotypes can be performed (Luijckx et al. 2012), which allows to investigate the genetic architecture of resistance. The genomic regions determining resistance to different *P. ramosa* isolates and associated genetic models were described using quantitative trait loci (QTL) approaches (Routtu and Ebert 2015; Bento et al. 2020; Fredericksen et al. in prep), genome-wide association studies (GWAS) (Bourgeois et al. 2017; Chapter 1, Ameline et al. 2021) and genetic crosses (Luijckx et al. 2011; Luijckx et al. 2012; Luijckx et al. 2013; Metzger et al. 2016; Chapter 1, Ameline et al. 2021). As more combinations of host and parasite genotypes are being studied, the complexity of the genetic model for resistance has

increased. In the present study, we provide a review of the genetic model of resistance in the system. We further investigate the mode of inheritance to two *P. ramosa* isolates, P15 and P21, using host clones from a focal population undergoing strong epidemics, the Aegelsee population, where interactions with these two isolates is thought to play a role in the dynamics of resistance (Chapter 2, Ameline et al. preprint). The genomic regions determining resistance to P15 and P21 have been described, but their mode of inheritance remains to be investigated (Bento et al. 2020; Fredericksen et al. in prep). The way they interact with the previously described resistance loci is unknown. We combine genetic crosses in the host and genomic PoolSeq association study to describe the epistatic interactions linking different resistance loci. However, the rare variation for resistance to P15 and P21 observed in our study population impede us to provide strong support to these interactions. Further studies are needed to confirm these interactions in other host populations where more diversity at the loci of interest is observed.

Materials and methods

The resistotype

In the *Daphnia magna–Pasteuria ramosa* host–parasite system, susceptibility (S) or resistance (R) to the parasite is mainly determined at the attachment step, when the bacterial spores attach or not, respectively to the host gut wall. The resistance phenotype, a.k.a. resistotype, corresponds to the attachment phenotype of a *P. ramosa* isolate in a given *D. magna* genotype. The here-used full resistotype depicts the host genotype attachment reaction to five well characterized bacterial isolates (Luijckx et al. 2011; Chapter 1, Ameline et al. 2021; Bento et al. 2020; Chapter 2, Ameline et al. preprint) in the following order: C1, C19, P15, P20 and P21. A host genotype with a RRRRR resistotype shows no attachment to any of the bacterial isolates, while a SSSSS host genotype allows attachment of all bacterial isolates. If isolates are not considered or tested, we use the placeholder "␣", e.g. "RR␣R␣ resistotype".

Host and parasite material

Bacterial isolates come from infected *D. magna* or sediment collected at different geographical locations. Isolates P20 and P21 come from the Aegelsee population and are believed to play a role in the epidemics (Chapters 1 & 2). Isolate P15 was collected in a Belgian *D. magna* population (Bento et al. 2020) and may also play a role in the epidemics of the Aegelsee population (Chapter 2). The inheritance mode of the P20 resistotype has been investigated in Chapter 1, and the present chapter investigates the inheritance mode of resistance to the P15 and P21 *P. ramosa* isolates.

Genetic crosses

To investigate the mode of inheritance of resistance to *P. ramosa* P15 and P21 isolates in the Aegelsee *Daphnia magna* population, we produced groups of F1 offspring by selfing parent clones. Here we consider F1 groups that showed segregation at the P15 and P21 resistotypes. Inbred F1 off-

spring groups were used in Chapter 1, where we considered resistance to C1, C19 and P20. In the present chapter, we consider resistance to P15 and P21 *P. ramosa* isolates. The parent clones used to produce the F1 groups derived from the Aegelsee study population. We selfed one to four *D. magna* clones of the three common resistotypes (RRSRS, RRSSS and SSSSS) and four clones of two rare resistotypes (RRRRR and SRSSS), following the protocol from (Luijckx et al. 2012). Hatching of selfed offspring is not always successful, resulting in uneven sample sizes. We obtained from 19 to 89 selfed F1 offspring from the 24 parent clones (Supplementary Table S3.1). Their resistotypes were assessed with the attachment test, as described in Chapter 2 (Ameline et al. preprint).

PoolSeq association study

From the 24 inbred F1 groups produced, two groups that showed segregation for the P21 resistotype were used for a genome-wide F_{ST} analysis. We categorized the F1 from these two groups into those that were P21 susceptible and those that were P21 resistant. Host clones from these two categories were sequenced as a pool (pool sequencing, or PoolSeq) (Schlötterer et al. 2014). By contrasting the whole genome data of the two pools of each category we expected that loci responsible for the difference between P21-susceptible and P21-resistant would show up with an elevated F_{ST} value.

Resistotype pools contained seven to 25 host genotypes, and one to ten individuals per genotype of approximately the same size were used. The animals went through a three-day antibiotic and gut-cleaning treatment to remove as much as possible alien DNA. We transferred the animals each day in a fresh antibiotics cocktail (50 $g.mL^{-1}$ of Streptomycin, Tetracycline, and Ampicillin) and fed them with small dextran beads as described in (http://evolution.unibas.ch/ebert/lab/daphnia_dna.htm). After the antibiotic treatment, genotypes within resistotype categories were pooled, using five individuals. For each pool, we extracted whole-genome DNA using a QIAGEN Blood and Tissue kit.

DNA was sequenced on an Illumina HiSeq2000, with no amplification step. Raw reads were trimmed using Trimmomatic v. 0.39 (Bolger et al. 2014). Quality of trimmed reads was checked using FastQC v. 0.11.9 (Andrews 2010). Trimmed reads were mapped to the *D. magna* reference genome v. 3.0 (Fields et al. in prep) using BWA MEM v. 0.7.17 (Li and Durbin 2009; Li 2013). We used SAMtools v. 1.10 for data manipulation, filtering and conversion (Li et al. 2009; Li 2011). Picard v. 2.22.8 was run to mark and remove duplicated reads (Broad Institute 2020). Reads with quality lower than 20 were discarded. Coverage along the genome was calculated using BEDTools v. 2.29.2 (Quinlan and Hall 2010) (Supplementary Fig. S3.1). We ran the Popoolation2 v. 1.201 pipeline (Kofler et al. 2011) to calculate SNP allele frequency difference and F_{ST} value between pools. F_{ST} was calculated with a sliding-window approach using 500 bp windows. Graphs were produced using R v. 3.6.2 (R Core Team 2021) and packages ggplot2 v. 3.3.0 (Wickham 2016) and cowplot v. 1.0.0 (Wilke 2019).

Results

Genetic model and resistance diversity

The genetic architecture of resistance to *Pasteuria ramosa* in *Daphnia magna* has been investigated using different approaches and a growing number of parasite isolates (Supplementary Table S3.2 and Figs. S3.2 to S3.8). Variation at the C1 and C19 resistotypes (resistance phenotypes) is determined in the Aegelsee *D. magna* population by variation at the B and C loci (Chapter 1, Ameline et al. 2021) (Metzger et al. 2016). Variation at the P20 resistotype is determined by variation at the C and E loci (Chapter 1, Ameline et al. 2021). Variation at the D and the C loci determines resistance to the P15 *P. ramosa* isolate (Bento et al. 2020). Using a QTL analysis, resistance to P21 was found to be dominant, and a novel genomic region determining resistance, the F locus, was found close to the C locus (Fredericksen et al. in prep). These studies result in a preliminary model of resistance including resistance variation at the five *P. ramosa* isolates (Fig. 3.1A). In this model we consider variation at the D and the F loci independently of variation at the other loci, i.e. without epistatic interaction linking these two loci to the others. However, previous work suggested there might be epistatic interactions among the C, D and F loci, although the nature of these interactions has yet to be resolved (Bento et al. 2020; Fredericksen et al. in prep). In the following, we investigate such potential epistatic relationships linking the C, D and the F loci using selfed F1 groups showing variation at the P15 and P21 resistotypes. We build up our hypothesis from our preliminary model (Fig. 3.1A).

In the Aegelsee *D. magna* population, variation at the resistotype (resistance phenotype) is mainly observed at the C1, C19 and P20 resistotypes and is determined by variation at the C and the E loci (Chapter 1, Ameline et al. 2021).

Here we consider data from 2016 to 2018, when the P15 and P21 *P. ramosa* isolates were additionally tested. We observed that the P15 and P21 resistotypes were mostly "S", as RRSRS, RRSSS and SSSSS (light blue, orange and light orange, respectively in Fig. 3.1A) making up for 80.8±2.3% of the host population across the planktonic phase of three consecutive years. At the time of the peak of the epidemics, we observed a drastic change in resistotype proportions, and resistance to P15 and P21 appeared (Chapter 2, Fig. 2.1A). Until the peak of the epidemic, the three common resistotypes RRSRS, RRSSS and SSSSS made up for 95.7±1.4% of the host population. In late summer, after the peak of the epidemic, the most resistant resistotypes RRRRR (medium blue), RRRRS (dark blue), RRSRS (light blue) and RRSRR (bright blue in Fig. 1A) represented 92.3±2.0% of the population (Chapter 2, Fig. 2.1A). Using genetic crossings and the genetic model of resistance, we inferred in the previous chapters that the "bbDD" genotype was almost fixed in the Aegelsee *D. magna* population (Chapters 1 and 2). Considering that the P21 resistotype is mostly "S", we suppose the "bbDDff" genotype is mostly fixed in the population (see Fig. 3.1A).

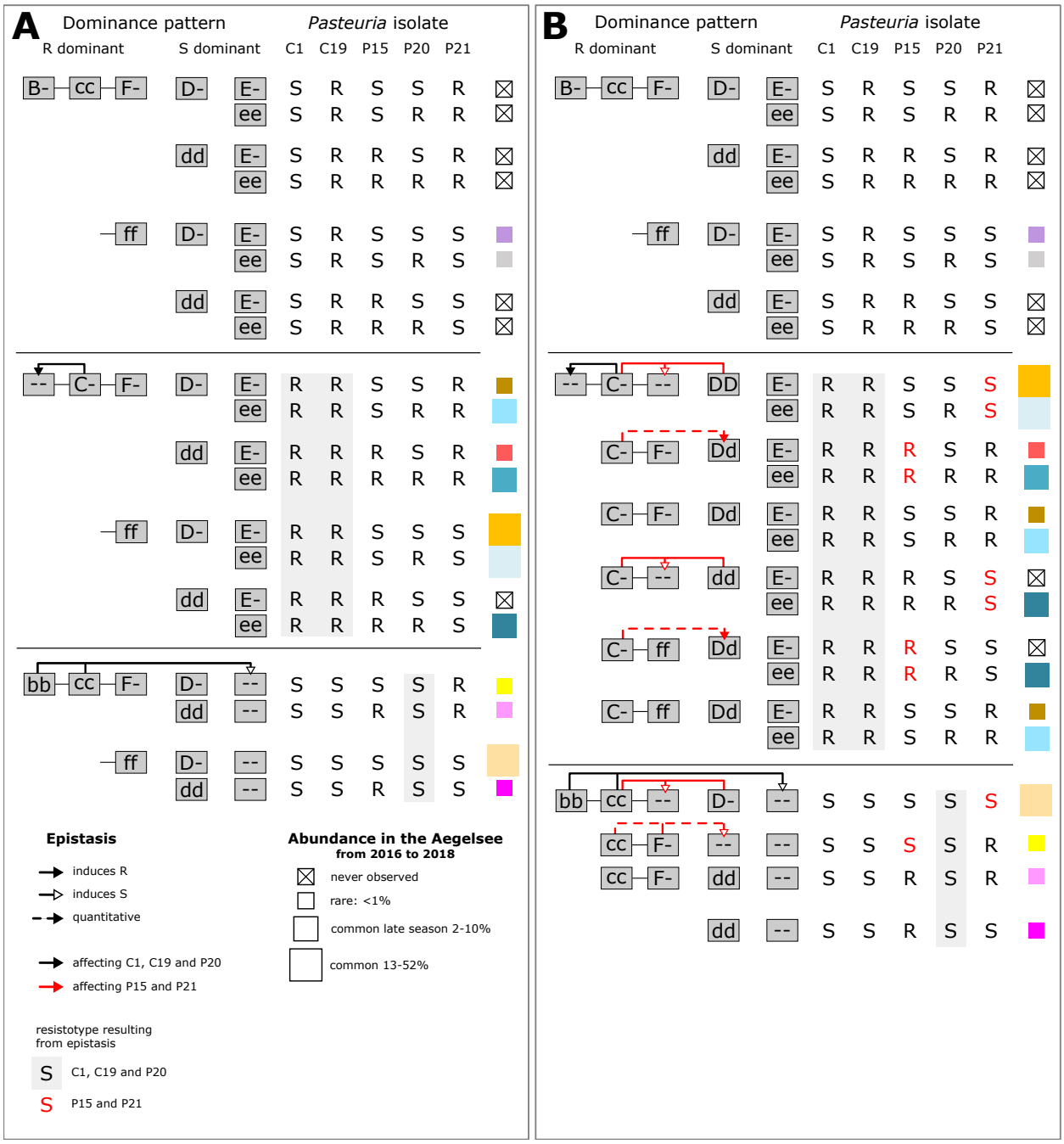

Figure 3.1

Genetic model of resistance to *Pasteuria ramosa* in the *Daphnia magna* Aegelsee population. Grey boxes in the left panel represent resistance loci and are linked with a black line when they are sitting on the same linkage group. Capital letters represent dominant alleles, and arrows represent epistatic interactions. The five-letter string in the right panel represents resistotypes, i.e. resistance phenotypes to the five *P. ramosa* isolates tested for attachment. **A**: Without interaction among the C, D and F loci. This preliminary model was used to investigate potential interactions, described in B. **B**: With interactions among the C, D and F loci described in the present study. The interactions including the C and the c alleles are described in Eq. 3.1 and 3.2, respectively

Genetic crossings

We selfed 24 clones from the Aegelsee population and raised their F1 offspring. Out of the 24 inbred F1 groups created we obtained:

#	Category of inbred group
1	19 groups where P15 and P21 resistotypes did not segregate (Tables 3.1 and 3.2). Results for each selfed F1 group are given in Supplementary Tables S3.3 to S3.14.
2	1 group where P15 and P21 resistotypes segregated and were perfectly coupled, i.e. both resistotypes are “S” or both resistotypes are “R”: parent clone t2_17.3_4 (Table 3.3)
3	1 group with independent segregation of resistance to P15 and P21. We used these F1 group in a PoolSeq association analysis: parent clone MS_2016_b_70 **(Group PoolSeq 1: Tables 3.4 and 3.5, Fig. 3.2)**
4	1 group with P21 resistotype segregation and no P15 resistotype segregation. We used this F1 group for a second PoolSeq association analysis: parent clone CH-H-2015-86 **(Group PoolSeq 2: Tables 3.6 and 3.7, Fig. 3.3)**
5	1 group with rare P15 resistotype variation, and no P21 resistotype segregation: parent clone CH-H-2015-16 (Table 3.8)
6	1 group with rare segregation at the P21 resistotype, and no segregation at the P15 resistotype: parent clone t1_10.3_2 (Table 3.9).

Table 3.1

Genetic crosses of resistance phenotypes (resistotypes) from the Aegelsee *Daphnia magna* population. Parent clones presenting the common variation at the C and E loci. Results for each selfed F1 offspring group are given in Supplementary Tables S3.3 to S3.11 and S3.14.

A

RRSSS aabbCcDDEeff	abCDEf	abCDef	abcDEf	abcDef
abCDEf	RRSSS	RRSSS	RRSSS	RRSSS
abCDef	RRSSS	RRSRS	RRSSS	RRSRS
abcDEf	RRSSS	RRSSS	SSSSS	SSSSS
abcDef	RRSSS	RRSRS	SSSSS	SSSSS

B

F0 parent		F1 offspring						
Inferred genotype	Resistotype	Inferred genotype	Resistotype	Proportion Expected	Observed Repeat a	b	c	C-M-H test on counts
aabbCCDDEEff	RRSSS	aabbCCDDEEff	RRSSS	1	*n* = 43 1	*n* = 37 1		NA
aabbCCDDEeff	RRSSS	aabbCCDDE-ff aabbCCDDeeff	RRSSS RRSRS	0,75 0,25	*n* = 89 0,79 0,21	*n* = 31 0,74 0,26	*n* = 79 0,84 0,16	X^2=0.85, *df*=1, *p*=0.36
aabbCCDDeeff	RRSRS	aabbCCDDeeff	RRSRS	1	*n* = 39 1			NA
aabbCcDDEEff	RRSSS	aabbC-DDEEff aabbccDDEEff	RRSSS SSSSS	0,75 0,25	*n* = 19 0,74 0,26			*Fisher test on counts* *p*=1
aabbCcDDEeff	RRSSS	aabbC-DDE-ff aabbccDD--ff aabbC-DDeeff	RRSSS SSSSS RRSRS	0,56 0,25 0,19	*n* = 48 0,48 0,29 0,23	*n* = 64 0,64 0,14 0,22	*n* = 65 0,52 0,22 0,26	M^2=1.9, *df*=2, *p*=0.39
aabbCcDDeeff	RRSRS	aabbC-DDeeff aabbccDDeeff	RRSRS SSSSS	0,75 0,25	*n* = 36 0,75 0,25	*n* = 49 0,80 0,20	*n*= 22 0,64 0,36	X^2=0.0062, *df*=1, *p*=0.94
aabbccDDEEff	SSSSS	aabbccDDEEff	SSSSS	1	*n* = 87 1			NA
aabbccDDEeff	SSSSS	aabbccDDE-ff	SSSSS	1	*n* = 84 1	*n* = 65 1		NA
aabbccDDeeff	SSSSS	aabbccDDeeff	SSSSS	1	*n* = 74 1			NA

A: Punnett square for all possible gamete combinations according to our genetic model of resistance inheritance (Fig. 3.1A). The table shows the resistotypes (grouped by background colour) resulting from the 16 combinations of gametes from a double heterozygote for the C and the E loci. The bottom right cell (P20 resistotype in red font) represents individuals in the offspring where the epistatic interaction between the C and the E loci is revealed (Fig. 3.1A). **B**: Results from selfing of *D. magna* clones. Resistotypes of F0 parents and F1 offspring groups were obtained using the attachment test and resistance genotypes of F0 parents at the C and E loci were inferred from their resistotypes and the segregation patterns of resistotypes in their F1 offspring. Expected resistotype proportions within F1 groups were calculated following the genetic model presented in the Punnett square. The detailed results and statistical analyses for each cross are presented in Supplementary Tables S3.3 to S3.14. Statistical tests were run on counts, but we present here segregation of offspring as proportions. One to three crosses using distinct parent clonal lines (repeats a to c) were conducted for each F0 parent resistance genotype at the C and E loci. No variation at the B locus was observed (all F0 parents are inferred to have the "bb" genotype according to F1 resistotype segregation).

1. The "bbDDff" genotype is almost fixed in the Aegelsee population

Most of our selfed F1 groups, 19 out of 24, presented no variation at the P15 and P21 resistotypes. Most of the segregation we observed was at the C1, C19 and P20 resistotypes. This segregation is mostly determined by variation at the C and E loci, and rarely by variation at the B locus, as described in Chapter 1. This confirms the result previously inferred from ob-

Table 3.2

Genetic crosses of resistance phenotypes (resistotypes) from the Aegelsee *Daphnia magna* population. The B and the E loci present variation, the C locus is fixed for genotype "cc". Results for each selfed F1 offspring group are given in Supplementary Tables S3.12 to S3.14.

A

SRSSS aaBbccDDEeff	aBcDEf	aBcDef	abcDEf	abcDef
aBcDEf	SRSSS	SRSSS	SRSSS	SRSSS
aBcDef	SRSSS	SRSRS	SRSSS	SRSRS
abcDEf	SRSSS	SRSSS	SSSSS	SSSSS
abcDef	SRSSS	SRSRS	SSSSS	SSSSS

B

F0 parent		F1 offspring				
				Proportion		
Inferred genotype	Resistotype	Inferred genotype	Resistotype	Expected	Observed	Fisher test on counts
					n = 37	
aaBbccDDEEff	SRSSS	aaB-ccDDEEff	SRSSS	0,75	0,76	
		aabbccDDEEff	SSSSS	0,25	0,22	*p*=1
		aaB-ccDDeeff	SRSRS	0,00	0,03	
					n = 38	
aaBbccDDEeff	SRSSS	aaB-ccDDE-ff	SRSSS	0,56	0,55	
		aabbccDDE-ff	SSSSS	0,25	0,32	*p*=0.58
		aaB-ccDDeeff	SRSRS	0,19	0,13	

A: Punnett square for all possible gamete combinations according to our genetic model of resistance inheritance (Fig. 3.1A). The table shows the resistotypes (grouped by background colour) resulting from the 16 combinations of gametes from a double heterozygote for the B and the E loci. The bottom right cell (P20 resistotype in red font) represents individuals in the offspring where the epistatic interaction between the B and the C, and the E loci is revealed (Fig. 3.1A). **B**: Results from selfing of *D. magna* clones. Resistotypes of F0 parents and F1 offspring were obtained using the attachment test and resistance genotypes of F0 parents at the B, C and E loci were inferred from their resistotypes and the segregation patterns of resistotypes in their F1 offspring. Expected resistotype proportions of F1 were calculated following the genetic model as outlined in the Punnett square. The detailed results and statistical analyses for each cross are presented in Supplementary Tables S3 to S14. Statistical tests were run on counts, but we present here segregation of offspring as proportions.

served resistotypes proportions, namely that at the B, D and F loci the b, D, and f alleles are nearly fixed, resulting in the multi-locus genotype "bbDDff" in the study population (Tables 3.1 and 3.2).

2. Variation at the P15 and P21 resistotypes is linked

In one of our selfed F1 group, we observed coupled segregation at the P15 and P21 resistotypes, meaning both resistotypes were "R", or both were "S". In this group, if we consider variation at the C, D and E loci, the genetic model predict well segregation in the F1 selfed offspring, although we observe much less SSSSS than expected (Table 3.3). We infer that the genotype at the F locus might be "ff" because most offspring are P21 susceptible. However, because variation at the P15 and P21 resistotypes is coupled, we cannot infer the genotype at the F locus with certainty. Additionally, this group presents variation at the C and E loci, so we cannot infer a simple epistatic interaction that would explain the observed segregation pattern.

Table 3.3

Selfed genotype aabbCcDdEeff. F0 parent: t2_17.3_4. This selfed F1 group shows coupled segregation for the P15 and P21 resistotypes. The C, D and the E loci present variation, the B locus is fixed for genotype "bb" and we suggest the genotype at the F locus might be "ff".

A

RRSSS aabbCcDdEeff	abCDEf	abCDef	abcDEf	abcDef	abCdEf	abCdef	abcdEf	abcdef
abCDEf	RRSSS	RRSSS	RRSSS	RRSSS	RRSSS	RRSSS	RRSSS	RRSSS
abCDef	RRSSS	RRSRS	RRSSS	RRSRS	RRSSS	RRSRS	RRSSS	RRSRS
abcDEf	RRSSS	RRSSS	SSSSS	SSSSS	RRSSS	RRSSS	SSSSS	SSSSS
abcDef	RRSSS	RRSRS	SSSSS	SSSSS	RRSSS	RRSRS	SSSSS	SSSSS
abCdEf	RRSSS	RRSSS	RRSSS	RRSSS	RRRSR	RRRSR	RRRSR	RRRSR
abCdef	RRSSS	RRSRS	RRSSS	RRSRS	RRRSR	RRRRR	RRRSR	RRRRR
abcdEf	RRSSS	RRSSS	SSSSS	SSSSS	RRRSR	RRRSR	SSRSR	SSRSR
abcdef	RRSSS	RRSRS	SSSSS	SSSSS	RRRSR	RRRRR	SSRSR	SSRSR

B

F0 parent		F1 offspring				
Inferred genotype	Resistotype	Inferred genotype	Resistotype	Proportion		Fisher test on counts
				Expected	Observed	
					n = 34	
aabbCcDdEeff	RRSSS	aabbC-DDE-ff	RRSSS	0,42	0,44	
		aabbccDD--ff	SSSSS	0,19	0,03	
		aabbC-DDeeff	RRSRS	0,14	0,26	
		aabbC-ddE-ff	RRRSR	0,14	0,12	*p* = 0.42
		aabbccdd--ff	SSRSR	0,06	0,06	
		aabbC-ddeeff	RRRRR	0,05	0,09	

A: Punnett square for all possible gamete combinations according to our genetic model of resistance inheritance (Fig. 3.1A). The table shows the resistotypes (grouped by background colour) resulting from the 64 combinations of gametes from a triple heterozygote for the C, D and E loci. Alleles at loci where the genotype does not vary are written in grey. The P20 resistotype in red font represents individuals in the offspring where the epistatic interaction between the B and the C, and the E loci is revealed (Fig. 3.1A). The P21 resistotype is written in bold in case where the phenotype does not match the underlying genotype. **B**: Results from selfing of the *D. magna* t2_17.3_4 clone compared to expectations from the Punnett square. Resistotypes of the F0 parent and F1 offspring were obtained using the attachment test and the resistance genotype of the F0 parent was inferred from its resistotype and the segregation pattern of resistotypes in its F1 offspring. Expected resistotype proportions of F1 were calculated following the genetic model as outlined in the Punnett square. Statistical test was run on counts, but we present here segregation of offspring as proportions.

3. Epistatic interaction #1 among the C, D and F loci

In one of our selfed F1 group, we observed uncoupled variation at the P15 and P21 resistotypes, meaning that all four combinations were observed (_ _S_S, _ _S_R, _ _R_S, and _ _R_R). From the observed resistotype segregation in the F1 offspring (Table 3.4), we inferred that this parent F0 clone presented a fixed genotype at the B, C and E loci ("bbCCee") and was heterozygous at the D and F loci (Table 3.5A and B). However, this inferred parent genotype produces a segregation in the F1 that fits qualitatively the expected one, but not qualitatively. This means that we observe the expected resistotype combinations, but not in the expected proportions (Table 3.5B). Additionally, the parent clone has a "RRRRR" resistotype whereas the inferred genotype would produce a "RRSRR" resistotype. There may thus exist epistatic interactions that explain this result and that would allow us to get a better fit between expected and observed resistotype segregation in the selfed F1 offspring.

F0 parent	F1 offspring			
Resistotype		n = 79	100%	n(PoolSeq)
RRRRR	RRRRR	24	30%	19
	RRSRS	32	41%	
	RRRRS	20	25%	20
	RRSRR	3	4%	

Table 3.4

Genetic crossing in the *Daphnia magna* Aegelsee population. Resistotype segregation in the selfed F1 offspring and sampling for the PoolSeq association analysis. Selfed F0 parent: CH-H-2016-b-70. This selfed F1 group presented decoupled segregation at the P15 and P21 resistotypes. The PoolSeq analysis aimed to investigate segregation at the P21 resistotype. This segregation is highlighted in white font, and the sample size of the PoolSeq corresponds to the number of clones pooled for subsequent sequencing within both resistotype groups.

Table 3.5

Genetic crossing in the Aegelsee *Daphnia magna* population. Selfed genotype bbCCDdeeFf. F0 parent: CH-H-2016-b-70. This selfed F1 offspring group shows decoupled segregation for the P15 and P21 resistotypes. PoolSeq association study shows evidence for segregation at the D locus. The D and F loci present variation, the B, C and the E loci are fixed for the "bbCCee" genotype.

A

RRSRR aabbCCDdeeFf	abCDeF	abCDef	abCdeF	abCdef
abCDeF	RRSRR	RRSRR	RRSRR	RRSRR
abCDef	RRSRR	RRSRS	RRSRR	RRSRS
abCdeF	RRSRR	RRSRR	RRRRR	RRRRR
abCdef	RRSRR	RRSRS	RRRRR	RRRRS

B

F0 parent		F1 offspring				
Inferred genotype	Resistotype	Inferred genotype	Resistotype	Proportion Expected	Proportion Observed	Fisher test on counts
					n = 79	
aabbCCDdeeFf	RRSRR	aabbCCD-eeF-	RRSRR	0,56	0,04	
		aabbCCD-eeff	RRSRS	0,19	0,42	
		aabbCCddeeF-	RRRRR	0,19	0,30	$p < 0.0001$
		aabbCCddeeff	RRRRS	0,06	0,24	

C

RRRRR aabbCCDdeeFf	abCDeF	abCDef	abCdeF	abCdef
abCDeF	RRSRS	RRSRS	RRRRR	RRRRR
abCDef	RRSRS	RRSRS	RRRRR	RRSRS
abCdeF	RRRRR	RRRRR	RRRRS	RRRRS
abCdef	RRRRR	RRSRS	RRRRS	RRRRS

D

F0 parent		F1 offspring				
Inferred genotype	Resistotype	Inferred genotype	Resistotype	Proportion Expected	Proportion Observed	Fisher test on counts
					n = 79	
aabbCCDdeeFf	RRRRR	aabbCCDdeeF-	RRRRR	0,38	0,30	
		aabbCCD-eeff	RRSRS	0,38	0,42	
		aabbCCDDeeF-	RRSRS			
		aabbCCddeeF-	RRRRS	0,25	0,24	$p = 0.34$
		aabbCCddeeff	RRRRS			
		aabbCCD-eeF-	RRSRR	0,00	0,04	

A and B: segregation without epistatic interaction. **A:** Punnett square for all possible gamete combinations according to our genetic model of resistance inheritance (Fig. 3.1A). The table shows the resistotypes (grouped by background colour) resulting from the 16 combinations of gametes from a double heterozygote for the D and F loci. Alleles at homozygous loci are written in grey. **B**: Results from selfing of the *D. magna* CH-H-2016-b-70 clone compared to expectations from the Punnett square. Resistotypes of the F0 parent and F1 offspring were obtained using the attachment test and the resistance genotype of the F0 parent was inferred from its resistotype and the segregation pattern of resistotypes in its F1 offspring. Expected resistotype proportions of F1 were calculated following the genetic model as outlined in the Punnett square. Statistical test was run on counts, but we present here segregation of offspring as proportions. **C and D: segregation with epistatic interaction**. **C**: Same as A, with added epistatic interactions that give a better fit between expected and observed resistotype segregation. Additionally, the presented epistatic interactions fit the PoolSeq analysis result that RRRRR ("dd" genotype) and RRRRS ("D-" genotype) F1 offspring clones present variation at the D locus. Resistotypes where an epistatic interaction is revealed are written in red font. **D**: Same as B, considering the epistatic interactions proposed in C. These epistatic interactions are described in Fig. 3.1B.

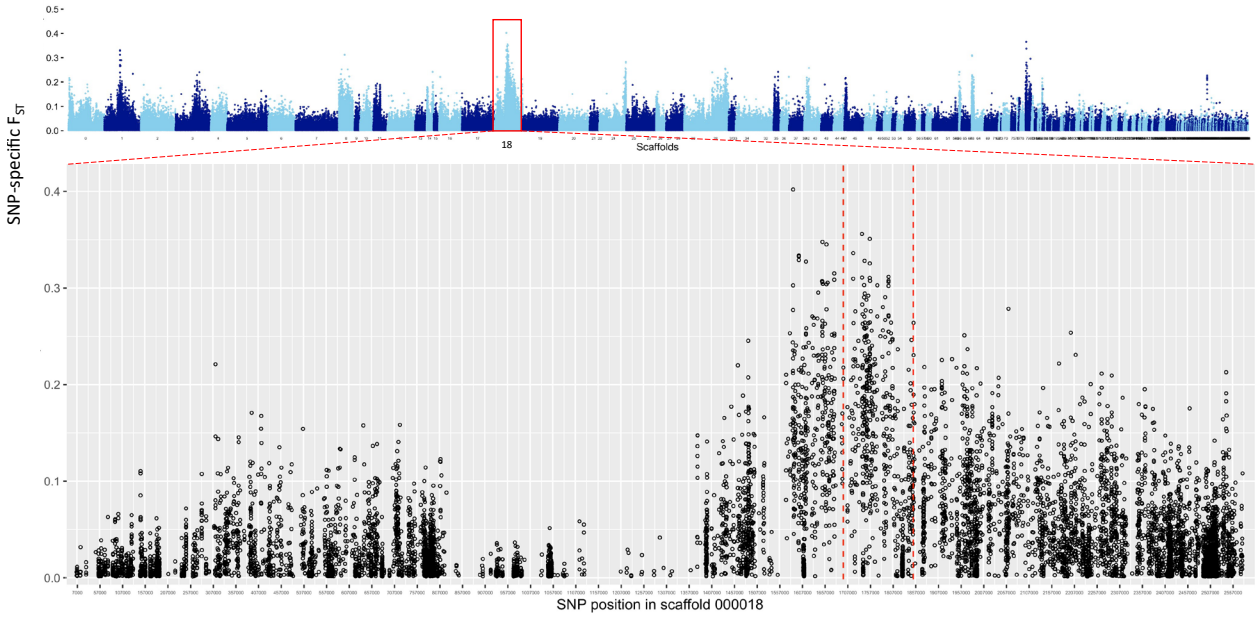

Figure 3.2

PoolSeq association for the selfed F1 offspring group from the MS_2016_b_70 parent *Daphnia magna* clone. The parent clone presents the RRRRR resistance phenotype (resistotype). The two pools present the RRRRR (n = 19) and RRRRS (n = 20) resistotypes. **A**: Genome-wide SNP-specific F_{ST} value, the x-axis represents single nucleotide polymorphisms (SNPs). **B**: SNP-specific F_{ST} value mapped on SNP position on scaffold 18 of the *D. magna* reference genome v. 3.0 (Fields et al. in prep). The D-locus position (falcon_000018F:1698391-1852181) is indicated with the red dotted lines.

To get a second line of evidence for potential epistatic interactions affecting the P15 and P21 resistotypes, we performed a PoolSeq association analysis between two resistotype groups. As this analysis was initially intended to investigate variation solely at the P21 resistotype, we compared pools of F1 clones within the selfed F1 group that presented variation only at the P21 resistotype. We compared clones with the RRRRR resistotype and clones with the RRRRS resistotype (Table 3.4), and found an F_{ST} peak on scaffold 18 (Fig. 3.2), where the D locus has been described (Bento et al. 2020). We did not find SNPs associated to the P21 resistotype in the genomic regions that we know determine resistance to the C1, C19 and P20 *P. ramosa* isolates (the ABC cluster and the E locus) (Bento et al. 2017; Chapter 1, Ameline et al. 2021). As variation at the P21 resistotype has been found to be determined by the F locus, standing next to the ABC cluster, we expected to pinpoint this region when confronting pools of clones with the RRRRR vs. RRRRS resistotypes. Rather, our result detected variation at the D locus between the two groups, showing that there may be epistatic interactions between the D and the F loci (and potentially the other resistance loci) influencing the P21 resistotype.

We thus intended to describe epistatic interactions that could explain these two results: (i) the observed resistotype segregation in the selfed F1 group and (ii) variation at the D locus between the RRRRR and the RRRRS resistotypes. We considered the Punnet square of the double heterozygote at the D and F loci (Table 3.5A) and modified resistotypes to obtain an expected resistotype segregation that would fit the observed one (Table 3.5C and D). To fit the PoolSeq association result, this segregation expectation should additionally have one of the RRRRR and RRRRS groups homozygous at the

D locus. Alternatively, one could be homozygous recessive and the other one dominant.

We find that variation at the D locus could explain the observed pattern, independently from variation at the F locus. Namely, a "DD" genotype would induce susceptibility to P21, a "Dd" genotype would induce resistance to P15 and a "dd" genotype would induce susceptibility to P21, regardless of the genotype at the F locus (Table 3.5C and D). We still find about 1/16 of RRSRR (bright blue), that are not expected, less RRRRR (medium blue) than expected and less RRSRS (light blue) than expected in the observed selfed F1 offspring. This could be explained by one of these interactions being quantitative, namely, the "Dd" genotype would not always induce susceptibility to P15 (Table 3.5C and D).

In the next example, we also infer a double heterozygote at the D and the F loci, but with a different genetic background. Namely, the present selfed F1 group has the "CC" genotype whereas the next F1 group has the "cc" genotype. As the epistatic interactions we deduce from both F1 groups are incompatible if we consider only the D and the F loci, we additionally consider the C locus as playing a role in these interactions. In summary, we obtain for the present F1 group the epistatic interactions presented in Eq. 3.1. Arrows represent epistatic interactions; a dashed arrow represents a quantitative epistatic interaction. We apply these interactions to our genetic model in Fig. 3.1B.

```
C-DD → P21 S
C-Dd ⇢ P15 R        ( Eq. 3.1 )
C-dd → P21 S
```

4. Epistatic interaction #2 among the C, D and F loci

In one of our selfed F1 group, we observed variation at the P21 resistotype, but not at the P15 resistotype, as these two combinations were observed: _ _S_S and _ _S_R. The parent F0 clone is SSSSS, and its selfed F1 offspring is SS_ _ _ (Table 3.6), thus the parent presents a fixed genotype at the B and C loci ("bbcc"). An epistatic interaction between the B, C and the E loci induces susceptibility to P20 when the "bbcc" genotype is present, regardless of the genotype at the E locus (Fig. 3.1A, Chapter 1, Ameline et al. 2021). We could thus not infer the genotype at the E locus from phenotypic data. However, these F1 groups were scored for their genotype at the C and E loci using genetic markers (Chapter 1, Ameline et al. 2021). This scoring revealed that this selfed F1 group was homozygous recessive at the E locus ("ee").

F0 parent	F1 offspring			
Resistotype		n = 35	100%	n(PoolSeq)
SSSSS	SSSSS	27	77%	25
	SSSSR	8	23%	7

Table 3.6

Genetic crossing in the *Daphnia magna* Aegelsee population. Resistotype segregation in the selfed F1 offspring and sampling for the PoolSeq association analysis. Selfed F0 parent: CH-H-2015-86. This selfed F1 group presented segregation at the P21 resistotype, decoupled from the P15 resistotype. The PoolSeq analysis aimed to investigate segregation at the P21 resistotype. This segregation is highlighted in black font, and the sample size of the PoolSeq corresponds to the number of clones pooled for subsequent sequencing within both resistotype groups.

Table 3.7

Genetic crossing in the Aegelsee *Daphnia magna* population. F0 parent: CH-H-2015-86. This selfed F1 offspring group shows segregation for the P21 resistotype, but not for the P15 resistotype. PoolSeq association study shows evidence for segregation at the D-locus. The B, C and the E loci are fixed for the "bbccee" genotype.

A

SSSSS aabbccDDeeFf	abcDeF	abcDef
abcDeF	SSSSS	SSSSS
abcDef	SSSSS	SSSSR

B

F0 parent		F1 offspring				
				Proportion		
Inferred genotype	Resistotype	Inferred genotype	Resistotype	Expected	Observed	Fisher test on counts
					n = 35	
aabbccDDeeFf	SSSSS	aabbccDDeeF-	SSSSS	0,75	0,77	*p* = 1
		aabbccDDeeff	SSSSR	0,25	0,23	

C

SSSSR aabbccDdeeFf	abcDeF	abcDef	abcdeF	abcdef
abcDeF	SSSSR	SSSSR	SSSSR	SSSSR
abcDef	SSSSR	SSSSS	SSSSR	SSSSS
abcdeF	SSSSR	SSSSR	SSRSR	SSRSR
abcdef	SSSSR	SSSSS	SSRSR	SSRSS

D

F0 parent		F1 offspring				
				Proportion		
Inferred genotype	Resistotype	Inferred genotype	Resistotype	Expected	Observed	Fisher test on counts
					n = 35	
aabbccD-eeF-	SSSSR	aabbccD-eeF-	SSSSR	0,56	0,23	
		aabbccD-eeff	SSSSS	0,19	0,77	*p* < 0.0001
		aabbccddeeff	SSRSR	0,19	0,00	
		aabbccddeeff	SSRSS	0,06	0,00	

E

SSSSS aabbccDdeeFf	abcDeF	abcDef	abcdeF	abcdef
abcDeF	SSSSS	SSSSS	SSSSS	SSSSS
abcDef	SSSSS	SSSSS	SSSSS	SSSSS
abcdeF	SSSSS	SSSSS	SSSSR	SSSSR
abcdef	SSSSS	SSSSS	SSSSR	SSRSS

F

F0 parent		F1 offspring				
				Proportion		
Inferred genotype	Resistotype	Inferred genotype	Resistotype	Expected	Observed	Fisher test on counts
					n = 35	
aabbccDdeeFf	SSSSS	aabbccD-eeF-	SSSSS	0,75	0,77	
		aabbccD-eeff	SSSSS			
		aabbccddeeF-	SSSSR	0,19	0,23	*p* = 0.62
		aabbccddeeff	SSRSS	0,06	0,00	

A and B: resistance is recessive at the F locus, variation only at the F locus, no epistatic interaction. **A:** Punnett square for all possible gamete combinations according to our genetic model of resistance inheritance (Fig. 3.1A). The table shows the resistotypes (grouped by background colour) resulting from the four combinations of gametes from a heterozygote at the F locus. Alleles at homozygous loci are written in grey. **B**: Results from selfing of the *D. magna* CH-H-2015-86 clone compared to expectations from the Punnett square. Resistotypes of the F0 parent and F1 offspring were obtained using the attachment test and the resistance genotype of the F0 parent was inferred from its resistotype and the segregation pattern of resistotypes in its F1 offspring. Expected resistotype proportions of F1 were calculated following the genetic model as outlined in the Punnett square. Statistical test was run on counts, but we present here segregation of offspring as proportions. **C to F: variation at the D and F loci. C and D: segregation without epistatic interaction**. **C:** Same as A, the table shows the resistotypes resulting from the 16 combinations of gametes from a double heterozygote at the D and F loci. **D**: Same as B, considering the Punnett square in C. **E and F: segregation with epistatic interaction**. **E**: Same as C, with added epistatic interactions that give a better fit between expected and observed resistotype segregation. Additionally, the presented epistatic interactions fit the PoolSeq analysis result that SSSSR ("dd" genotype) and SSSSS ("D-" genotype) F1 offspring clones present variation at the D locus. Resistotypes where an epistatic interaction is revealed are written in red font. **F**: Same as D, considering the epistatic interactions proposed in E. These epistatic interactions are described in Fig. 3.1B

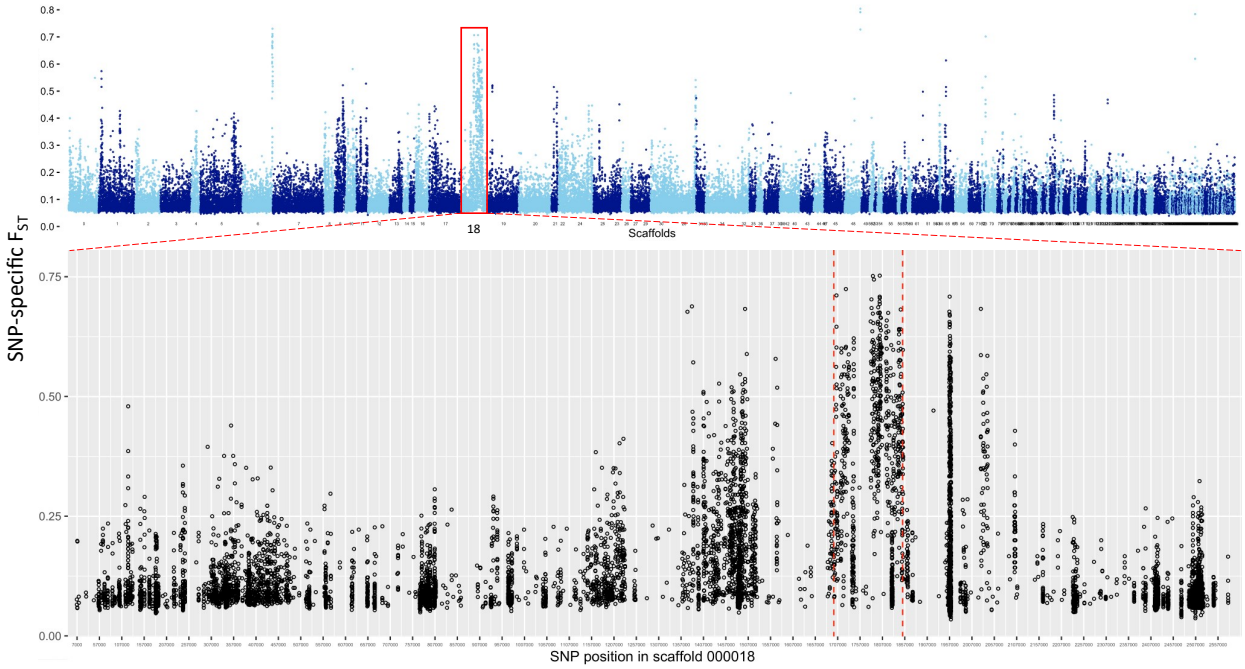

Figure 3.3

PoolSeq association for the F1 inbred offspring group from the CH-H-2015-86 parent *Daphnia magna* clone. The parent clone presents the SSSSS resistance phenotype (resistotype). The two pools present the SSSSS (n = 25) and SSSSR (n = 7) resistotypes. **A**: Genome-wide SNP-specific F_{ST} value, the x-axis represents single nucleotide polymorphisms (SNPs). **B**: SNP-specific F_{ST} value mapped on SNP position on scaffold 18 of the *D. magna* reference genome v. 3.0 (Fields et al. in prep). The D-locus position (falcon_000018F:1698391-1852181) is indicated with the red dotted lines.

In the present selfed F1 group, we observed a roughly ¾ P21-susceptible: ¼ P21-resistant segregation. This suggested that resistance could be recessive at the F locus (Table 3.7A and B), although the opposite was found in the previous study using a QTL analysis (Fredericksen et al. in prep). However, similarly to the previous F1 group, we performed a PoolSeq analysis opposing SSSSS and SSSSR, and found that the genomic region responsible for this variation at the P21 resistotype was not the F locus, but the D locus (Fig. 3.3), revealing that the genotype at the D locus was varying in the offspring. As this could not be explained in a scenario where resistance would be recessive at the F locus, we considered resistance dominant at the F locus.

The expected resistotype segregation from selfing of a double heterozygote at the D and the F loci, with the "bbccee" genotype does not fit our observed segregation, neither qualitatively nor quantitatively (Table 3.7C and D). Additionally, the parent clone has a "SSSSS" resistotype whereas the inferred genotype would produce a "SSSSR" resistotype. We thus investigated potential epistatic interactions that could explain the observed resistotype segregation. Following the same reasoning as in the previous F1 group, we considered the Punnett square of the selfing of the F0 "bbccDdeeFf" parent (Table 3.7C) and modified resistotypes to obtain an expected resistotype segregation that would fit the observed one (Table 3.7E and F). To fit the PoolSeq association result, this segregation expectation should additionally have one of the SSSSS and SSSSR groups homozygous at the D locus. Alternatively, one could be homozygous recessive and the other one dominant.

We find that variation at the D and the F loci could explain the observed pattern. Namely, a "D-" genotype would induce susceptibility to P21, and a "F-" genotype would induce susceptibility to P15 (Table 3.7E and F). These interactions produce and expected segregation that fits much better the observed one, however, we expect SSRSS in the offspring, which we do not observe. This could be explained by one of these interactions being quantitative, namely, the "F-" genotype would not always induce susceptibility to P15 (Table 3.7E and F).

Like in the previous example, we consider here the genotype at the C locus to take part in the proposed epistatic interaction. Indeed, we also infer a double heterozygote at the D and the F loci, but with a different genetic background at the C locus. Namely, the present selfed F1 group has the "cc" genotype whereas the previous F1 group has the "CC" genotype. As the epistatic interactions we deduce from both F1 groups are incompatible if we consider only the D and the F loci, we additionally consider the C locus as playing a role in these interactions. In summary, we obtain for the present F1 group the epistatic interactions presented in Eq. 3.2. Arrows represent epistatic interactions; a dashed arrow represents a quantitative epistatic interaction. We apply these interactions to our genetic model in Fig. 3.1B.

$$\begin{aligned} ccD- &\rightarrow P21\ S \\ ccF- &\dashrightarrow P15\ S \end{aligned} \qquad \text{(Eq. 3.2)}$$

5. The C allele may confer some resistance to P15

In one of our selfed F1 group, we observed rare variation at the P15 resistotype, but no variation at the P21 resistotype. The F0 parent and most of the selfed F1 offspring were RRSRS. From the genetic model (Fig. 3.1A) we inferred that the genotype in this group should be "bbCCDDeeff". However, we observed rare variation in the offspring as we got a few RRRRS individuals (Table 3.8). In the QTL analysis investigating variation at the P15 resistotype, it was suggested that the C allele may induce quantitative resistance to P15, regardless of the genotype at the D locus (Bento et al. 2020). This could explain the pattern observed here, as the C allele is present in this F1 group and we observe unexpected resistance to P15. However, we did not observe unexpected resistance to P15 in the F1 group presented in Table 3.5, where the same inferred genotype was present.

6. Rare segregation at the P21-resistotype

In one of our selfed F1 groups, we observed rare resistotype segregation at the P21 resistotype, but not at the P15 resistotype. The F0 parent and most of the offspring were RRRRR. From the genetic model (Fig. 3.1A) we inferred the genotype in this group to be "bbCCddeeFF". However, we observed one RRRRS individual in the offspring (Table 3.9). This result is consistent with the epistatic interaction described in (Eq. 3.1) stating that a "C-dd" would confer susceptibility to P21, although this interaction would work very weakly in the present F1 group.

Table 3.8

Genetic crossing in the Aegelsee *Daphnia magna* population. F0 parent: CH-H-2015-16. This selfed F1 offspring group shows rare segregation at the P15 resistotype, but no segregation at the P21 resistotype.

A

RRSRS aabbCCDDeeff	abCDef
abCDef	RRSRS RRRRS

B

F0 parent		F1 offspring				
Inferred genotype	Resistotype	Inferred genotype	Resistotype	Proportion		Fisher test on counts
				Expected	Observed	
					n = 70	
aabbCCDDeeff	RRSRS	aabbCCDDeeff	RRSRS	1	0,96	*p* = 0.24
			RRRRS	0	0,04	

A: Punnett square for the unique possible gamete combination according to our genetic model of resistance inheritance (Fig. 3.1A). The table shows the resistotypes (grouped by background colour) resulting from the unique combination of gametes resulting from a homozygous parent, and from a possible epistatic interaction. **B**: Results from selfing of the *D. magna* CH-H-2015-16 clone compared to expectations from the Punnett square. Resistotypes of the F0 parent and F1 offspring were obtained using the attachment test and the resistance genotype of the F0 parent was inferred from its resistotype and the segregation pattern of resistotypes in its F1 offspring. Expected resistotype proportions of F1 were calculated following the genetic model as outlined in the Punnett square. Statistical test was run on counts, but we present here segregation of offspring as proportions.

Table 3.9

Genetic crossing in the Aegelsee *Daphnia magna* population. F0 parent: t1_10.3_2. This selfed F1 offspring group shows rare segregation at the P21 resistotype, but no segregation at the P15 resistotype.

A

RRRRR aabbCCddeeFF	abCdeF
abCdeF	RRRRR RRRRS

B

F0 parent		F1 offspring				
Inferred genotype	Resistotype	Inferred genotype	Resistotype	Proportion		Fisher test on counts
				Expected	Observed	
					n = 42	
aabbCCddeeFF	RRRRR	aabbCCddeeFF	RRRRR	1	0,98	*p* = 1
			RRRRS	0	0,02	

A: Punnett square for the unique possible gamete combination according to our genetic model of resistance inheritance (Fig. 3.1A). The table shows the resistotypes (grouped by background colour) resulting from the unique combination of gametes resulting from a homozygous parent, and from a possible epistatic interaction. **B**: Results from selfing of the *D. magna* t1_10.3_2 clone compared to expectations from the Punnett square. Resistotypes of the F0 parent and F1 offspring were obtained using the attachment test and the resistance genotype of the F0 parent was inferred from its resistotype and the segregation pattern of resistotypes in its F1 offspring. Expected resistotype proportions of F1 were calculated following the genetic model as outlined in the Punnett square. Statistical test was run on counts, but we present here segregation of offspring as proportions.

Discussion and perspectives

In the present study we investigated the mode of inheritance of *Pasteuria ramosa* P15 and P21 resistotypes (resistance phenotypes) in the Aegelsee *Daphnia magna* population. These resistotypes are susceptible in about 80% of the host population across the planktonic season. Variation at the P15 and P21 resistotypes is thus rare in the population, which makes it difficult to test hypotheses about their mode of inheritance. Towards the end of the planktonic season, however, we observe variation at these resistotypes, which we used to produce genetic crosses to investigate the mode of inheritance of resistance to P15 and P21.

We describe in this study genetic crosses and genomic associations from which we infer possible epistatic interactions among the C, D and F loci determining resistance to P15 and P21. Our results emphasize, along with other studies on plants and animals (Kover and Caicedo 2001; Wilfert and Schmid-Hempel 2008; Jones et al. 2014; González et al. 2015; Metzger et al. 2016), the essential role of epistasis and dominance in shaping the genetic architecture of resistance to parasites. Indeed, all the resistance loci described in *D. magna* have been found to epistatically interact among one another and to present dominance patterns. Multi-locus polymorphisms have been shown to determine resistance to parasites (Sasaki 2000; Cerqueira et al. 2017). To date, in the *D. magna–P. ramosa* system, a total of seven resistance loci determining attachment of the parasite have been described (Metzger et al. 2016; Bento et al. 2017; Gattis 2018; Chapter 1, Ameline et al. 2021; Fredericksen et al. 2021), which is consistent with the theoretical importance of multi-locus polymorphisms in a host–parasite coevolution context (Tellier and Brown 2007).

We describe here epistatic interactions that display more complexity than the previous ones described, as they consider variation at three different loci and present quantitative effects (Fig. 3.1B). Although some of the epistatic interactions described here seem weaker, strong epistasis is involved in the genetic architecture of resistance in the system overall. Additionally, a weaker epistatic interaction could be the result of interactions with other loci that we do not consider.

To confirm the interactions described here among the C, D and F loci, we further need to test all the possible allele combinations at these three loci. Additionally, these interactions should be tested in different genetic backgrounds at the other three resistance loci we know of, the A, B and E loci. The A locus is fixed for the recessive allele in the Aegelsee population, we thus do not know how it interacts with the other loci in this population. The B allele is rare in the population, and we do not take it into account in the described interactions. More variation is observed in other populations of *D. magna*, where it can be used in further genetic crossings and genomic association studies. The genetic model of resistance to C1, C19 and P20 was described using host clones coming from Finland, Germany and the Aegelsee population (Metzger et al. 2016; Chapter 1, Ameline et al. 2021). Previous work showed that this model was mostly consistent when using a wide diversity of host clones coming from the whole geographic distribution of *D. magna* (Gattis 2018). We thus suppose that the genetic model described here should mostly hold in other *D. magna* populations, allowing us to use these populations to investigate additional variation at the P15 and P21 resistotypes.

Looking at the resistotype abundances in the Aegelsee population, we initially inferred that the "DDff" genotype might be almost fixed. However, the new epistatic interactions described here reveal that the genotype at the F locus might not play an important role in the observed resistotype abundances in the population, as it is mostly "hidden" by epistatic interactions (Fig. 3.1B).

This study provides insights into the inheritance mode of resistance in a well-studied host–parasite system. We unveil strong and complex epistatic interactions determining resistance in the host. Epistasis being central in the Red Queen theory for the maintenance of genetic diversity and recombination in the host (Hamilton 1980; Hamilton et al. 1990; Howard and Lively 1998; Salathé et al. 2008; Engelstädter and Bonhoeffer 2009; Kouyos et al. 2009), we therefore provide empirical evidence to support theories in the wider context of host–parasite coevolution and the maintenance of sex.

Acknowledgments

We thank Jürgen Hottinger, Urs Stiefel, Kristina Müller, Michelle Krebs, Peter Fields and Jelena Rakov for help in the laboratory. Sequencing for the PoolSeq analysis was performed at the Genomics Facility at the Department of Biosystem Science and Engineering (D-BSSE, ETH) in Basel. The AB3130xl sequencer used for the markers analysis was operated by Nicolas Boileau. Members of the Ebert group provided valuable feedback on the study. This work was funded by the Swiss National Science Foundation (SNSF) grant No 310030B_166677 to DE, the Freiwillige Akademische Gesellschaft (FAG) Basel to CA, the University of Basel to DE.

Authors contribution

DE and CA designed the study. CA produced the genetic crossings and the genomic raw data. CCA conducted the PoolSeq analysis and produced the corresponding figures. MH provided a pipeline for PoolSeq data analysis. CA analyzed the data, wrote the manuscript, and produced the figures.

References

Agrawal A, Lively CM. 2002. Infection genetics: gene-for-gene versus matching-alleles models and all points in between. *Evolutionary Ecology Research* **4**:79–90.

Ameline C, Vögtli F, Andras JP, Dexter E, Engelstädter J, Ebert D. preprint. Genetic slippage after sex maintains diversity for parasite resistance in a natural host population. *bioRxiv*.

Ameline C, Vögtli F, Savola E, Bourgeois Y, Andras JP, Engelstädter J, Ebert D. 2021. A two-locus system with strong epistasis underlies rapid parasite-mediated evolution of host resistance. *Molecular Biology and Evolution* **38**:1512–1528.

Andrews S. 2010. FastQC: A quality control tool for high throughput sequence data. Available from: http://www.bioinformatics.babraham.ac.uk/projects/fastqc/

Bangham J, Knott SA, Kim K-W, Young RS, Jiggins FM. 2008. Genetic variation affecting host–parasite interactions: major-effect quantitative trait loci affect the transmission of sigma virus in *Drosophila melanogaster*. *Molecular Ecology* **17**:3800–3807.

Bento G, Fields PD, Duneau D, Ebert D. 2020. An alternative route of bacterial infection associated with a novel resistance locus in the *Daphnia–Pasteuria* host–parasite system. *Heredity* **125**:173–183.

Bento G, Routtu J, Fields PD, Bourgeois Y, Du Pasquier L, Ebert D. 2017. The genetic basis of resistance and matching-allele interactions of a host–parasite system: The *Daphnia magna–Pasteuria ramosa* model. *PLOS Genetics* **13**:e1006596.

Bolger AM, Lohse M, Usadel B. 2014. Trimmomatic: a flexible trimmer for Illumina sequence data. *Bioinformatics* **30**:2114–2120.

Bourgeois Y, Roulin AC, Müller K, Ebert D. 2017. Parasitism drives host genome evolution: Insights from the *Pasteuria ramosa–Daphnia magna* system. *Evolution* **71**:1106–1113.

Broad Institute. 2020. Picard Tools. Available from: http://broadinstitute.github.io/picard/

Cao C, Magwire MM, Bayer F, Jiggins FM. 2016. A polymorphism in the processing body component Ge-1 controls resistance to a naturally occurring Rhabdovirus in *Drosophila*.Schneider DS, editor. *PLOS Pathogens* **12**:e1005387.

Cerqueira GC, Cheeseman IH, Schaffner SF, Nair S, McDew-White M, Phyo AP, Ashley EA, Melnikov A, Rogov P, Birren BW, et al. 2017. Longitudinal genomic surveillance of *Plasmodium falciparum* malaria parasites reveals complex genomic architecture of emerging artemisinin resistance. *Genome Biology* **18**:1–13.

Cogni R, Cao C, Day JP, Bridson C, Jiggins FM. 2016. The genetic architecture of resistance to virus infection in *Drosophila*. *Molecular Ecology* **25**:5228–5241.

Duneau D, Luijckx P, Ben-Ami F, Laforsch C, Ebert D. 2011. Resolving the infection process reveals striking differences in the contribution of environment, genetics and phylogeny to host–parasite interactions. *BMC biology* **9**:1–11.

Ebert D. 2005. Ecology, epidemiology, and evolution of parasitism in *Daphnia*. Bethesda, MD: National Library of Medicine (US), National Center for Biotechnology Information

Engelstädter J, Bonhoeffer S. 2009. Red Queen dynamics with non-standard fitness interactions.Stormo GD, editor. *PLoS Computational Biology* **5**:e1000469.

Fields PD et al. in prep. *Daphnia magna* reference genome 3.0.

Fredericksen M, Fields PD, Bento G, Ebert D. in prep. QTL and fine mapping parasite resistance in *Daphnia magna*.

Gattis S. 2018. Segregation of resistance to the parasite *Pasteuria ramosa* in the freshwater crustacean *Daphnia magna*.

González AM, Yuste-Lisbona FJ, Rodiño AP, De Ron AM, Capel C, García-Alcázar M, Lozano R, Santalla M. 2015. Uncovering the genetic architecture of *Colletotrichum lindemuthianum* resistance through QTL mapping and epistatic interaction analysis in common bean. *Frontiers in Plant Science* **6**:1–13.

Hamilton WD. 1980. Sex versus non-sex versus parasite. *Oikos* **35**:282.

Hamilton WD, Axelrod R, Tanese R. 1990. Sexual reproduction as an adaptation to resist parasites (a review). *Proceedings of the National Academy of Sciences* **87**:3566–3573.

Hooker AL, Saxena KMS. 1971. Genetics of disease resistance in plants. *Annual Review of Genetics* **5**:407–424.

Howard RS, Lively CM. 1998. The maintenance of sex by parasitism and mutation accumulation under epistatic fitness functions. *Evolution* **52**:604–610.

Jones AG, Bürger R, Arnold SJ. 2014. Epistasis and natural selection shape the mutational architecture of complex traits. *Nature Communications* **5**:1–10.

Juneja P, Ariani CV, Ho YS, Akorli J, Palmer WJ, Pain A, Jiggins FM. 2015. Exome and transcriptome sequencing of *Aedes aegypti* identifies a locus that confers resistance to *Brugia malayi* and alters the immune response. Besansky NJ, editor. *PLOS Pathogens* **11**:e1004765.

Kofler R, Pandey RV, Schlotterer C. 2011. PoPoolation2: identifying differentiation between populations using sequencing of pooled DNA samples (Pool-Seq). *Bioinformatics* **27**:3435–3436.

Kouyos RD, Salathé M, Otto SP, Bonhoeffer S. 2009. The role of epistasis on the evolution of recombination in host–parasite coevolution. *Theoretical Population Biology* **75**:1–13.

Kover PX, Caicedo AL. 2001. The genetic architecture of disease resistance in plants and the maintenance of recombination by parasites. *Molecular Ecology* **10**:1–16.

Li H. 2011. A statistical framework for SNP calling, mutation discovery, association mapping and population genetical parameter estimation from sequencing data. *Bioinformatics* **27**:2987–2993.

Li H. 2013. Aligning sequence reads, clone sequences and assembly contigs with BWA-MEM. *arXiv:1303.3997 [q-bio]*:1–3.

Li H, Durbin R. 2009. Fast and accurate short read alignment with Burrows–Wheeler transform. *Bioinformatics* **25**:1754–1760.

Li H, Handsaker B, Wysoker A, Fennell T, Ruan J, Homer N, Marth G, Abecasis G, Durbin R, 1000 Genome Project Data Processing Subgroup. 2009. The Sequence Alignment/Map format and SAMtools. *Bioinformatics* **25**:2078–2079.

Li W, Zhu Z, Chern M, Yin J, Yang C, Ran L, Cheng M, He M, Wang K, Wang Jing, et al. 2017. A natural allele of a transcription factor in rice confers broad-spectrum blast resistance. *Cell* **170**:114-126.e15.

Lively CM. 2010. A review of Red Queen models for the persistence of obligate sexual reproduction. *Journal of Heredity* **101**:S13–S20.

Luijckx P, Ben-Ami F, Mouton L, Du Pasquier L, Ebert D. 2011. Cloning of the unculturable parasite *Pasteuria ramosa* and its *Daphnia* host reveals extreme genotype–genotype interactions. *Ecology Letters* **14**:125–131.

Luijckx P, Fienberg H, Duneau D, Ebert D. 2012. Resistance to a bacterial parasite in the crustacean *Daphnia magna* shows Mendelian segregation with dominance. *Heredity* **108**:547–551.

Luijckx P, Fienberg H, Duneau D, Ebert D. 2013. A matching-allele model explains host resistance to parasites. *Current Biology* **23**:1085–1088.

Magalhães S, Sucena É. 2016. Genetics of host–parasite interactions: towards a comprehensive dissection of *Drosophila* resistance to viral infection. *Mole-*

cular Ecology **25**:4981–4983.

Magwire MM, Fabian DK, Schweyen H, Cao C, Longdon B, Bayer F, Jiggins FM. 2012. Genome-wide association studies reveal a simple genetic basis of resistance to naturally coevolving viruses in *Drosophila melanogaster*. *PLoS Genetics* **8**:e1003057.

Mendel G. 1865. Versuche über Plflanzenhybriden. *Verhandlungen des naturforschenden Vereines in Brünn, Bd. IV für das Jahr 1865* **Abhandlungen**:3–47.

Metzger CMJA, Luijckx P, Bento G, Mariadassou M, Ebert D. 2016. The Red Queen lives: Epistasis between linked resistance loci. *Evolution* **70**:480–487.

Quinlan AR, Hall IM. 2010. BEDTools: a flexible suite of utilities for comparing genomic features. *Bioinformatics* **26**:841–842.

R Core Team. 2021. R: A language and environment for statistical computing. R Foundation for Statistical Computing, Vienna, Austria. Available from: http://www.R-project.org

Routtu J, Ebert D. 2015. Genetic architecture of resistance in *Daphnia* hosts against two species of host-specific parasites. *Heredity* **114**:241–248.

Salathé M, Kouyos R, Bonhoeffer S. 2008. The state of affairs in the kingdom of the Red Queen. *Trends in Ecology & Evolution* **23**:439–445.

Samson M, Libert F, Doranz BJ, Rucker J, Liesnard C, Farber C-M, Saragosti S, Lapouméroulie C, Cognaux J, Forceille C, et al. 1996. Resistance to HIV-1 infection in Caucasian individuals bearing mutant alleles of the CCR-5 chemokine receptor gene. *Nature* **382**:722–725.

Sasaki A. 2000. Host–parasite coevolution in a multilocus gene-for-gene system. *Proceedings of the Royal Society B: Biological Sciences* **267**:2183–2188.

Schlötterer C, Tobler R, Kofler R, Nolte V. 2014. Sequencing pools of individuals — mining genome-wide polymorphism data without big funding. *Nature Reviews Genetics* **15**:749–763.

Tellier A, Brown JKM. 2007. Polymorphism in multilocus host–parasite coevolutionary interactions. *Genetics* **177**:1777–1790.

Thrall PH, Barrett LG, Dodds PN, Burdon JJ. 2016. Epidemiological and evolutionary outcomes in gene-for-gene and matching allele models. *Frontiers in Plant Science* **6**:1–12.

Wickham H. 2016. ggplot2: Elegant graphics for data analysis. New York: Springer-Verlag

Wilfert L, Schmid-Hempel P. 2008. The genetic architecture of susceptibility to parasites. *BMC Evolutionary Biology* **8**:187.

Wilke CO. 2019. cowplot: Streamlined plot theme and plot annotations for "ggplot2." Available from: https://CRAN.R-project.org/package=cowplot

Xiao Y, Dai Q, Hu R, Pacheco S, Yang Y, Liang G, Soberón M, Bravo A, Liu K, Wu K. 2017. A single point mutation resulting in cadherin mislocalization underpins resistance against *Bacillus thuringiensis* toxin in cotton bollworm. *Journal of Biological Chemistry* **292**:2933–2943.

CHAPTER 4

New attachment sites and patterns of *Pasteuria ramosa* spores on the cuticle of *Daphnia magna*

Camille Ameline, Maridel Fredericksen, Benjamin Huessy and Dieter Ebert

This chapter is included in the publication:

Fredericksen M, Ameline C, Krebs M, Hüssy B, Fields PD, Andras JP, Ebert D. 2021. Infection phenotypes of a coevolving parasite are highly diverse, structured, and specific. Evolution 75:2540–2554.

Abstract Infection by different genotypes of the endospore-forming bacteria *Pasteuria ramosa* in the crustacean *Daphnia magna* is highly specific to the host genotype. Consequently, this host−parasite system is intensively studied as a model system in coevolution research. Infection by *P. ramosa* is determined by the attachment of bacterial spores to the gut wall of the host. Hosts without attachment are resistant to the parasite. Resistance is scored in the laboratory using the so-called attachment test, where fluorescently labelled spores are fed to the *Daphnia* and attachment is observed under the microscope. Attachment tests have been so far conducted using a small number of *P. ramosa* clones and isolates, revealing two sites in the host where attachment is observed, the foregut (= esophagus) and the hindgut. Occasional observation of attachment to other parts of the host body prompted us to systematically look for other possible attachment sites in the host. In this study we use novel *P. ramosa* isolates from different populations and describe several previously unknown attachment sites in the host gut, postabdomen, and body appendages. These attachment sites were observed consistently within host genotypes, although the intensity of attachment varies strongly, making them more difficult to score than the previously described foregut and hindgut sites. Infection trials are needed to confirm that these novel attachment sites can lead to infections. We recommend caution using the attachment test at these new sites, as the observed variation suggests more stochasticity in the attachment process. Clearly, the infection process in this host−parasite system is more diverse and complex than previously thought.

Keywords attachment test, bacterial spores, cuticle, gut, specificity

Introduction

Specificity in infection by parasites has strong implications in epidemiology and ultimately host–parasite coevolution theory (Fortuna et al. 2019; Orlansky and Ben-Ami 2019). Indeed, when coupled with strong fitness costs, high specificity has the potential to induce tight coevolution between a host and its parasites (Martinů et al. 2018). However, the degree of specificity between a host and its parasites can be hard to detect because multi-genotypic parasite isolates are often used in experiments, or because epidemiological and environmental factors are not controlled. Additionally, specificity can result from epidemiological and geographical factors (Piecyk et al. 2019) or genotype–genotype interactions (Luijckx et al. 2011).

To characterize such specificity and include it in a host–parasite coevolution context, it is essential to possess reliable infection scoring in the laboratory, such as infection trials or direct histological observations. Indeed, in the case of genotype–genotype interactions, infection scoring allows to investigate the genetic architecture of resistance and infectivity, i.e. finding the coevolving genes and understanding how they interact (Magwire et al. 2012; Cogni et al. 2016; Zueva et al. 2018). Additionally, coevolutionary dynamics can be investigated (Decaestecker et al. 2007; Ford et al. 2017), and population genomics studies can look for potential signatures of selection (Bourgeois et al. 2017). Such studies rely on a clear phenotypic scoring to detect statistical association.

In the *Daphnia magna–Pasteuria ramosa* host–parasite system, cloning of the parasite and controlled infections revealed a high genotype–genotype specificity between the host and the parasite (Luijckx et al. 2011). The mode of infection was later determined, as it was found that bacterial spores can attach to the gut wall of the host and thus cause infection, while host are resistant when spores do not attach (Duneau et al. 2011). Attachment is the first step of the infection process, as it allows penetration into the host body cavity and then multiplication of the bacteria (Ebert et al. 2016). In the first study describing the attachment test, attachment showed a clear site-specific pattern (at the host foregut/esophagus), was binary, and independent of environmental factors (Duneau et al. 2011). Later a second attachment site was described, namely the host hindgut (Bento et al. 2020).

Because it is fast and reliable, the attachment test has become the standard method for scoring resistance and infectivity phenotypes in the *P. ramosa–D. magna* system (Luijckx et al. 2013; Metzger et al. 2016; Chapter 1: Ameline et al. 2021). However, as new *P. ramosa* isolates were used in the laboratory, observations of new attachment sites were made, prompting a systematic search for novel attachment sites (Bento et al. 2020; Ameline et al. 2021). Here we report the results of this systematic search.

Materials and methods

Host and parasite genotypes

The five *Pasteuria ramosa* isolates routinely used in the laboratory are C1, C19, P15, P20 and P21 (Luijckx et al. 2011; Bento et al. 2020; Chapter 1:

Ameline et al. 2021). The resistance phenotype—a.k.a. resistotype—of a *Daphnia magna* clone (= genotype) depicts resistance (R: no attachment) or susceptibility (S: attachment) to these five isolates. We aimed to get more diversity of *P. ramosa* isolates by exposing *D. magna* clones from the Aegelsee population that were fully resistant to the five known *P. ramosa* isolates (RRRRR resistotype) to pond sediment. We isolated the parasite from five different host genotypes (t1_10.3_2i_2, 5, 6, 11, and 15) and passaged them once in the host genotype used to isolate them from the sediments, aiming to yield larger amounts of spores and to reduce a possible multiplicity of parasite strains within isolates. We renamed these five isolates P38 to P42.

These five new isolates—P38 to P42—were then tested on a diverse panel of host genotypes from the Aegelsee population. We used 91 *D. magna* genotypes collected from 2015 to 2018 sampled across the summer season. We performed the attachment test as described in (Duneau et al. 2011), using *P. ramosa* fluorescently labelled spores. This attachment test revealed three new attachment sites consistently observed across repeats.

In parallel, attachment test performed in the laboratory in sexual offspring of selfed host cloned (F1 groups) revealed two other new attachment sites. Six selfed F1 groups with 19 to 89 offspring were used, representing a total of 340 genotypes (Supplementary Table S4.1). These selfed F1 groups correspond to the groups used in Chapter 1 (Ameline et al. 2021) and Chapter 3 (Fredericksen et al. 2021) to investigate the genetic model of resistance in the host. Finally, attachment test performed using host and parasite genotypes from other populations revealed one further unknown attachment site.

Attachment pictures

To describe the new attachment sites observed, we developed a protocol to take good quality images of the attachment. We infected juvenile host individuals (about 1 mm body length) with fluorescently labelled spores in 96-well plates as described in Duneau et al. (2011), using varying amounts of spores. In the attachment test, depending on the bacterial isolate, we routinely feed one individual 4000–10000 spores. The spore suspension used in the standard attachment test were created from the macerated whole-body tissue of five to ten infected *D. magna* individuals and diluted ten times (1:10 dilution). To avoid too strong fluorescence that would impede taking clear pictures, we used 500–2000 spores of 1:10 dilutions or 500–1000 *P. ramosa* spores of 1:100 dilutions. The attachment test is normally performed using alive *D. magna*, but to obtain better pictures we immobilized the hosts after exposure to the parasite. After the incubation period (about 30 min), we removed the medium and added 150 µL of 18% EtOH solution, in which individuals were left for 10 min. Individuals were then placed with a drop of medium on a glass slide and covered with a cover slip, with play-dough distance holder at the corners. We took images under a fluorescent lens microscope, within 10 minutes to avoid autofluorescence. Unless mentioned otherwise, we used a Leica DM6 B microscope, objective 10x with 1x or 1.6x magnification, FluoCube: GFP. Images were produced using a Leica DFC7000 T camera connected to the microscope, using the program LAS v.

4.12 and the package "montage", with a Z-step size of 2 (30–50 pictures per image). Details on the host and parasite genotypes, number of spores and dilutions used to produce the attachment images are given in Table 4.1 and Supplementary Table S4.2.

Results

Attachment of *Pasteuria ramosa* spores has been reported in *Daphnia magna* in the foregut ("F" attachment) and in the hindgut (Figs. 4.1, 4.2 and 4.3) (Duneau et al. 2011; Bento et al. 2020). However, the hindgut has various clearly differentiable regions, and attachment in these regions has not yet been characterized. New attachment sites were observed in the postabdomen region of the host (Fig. 4.2).

Table 4.1

Details about the *Daphnia magna* genotypes used in the pictures of this chapter.

***D. magna* clone**		**Resistotype**										**Attachment site observed with high spore concentration**										**Comment**
Name	**Origin**	C1	C19	P15	P20	P21	P38	P39	P40	P41	P42	C1	C19	P15	P20	P21	P38	P39	P40	P41	P42	
CH-H-2015-9	Aegelsee	R	R	S	R	S	S	S	S	S	S	NA	NA	D or DR	NA	D or DR	RE	E, REA	RE	RE	E, REA	NA
CH-H-2015-20	Aegelsee	R	R	S	R	S	S	S	S	S	S	NA	NA	D or DR	NA	D or DR	RE	REA	REA	E, REA	RE	NA
CH-H-2015-35	Aegelsee	S	S	S	S	S	S	S	S	S	S	F	F	D or DR	F	D or DR	E	E, REA	E	E	E, RE	NA
CH-H-2015-36	Aegelsee	R	R	S	S	S	S	S	S	S	S	NA	NA	D or DR	F	D or DR	REA	REA	RE	REA, RE	REA, RE	NA
CH-H-2015-42	Aegelsee	R	R	S	S	S	S	S	S	S	S	NA	NA	D or DR	F	D or DR	RE	E, REA	REA	REA, RE	E, RE	NA
t1_10.3_2i_2	Aegelsee	R	R	R	R	R	S	S	S	S	S	NA	NA	NA	NA	NA	REA, DE	E, REA, DE	REA, DE	DE	DE	P38 host
t1_10.3_2i_3	Aegelsee	R	R	R	R	R	S	S	S	S	S	NA	NA	NA	NA	NA	EA	E, REA	E, REA, DE	E, RE	REA, DE	P39 host
t1_10.3_2i_6	Aegelsee	R	R	R	R	R	S	S	S	S	S	NA	NA	NA	NA	NA	RE	DE, RE	REA, DE	E, DE, RE	E, REA	P40 host
t1_10.3_2i_11	Aegelsee	R	R	R	R	R	S	S	S	S	S	NA	NA	NA	NA	NA	REA, EA, RE	E, REA	REA	REA, DE	DE, RE	P41 host
t1_10.3_2i_15	Aegelsee	R	R	R	R	R	S	S	S	S	S	NA	NA	NA	NA	NA	REA	REA, DE	E, REA	REA	REA	P42 host
t2_17.3_4	Aegelsee	R	R	S	S	S	NA	NA	NA	NA	NA	NA	NA	D	FLA	DL4	NA	NA	NA	NA	NA	NA
t2_17.3_4i_12i_10	Aegelsee	R	R	S	S	S	NA	NA	NA	NA	NA	NA	NA	D	FLA	DL4	NA	NA	NA	NA	NA	NA
CH-H-2015-97	Aegelsee	S	S	S	S	S	NA	NA	NA	NA	NA	F	F	D	FLA	D	NA	NA	NA	NA	NA	NA
CH-H-2015-97i-6	Aegelsee	S	S	S	S	S	NA	NA	NA	NA	NA	F	F	D	FLA	D	NA	NA	NA	NA	NA	NA
RU-BOL-1	Russia	NA	NA	NA	NA	NA	NA	NA	NA	NA	NA	NA	NA	NA	NA	NA	NA	NA	NA	NA	NA	NA

Attachment is described as a string of letters containing all sites where attachment was observed in one host individual. For example, in the CH-H-2015-9 host clone, we observed attachment on the external postabdomen (site E) in some repeats (attachment "E"); and attachment on the postabdomen (site E), rectum (site R) and anus (site A) in other repeats (attachment "REA"). Previous scoring did not distinguish attachment on the distal hindgut (site D) from attachment on the rectum (site R). Hence, in some cases, we do not know if the observed attachment was "D" or "DR".

Figure 4.1

Daphnia magna female morphology. **A**: Structures relevant for the attachment test. Appendages morphology and structures names taken form (Fryer 1991). Going around the animal, from the upper left to the upper right: **TL1**: Trunk limb 1. Trunk limbs are also called thoracopods, thoracic appendages and phyllopods, **Ex**: Exopod of trunk limb 1. Exopods are present on all trunk limbs, **Se**: Setae of trunk limb 1. Setae are present on all trunk limbs, and are themselves covered with setules, also called spinules, not represented here, **FCh**: Filter chamber, **TL2 and 3** Trunk limbs 2 and 3, **FP**: Gnathobasic filter plate of trunk limb 3, also present on trunk limb 4, **TL4 and 5**: Trunk limbs 4 and 5, **Ep**: Epipodite of trunk limb 5, also present in the other trunk limbs, **Abdomen**: see Fig. 4.2, **C**: Carapace, **FG**: Food groove. The *Daphnia* filters the water, creating a water flow from the posterior part of the filter chamber to the anterior part where the mouth is. Particles are accumulated through the food groove to the mouth, **Th**: Thorax, **MG**: Midgut, **GS**: Grinding surface, autofluorescent in our samples. The grinding surface of the second mandible is represented, but not the rest of the mandible, as it is hidden behind, **Mand.**: Mandible, **M**: Mouth, **F**: Foregut, or esophagus. **B**: Picture showing the trunk limbs of the *D. magna*. A few *P. ramosa* spores are visible in the gut, the food groove and on the expod of trunk limb 4. The fluorescent mass below the mandible is the supra-oesophagal ganglion, not spores. The antenna hides the foregut and the grinding surfaces of the mandibles. **C**: Picture showing the filter plates of *D. magna*. The foregut and mandible are also well visible. A few *P. ramosa* spores are visible in the distal part of the gut, one spore is visible on the filter plate. **D**: Picture showing the foregut and mandibles of *D. magna*.

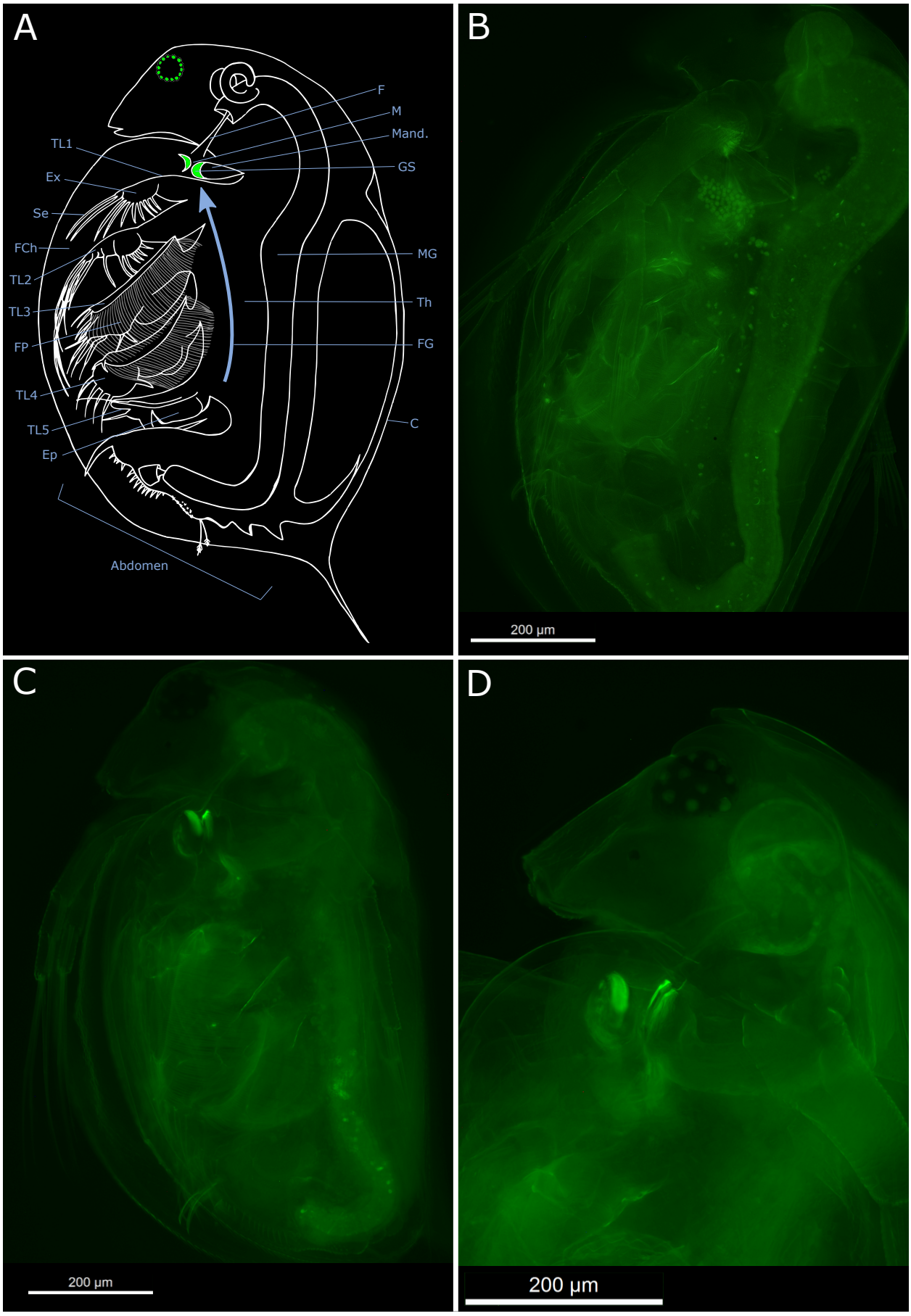

Figure 4.1 *Daphnia magna* female morphology.

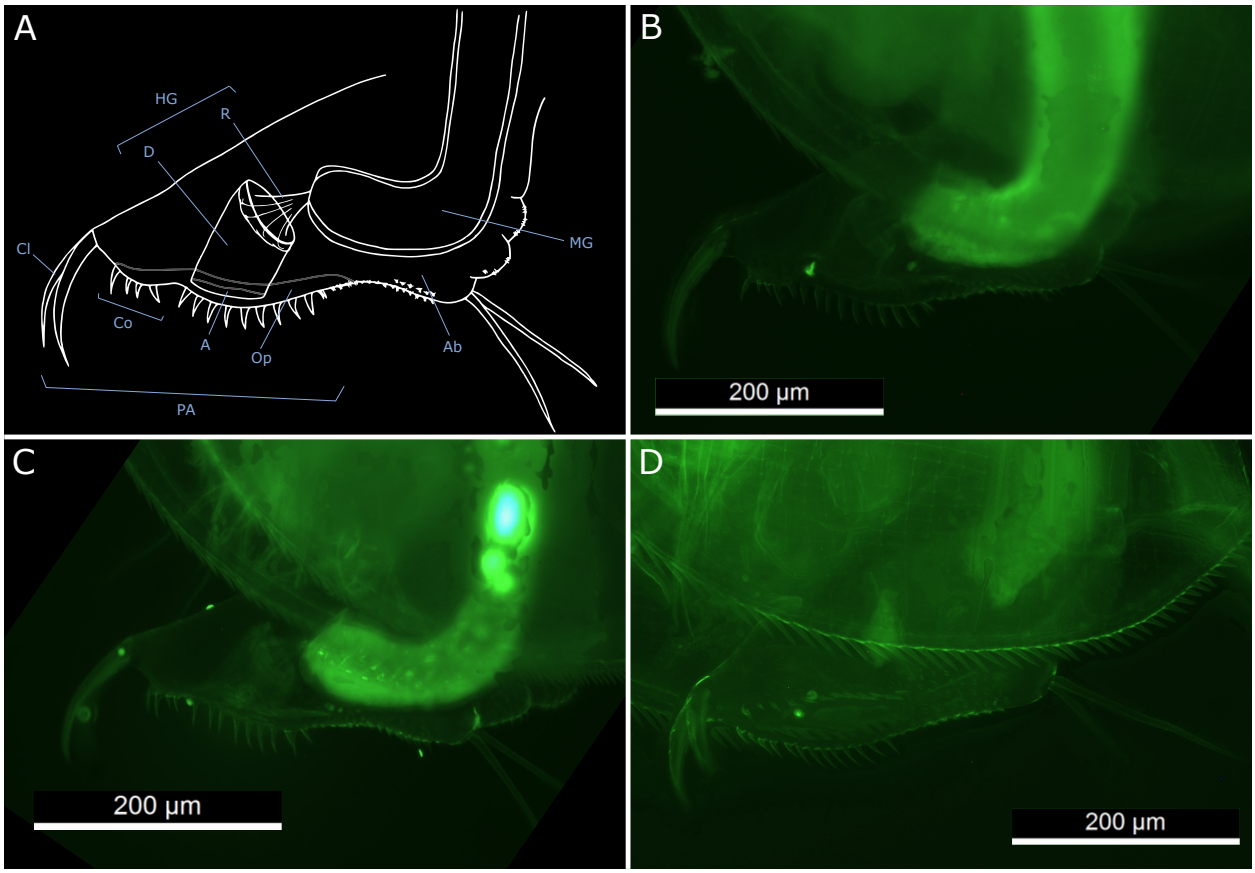

Figure 4.2

Daphnia magna female abdomen morphology. **A**: Structures relevant for the attachment test. Structures names taken form (Fryer 1991). A male abdomen is shown in Fig. 4.4C. Going around the abdomen, from the upper left to the upper right: **HG**: Hindgut, **R**: Rectum. The rectum is a flexible structure that links the midgut to the distal hindgut. It is represented here "folded" as the midgut and the distal hindgut are close to each other. However, the rectum can be elongated, as seen in Fig. 4.5C. **D**: Distal hindgut, **Cl**: Postabdominal claw. Setules present on the posterior part of the claws (not represented here) are visible in A to D. **Co**: Comb. The disposition of the two combs is specific to the species and the sex of the individual. The anus is positioned where the proximal larger comb is. **A**: Anus, **Op**: Postabdominal opening, **PA**: Postabdomen, **Ab**: Abdomen, **MG**: Midgut. **B**: Picture showing the abdominal structures in *D. magna*. A few *P. ramosa* spores are visible on the anus. **C**: Picture showing the abdominal structures in *D. magna*. A few *P. ramosa* spores are visible on the external postabdomen. **D**: Picture showing the postabdominal opening and the anus from below in *D. magna*. One *P. ramosa* spore attaches to the larger postabdominal comb and one to the anterior part of the anus.

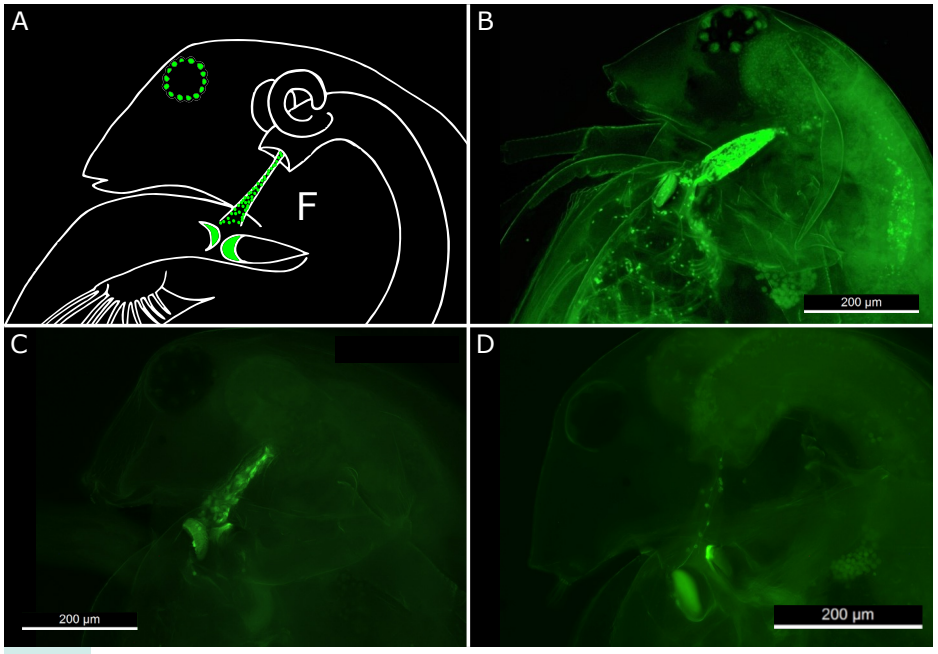

Figure 4.3

Foregut attachment "F" of *Pasteuria ramosa* in *Daphnia magna*. **A**: Schematic view of the foregut attachment. The grinding surfaces on the mandibles autofluoresce. Spores of *P. ramosa* are represented as green dots. Spores cover the internal part of the foregut. **B**: Picture showing the foregut attachment in *D. magna* with a high spore concentration. Spores also attach to the appendices in this sample. **C**: Picture showing the foregut attachment in *D. magna* with a medium spore concentration. **D**: Picture showing the foregut attachment in *D. magna* with a low spore concentration.

Attachment to the postabdomen

First, we observed that attachment could occur in different parts of the hindgut, namely the distal hindgut ("D" attachment) and the rectum ("R" attachment) (Figs. 4.4 and 4.5). The rectum is a muscular tube linking the distal end of the midgut to the seemingly harder distal hindgut (Fig. 4.2), which closes the gut. At the rectum we observed variable patterns depending on the degree of extension of the tissue (compare Fig. 4.5B and C). Because of this, the attachment to the rectum is difficult to score. For example, Figure 4.5D shows a possible artefact created by the mobility of the outer membrane of the midgut that looks like a rectum attachment but is probably not one. Attachment to both the distal part of the hindgut and the rectum is often observed. Attachment in the distal part of the hindgut has been observed before with the P15 and P21 *P. ramosa* isolates, and the attachment pattern is clear, covering the whole cavity of the distal part of the hindgut (Bento et al. 2020; Fredericksen et al. in prep) (Fig. 4.4B and C), although attachment intensity can vary. As we tested new *P. ramosa* isolates, we observed much more variable attachment in the distal hindgut. Figures 4.4D to G show examples of different patterns of partial attachment in the distal hindgut observed consistently across host and parasite genotypes.

Second, we observed that spores also attached to the outer part of the postabdomen. We describe two further attachment sites, the anus region "A" (Fig. 4.6) and the external abdomen "E" (Fig. 4.7). The anus attachment describes spores attaching to the opening of the distal hindgut and to the larger postabdominal comb, while the external abdomen attachment describes attachment of spores to large parts of the surface of the postabdomen. These two attachments were observed separately (only "A": Fig. 4.6B to E, only "E": Fig. 4.7B and C) or together (Fig. 4.7D). The intensity of attachment to these sites can vary greatly. For example, both are observed in Figure 4.7D at the relative same intensity, but Figure 4.6F shows a more intense attachment to the anus than to the external abdomen. Figure 4.6F also shows that the anus attachment can be difficult to disentangle from a partial attachment in the distal hindgut. The external postabdomen attachment—"E"—of the P38 to P42 *P. ramosa* isolates was observed in all the 91 tested host genotypes from the Aegelsee population, at varying intensities. All possible combinations of the other postabdomen attachments—"D", "R" and "A"—were observed (Table 4.1). We observed this variation in attachment intensity and patterns across and within host genotypes, which made the scoring of the postabdominal attachment often difficult.

We tested attachment of the new isolates P38 to P42 on the host genotypes from which they were isolated and passaged, and observed attachment at the rectum, anus, and external abdomen (Table 4.1), suggesting that attachment at these sites does lead to infection.

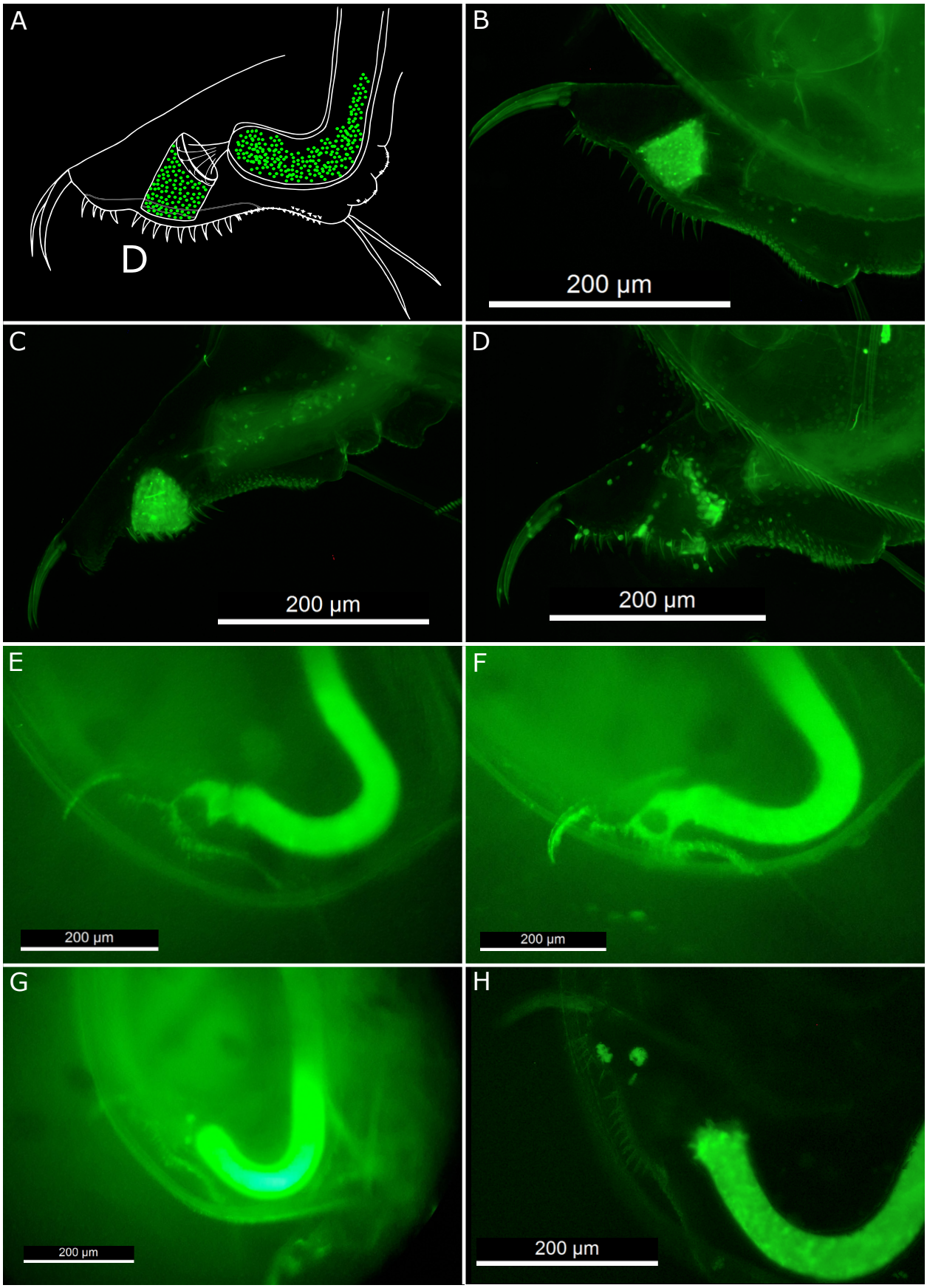

Figure 4.4

Distal hindgut attachment "D" of *Pasteuria ramosa* in *Daphnia magna*.

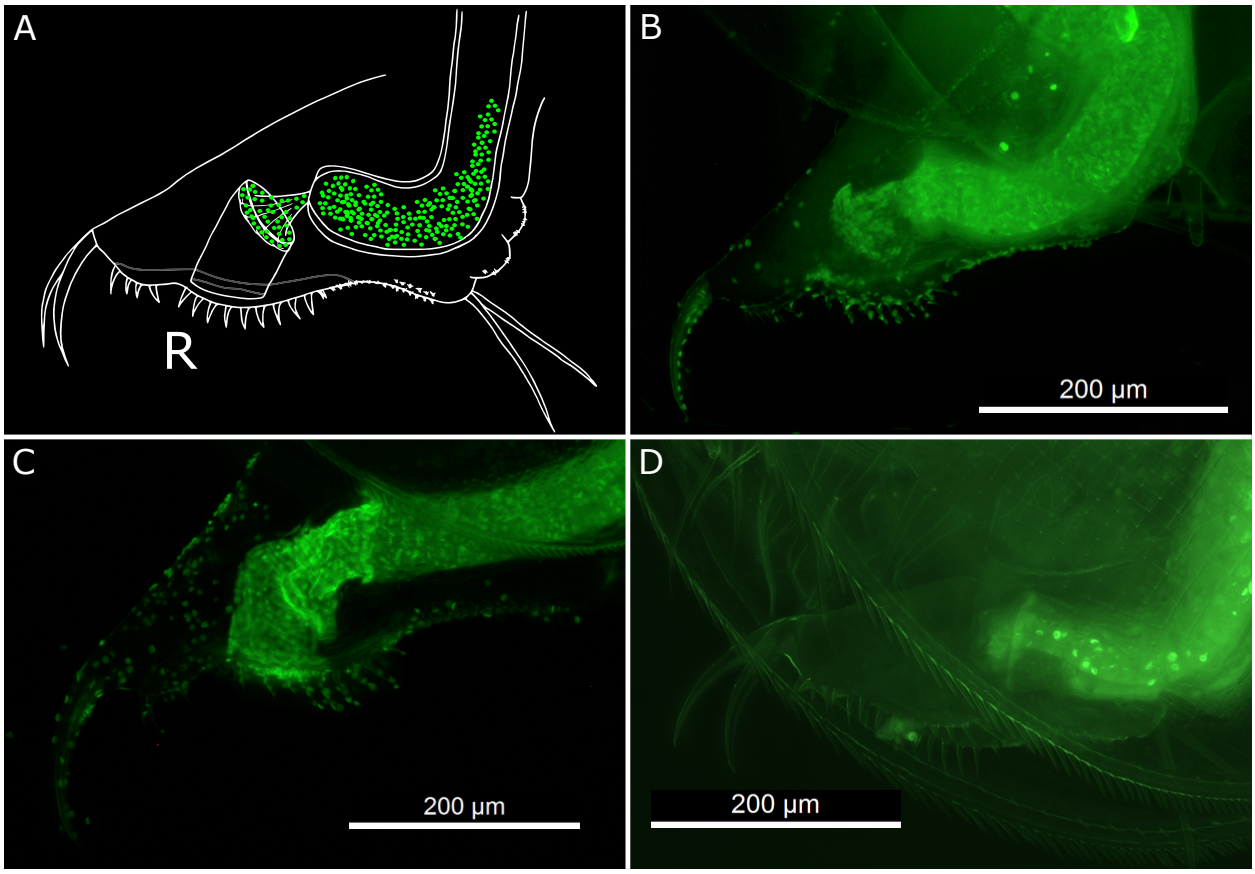

Figure 4.5

Rectum attachment "R" of *Pasteuria ramosa* in *Daphnia magna*. **A**: Schematic view of the rectum attachment. Spores of *P. ramosa* are represented as green dots. Spores cover the internal part of the rectum. **B**: Picture showing the "folded" rectum attachment. In this sample spores also attach to the external postabdomen. **C**: Picture showing the "unfolded" rectum attachment. In this sample spores also attach to the external postabdomen. **D**: Picture showing a possible artefact looking similar to the rectum attachment. In this sample it seems like the distal part of the midgut would be protruding from the midgut, making it look like a rectum attachment In this sample a few spores attach to the external postabdomen, on the larger comb.

Figure 4.4

Distal hindgut attachment "D" of *Pasteuria ramosa* in *Daphnia magna*. **A**: Schematic view of the distal hindgut attachment. Spores of *P. ramosa* are represented as green dots. Spores cover the internal part of the distal hindgut. **B**: Picture showing the distal hindgut attachment in a female *D. magna*. **C**: Picture showing the distal hindgut attachment in a male *D. magna*. **D**: Picture showing a specific distal hindgut attachment in *D. magna*. Spores attach mostly at the corners of the distal hindgut. In this sample, spores also attach to the external postabdomen. **E**: Picture showing a specific distal hindgut attachment in *D. magna*. Spores attach to the rectum and to the proximal part of the distal hindgut. In this sample, spores also attach to the external postabdomen. Picture taken with a smartphone camera through a fluorescent-lens microscope LEICA DMI4000B. **F**: Picture showing a specific distal hindgut attachment in *D. magna*. Spores attach to the rectum and seem to attach to the medial part of the distal hindgut more than the lateral part. In this sample, spores also attach to the external postabdomen. Picture taken with a smartphone camera through a fluorescent-lens microscope LEICA DMI4000B. **G**: Picture showing a specific distal hindgut attachment in *D. magna*. Spores attach to proximal part of the distal hindgut, where it meets the rectum. Picture taken with a smartphone camera through a fluorescent-lens microscope LEICA DMI4000B. **H**: Possibly same as G, if the sample was slightly crushed and the distal hindgut was moved towards the distal part of the postabdomen. Alternatively, this could represent yet another attachment pattern not described in the present study. Another possibility would be that this pattern comes from an artefact.

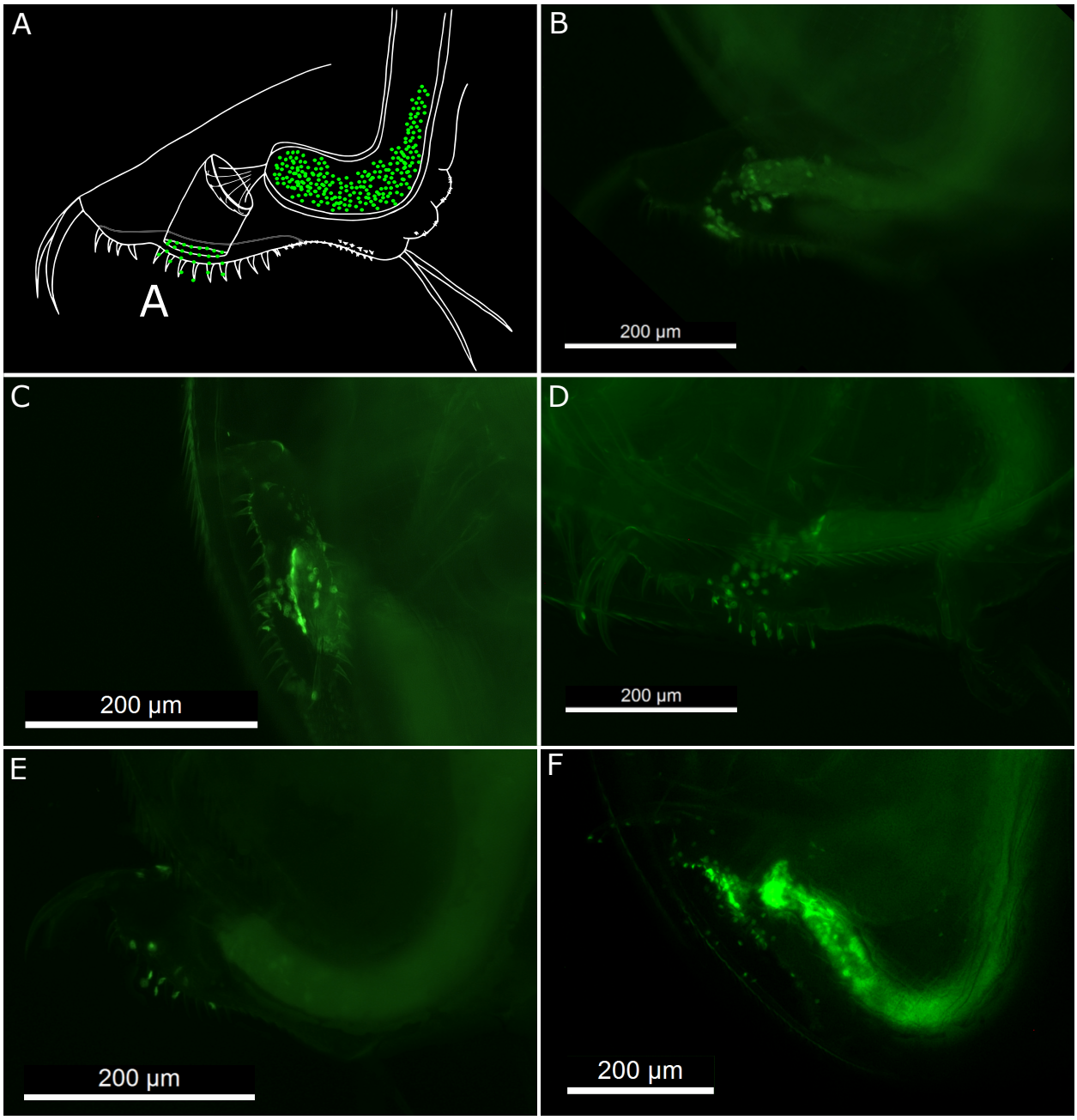

Figure 4.6

Anus attachment "A" of *Pasteuria ramosa* in *Daphnia magna*. **A**: Schematic view of the anus attachment. Spores of *P. ramosa* are represented as green dots. Spores attach to the anus and to the larger comb of the postabdomen. **B**: Picture showing the anus attachment. In this sample a few spores attach to the distal hindgut. **C**: Picture showing the anus attachment from below. **D**: Same as B, with a stronger attachment in the distal hindgut. One spore attaches to the postabdominal claw. **E**: Picture showing the anus attachment with a low spore concentration. In this sample a few spores attach to the external abdomen. **F**: Picture showing the anus attachment with a high spore concentration. In this sample spores also attach to the rectum and a few spores attach to the external abdomen. Picture taken with a reflex camera through a fluorescent-lens microscope LEICA DMI4000B.

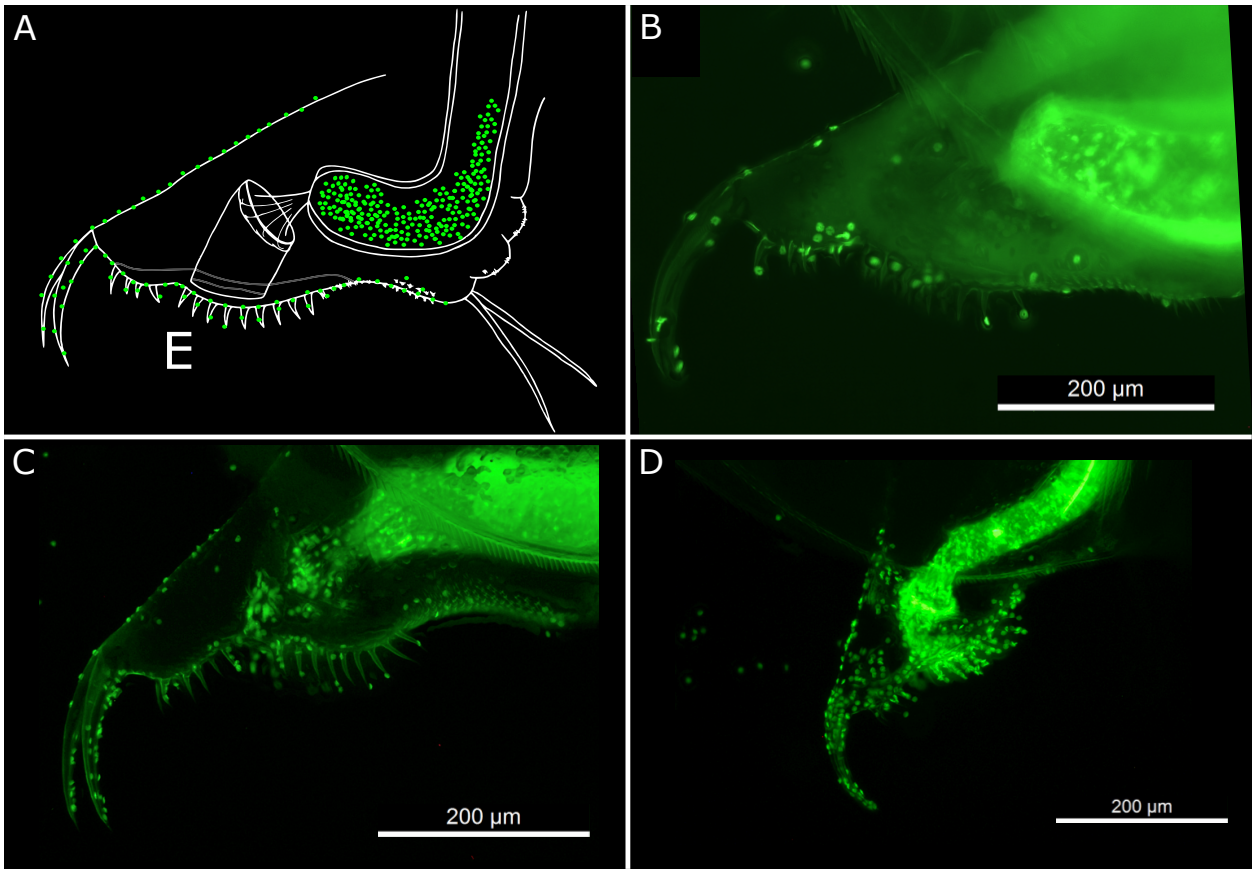

Figure 4.7

External postabdomen attachment "E" of *Pasteuria ramosa* in *Daphnia magna*. **A**: Schematic view of the external postabdomen attachment. Spores of *P. ramosa* are represented as green dots. Spores attach to the carapace outside of the postabdomen. **B**: Picture showing the external postabdomen attachment with a low spore concentration. **C**: Picture showing the external postabdomen attachment with a medium spore concentration. Note that spores attach more to the posterior part of the postabdominal claws, where the setules are (see Fig. 4.2). In this sample spores also attach to the rectum and the distal hindgut. **D**: Picture showing the external postabdomen attachment with a high spore concentration. In this sample spores also attach to the rectum and the distal hindgut. Picture taken with a reflex camera through a fluorescent-lens microscope LEICA DMI4000B.

Attachment to the appendages

Using new *P. ramosa* isolates further revealed a clear attachment site to one of the appendages of the host, trunk limb 5 "L5" (Fig. 4.8). Performing the attachment test in six selfed F1 groups with isolates routinely used in the laboratory revealed two additional consistent attachment sites. Isolates P15 and P21 showed attachment to the exopodic setae of trunk limb 4 "L4" (Fig. 4.9), and P20 showed attachment to all trunk limbs "LA" (Fig. 4.10, Supplementary Table S4.1). The *P. ramosa* isolates P20 and P21 showed attachment at the "T" and "L4" sites, respectively in all the five selfed F1 groups tested, but P15 showed attachment at the "L4" site only in three out of six F1 groups (Supplementary Table S4.1). All trunk limbs attachment seems to be mostly happening on the exopodic setae, but also on the filter plates of limbs 3 and 4 (Figs. 4.1A and 4.10). All trunk limbs attachment also seemed to touch trunk limb 5, but with a lower intensity than the "L5" attachment (compare Figs. 4.8B and 4.10B). Overall, attachment on the trunk limbs is mostly difficult characterize. This may be in part caused by their complex morphology.

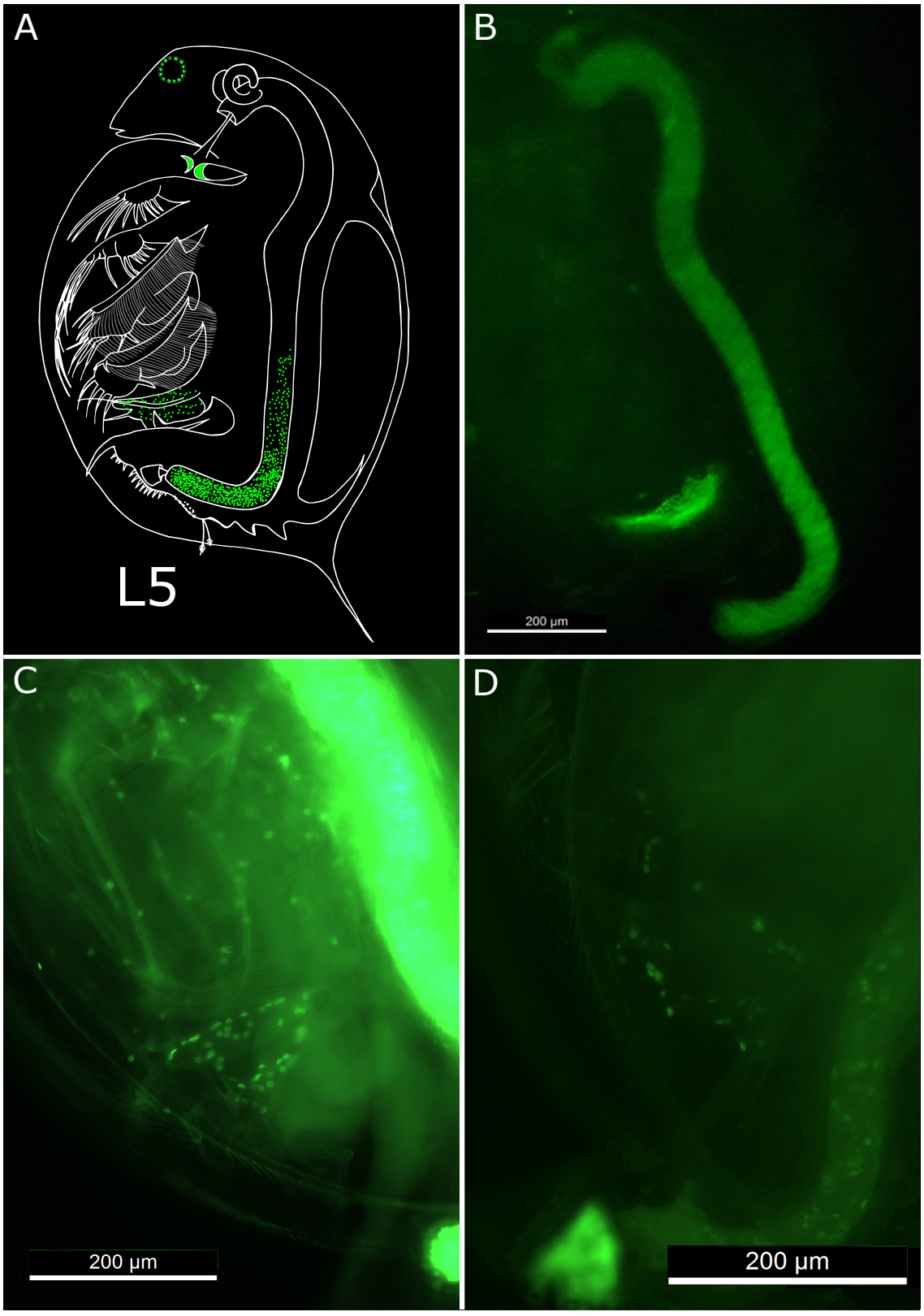

Figure 4.8

Trunk limb 5 attachment "L5" of *Pasteuria ramosa* in *Daphnia magna*. **A**: Schematic view of the trunk limb 5 attachment. Spores of *P. ramosa* are represented as green dots. **B**: Picture showing the trunk limb 5 attachment with a high spore concentration (10000 spores). Picture taken with a smartphone camera through a fluorescent-lens microscope LEICA DMI4000B. **C**: Picture showing the trunk limb 5 attachment with a medium spore concentration (2000 spores). In this sample spores also attach to the filter plate. **D**: Picture showing the trunk limb 5 attachment with a medium spore concentration (2000 spores). In this sample spores also attach to the distal hindgut.

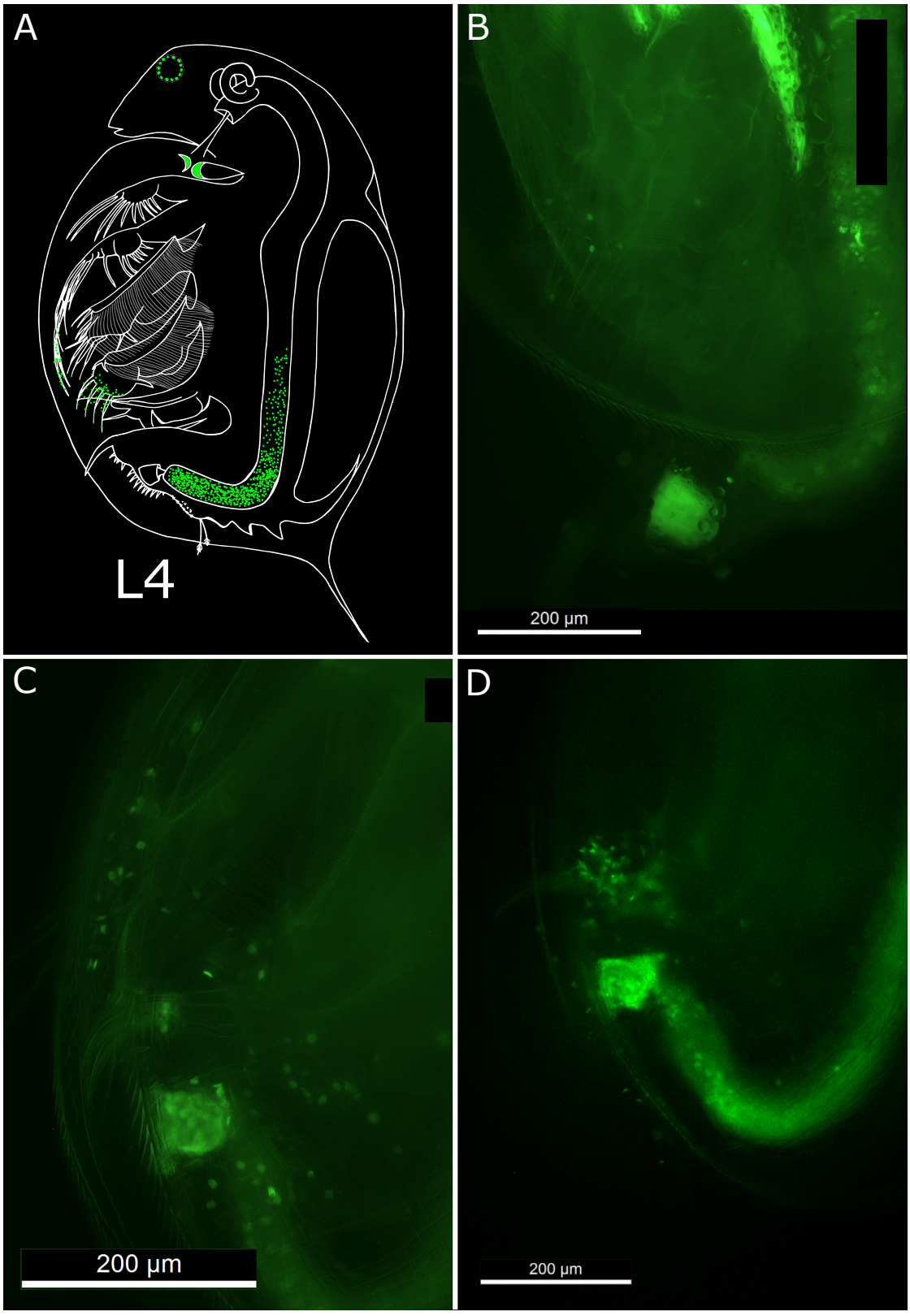

Figure 4.9

Trunk limb 4 attachment "L4" of *Pasteuria ramosa* in *Daphnia magna*. **A**: Schematic view of the trunk limb 4 attachment. Spores of *P. ramosa* are represented as green dots. **B**: Picture showing the trunk limb 4 attachment with a low spore concentration (500 spores). Spores are attached to the exopod of trunk limb 4 and to its setae. In this sample spores also attach to the distal hindgut. **C and D**: It is not clear where the spores attach, but they possibly attach to the distal part of the exopodic setae of the trunk limbs. In A, for clarity, we represent the trunk limbs separated from one other, but in reality, the trunk limbs overlap and exopodic setae from possibly all trunk limbs meet above the postabdominal claws. **C**: Picture showing the trunk limb 4 attachment with a medium spore concentration (2000 spores). In this sample spores also attach to the distal hindgut. **D**: Picture showing the trunk limb 4 attachment with a high spore concentration (10000 spores). In this sample spores also attach to the distal hindgut. Picture taken with a reflex camera through a fluorescent-lens microscope LEICA DMI4000B.

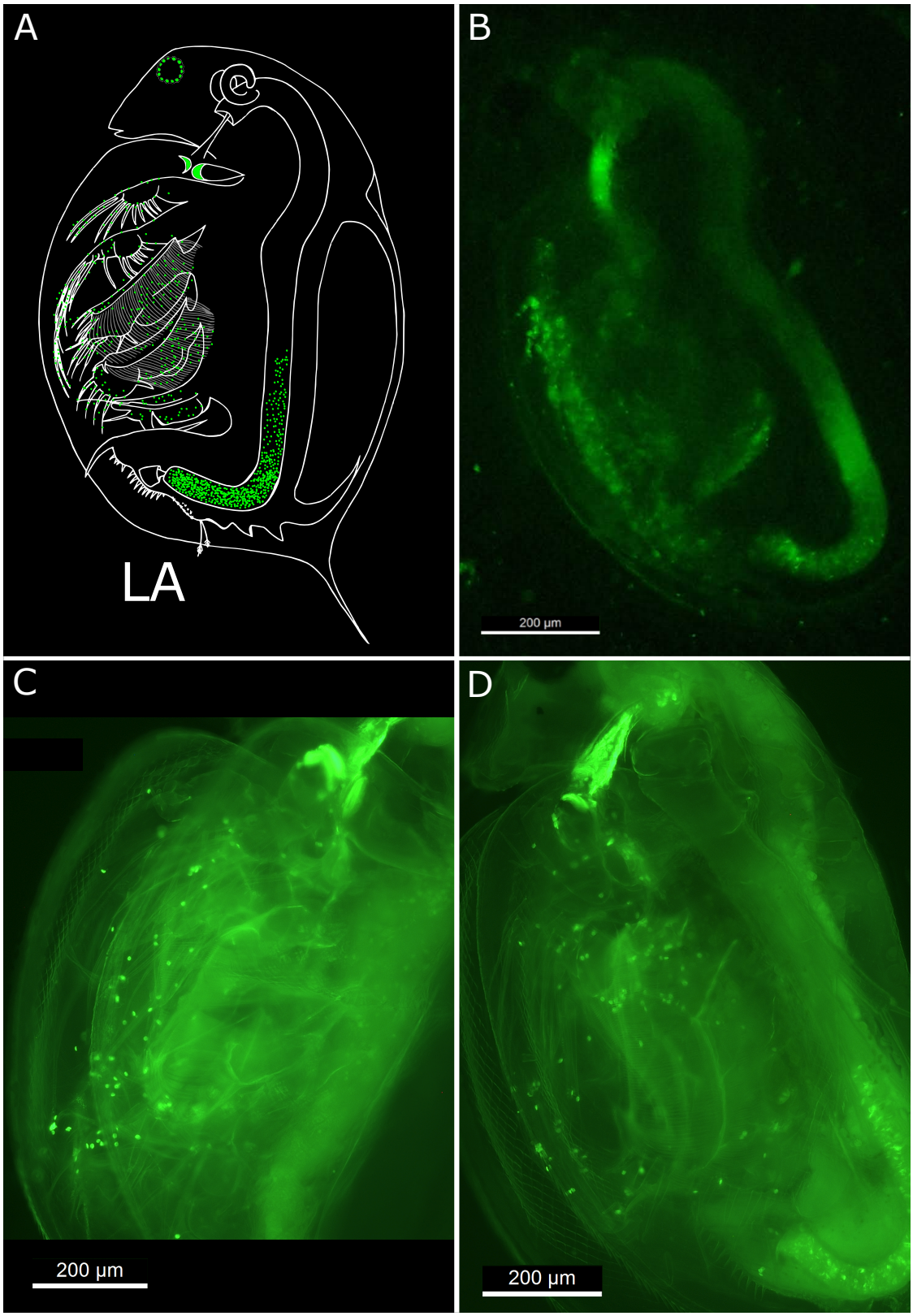

Figure 4.10

All trunk limbs attachment "LA" of *Pasteuria ramosa* in *Daphnia magna*. **A**: Schematic view of the trunk limbs attachment. Spores of *P. ramosa* are represented as green dots. Spores seem to attach to all trunk limbs, primarily on the exopodic setae and on trunk limb 5. **B**: Picture showing the trunk limbs attachment with a high spore concentration (10000 spores). Spores seem to attach to all trunk limbs, primarily on the exopodic setae and on trunk limb 5. In this sample spores also attach to the foregut. Picture taken with a reflex camera through a fluorescent-lens microscope LEICA DMI4000B. **C**: Picture showing the trunk limbs attachment with a medium spore concentration (2000 spores). Spores seem to attach to the exopodic setae of all trunk limbs. In this sample spores also attach to the foregut. **D**: Picture showing the trunk limbs attachment with a medium spore concentration (2000 spores). Spores seem to attach to the filter plates of trunk limbs 3 and 4. In this sample spores also attach to the foregut.

Molting possibly affects all attachment sites

Observations of cuticle molts of the *D. magna* during the attachment test revealed that attached spores at the foregut and postabdominal attachment sites were shed by the animal along with the molt (Fig. 4.11A and B). As we did not observe a molt of rectum attachment, we do not know if spores attached to this part of the hindgut get shed. Observations of cuticle molts under a stereomicroscope revealed that the entire structure of the appendages, including the setae, also get shed by the *D. magna* (Fig. 4.11C and D).

Discussion and perspectives

Attachment is diverse and complex

In the present study we describe new attachment sites of *Pasteuria ramosa* spores to the cuticle of it crustacean host *Daphnia magna*. We characterize a total of eight attachment sites in the foregut, the hindgut, the postabdomen and the appendages of *D. magna*. The previously described attachment sites, namely the foregut and the hindgut attachment, showed very clear and consistent patterns (Duneau et al. 2011; Bento et al. 2020), while these new sites showed more diverse and variable phenotypes. First, the new attachment sites we describe are situated on morphologically and anatomically complex structures. To our knowledge, attachment of *P. ramosa* has not been characterized in other species of *Daphnia*. A closely related species of *P. ramosa*, *P. penetrans*—infecting root-knot nematodes—seems to be able to attach to the entire cuticle of the worm (see Fig. 2 in Preston et al. 2003). Second, different attachment phenotypes were observed at the same attachment sites across host or parasite lines. Third, attachment was often observed to occur simultaneously at more than one site in a given combination of parasite and host genotype. As the new *P. ramosa* isolates were only passaged once in their host genotype, they might contain multiple genotypes of *P. ramosa*, which could blur the observed attachment phenotype and may contribute to the finding that isolates attach to several sites. However, we observed that three of the *P. ramosa* isolates used routinely in the laboratory (P15, P20 and P21) attached simultaneously to several sites in the same host genotype, with clear phenotypes. Additionally, isolate P15 was observed to attach to both the foregut and the hindgut of some host clones (Gattis 2018; Bento et al. 2020). These isolates were passaged several times in the laboratory and are mostly clonal. Thus, attachment to multiple sites by the same isolate seems to be a real possibility. Fourth, attachment phenotypes and intensity of attachment was observed to vary between and within tested host and parasite genotype combinations. However, we observed much more variation between than within tested combinations, which suggests that the observed patterns are genetic. Validation of the attachment phenotypes described here and confirmation that attachment leads to infection require further infection trials.

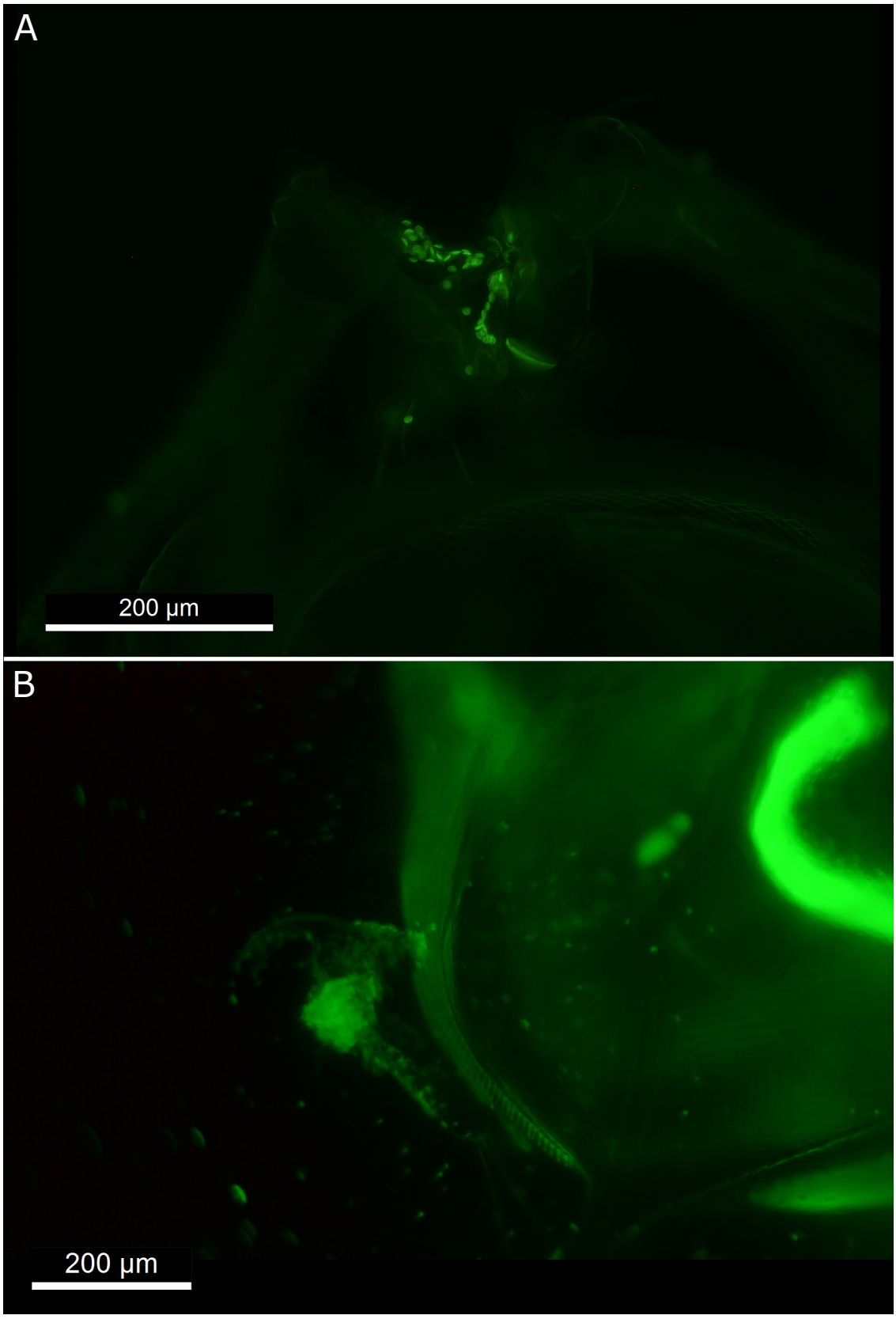

Figure 4.11

Cuticle molts in *Daphnia magna*. **A**: Picture of a cuticle molt of a foregut attachment with a low spore concentration. The foregut seems to have been split in two parts. The antennas are visible on both sides of the foregut, and one of the mandibles is visible at the bottom of the foregut. **B**: Picture showing the cuticle molt of a distal hindgut and external postabdomen attachment with a high spore concentration (10000 spores). The animal is in the process of molting and the gut is visible on the right side of the picture. Picture taken with a reflex camera through a fluorescent-lens microscope LEICA DMI4000B.

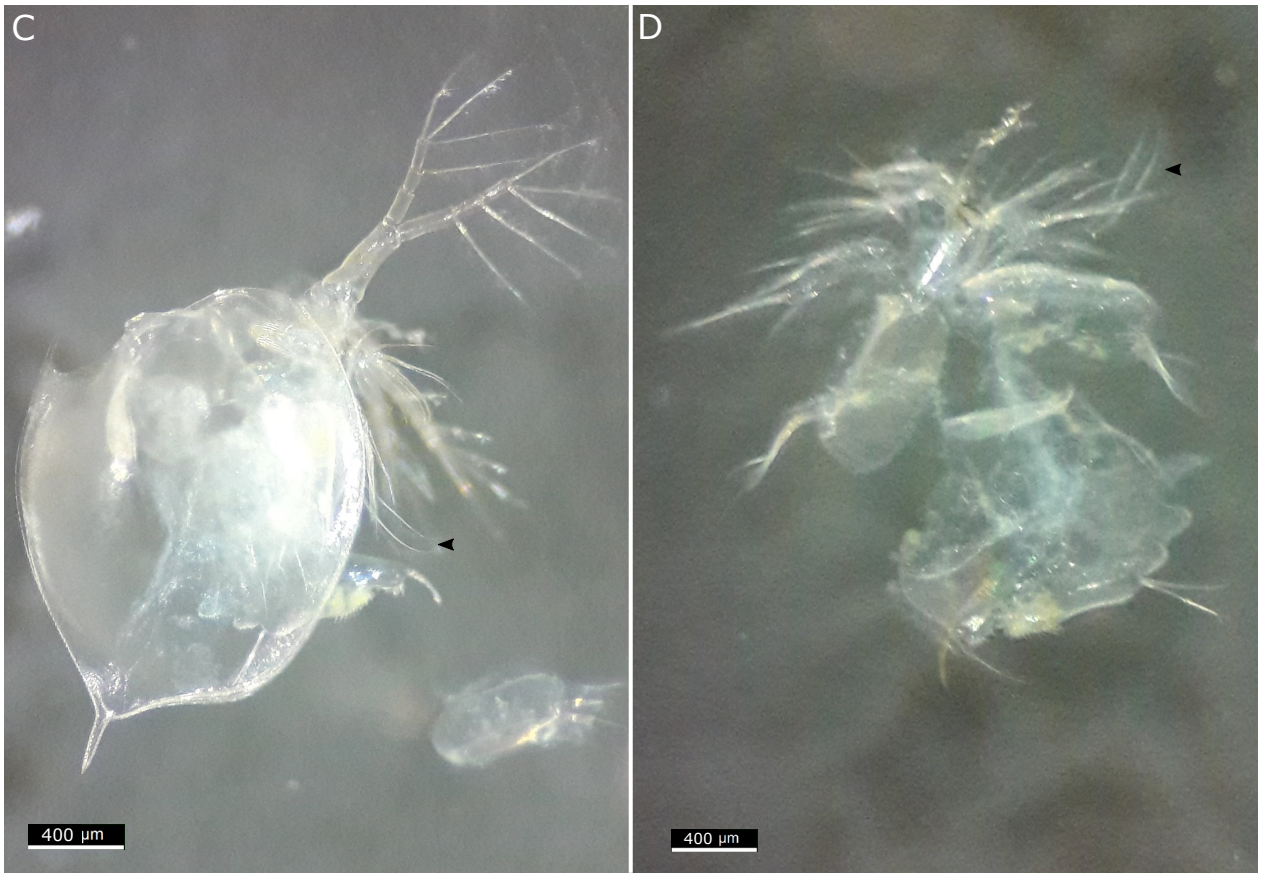

Figure 4.11 (continued)

Cuticle molts in *Daphnia magna*. **C and D**: Pictures showing the cuticle molt of entire *D. magna* individuals. Arrow heads point to the setae of the exopods. Pictures taken with a smartphone camera through a stereomicroscope.

Genotype–genotype specificity

High specificity between *D. magna* genotypes and *P. ramosa* clones has previously been observed (Luijckx et al. 2011). The five new isolates, P38 to P42, that we tested against a diverse panel of 91 host genotypes from the Aegelsee population all resulted to attach to at least the external postabdomen site "E", although with varying intensity. However, attachment to the external postabdomen does not seem to lead to infection (Fredericksen et al. 2021). This would mean that, similarly to P20 and P21 which were isolated from the same population, these new isolates cannot infect most host genotypes present in the population. While isolates possibly contain several bacterial genotypes, we did observe variation of attachment patterns and intensity across host genotypes. We thus suggest that these new *P. ramosa* isolates display some degree of specificity, even more so if we consider that the "E" attachment does not lead to infection (Table 4.1). High specificity has been observed between *Pasteuria* species and their nematode host species (Mendoza de Gives et al. 1999; Giblin-Davis et al. 2001; Davies 2009), although some species show a larger host range than others, as they are able to adhere to several host species (Mendoza de Gives et al. 1999; Mohan et al. 2012).

The mechanisms of adhesion

We describe in this study attachment of *P. ramosa* spores on specific sites of the cuticle: the foregut, the hindgut, the postabdomen, and appendages and their setae. Attachment of *P. penetrans* to nematode hosts has been hypothesized to happen in a Velcro-like fashion through a hair-like nap produced by collagen-like proteins in the bacteria (Davies 2009; Srivastava et al. 2018). This Velcro is thought to result from the interaction of carbohydrates of the collagen-like proteins of the bacteria with the glycans of mucin peptides of the nematodes cuticle (Davies 2009; Phani et al. 2017; Phani et al. 2018). Attachment specificity in our study system is hypothesized to function in a similar way, as collagen-like proteins are believed to play a role in adhesion to the host in *P. ramosa* (Mouton et al. 2009; Andras et al. 2020).

All previously known attachments sites, as well as the here described new sites are part of the cuticle of the host and are shed with the carapace when the host molts. As such, all sites are of ectodermal origin, in contrast with the midgut, which is of endodermal origin. Attachment on the midgut wall, which is not molted, has never been observed. The cuticle of crustaceans has been described in detail (Nagasawa 2012), as well as the internal structure of the carapace of *D. magna* (Christensen et al. 2018), but we lack knowledge about potential differences in the cuticle surface molecules between the different attachment sites.

Some attachment sites, such as the rectum, distal hindgut and anus, necessitate that the bacterial spores go through the digestive tract to reach them. This could cause differences in the adhesion mechanism, as spores going through the gut might be affected by the digestive process of the host. Attachment to the external abdomen and the trunk limbs does not require a gut passage of the spores.

Implications for the underlying genetics of resistance

In the present host–parasite system, attachment to different sites, namely the foregut and the hindgut, has been shown to be determined by distinct resistance loci in the host (Bento et al. 2017; Gattis 2018; Bento et al. 2020; Chapter 1: Ameline et al. 2021; Fredericksen et al. in prep). Resistance to the same *P. ramosa* isolate (P15) attaching at different sites in the host has been observed to independently segregate in selfed F1 offspring groups (Gattis 2018), showing that resistance to the same parasite genotype attaching at different sites might be determined by distinct resistance loci. A locus involved in hindgut attachment was shown to be distinct from the known loci involved in foregut attachment, but did interact with them (Bento et al. 2020). Attachment to the new sites described here may similarly be determined by distinct resistance loci. As specificity has implications in the type of selection the resistance genes involved undergo, varying specificity across bacterial genotypes might result in different evolutionary dynamics of resistance alleles and genetic architectures of resistance (Agrawal and Lively 2002; Salathé et al. 2008; Dybdahl et al. 2014). Considering the importance of the attachment step in the infection process of *D. magna* by *P.*

ramosa, and the implications of specificity in the system in host-parasite coevolution theory, further investigation of the diversity and complexity of attachment and their underlying mechanisms is essential.

Authors contribution

CA and DE designed the study. CA and MF observed and categorized new patterns of attachment. BH designed the protocol for acquiring attachment images. CA analyzed the data, wrote the manuscript, and produced the images and figures.

References

Agrawal A, Lively CM. 2002. Infection genetics: gene-for-gene versus matching-alleles models and all points in between. *Evolutionary Ecology Research* **4**:79–90.

Ameline C, Bourgeois Y, Vögtli F, Savola E, Andras J, Engelstädter J, Ebert D. 2021. A two-locus system with strong epistasis underlies rapid parasite-mediated evolution of host resistance. *Molecular Biology and Evolution* **38**:1512–1528.

Andras JP, Fields PD, Du Pasquier L, Fredericksen M, Ebert D. 2020. Genome-wide association analysis identifies a genetic basis of infectivity in a model bacterial pathogen. *Molecular Biology and Evolution* **37**:3439–3452.

Bento G, Fields PD, Duneau D, Ebert D. 2020. An alternative route of bacterial infection associated with a novel resistance locus in the *Daphnia–Pasteuria* host–parasite system. *Heredity* **125**:173–183.

Bento G, Routtu J, Fields PD, Bourgeois Y, Du Pasquier L, Ebert D. 2017. The genetic basis of resistance and matching-allele interactions of a host–parasite system: The *Daphnia magna–Pasteuria ramosa* model. *PLOS Genetics* **13**:e1006596.

Bourgeois Y, Roulin AC, Müller K, Ebert D. 2017. Parasitism drives host genome evolution: Insights from the *Pasteuria ramosa–Daphnia magna* system. *Evolution* **71**:1106–1113.

Christensen AK, Owusu NG, Jean-Louis D. 2018. Carapace epithelia are rich in large filamentous actin bundles in *Daphnia magna, Daphnia pulex,* and *Sida crystallina* (Crustacea: Cladocera). *Invertebrate Biology* **137**:49–59.

Cogni R, Cao C, Day JP, Bridson C, Jiggins FM. 2016. The genetic architecture of resistance to virus infection in *Drosophila*. *Molecular Ecology* **25**:5228–5241.

Davies KG. 2009. Understanding the interaction between an obligate hyperparasitic bacterium, *Pasteuria penetrans* and its obligate plant‐parasitic nematode host, *Meloidogyne* spp. *Advances in Parasitology* **68**:211–245.

Decaestecker E, Gaba S, Raeymaekers JAM, Stoks R, Van Kerckhoven L, Ebert D, De Meester L. 2007. Host–parasite 'Red Queen' dynamics archived in pond sediment. *Nature* **450**:870–873.

Duneau D, Luijckx P, Ben-Ami F, Laforsch C, Ebert D. 2011. Resolving the infection process reveals striking differences in the contribution of environment, genetics and phylogeny to host–parasite interactions. *BMC biology* **9**:1–11.

Dybdahl MF, Jenkins CE, Nuismer SL. 2014. Identifying the molecular basis of host-parasite coevolution: merging models and mechanisms. *The American Naturalist* **184**:1–13.

Ebert D, Duneau D, Hall MD, Luijckx P, Andras JP, Du Pasquier L, Ben-Ami F. 2016. A population biology perspective on the stepwise infection process of the bacterial pathogen *Pasteuria ramosa* in *Daphnia*. *Advances in Parasitology* **91**:265–310.

Ford SA, Williams D, Paterson S, King KC. 2017. Co-evolutionary dynamics between a defensive microbe and a pathogen driven by fluctuating selection. *Molecular Ecology* **26**:1778–1789.

Fortuna MA, Barbour MA, Zaman L, Hall AR, Buckling A, Bascompte J. 2019. Coevolutionary dynamics shape the structure of bacteria‐phage infection networks. *Evolution* **73**:1001–1011.

Fredericksen M, Ameline C, Krebs M, Hüssy B, Fields PD, Andras JP, Ebert D. 2021. Infection phenotypes of a coevolving parasite are highly diverse, structured, and specific. *Evolution* **75**:2540–2554.

Fredericksen M, Fields PD, Bento G, Ebert D. in prep. QTL and fine mapping parasite resistance in *Daphnia magna*.

Fryer G. 1991. Functional morphology and the adaptive radiation of the Daphniidae (Branchiopoda: Anomopoda). *Philosophical Transactions of the Royal Society B: Biological Sciences* **331**:1–99.

Gattis S. 2018. Segregation of resistance to the parasite *Pasteuria ramosa* in the freshwater crustacean *Daphnia magna*.

Giblin-Davis R, Williams D, Wergin W, Dickson D, Hewlett T, Bekal S, Becker J. 2001. Ultrastructure and development of *Pasteuria* sp. (S-1 strain), an obligate endoparasite of *Belonolaimus longicaudatus* (Nemata: Tylenchida). *Journal of Nematology* **33**:227–238.

Luijckx P, Ben-Ami F, Mouton L, Du Pasquier L, Ebert D. 2011. Cloning of the unculturable parasite *Pasteuria ramosa* and its *Daphnia* host reveals extreme genotype–genotype interactions. *Ecology Letters* **14**:125–131.

Luijckx P, Fienberg H, Duneau D, Ebert D. 2013. A matching-allele model explains host resistance to parasites. *Current Biology* **23**:1085–1088.

Magwire MM, Fabian DK, Schweyen H, Cao C, Longdon B, Bayer F, Jiggins FM. 2012. Genome-wide association studies reveal a simple genetic basis of resistance to naturally coevolving viruses in *Drosophila melanogaster*. *PLoS Genetics* **8**:e1003057.

Martinů J, Hypša V, Štefka J. 2018. Host specificity driving genetic structure and diversity in ectoparasite populations: Coevolutionary patterns in *Apodemus* mice and their lice. *Ecology and Evolution* **8**:10008–10022.

Mendoza de Gives P, Davies KG, Morgan M, Behnke JM. 1999. Attachment tests of *Pasteuria penetrans* to the cuticle of plant and animal parasitic nematodes, free living nematodes and *srf* mutants of *Caenorhabditis elegans*. *Journal of Helminthology* **73**:67–71.

Metzger CMJA, Luijckx P, Bento G, Mariadassou M, Ebert D. 2016. The Red Queen lives: Epistasis between linked resistance loci. *Evolution* **70**:480–487.

Mohan S, Mauchline TH, Rowe J, Hirsch PR, Davies KG. 2012. *Pasteuria* endospores from *Heterodera cajani* (Nematoda: Heteroderidae) exhibit inverted attachment and altered germination in cross-infection studies with *Globodera pallida* (Nematoda: Heteroderidae). *FEMS Microbiology Ecology* **79**:675–684.

Mouton L, Traunecker E, McElroy K, Du Pasquier L, Ebert D. 2009. Identification of a polymorphic collagen-like protein in the crustacean bacteria *Pasteuria ramosa*. *Research in Microbiology* **160**:792–799.

Nagasawa H. 2012. The crustacean cuticle: structure, composition and mineralization. *Frontiers in Bioscience* **E4**:711–720.

Orlansky S, Ben-Ami F. 2019. Genetic resistance and specificity in sister taxa of *Daphnia*: insights from the range of host susceptibilities. *Parasites & Vectors* **12**:545.

Phani V, Shivakumara TN, Davies KG, Rao U. 2017. *Meloidogyne incognita* Fatty Acid- and Retinol- binding protein (Mi-FAR-1) affects nematode infection of plant roots and the attachment of *Pasteuria penetrans* endospores. *Frontiers in Microbiology* **8**:1–13.

Phani V, Shivakumara TN, Davies KG, Rao U. 2018. Knockdown of a mucin-like gene in *Meloidogyne incognita* (Nematoda) decreases attachment of endospores of *Pasteuria penetrans* to the infective juveniles and reduces nematode fecundity. *Molecular Plant Pathology* **19**:2370–2383.

Piecyk A, Roth O, Kalbe M. 2019. Specificity of resistance and geographic patterns of virulence in a vertebrate host-parasite system. *BMC Evolutionary Biology* **19**:1–14.

Preston JF, Dickson D, Maruniak J, Nong G, Brito J, Schmidt LM, Giblin-Davis R. 2003. *Pasteuria* spp.: Systematics and phylogeny of these bacterial parasites of phytopathogenic nematodes. *Journal of Nematology* **35**:198–207.

Salathé M, Kouyos R, Bonhoeffer S. 2008. The state of affairs in the kingdom of the Red Queen. *Trends in Ecology & Evolution* **23**:439–445.

Srivastava A, Mohan S, Mauchline TH, Davies KG. 2018. Evidence for diversifying selection of genetic regions of encoding putative collagen-like host-adhesive fibers in *Pasteuria penetrans*. *FEMS Microbiology Ecology* **95**:1–8.

Zueva KJ, Lumme J, Veselov AE, Kent MP, Primmer CR. 2018. Genomic signatures of parasite-driven natural selection in north European Atlantic salmon (*Salmo salar*). *Marine Genomics* **39**:26–38.

Supplementary Material

Chapter 1

Overview

Section in main manuscript	Element	Description	Page
Results			
Parasite-mediated selection explains phenotypic dynamics			
Monitoring	Fig. S1.1	*Pasteuria* genotypes	p. 104
Linking resistance phenotypes to genotypes	Fig. S1.2	ABC genetic model	
Genomic regions of resistance to the parasite	Tables S1.1 and S1.2	E locus description	p. 105
Genetic model of resistance inheritance	Table S1.3	GWAS genotypes	p. 106
	Tables S1.4 to S1.15	Selfing results	p. 106–111
Linking the genomic regions and the genetic model of resistance	Tables S1.16 to S1.18	Markers linkage	p. 112–113
Materials and methods			
Assessment of resistotype segregation	Table S1.19	Selfing methods	p. 114
Predictions of segregation patterns	Documents S1.1 and S1.2	Peas program	p. 115–118
Linking the phenotype to the genotype	Tables S1.20 and S1.21	Genetic markers	p. 119
	References		p. 120

Results

Parasite-mediated selection explains phenotypic dynamics

Monitoring

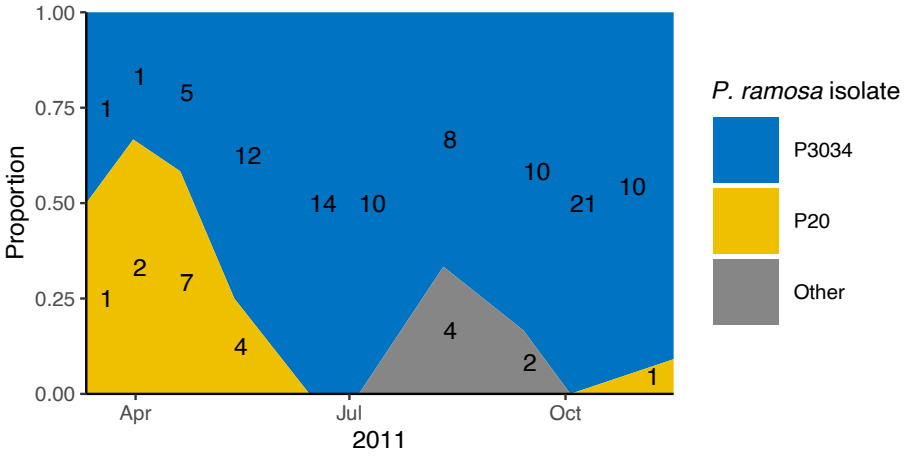

Figure S1.1

Pasteuria ramosa genotypes frequency over time during the 2011 active season of *Daphnia magna*. Infected animals were collected throughout the season, and the genotype of the parasite was determined using microsatellite markers following the protocol described in (Andras and Ebert 2013). A total of 113 infected *D. magna* individuals were sampled throughout the season and their parasite genotype was assessed. The P20 genotype represents about 50% of the parasite diversity among infected hosts at the beginning of the season, a proportion that then drops off during the epidemics. The P3034 genotype represents the most diversity of the parasite population among infected hosts but was not used in this study to score host resistotype (resistance phenotype). Numbers represent the amount of *D. magna* individuals sampled on each collection date.

Linking resistance phenotypes to genotypes

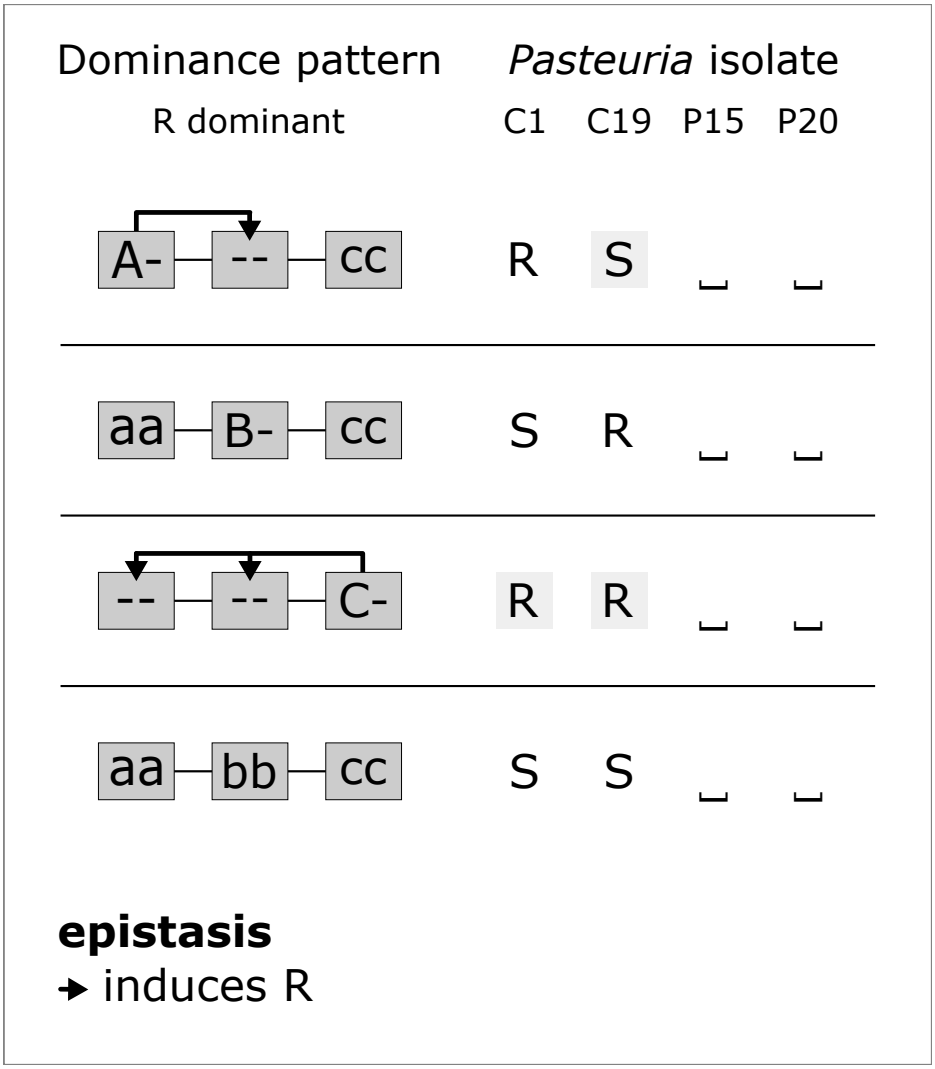

Figure S1.2

Genetic model of resistance inheritance at the ABC cluster in the *D. magna–P. ramosa* system. Resistance is dominant at the A, B and C loci. The dominant allele at the A locus confers resistance to C1 and susceptibility to C19, regardless of the genotype at the B locus (epistasis). The dominant allele at the B locus confers resistance to C19, in the right genetic background, i.e. when an individual is double recessive at the A locus ("aa" genotype). The dominant allele at the C locus acts epistatically on the A and B loci and confers resistance to C1 and C19, regardless of the genotype at the A and B loci. Figure adapted from (Metzger et al. 2016).

Genomic regions of resistance to the parasite

Scaffold	Length (bp)
scaffold02167	358328
contig71262	772
scaffold00149	66134
scaffold00715	344834
scaffold01200	81121
scaffold01244	6526
scaffold01745	65595
scaffold01839	55648
scaffold01865	165487
scaffold02315	259660
scaffold02388	172183
scaffold02489	70866
scaffold02560	89801
scaffold02708	22268
scaffold02913	44097
scaffold02970	253762
scaffold02993	133684
scaffold03031	266621
scaffold03154	80879
scaffold03356	21979
scaffold02031	8800
scaffold02207	115428
scaffold00872	416603

Table S1.1

Genomic description of the E locus. The region displaying the most markers discriminating between _-_-_R and _-_-_S encompassed 22 scaffolds and one contig on version 2.4 of the *Daphnia magna* reference genome (Routtu et al. 2014), with a cumulated length of 3101076 bp. The strongest signals of association were found on scaffolds 2167 and 2560. Scaffolds are ordered following the genetic map of (Dukić et al. 2016).

Table S1.2

We found 485 genes on all associated scaffolds. Scaffolds 2167 and 2560 harbored 82 candidate genes. Some of these genes had annotations similar to genes identified in a previous study of the ABC locus (Bento et al. 2017), with a glucosyltransferase found on scaffold 2167. Three other sugar transferases (galactosyltransferases) were identified on the 22 associated scaffolds, two of them found on scaffold 2560.

Scaffold	Start	End	Name
scaffold02489	49633	55225	udp-galactose:n-acetylgalactosamine-alpha-r beta galactosyltransferase/ARP2_G2977
scaffold02560	1296	4007	udp-galactose:n-acetylgalactosamine-alpha-r beta galactosyltransferase/ARP2_G2977
scaffold02560	4186	14123	udp-galactose:n-acetylgalactosamine-alpha-r beta galactosyltransferase/ARP2_G2977
scaffold02167	334036	335960	glucosyl/glucuronosyl tr_G27

Genetic model of resistance inheritance

Table S1.3

List of *D. magna* genotypes used for the association analysis. Genotypes whose name starts with "CH-H" were collected directly from the pond between 2010 and 2014. Names starting with "t" depict animals hatched in the laboratory from resting eggs collected in early 2014, before the natural hatching of the *D. magna* population.

Clone	Resistotype C1, C19, P15, P20	Resistotype C1, C19, _, P20	C-locus genotype	E-locus genotype
CH-H-1769	RRRR	RR_R	Cc	ee
CH-H-2029	RRRR	RR_R	Cc	ee
CH-H-2299	RRRR	RR_R	CC	ee
t1_10.3_2	RRRR	RR_R	CC	ee
t2_14.3_10	RRRR	RR_R	CC	ee
CH-H-1	RRSR	RR_R	Cc	ee
t1_10.3_4	RRSR	RR_R	Cc	ee
t3_10.3_12	RRSR	RR_R	Cc	unsure
t3_14.3_4	RRSR	RR_R	CC	ee
t3_14.3_5	RRSR	RR_R	Cc	ee
t3_31.3_1	RRSR	RR_R	Cc	ee
t4_10.3_11	RRSR	RR_R	CC	ee
t4_10.3_12	RRSR	RR_R	Cc	ee
t4_10.3_2	RRSR	RR_R	Cc	ee
t5_10.3_5	RRSR	RR_R	CC	ee
t5_20.3_1	RRSR	RR_R	CC	ee
t2_17.3_1	RRSS	RR_S	Cc	Ee
t2_17.3_4	RRSS	RR_S	Cc	Ee
t2_17.3_5	RRSS	RR_S	Cc	EE
t3_12.3_1	RRSS	RR_S	CC	Ee
t3_31.3_3	RRSS	RR_S	CC	EE
t4_13.3_10	RRSS	RR_S	Cc	EE
t4_17.3_8	RRSS	RR_S	Cc	Ee
t4_17.3_9	RRSS	RR_S	CC	Ee
t5_12.3_3	RRSS	RR_S	CC	Ee
t5_12.3_4	RRSS	RR_S	Cc	Ee
CH-H-16	SSSS	SS_S	cc	Ee
t2_12.3_10	SSSS	SS_S	cc	Ee
t2_12.3_11	SSSS	SS_S	cc	ee
t2_12.3_12	SSSS	SS_S	cc	ee
t2_14.3_9	SSSS	SS_S	cc	EE
t3_12.3_6	SSSS	SS_S	cc	ee
t3_12.3_8	SSSS	SS_S	cc	EE
t3_13.3_5	SSSS	SS_S	cc	Ee
t3_18.3_3	SSSS	SS_S	cc	Ee
t4_12.3_3	SSSS	SS_S	cc	EE
t4_7.3_4	SSSS	SS_S	cc	Ee

Tables S1.4 to S1.15

Selfing results in the Aegelsee *Daphnia magna* population: phenotypic and genotypic segregation. **Tables S1.4 to S1.12:** Selfing results for parents with variation at C and E loci. **Tables S1.13 and 1.S14:** Selfing results for parents with variation at B, C and E loci. **Table S1.15:** Detailed results of statistical analyses applied to F1 groups.

Tables S1.4 to S1.12

Expected and observed genotypes and phenotypes of F1 offspring groups resulting from the selfing of F0 parents where variation at the C and E loci was observed (see Supplementary Table S1.21 for clones' details). Observed resistance genotype for parents and offspring was assessed using markers DMPR1 and DMPR3 for the C and the E loci, respectively (see results). Resistance is dominant at the C locus (resistance to C1/C19) whereas resistance is recessive at the E locus (resistance to P20). In addition, an epistatic relationship linking both loci confers susceptibility to P20 to an individual that shows susceptibility to C1 and C19, disregarding the individual genotype at the E locus (see results section Fig. 1.5). Text in red denotes genotypes and their corresponding phenotypes where the epistatic relationship between the C and the E loci is expected to be revealed in the phenotype. The epistatic relationship "confers" to "cc--" individuals a susceptibility to P20, whatever their genotype at the E locus. Hence the epistasis can only be observed phenotypically in "ccee" offspring. If the epistatic relationship is not present in this case, the observed phenotype would be SS_R, whereas if the epistatic relationship is present, the observed phenotype would be SS_S. **A.** Expected Punnett square for the selfed genotype according to the genetic model. **B.** Expected vs. observed genotypes and phenotypes of selfed F1 offspring. Differences in offspring number between the genotype and the phenotype correspond to instances where either genetic markers analysis did not work, or attachment test was

not conducted because the *D. magna* clone got extinct. Expected genotypes and phenotypes were calculated from the Punnett square and using the R package "peas" (Supplementary Doc. S1.1). Genotypes are ordered in upper-case then lower-case fashion. We compared expected vs. observed genotype and resistotype segregation separately in the F1 groups using the Cochran–Mantel–Haenszel (C-M-H) test for repeated tests of independence. When there was only one repeat (Supplementary Table S1.7), we used the Fisher test. In cases where there was only one category of expected and observed genotype or phenotype, no test was run (Supplementary Tables S1.4, S1.6, S1.10, S1.11 (resistotype only) and S1.12). In these cases, expectation and observation show a perfect match. Following each C-M-H test, assumption of homogeneity of the odds ratio across repeats was confirmed using a Breslow-Day test (R package DescTools: (Signorell et al. 2018)). However, this test can only be operated in 2x2 tables (phenotype only Supplementary Tables S1.5, S1.7, S1.8). We then ran a Fisher test of independence for each comparison (expected vs. observed for each repeat, Bonferroni corrected) to detect possible significant differences in opposite directions across repeats, which would result in a non-significant C-M-H test. We did not detect such differences in direction (see Supplementary Table S1.15 below for all detailed results of statistical analyses). Tests were run on counts, although we present here segregation of offspring as proportions.

Table S1.4

Selfed genotype "CCEE". F0 parents: **a**: t3_12.3_1i_12, **b**: t3_12.3_1i_21.

A

RR_S CCEE	**CE**
CE	RR_S

B

Markers genotype	Fraction Expected	Fraction Observed Repeat **a** n = 43	Fraction Observed Repeat **b** n = 37	C-M-H test on counts	Resistotype	Fraction Expected	Fraction Observed Repeat **a** n = 43	Fraction Observed Repeat **b** n = 37	C-M-H test on counts
CCEE	1	1	1	NA	RR_S	1	1	1	NA

Table S1.5

Selfed genotype "CCEe". F0 parents: **a**: CH-2015-36, **b**: t3_12.3_1, **c**: CH-H-2015-49. Repeat "c" was not tested genotypically as the E locus marker appeared not to be linked to the E locus.

A

RR_S CCEe	**CE**	**Ce**
CE	RR_S	RR_S
Ce	RR_S	RR_R

B

Markers genotype	Fraction Expected	Fraction Observed Repeat **a** n = 89	Fraction Observed Repeat **b** n = 31	Fraction Observed Repeat **c** n = 81	C-M-H test on counts (a+b)	Resistotype	Fraction Expected	Fraction Observed Repeat **a** n = 89	Fraction Observed Repeat **b** n = 31	Fraction Observed Repeat **c** n = 79	C-M-H test on counts
CCEE	0,25	0,31	0,19	1			0,75	0,79	0,74	0,84	
CCEe	0,50	0,46	0,55	0	$M^2 = 0.35$, $df = 2$, $p = 0.84$	RR_S					$X^2 = 0.85$, $df = 1$, $p = 0.36$
CCee	0,25	0,22	0,26	0		RR_R	0,25	0,21	0,26	0,16	

Table S1.6

Selfed genotype "CCee". F0 parents: **a**: CH-H-434-inb2-1, **b**: t1_10.3_2, **c**: CH-H-2015-16, **d**: CH-H-2016-b-70.

A

RR_R CCee	**Ce**
Ce	RR_R

B

Markers genotype	Fraction Expected	Fraction Observed Repeat **a** n = 39	Fraction Observed Repeat **b** n = 42	Fraction Observed Repeat **c** n= 66	Fraction Observed Repeat **d** n = 84	C-M-H test on counts	Resistotype	Fraction Expected	Fraction Observed Repeat **a** n = 39	Fraction Observed Repeat **b** n = 42	Fraction Observed Repeat **c** n = 70	Fraction Observed Repeat **d** n = 79	C-M-H test on counts
CCee	1	1	1	1	1	NA	RR_R	1	1	1	1	1	NA

Table S1.7

Selfed genotype "CcEE". F0 parent: **a**: t2_17.3_4i_12.

A

RR_S CcEE	CE	cE
CE	RR_R	RR_R
cE	RR_R	SS_S

B

Markers genotype	Fraction: Expected	Fraction: Observed, Repeat a n = 19	Fisher test on counts	Resistotype	Fraction: Expected	Fraction: Observed, Repeat a n = 19	Fisher test on counts
CCEE	0,25	0,32	$p = 0.92$	RR_S	0,75	0,74	$p = 1$
CcEE	0,50	0,42					
ccEE	0,25	0,26		SS_S	0,25	0,26	

Table S1.8

Selfed genotype "CcEe". F0 parents: **a**: t3_14.3_1, **b**: t2_17.3_4, **c**: t2_17.3_1, **d**: CH-H-2015-59. Repeat "d" was not tested genotypically as the E locus marker appeared not to be linked to the E locus. Text in grey corresponds to non-matching marker genotypes with their observed resistotypes according to the genetic model. Those non-matching observations are included above in the observed proportions of genotypes.

A

RR_S CcEe	CE	Ce	cE	ce
CE	RR_S	RR_S	RR_S	RR_S
Ce	RR_S	RR_R	RR_S	RR_R
cE	RR_S	RR_S	SS_S	SS_S
ce	RR_S	RR_R	SS_S	SS_S

B

Markers genotype	Fraction: Expected	Fraction: Observed, Repeat a n = 47	b n = 32	c n= 80	d n = 61	C-M-H test on counts (a+b+c)	Resistotype	Fraction: Expected	Fraction: Observed, Repeat a n = 48	b n = 32	c n = 64	d n = 65	C-M-H test on counts
CCEE	0,06	0	0,16	0,05	0,20	$M^2 = 6.79$, $df = 8$, $p = 0.56$	RR_S	0,56	0,47	0,56	0,65	0,51	$M^2 = 4.61$, $df = 2$, $p = 0.10$
CCEe	0,13	0	0,19	0,12	0								
CcEE	0,13	0,13	0,06	0,18	0,57								
CcEe	0,25	0,40	0,25	0,28	0								
ccEE	0,06	0,09	0	0,03	0,23		SS_S	0,25	0,30	0,06	0,13	0,21	
ccEe	0,13	0,11	0,03	0,03	0								
ccee	0,06	0,11	0,03	0,03	0								
CCee	0,06	0	0,09	0,17	0		RR_R	0,19	0,23	0,38	0,22	0,28	
Ccee	0,13	0,17	0,19	0,10	0								
CCEE					0,11		RR_R						
CCEe			0,06				RR_R						
CcEE		0,02	0,03		0,16		RR_R						
CcEe		0,06	0,06				RR_R						
CCee				0,05			RR_S						
Ccee		0,02	0,06				RR_S						
CcEE				0,02	0,02		SS_S						
CcEe				0,02			SS_S						
ccEE					0,03		RR_S						

Table S1.9

Selfed genotype "Ccee". F0 parents: **a**: t1_10.3_4, **b**: t5_10.3_3, **c**: CH-H-434-inb2-2.

A

RR_R Ccee	Ce	ce
Ce	RR_R	RR_R
ce	RR_R	SS_S

B

Markers genotype	Fraction Expected	Fraction Observed Repeat a n = 36	b n = 49	c n= 21	C-M-H test on counts	Resistotype	Fraction Expected	Fraction Observed Repeat a n = 36	b n = 49	c n= 22	C-M-H test on counts
CCee	0,25	0,19	0,16	0,14		RR_R	0,75	0,75	0,80	0,62	
Ccee	0,50	0,56	0,63	0,48	M^2 = 2.16, *df* = 2, *p* = 0.34						X^2 = 0.0062, *df* = 1, *p* = 0.94
ccee	0,25	0,25	0,20	0,38		SS_S	0,25	0,25	0,20	0,38	

Table S1.10

Selfed genotype "ccEE". F0 parent: **a**: CH-H-2015-97.

A

SS_S ccEE	cE
cE	SS_S

B

Markers genotype	Fraction Expected	Fraction Observed Repeat a n = 89	Fisher test on counts	Resistotype	Fraction Expected	Fraction Observed Repeat a n = 87	Fisher test on counts
ccEE	1	1	NA	SS_S	1	1	NA

Table S1.11

Selfed genotype "ccEe". F0 parents: **a**: CH-H-2015-113, **b**: t4_10.3_16.

A

SS_S ccEe	cE	ce
cE	SS_S	SS_S
ce	SS_S	SS_S

B

Markers genotype	Fraction Expected	Fraction Observed Repeat a n = 82	b n = 63	C-M-H test on counts	Resistotype	Fraction Expected	Fraction Observed Repeat a n = 84	b n = 65	C-M-H test on counts
ccEE	0,25	0,27	0,15		SS_S	1	1	1	
ccEe	0,50	0,55	0,44	M^2 = 0.58, *df* = 2, *p* = 0.75					NA
ccee	0,25	0,18	0,41						

Table S1.12

Selfed genotype "ccee". F0 parents: **a**: t4_13.3_2, **b**: CH-H-2015-86.

A

SS_S ccee	ce
ce	SS_S

B

Markers genotype	Fraction Expected	Fraction Observed Repeat a n = 76	b n = 36	C-M-H test on counts	Resistotype	Fraction Expected	Fraction Observed Repeat a n = 74	b n = 35	C-M-H test on counts
ccee	1	1	1	NA	SS_S	1	1	1	NA

Tables S1.13 and S1.14

Expected and observed phenotypes of F1 offspring resulting from the selfing of F0 parents where variation at the B- and E loci was observed (see Supplementary Table S1.21 for clones' details). Individuals bearing the dominant allele at the B locus display a SR_ _ resistotype underlined by a "--B-cc" genotype. In the Swisspond population we assume the recessive allele is fixed at the A locus and the dominant allele at the B locus is rare (see results section). Individuals with a SR_ _ resistotype are thus expected to possess an "aaB-cc" genotype in our study population. As genetic markers were not designed to discriminate variation at the B locus and consequently do not show linkage with expected genotypes, we present only phenotype segregation. We deduced the resistance genotypes of the present F0 parents based on their resistotype and on the segregation patterns of their F1 offspring. In these F1 offspring, we observed SR_R individuals, supposedly "aaB-ccee", which indicates that the epistatic relationship described before between the C and the E loci (results section Fig. 1.5) should also include the B locus. If the epistasis was only between the C and the E locus, SR_ _ individuals would necessarily be SR_S. However, we do find SR_R individuals among F1 offspring of SR_S parents, which indicates that the "bbcc--" genotype induces susceptibility to P20, regardless of the genotype at the E locus. As SR_ _ individuals are rare in the population, we base this hypothesis solely on the selfed offspring presented below. As the recessive allele at the A locus is fixed in the population, we cannot infer a possible role of the A locus in this epistatic relationship. Text in red denotes phenotypes and genotypes where this epistatic relationship between the B/C and the E loci is expected to be revealed in the phenotype. The epistatic relationship "confers" to "bbcc--" individuals a susceptibility to P20, whatever their genotype at the E locus. Hence the epistasis can only be observed phenotypically in "bbccee" offspring. If the epistatic relationship was not present in this case, the observed phenotype would be SS_R, whereas if the epistatic relationship is present, the observed phenotype is SS_S. This genetic model is presented in Fig. 1.5 in the results section. **A.** Expected Punnett square for the selfed genotype according to the genetic model including the B locus. **B.** Expected and observed phenotypes of selfed F1 offspring. Expected phenotypes were calculated from the Punnett square and using the R package "peas" (Supplementary Doc. S1.2). Genotypes are ordered in upper-case then lower-case fashion. We compared expected vs. observed resistotype segregation in the F1 groups using the Fisher test of independence (see Table S1.15 below for all detailed results of statistical analyses). Tests were run on counts, although we present here segregation of offspring as proportions.

Table S1.13

Selfed genotype "BbccEE". F0 parent: **a**: t0_9.3_7.

A

SR_S BbccEE	BcE	bcE
BcE	SR_S	SR_S
bcE	SR_S	SS_S

B

Markers genotype	Fraction: Expected	Fraction: Observed: Repeat: a n = 35	Fisher test on counts	Resistotype	Fraction: Expected	Fraction: Observed: Repeat: a n = 37	Fisher test on counts
BBccEE	0,25	NA		SR_S	0,75	0,76	
BbccEE	0,50	NA	NA	SS_S	0,25	0,22	$p = 1$
bbccEE	0,25	NA		SR_R	0,00	0,03	
CCee		0,29		SR_S			
CCee		0,03		SR_R			
Ccee		0,46		SR_S			
ccee		0,23		SS_S			

Table S1.14

Selfed genotype "BbccEe". F0 parent: **a**: t0_28.2_43.

A

SR_S BbccEe	BcE	Bce	bcE	bce
BcE	SR_S	SR_S	SR_S	SR_S
Bce	SR_S	SR_R	SR_S	SR_R
bcE	SR_S	SR_S	SS_S	SS_S
bce	SR_S	SR_R	SS_S	SS_S

B

Markers genotype	Fraction Expected	Fraction Observed Repeat a n = 36	Fisher test on counts	Resistotype	Fraction Expected	Fraction Observed Repeat a n = 38	Fisher test on counts
BBccEE	0,06	NA		SR_S	0,56	0,55	
BBccEe	0,13	NA					
BbccEE	0,13	NA					
BbccEe	0,25	NA					
bbccEE	0,06	NA	NA	SS_S	0,25	0,32	$p = 0.58$
bbccEe	0,13	NA					
bbccee	0,06	NA					
BBccee	0,06	NA		SR_R	0,19	0,13	
Bbccee	0,13	NA					
CCEE		0,06		SR_S			
CCEe		0,11		SR_S			
CcEE		0,08		SR_S			
CcEe		0,19		SR_S			
CcEe		0,06		SR_R			
Ccee		0,11		SR_S			
Ccee		0,06		SR_R			
ccEE		0,06		SS_S			
ccEe		0,17		SS_S			
ccee		0,11		SS_S			

Table S1.15

Detailed results of statistical analyses applied to F1 offspring groups. Analyses are described in tables' legends above.

Phenotype

	CMH test				BD test			Fisher test							
								repeat a		repeat b		repeat c		repeat d	
	M^2	*df*	*p*		X^2	*df*	*p*	*p*	*p + Bonf.*	*p*	*p + Bonf.*	*p*	*p + Bonf.*	*p*	*p + Bonf.*
Table S1.4	NA	NA	NA	NA	NA	NA	NA	NA	NA	NA	NA	NA	NA	NA	NA
Table S1.5	$X^2 = 0.85$	1	0,36	CI = (0.49, 1.25), estimate = 0.78, null value = 1	0,83	2	0,66	0,86	1	1	1	0,24	0,72	NA	NA
Table S1.6	NA	NA	NA	NA	NA	NA	NA	NA	NA	NA	NA	NA	NA	NA	NA
Table S1.7	NA	NA	NA	NA	NA	NA	NA	1	NA	NA	NA	NA	NA	NA	NA
Table S1.8	4,61	2	0,1	NA	NA	NA	NA	0,76	1	0,07	0,27	0,29	1	0,49	1
Table S1.9	$X^2 = 0.0062$	1	0,94	CI = (0.55, 1.9), estimate = 1.03, null value = 1	1,12	2	0,57	1	1	0,81	1	0,51	1	NA	NA
Table S1.10	NA	NA	NA	NA	NA	NA	NA	NA	NA	NA	NA	NA	NA	NA	NA
Table S1.11	NA	NA	NA	NA	NA	NA	NA	NA	NA	NA	NA	NA	NA	NA	NA
Table S1.12	NA	NA	NA	NA	NA	NA	NA	NA	NA	NA	NA	NA	NA	NA	NA
Table S1.13	NA	NA	NA	NA	NA	NA	NA	1	NA	NA	NA	NA	NA	NA	NA
Table S1.14	NA	NA	NA	NA	NA	NA	NA	0,58	NA	NA	NA	NA	NA	NA	NA

Genotype

	CMH test			Fisher test					
				repeat a		repeat b		repeat c	
	M^2	*df*	*p*	*p*	*p + Bonf.*	*p*	*p + Bonf.*	*p*	*p + Bonf.*
Table S1.4	NA	NA	NA	NA	NA	NA	NA	NA	NA
Table S1.5	0,35	2	0,84	0,67	1	0,89	1	NA	NA
Table S1.6	NA	NA	NA	NA	NA	NA	NA	NA	NA
Table S1.7	NA	NA	NA	0,92	NA	NA	NA	NA	NA
Table S1.8	6,79	8	0,56	0,06	0,19	0,61	1	0,39	1
Table S1.9	2,16	2	0,34	0,86	1	0,42	1	0,6	1
Table S1.10	NA	NA	NA	NA	NA	NA	NA	NA	NA
Table S1.11	0,58	2	0,75	0,64	1	0,13	0,25	NA	NA
Table S1.12	NA	NA	NA	NA	NA	NA	NA	NA	NA
Table S1.13	NA	NA	NA	NA	NA	NA	NA	NA	NA
Table S1.14	NA	NA	NA	NA	NA	NA	NA	NA	NA

Linking the genomic regions and the genetic model of resistance

Table S1.16

Multi-marker genotypes and their expected corresponding resistance genotype at the C and E loci and resistotypes (resistance phenotypes) of *Daphnia magna* in the Swisspond population, assuming perfect linkage between markers and resistance loci. All possible allele combinations for the four markers DMPR1, 2, 3 and 4 (DMPR: *Daphnia magna–Pasteuria ramosa*). DMPR1 and 2 are physically linked to the C locus while DMPR3 and 4 are physically linked to the E locus. Zeros (0) and ones (1) correspond to absence and presence of an allele, respectively. The size of an amplicon containing an allele is denoted next to the name of the allele (see Supplementary Table S1.20 for details on the markers). For example, DMPR1_R1_89 corresponds to the amplicon of 89 bp yielded by the PCR for the first R allele of the DMPR1 marker. Inferred resistotypes in red denote resistotypes where the epistatic interaction between the C and the E loci is detectable. In order to show the logic of the different possible combinations, lines with zeros and ones identical to the line directly above them are shown in grey.

Alleles associated to the C locus					Alleles associated to the E locus							
DMPR1_R1_89	DMPR1_R2_113	DMPR1_S_118	DMPR2_S_176	DMPR2_R_184	DMPR3_S_206	DMPR3_R1_211	DMPR3_R2_212	DMPR4_R_128	DMPR4_S_136	Multi-marker genotype	Inferred resistance genotype	Inferred resistotype
0	0	1	1	0	0	0	1	1	0	001_10_001_10	ccee	SS_S
0	0	1	1	0	0	1	0	1	0	001_10_010_10	ccee	SS_S
0	0	1	1	0	0	1	1	1	0	001_10_011_10	ccee	SS_S
0	0	1	1	0	1	0	0	0	1	001_10_100_01	ccEE	SS_S
0	0	1	1	0	1	0	1	1	1	001_10_101_11	ccEe	SS_S
0	0	1	1	0	1	1	0	1	1	001_10_110_11	ccEe	SS_S
0	1	0	0	1	0	0	1	1	0	010_01_001_10	CCee	RR_R
0	1	0	0	1	0	1	0	1	0	010_01_010_10	CCee	RR_R
0	1	0	0	1	0	1	1	1	0	010_01_011_10	CCee	RR_R
0	1	0	0	1	1	0	0	0	1	010_01_100_01	CCEE	RR_S
0	1	0	0	1	1	0	1	1	1	010_01_101_11	CCEe	RR_S
0	1	0	0	1	1	1	0	1	1	010_01_110_11	CCEe	RR_S
0	1	1	1	1	0	0	1	1	0	011_11_001_10	Ccee	RR_R
0	1	1	1	1	0	1	0	1	0	011_11_010_10	Ccee	RR_R
0	1	1	1	1	0	1	1	1	0	011_11_011_10	Ccee	RR_R
0	1	1	1	1	1	0	0	0	1	011_11_100_01	CcEE	RR_S
0	1	1	1	1	1	0	1	1	1	011_11_101_11	CcEe	RR_S
0	1	1	1	1	1	1	0	1	1	011_11_110_11	CcEe	RR_S
1	0	0	0	1	0	0	1	1	0	100_01_001_10	CCee	RR_R
1	0	0	0	1	0	1	0	1	0	100_01_010_10	CCee	RR_R
1	0	0	0	1	0	1	1	1	0	100_01_011_10	CCee	RR_R
1	0	0	0	1	1	0	0	0	1	100_01_100_01	CCEE	RR_S
1	0	0	0	1	1	0	1	1	1	100_01_101_11	CCEe	RR_S
1	0	0	0	1	1	1	0	1	1	100_01_110_11	CCEe	RR_S
1	0	1	1	1	0	0	1	1	0	101_11_001_10	Ccee	RR_R
1	0	1	1	1	0	1	0	1	0	101_11_010_10	Ccee	RR_R
1	0	1	1	1	0	1	1	1	0	101_11_011_10	Ccee	RR_R
1	0	1	1	1	1	0	0	0	1	101_11_100_01	CcEE	RR_S
1	0	1	1	1	1	0	1	1	1	101_11_101_11	CcEe	RR_S
1	0	1	1	1	1	1	0	1	1	101_11_110_11	CcEe	RR_S
1	1	0	0	1	0	0	1	1	0	110_01_001_10	CCee	RR_R
1	1	0	0	1	0	1	0	1	0	110_01_010_10	CCee	RR_R
1	1	0	0	1	0	1	1	1	0	110_01_011_10	CCee	RR_R
1	1	0	0	1	1	0	0	0	1	110_01_100_01	CCEE	RR_S
1	1	0	0	1	1	0	1	1	1	110_01_101_11	CCEe	RR_S
1	1	0	0	1	1	1	0	1	1	110_01_110_11	CCEe	RR_S

Table S1.18 (next page)

Observed allele combinations for markers DMPR3 and 4 and their corresponding inferred resistance genotype, expected and observed resistotypes. DMPR1 and 2 are linked to the E locus. Details about the markers and their expected signatures from the genetic model of resistance are given in Supplementary Table S1.20. Within the groups of "ee" genotypes, we separately present the "SS_ _" C1/C19 resistotype as we expect in that case the P20 resistotype to be "_ _ _S", due to the epistatic relationship between the C and the E locus. Text in grey represents occurrences where the measured and expected resistotypes do not match. Text in red denotes resistotypes where the epistatic interaction between the C and the E loci is detectable. For each genotype, the expected count of resistotypes is calculated as the total count of observed resistotypes. The panel of clones used represents 24 selfed offspring groups (F1) ranging from 12 to 84 individual clones (Supplementary Table S1.19), as well as three random samples from the Swisspond from 2014 to 2016 (22 to 108 clones), either hatched from resting eggs of directly sampled in the pond. Differences in total sample size correspond to occurrences where a marker did not amplify or when the marker signature could not be clearly identified. The initial total sample size of phenotyped clones is n = 1550. Individuals with a "SR_ _" resistotype were excluded from the analysis as they were not used in the GWAS from which the markers were designed. Better linkage is observed between the E locus and DMPR3 than between the E locus and DMPR4. Note that marker DMPR4 did not amplify as well as the other markers (n = 911). This marker showed better amplification when put alone in a PCR reaction however we decided not to use it further as it showed poor linkage to the E locus.

Table S1.17

Observed allele combinations for markers DMPR1 and 2 and their corresponding inferred resistance genotype, expected and observed resistotypes. DMPR1 and 2 are linked to the C locus. Details about the markers and their expected signatures from the genetic model of resistance are given in Supplementary Table S1.20. Text in grey represents occurrences where the measured and expected resistotypes do not match. For each genotype, the expected count of resistotypes is calculated as the total count of observed resistotypes. The panel of clones used represents 24 selfed offspring groups (F1) ranging from 19 to 89 individual clones (Supplementary Table S1.19), as well as three random samples from the Swisspond from 2014 to 2016 (22 to 108 clones), either hatched from resting eggs of directly sampled from the pond. Differences in total sample size correspond to occurrences where a marker did not amplify or when the marker signature could not be clearly identified. The initial total sample size of phenotyped clones is n = 1550. Individuals with a "SR_ _" resistotype were excluded from the analysis as they were not used in the GWAS from which the markers were designed. Better linkage is observed between the C locus and DMPR1 than between the C locus and DMPR2.

DMPR1_R1_89	DMPR1_R2_113	DMPR1_S_118	DMPR1 genotype	Inferred resistance genotype	Inferred resistotype	Measured resistotype	Count (n = 1442)	Expected count from inferred resistotypes	Frequency (n = 1442)	Expected frequency from inferred resistotypes
0	0	1	001	cc	SS_ _	SS_ _	488	490	0,338	0,340
						RR_ _	*2*	*0*	*0,001*	*0*
0	1	0	010	CC	RR_ _	RR_ _	515	515	0,357	0,357
0	1	1	011	Cc	RR_ _	RR_ _	251	254	0,174	0,176
						SS_ _	*3*	*0*	*0,002*	*0*
1	0	0	100	CC	RR_ _	RR_ _	76	76	0,053	0,053
1	0	1	101	Cc	RR_ _	RR_ _	67	68	0,046	0,047
						SS_ _	*1*	*0*	*0,001*	*0*
1	1	0	110	CC	RR_ _	RR_ _	39	39	0,027	0,027
							Fisher's exact test $p = 0.77$			

DMPR2_S_176	DMPR2_R_184	DMPR2 genotype	Inferred resistance genotype	Inferred resistotype	Measured resistotype	Count (n = 1434)	Expected count from inferred resistotypes	Frequency (n = 1434)	Expected frequency from inferred resistotypes
0	1	01	CC	RR_ _	RR_ _	548	549	0,382	0,383
					SS_ _	*1*	*0*	*0,001*	*0*
1	0	10	cc	SS_ _	SS_ _	480	599	0,335	0,418
					RR_ _	*119*	*0*	*0,083*	*0*
1	1	11	Cc	RR_ _	RR_ _	283	286	0,197	0,199
					SS_ _	*3*	*0*	*0,002*	*0*
						Fisher's exact test $p = 1.25.10^{-37}$			

Table S1.18 (see left page)

Observed allele combinations for markers DMPR3 and 4 and their corresponding inferred resistance genotype, expected and observed resistotypes.

DMPR3_S_206	DMPR3_R1_211	DMPR3_R2_212	DMPR3 genotype	Inferred resistance genotype	Measured resistotype to C1/C19	Inferred resistotype to P20	Measured resistotype to P20	Count (n = 1438)	Expected count from inferred resistotypes	Frequency (n = 1438)	Expected frequency from inferred resistotypes
0	1	0	010	ee	RR_ _	_ _ _R	_ _ _R	468	481	0,325	0,334
							_ _ _S	*13*	*0*	*0,009*	*0*
					SS_ _	_ _ _S	_ _ _S	227	227	0,158	0,158
							_ _ _R				
0	1	1	011	ee	RR_ _	_ _ _R	_ _ _R	3	3	0,002	0,002
1	0	0	100	EE	XX_ _	_ _ _S	_ _ _S	417	450	0,290	0,313
							_ _ _R	*33*	*0*	*0,023*	*0*
1	0	1	101	Ee	XX_ _	_ _ _S	_ _ _S	1	1	0,001	0,001
1	1	0	110	Ee	XX_ _	_ _ _S	_ _ _S	247	276	0,172	0,192
							_ _ _R	*29*	*0*	*0,020*	*0*
								Fisher's exact test $p = 5.34.10^{-19}$			

DMPR4_R_128	DMPR4_S_136	DMPR4 genotype	Inferred resistance genotype	Measured resistotype to C1/C19	Inferred resistotype to P20	Measured resistotype to P20	Count (n = 911)	Expected count from inferred resistotypes	Frequency (n = 911)	Expected frequency from inferred resistotypes
0	1	01	EE	XX_ _	_ _ _S	_ _ _S	357	374	0,392	0,411
						_ _ _R	*17*	*0*	*0,019*	*0*
1	0	10	ee	RR_ _	_ _ _R	_ _ _R	18	19	0,020	0,021
						_ _ _S	*1*	*0*	*0,001*	*0*
				SS_ _	_ _ _S	_ _ _S	6	6	0,007	0,007
1	1	11	Ee	XX_ _	_ _ _S	_ _ _S	251	512	0,276	0,562
						_ _ _R	*261*	*0*	*0,286*	*0*
							Fisher's exact test $p = 1.00.10^{-100}$			

Materials and methods

Assessment of resistotype segregation

Table S1.19

Overview of the parent clones used to produce the selfed offspring sorted by their inferred genotypes. Resistotype corresponds to the resistance phenotype to the *Pasteuria ramosa* isolates C1, C19 and P20, in that order. The inferred genotypes at the C and E loci are the result of the markers analysis of the parent clones (see Supplementary Table S1.20). Two exceptions (marked with an asterisk "*") are cases where the marker genotype at the E locus was "EE", although segregation in the selfed F1 offspring revealed a "Ee" genotype. We selfed one to four parents of each homozygous genotype category, and one to four parents of each simple or double heterozygous genotype category. The genotype of the two "SR_S" parents was inferred using only the segregation pattern of their selfed offspring. The markers were designed to map resistance to C1, C19 and P20 in the Aegelsee population, using the three main resistotypes only: RR_S, RR_R and SS_S, and were consequently not linked to the genotype in SR_ _ individuals. F0 parents correspond to females caught from plankton (clone name starting with "CH") or hatched from resting eggs (clone name starting with "t") collected from the natural population between 2011 and 2016. Differences in offspring number between the genotype and the phenotype correspond to instances where either genetic markers analysis did not work, or attachment test was not conducted because the *D. magna* clone got extinct.

Resistotype	Inferred genotype	Repeat name	Parent clone name	n (offspring)		Segregation results
				Genotype n = 1274	Phenotype n = 1266	
RR_S	CCEE	a	t3_12.3_1i_12	43	43	Table S1.4
		b	t3_12.3_1i_21	37	37	
RR_S	CCEe	a	CH-2015-36	89	89	Table S1.5
		b	t3_12.3_1	31	31	
		c	CH-H-2015-49*	81	79	
RR_R	CCee	a	CH-H-434-inb2-1	39	39	Table S1.6
		b	t1_10.3_2	42	42	
		c	CH-H-2015-16	66	70	
		d	CH-H-2016-b-70	84	79	
RR_S	CcEE	a	t2_17.3_4i_12	19	19	Table S1.7
RR_S	CcEe	a	t3_14.3_1	47	48	Table S1.8
		b	t2_17.3_4	32	34	
		c	t2_17.3_1	80	64	
		d	CH-H-2015-59*	61	65	
RR_R	Ccee	a	t1_10.3_4	36	36	Table S1.9
		b	t5_10.3_3	49	49	
		c	CH-H-434-inb2-2	21	22	
SS_S	ccEE	a	CH-H-2015-97	89	87	Table S1.10
SS_S	ccEe	a	CH-H-2015-113	82	84	Table S1.11
		b	t4_10.3_16	63	65	
SS_S	ccee	a	t4_13.3_2	76	74	Table S1.12
		b	CH-H-2015-86	36	35	
SR_S	BbccEE	a	t0_9.3_7	35	37	Table S1.13
SR_S	BbccEe	a	t0_28.2_43	36	38	Table S1.14

Predictions of segregation patterns

Documents S1.1 and S1.2

Implementation of the genetic model of resistance using the "peas" package. **Doc. S1.1:** Variation at the C and E loci. **Doc S1.2:** Variation at the B, C and E loci.

Document S1.1

Implementation of the genetic model of resistance using the "peas" package. Variation at the C and E loci. The R package "peas" is available at https://github.com/JanEngelstaedter/peas. We consider variation at the C and E loci. In **step 2.1** we define the genetic system as two loci: C and E presenting each two alleles. Both loci sit on different linkage groups. In **step 2.2** we set the genetic model itself, defining resistance genotypes and their corresponding resistance phenotypes (resistotypes). Resistotypes are presented as resistant (R) or susceptible (S) to the bacteria strains C1, C19 and P20, in that order. Resistance to the bacteria is dominant for the C locus (Metzger et al. 2016) whereas resistance is recessive at the E locus. The dominant allele at the C locus confers resistance to C1 and C19. The recessive allele at the E locus confers resistance to P20. The epistatic interaction acts between the C and the E loci. Recessive individuals at C locus are susceptible to P20, regardless of their genotype at the E locus. The genetic model produces 9 possible genotypes coding for 3 different resistotypes. The number of possible genotypes corresponds to the draw of one element among three (AA, Aa or aa genotype) two consecutive times (at two different loci): *n(possible genotypes) = 2(3¦1) = 9*. In **step 3** we produce the expected results from the selfing of F0 mothers with all possible combinations of the two loci C and E and store them in a spreadsheet (Results section Table 1.1 & Supplementary Tables S1.4 to S1.12).

Genetic model for resistance to P20 in the Aegelsee

implemented in peas R package

1. Install the package

```
#install.packages("devtools")
#devtools::install_github("JanEngelstaedter/peas",
build_vignettes = TRUE)
library(peas)
```

C_E genetic model of resistance

2. Set up the genetic model

2.1 Defining the genetic system

```
# 2 loci with 2 alleles each, on different chromosomes
CE <- newGenopheno(nloci = 1,
                   alleleNames = list(c("c", "C")))
CE <- addLinkageGroup(CE, alleleNames = list(c("e",
"E")))
CE
```

```
## Genetic system comprising 2 linkage groups:
##   Linkage group 1: autosomal, 1 locus
##     Alleles at locus 1: c, C
##   Linkage group 2: autosomal, 1 locus
##     Alleles at locus 1: e, E
## No phenotypes defined.
```

2.2 Set genotypes and their corresponding phenotypes: THE GENETIC MODEL

```
CE <- setPhenotypes(CE, "S/R", "__ | __","SS_R") #
default all recessive --> SS_R
# (we don't take the epistasis relation into account,
this will be the last line of the model)

CE <- setPhenotypes(CE, "S/R", "C_ | __","RR_R") # C
--> R to C1 and C19
CE <- setPhenotypes(CE, "S/R", "C_ | E_","RR_S") # E
--> S to P20

CE <- setPhenotypes(CE, "S/R", "cc | __","SS_S") # cc
--> S to P20, hides E
```

Summary of model

```
CE
```

```
## Genetic system comprising 2 linkage groups:
##   Linkage group 1: autosomal, 1 locus
##     Alleles at locus 1: c, C
##   Linkage group 2: autosomal, 1 locus
##     Alleles at locus 1: e, E
## Phenotypes defined for the following traits:
##   S/R (trait values: SS_S, RR_R, RR_S)
```

List of all possible genotype combinations and corresponding phenotypes

```
CEallgeno<-getPhenotypes(CE)
CEallgeno # all possible combinations
```

```
##       S/R
## cc | ee SS_S
## Cc | ee RR_R
## CC | ee RR_R
## cc | Ee SS_S
## Cc | Ee RR_S
## CC | Ee RR_S
## cc | EE SS_S
## Cc | EE RR_S
## CC | EE RR_S
```

```
nrow(CEallgeno) # 9 possible genotypes
```

```
## [1] 9
```

```
nrow(unique(CEallgeno)) # 3 possible resistotypes
```

```
## [1] 3
```

3. Predict crosses

```
CEcombi<-row.names(CEallgeno) # all possible geno
combinations from the model
CEcombi<-c(CEcombi[9],CEcombi[6],CEcombi[3],
      CEcombi[8],CEcombi[5],CEcombi[2],
      CEcombi[7],CEcombi[4],CEcombi[1]) # reorder
them (optional)
allcrossCE<-list() # create empty list to  store the
```

crossing results

```
library(xlsx)

# for all the nine possible combinations with C and E
varying (F0 mothers)

# we calculate the genotypes and phenotypes fractions
in the F1 offspring with the predictCross function
(from the selfing of F0 mothers)

for (i in 1:9) {

# using the "CE" genetic model, we cross the "i"
combination with itself
 allcrossCE[[i]]<-predictCross(CE, CEcombi[i],
CEcombi[i])


# we add the corresponding resistotypes to the
genotype output
 allcrossCE[[i]]$genotypes$SRtrait <-
getPhenotypes(CE, equivalent = "none")[row.
names(allcrossCE[[i]]$genotypes), ]


# we store the result in a spreadsheet (genotype
output)
 write.xlsx(allcrossCE[[i]]$genotypes,"CEcross.
xlsx", sheetName= paste(CEcombi[i],"geno",
as.character(i)), append=T)


# then the phenotype output in another sheet of the
same document
 write.xlsx(allcrossCE[[i]]$phenotypes,"CEcross.
xlsx", sheetName= paste(CEcombi[i],"pheno",
as.character(i)), append=T)
 }
allcrossCE
```

```
## [[1]]
## [[1]]$genotypes
##       fraction SRtrait
## CC | EE      1   RR_S
##
## [[1]]$phenotypes
##   S/R fraction
## 1 RR_S      1
##
##
## [[2]]
## [[2]]$genotypes
##       fraction SRtrait
## CC | EE    0.25   RR_S
## CC | Ee    0.50   RR_S
## CC | ee    0.25   RR_R
##
## [[2]]$phenotypes
##   S/R fraction
## 1 RR_R    0.25
## 2 RR_S    0.75
##
##
## [[3]]
## [[3]]$genotypes
##       fraction SRtrait
## CC | ee      1   RR_R
##
## [[3]]$phenotypes
##   S/R fraction
## 1 RR_R      1
##
##
## [[4]]
## [[4]]$genotypes
##       fraction SRtrait
## CC | EE    0.25   RR_S
## Cc | EE    0.50   RR_S
## cc | EE    0.25   SS_S
##
## [[4]]$phenotypes
##   S/R fraction
## 1 RR_S    0.75
## 2 SS_S    0.25
##
##
## [[5]]
## [[5]]$genotypes
##       fraction SRtrait
## CC | EE  0.0625   RR_S
## Cc | EE  0.1250   RR_S
## CC | Ee  0.1250   RR_S
## Cc | Ee  0.2500   RR_S
## cc | EE  0.0625   SS_S
## cc | Ee  0.1250   SS_S
## CC | ee  0.0625   RR_R
## Cc | ee  0.1250   RR_R
## cc | ee  0.0625   SS_S
##
## [[5]]$phenotypes
##   S/R fraction
## 1 RR_R  0.1875
## 2 RR_S  0.5625
## 3 SS_S  0.2500
##
##
## [[6]]
## [[6]]$genotypes
##       fraction SRtrait
## CC | ee    0.25   RR_R
## Cc | ee    0.50   RR_R
## cc | ee    0.25   SS_S
##
## [[6]]$phenotypes
##   S/R fraction
## 1 RR_R    0.75
## 2 SS_S    0.25
##
##
## [[7]]
## [[7]]$genotypes
##       fraction SRtrait
## cc | EE      1   SS_S
##
## [[7]]$phenotypes
##   S/R fraction
## 1 SS_S      1
##
##
## [[8]]
## [[8]]$genotypes
##       fraction SRtrait
## cc | EE    0.25   SS_S
## cc | Ee    0.50   SS_S
## cc | ee    0.25   SS_S
##
## [[8]]$phenotypes
##   S/R fraction
## 1 SS_S      1
##
##
## [[9]]
## [[9]]$genotypes
##       fraction SRtrait
## cc | ee      1   SS_S
##
## [[9]]$phenotypes
##   S/R fraction
## 1 SS_S      1
```

Document S1.2

Implementation of the genetic model of resistance using the "peas" package. Variation at the B, C and E loci. In **step 2.1** we define the genetic system as three loci: B, C and E presenting each two alleles. The B and C loci sit on the same linkage group and recombination rate between them is set to r2 = (1-exp(-2*23.1/100))/2 as calculated in (Metzger et al. 2016). The E locus sits on a different linkage group. In **step 2.2** we set the genetic model itself, defining resistance genotypes and their corresponding resistance phenotypes (resistotypes). Resistotypes are presented as resistant (R) or susceptible (S) to the bacteria strains C1, C19 and P20, in that order. Resistance to the bacteria is dominant for the B and C loci (Metzger et al. 2016) whereas resistance is recessive at the E locus. The dominant allele at the B locus confers resistance to C19. The first epistatic interaction acts between the B and C loci. The dominant allele at the C locus confers resistance to C1 and C19, regardless of the genotype at the B locus. The recessive allele at the E locus confers resistance to P20. The second epistatic interaction acts between the B/C loci and the E locus. Double recessive individuals at the B and C loci are susceptible to P20, regardless of their genotype at the E locus. The genetic model produces 27 possible genotypes coding for 5 different resistotypes. The number of possible genotypes corresponds to the draw of one element among three (AA, Aa or aa genotype) three consecutive times (at three different loci): $n(possible\ genotypes) = 3(3¦1) = 27$. In **step 3** we produce the expected results from the selfing of F0 mothers with all possible combinations of the three loci B, C and E and store them in a spreadsheet. From these we extract the results of the F1 selfed offspring groups produced in the present study (Results section Table 1.2 & Supplementary Table S1.13 and S1.14).

BC_E genetic model of resistance

2. Set up the genetic model

2.1 Defining the genetic system

```
library(peas)
r2<-(1-exp(-2*23.1/100))/2 ## recombination rate between B and C loci (Metzger et al. 2016)

# 3 loci with 2 alleles each, BC clustered together (Metzger et al. 2016).
BCE <- newGenopheno(nloci = 2,
                    alleleNames = list(c("b", "B"), c("c", "C")),
                    rec = r2)
BCE <- addLinkageGroup(BCE, alleleNames = list(c("e", "E")))
```

2.2 Set genotypes and their corresponding phenotypes: THE GENETIC MODEL

```
BCE <- setPhenotypes(BCE, "S/R", "__~__ | __","SS_R")
# default all recessive --> SS_R
# (we don't take the epistasis relation into account, this will be the last line of the model)

BCE <- setPhenotypes(BCE, "S/R", "B_~__ | __","SR_R") # B --> R to C19

BCE <- setPhenotypes(BCE, "S/R", "B_~__ | E_","SR_S") # E --> S to P20

BCE <- setPhenotypes(BCE, "S/R", "__~C_ | __","RR_R") # C hides B and --> R to C1 and C19

BCE <- setPhenotypes(BCE, "S/R", "__~C_ | E_","RR_S") # E --> S to P20

BCE <- setPhenotypes(BCE, "S/R", "bb~cc | __","SS_S") # bb and cc --> S to P20, hides E
```

Summary of model

```
BCE
```

```
## Genetic system comprising 2 linkage groups:
##   Linkage group 1: autosomal, 2 loci with recombination rate 0.1849888
##     Alleles at locus 1: b, B
##     Alleles at locus 2: c, C
##   Linkage group 2: autosomal, 1 locus
##     Alleles at locus 1: e, E
## Phenotypes defined for the following traits:
##   S/R (trait values: SS_S, SR_R, RR_R, SR_S, RR_S)
```

List of all possible genotype combinations and corresponding phenotypes

```
BCEallgeno<-getPhenotypes(BCE)
nrow(BCEallgeno) # 27 possible genotypes
```

```
## [1] 27
```

```
nrow(unique(BCEallgeno)) # 5 possible resistotypes
```

```
## [1] 5
```

3. Predict crosses

```
BCEcombi<-row.names(BCEallgeno) # all possible geno combinations from the model
allcrossBCE<-list() # create empty list to  store the crossing results

library(xlsx)

for (i in 1:27) {

# using the "BCE" genetic model, we cross the "i" combination with itself
 allcrossBCE[[i]]<-predictCross(BCE, BCEcombi[i],
```

```
BCEcombi[i])


# we add the corresponding resistotypes to the genotype output
 allcrossBCE[[i]]$genotypes$SRtrait <- getPhenotypes(BCE, equivalent = "none")[row.names(allcrossBCE[[i]]$genotypes), ]


# we store the result in a spreadsheet (genotype output)
 write.xlsx(allcrossBCE[[i]]$genotypes,"BCEcross.xlsx", sheetName= paste(BCEcombi[i],"geno", as.character(i)), append=T)

# then the phenotype output in another sheet of the same document
 write.xlsx(allcrossBCE[[i]]$phenotypes,"BCEcross.xlsx", sheetName= paste(BCEcombi[i],"pheno", as.character(i)), append=T)}

# get a specific crossing

match("Bb~cc | Ee", BCEcombi) # position 11

## [1] 11

allcrossBCE[[11]]

## $genotypes
##          fraction SRtrait
## BB~cc | EE   0.0625   SR_S
## Bb~cc | EE   0.1250   SR_S
## BB~cc | Ee   0.1250   SR_S
## Bb~cc | Ee   0.2500   SR_S
## bb~cc | EE   0.0625   SS_S
## bb~cc | Ee   0.1250   SS_S
## BB~cc | ee   0.0625   SR_R
## Bb~cc | ee   0.1250   SR_R
## bb~cc | ee   0.0625   SS_S
##
## $phenotypes
##   S/R fraction
## 1 SR_R   0.1875
## 2 SR_S   0.5625
## 3 SS_S   0.2500

match("Bb~cc | EE", BCEcombi) # position 20

## [1] 20

allcrossBCE[[20]]

## $genotypes
##          fraction SRtrait
## BB~cc | EE     0.25   SR_S
## Bb~cc | EE     0.50   SR_S
## bb~cc | EE     0.25   SS_S
##
## $phenotypes
##   S/R fraction
## 1 SR_S     0.75
## 2 SS_S     0.25
```

Linking the phenotype to the genotype

Tables S1.20 and S1.21

Markers developed around GWAS peaks and further used to genotype selfed offspring at the C and E loci. DMPR (*Daphnia magna–Pasteuria ramosa*) markers information. Map 2.4 corresponds to the currently available *D. magna* draft genome version 2.4 (Routtu et al. 2014). DMPR1 and 2 are physically linked to the C locus while DMPR3 and 4 are physically linked to the E locus. According to the genetic model underlying resistance to *P. ramosa* yielded from the GWAS analysis and previous studies (Metzger et al. 2016), resistance is dominant at the C locus (resistance to C1 and C19) whereas resistance is recessive at the E locus (resistance to P20). In addition, an epistatic relationship linking both loci confers susceptibility to P20 to an individual that shows susceptibility to C1 and C19, disregarding the individual genotype at the E locus. This model is described in Fig. 1.5. In individuals showing resistance to C1 and C19 (RR_ _ phenotype, "Cc" or "CC" genotype), DMPR1 and 2 display either a heterozygous pattern with an allele linked to the C locus dominant allele (called R allele) and a recessive allele (S allele) ("Cc" genotype) or a homozygous pattern with one (or two: R1 and R2) dominant allele(s) ("CC" genotype). Note that at markers DMPR1, 3 and 4, two R alleles (called R1 and R2) are found, although R1 and R2 of DMPR4 have identical size. In individuals showing susceptibility to C1 and C19 (SS_ _ phenotype, "cc" genotype), DMPR1 and 2 display a homozygous pattern with an allele linked to the C locus recessive allele (called S allele) ("cc" genotype). In individuals showing resistance to C1 and C19 (without epistatic relationship between C and E loci) and susceptibility to P20 (RR_S phenotype, "Ee" or "EE" genotype at E locus), DMPR3 and 4 display either a heterozygous pattern with an allele linked to the E locus dominant allele (called S allele) and a recessive allele (R allele) ("Ee" genotype) or a homozygous pattern with an allele linked to the E locus dominant allele (called S allele) ("EE" genotype). In individuals showing resistance to C1 and C19 (without epistatic relationship between C and E loci) and resistance to P20 (RR_R phenotype, "ee" genotype at E locus), DMPR3 and 4 display a homozygous pattern with an allele linked to the E locus recessive allele (called R allele) ("ee" genotype). In individuals susceptible to C1 and C19 (SS_ _ phenotype), DMPR3 and 4 can show one of the three patterns described above (corresponding to "Ee", "EE" or "ee" genotype) because of the epistatic relationship linking the C and the E loci.

Table S1.20

DMPR (*Daphnia magna−Pasteuria ramosa*) markers information. **A:** Description of the positions and sizes of the markers. All primers were used in the same master mix. The size of a marker corresponds to the size of the sequence from the beginning of the F-primer to the end of the R-primer on the reference genome (map 2.4): *size marker = end position − start position of the marker*. **B and C:** Description of primers and motifs. Reference motifs correspond to the motifs that are present in the reference genome (map 2.4). The size of an amplicon is calculated as follows: *size amplicon = size of the marker − size of the reference motif + size of the motif of interest*. For example, to obtain the size of the R1 allele of DMPR1 we get: *size of DMPR_R1 amplicon = size of DMPR1 − size of DMPR1 reference motif + size of DMPR1_R1 motif=118 − 31 + 2 = 89*. **D:** Expected marker signatures for all possible genotypes. Here we consider alleles as the observable peaks yielded by the marker analysis, as two copies of the same sequence in a homozygous individual will be observed as a single amplicon of a given size. A "resistance" (R) or "susceptibility" (S) allele does not necessarily confer resistance or susceptibility to the individual that carries it. Resistance phenotype will depend on the genetic model described above. For DMPR1, 3 and 4, we expect R homozygous individuals ("CC" or "ee" genotype) to present one of the two R alleles (R1 or R2) or both. Heterozygous individuals ("Cc" or "Ee" genotype) should present one R allele (R1 or R2) together with the S allele. Finally, S homozygous individuals ("cc" or "EE" genotype) should present only the S allele. Similarly, for DMPR2, we expect R homozygous individuals to present only the R allele (R1), heterozygous individuals to present the R allele (R1) together with the S allele and S homozygous individuals should present the S allele. Note that for DMPR4, because both R1 and R2 alleles have the same size, they will appear as a single peak during the marker analysis.

A

Name of marker	Concentration in master mix (µM)	Locus to which marker is physically linked	Scaffold (map 2.4)	Start position of the marker (map 2.4)	End position of the marker (map 2.4)	Size of the marker (bp) (map 2.4)	Position of the motif (map 2.4)
DMPR1	0,1	C	944	1350608	1350726	118	1350644
DMPR2	0,1	C	944	1563359	1563543	184	1563391
DMPR3	0,6	E	2167	19662	19874	212	19793
DMPR4	0,6	E	2560	81434	81570	136	81471

B

Name of marker	Sequence of forward (F) primer	F Primer size (bp)	Sequence of reverse (R) primer	R Primer size (bp)	Melting tempera-ture (°C)	Reference motif (RM) (map 2.4)	RM length (bp)
DMPR1	ACAGCACGTCTCCGACTAAGG	21	GACGCCAAMAMCTACGCAACC	21	50	AAACGCACGGATCCTATATGTATCGAGCTTA	31
DMPR2	CAAATCTGCAATGGAATGAAAG	22	AACGCAACCGTTACGGTTAC	20	50	CTCCTGCTGGCT	12
DMPR3	TTACGTTCGGTTTGGCTCCG	20	TGAAACATTGGTAAGAGACG	20	48	TACAACAACAACAACAACAACAA	23
DMPR4	GATAGATATTTATTGAACAG	20	TTTTGTCTTCGGAAGAACG	19	48	AATGCCTCCATGCCTCCATGCCTCCA	26

C

Name of marker	Motif of allele(s) confering resistance (R1 and R2) (dominant at C-locus and recessive at E-locus)	Motif R1 length (bp)	Motif R2 length (bp)	Motif of allele confering susceptibility (S) (recessive at C-locus and dominant at E-locus)	Motif S length (bp)	Size of R1 amplicon (bp)	Size of R2 amplicon (bp)	Size of S amplicon (bp)
DMPR1	AAATGCATATGTATATATCGAGCTTA ; AA	2	26	AAACGCACGGATCCTATATGTATC-GAGCTTA	31	89	113	118
DMPR2	ATCCTGCTGGCT	12	NA	ATCG	4	184	NA	176
DMPR3	TACAACAACAACAACAACAAAA ; TACAACAACAACAACAACAACAA	22	23	TACAACAACAACAAAAA	17	211	212	206
DMPR4	AATGCCTCCATGCCTCCA ; AATACCTCCATGCCTCCA	18	18	AATGCCTCCATGCCTCCATGCCTCCA	26	128	128	136

D

Name of marker	Expected marker signature of R homozygous individual ("CC" or "ee" genotype)	Expected marker signature of heterozygous individual ("Cc" or "Ee" genotype)	Expected marker signature of S homozygous individual ("cc" or "EE" genotype)
DMPR1	R1 / R2 or R1 + R2	R1 + S or R2 + S	S
DMPR2	R1	R1 + S	S
DMPR3	R1 / R2 or R1 + R2	R1 + S or R2 + S	S
DMPR4	R1 / R2 or R1 + R2	R1 + S or R2 + S	S

Table S1.21

PCR reaction cycles using DMPR1 to 4.

Temperature	Time	Cycles
95 °C	15 min	
94 °C	30 sec	
60 °C	1 min 30 sec	30 x
72 °C	1 min 30 sec	
94 °C	30 sec	
47 °C	1 min 30 sec	10 x
72 °C	1 min 30 sec	
72 °C	10 min	
8 °C	∞	

References

Andras JP, Ebert D. 2013. A novel approach to parasite population genetics: Experimental infection reveals geographic differentiation, recombination and host-mediated population structure in *Pasteuria ramosa*, a bacterial parasite of *Daphnia*. *Molecular Ecology* **22**:972–986.

Bento G, Routtu J, Fields PD, Bourgeois Y, Du Pasquier L, Ebert D. 2017. The genetic basis of resistance and matching-allele interactions of a host–parasite system: The *Daphnia magna–Pasteuria ramosa* model. *PLOS Genetics* **13**:e1006596.

Dukić M, Berner D, Roesti M, Haag CR, Ebert D. 2016. A high-density genetic map reveals variation in recombination rate across the genome of *Daphnia magna*. *BMC Genetics* **17**:137.

Metzger CMJA, Luijckx P, Bento G, Mariadassou M, Ebert D. 2016. The Red Queen lives: Epistasis between linked resistance loci. *Evolution* **70**:480–487.

Routtu J, Hall MD, Albere B, Beisel C, Bergeron RD, Chaturvedi A, Choi J-H, Colbourne J, De Meester L, Stephens MT, et al. 2014. An SNP-based second-generation genetic map of *Daphnia magna* and its application to QTL analysis of phenotypic traits. *BMC genomics* **15**:1–15.

Signorell A et al. 2018. DescTools: Tools for descriptive statistics. R package version 0.99.26.

SUPPLEMENTARY MATERIAL CHAPTER 2

Overview

Section in main manuscript	Element	Description	Page
Results			
Seasonal epidemics			
	Fig. S2.1	Environment and ecology	p. 122
	Discussion S2.1	Discussion about the ecology	p. 123
Selection and sexual reproduction			
	Fig. S2.2	Hatching of planktonic resting stages	p. 124
	Fig. S2.3	Hatching of sediment-collected resting stages	p. 125
	Fig. S2.4	Overwintering resting stages	p. 125
Calculation of expected resistotype frequencies in resting stages			
	Fig. S2.5	BCDE genetic model	p. 126
		Description of allele frequency scenarios	p. 127
	Fig. S2.6	Results all scenarios	p. 128
	Fig. S2.7	Results best scenario	p. 129
	Table S2.1	Allele frequency scenarios	p. 130
	Table S2.2	Allele frequency best scenario	p. 131
	Fig. S2.8	Resistotype participation in sex	p. 132
Materials and methods			
Hatching modelling			
	Doc. S2.1	"peas" genetic model	p. 132–133
	Doc. S2.2	Resistotype frequency calculations	p. 134–136
	Fig. S2.9	Summary of calculations	p. 136
Statistical software	Doc. S2.3	Statistical software	p. 136
References			p. 137

Results

Seasonal epidemics—Environment and ecology in the Aegelsee

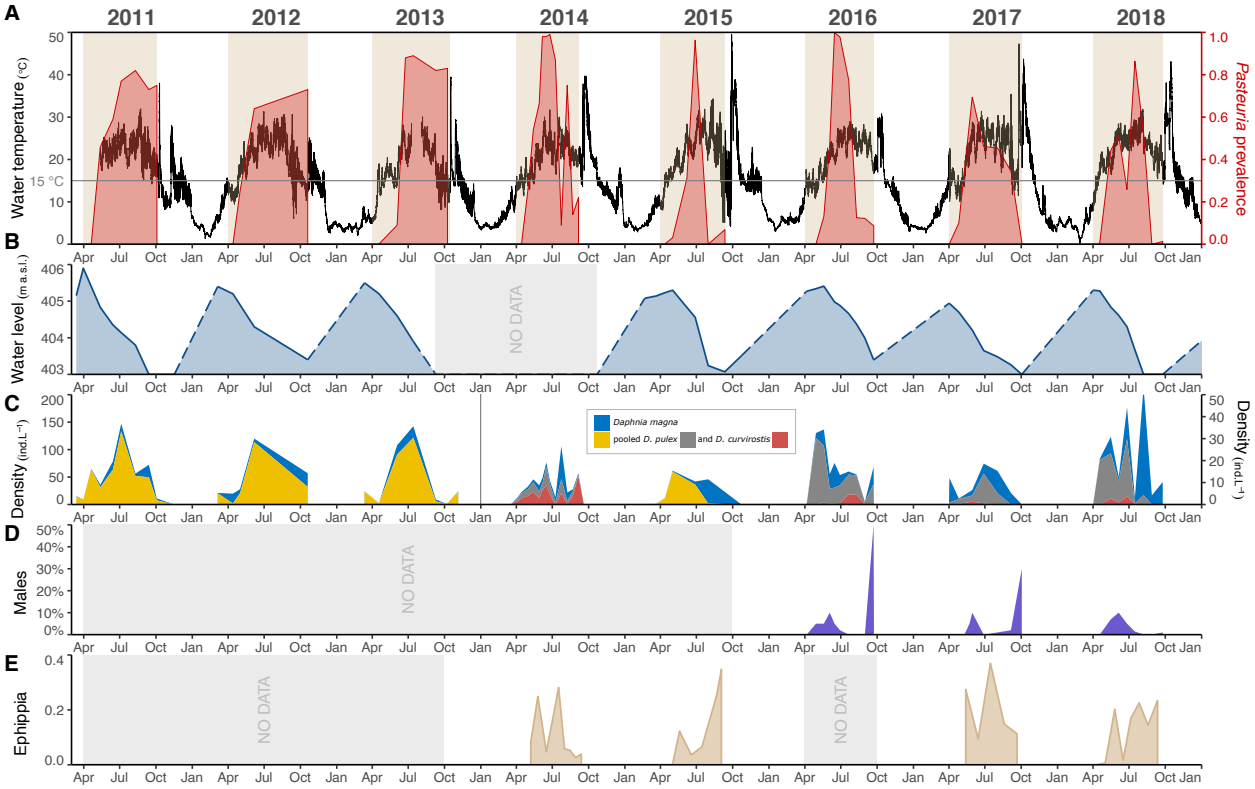

Figure S2.1

Environmental conditions and sexual reproduction of *Daphnia magna* in the Aegelsee. **A:** Water temperature rise in the Aegelsee goes hand in hand with the appearance of the *Pasteuria ramosa* epidemics in the *D. magna* population. **Water temperature**: a temperature logger was installed in the pond from 2011 to 2018. No data is plotted in July 2013 because of vandalism of the data logger. The yearly temperature peaks in early October represent the release of warm ammoniacal condensation water in the pond. ***Pasteuria* prevalence**: red area plot represents *P. ramosa* prevalence in the *D. magna* population from 2011 to 2018. The grey horizontal line represents a water temperature threshold of 15 °C. When the water temperature rises above about 15 °C, the bacterial epidemics starts. **B:** Water level in the Aegelsee. Water level above sea level (a.s.l.) was read on a fixed floating device installed in the pond where the animals were sampled. We measured water level during the active season of the *D. magna*, from early April to early October. During this period, water level decreases progressively because of evaporation and agricultural and industrial use of the water. Solid line corresponds to data collected during the sampling period while dashed line corresponds to inferred data. Note that 403 m a.s.l. is the lower limit of the floating device. Every year in early October, warm condensation water is released in the pond. Over winter the pond is progressively filled up to a level of about 405 m a.s.l. **C:** *Daphnia* species density in the Aegelsee, measured as the number of individuals per liter of water. We sampled the water column during the active season, from early April to early October. From 2011 to 2013, pond water was directly sampled in 1-L bottles. From 2014 on, a plankton net was used. These two protocols created a four-fold magnitude difference between values obtained in 2011−2013 and 2014−2018, which we represent on distinct y-axes. *Daphnia* species were subsequently determined in the laboratory. As *D. pulex* and *D. curvirostis* are difficult to tell apart, a subset of 100 individuals of these two species was used to infer their respective densities in 2014, 2016, 2017 and 2018. They are pooled in the other years. In early October, warm ammoniacal condensation water is released in the pond, killing all plankton. No *Daphnia* overwinter in this population, neither do resting stages hatch before early April. **D:** *D. magna* male production in the Aegelsee. We counted males in a subset of 100 *D. magna* at each collection point from 2016 to 2018. **E:** *D. magna* ephippia production in the Aegelsee. Five to nine sediment traps were installed on the pond floor and retrieved at each collection date in 2014, 2015, 2017 and 2018. The y-axis represents ephippia number relative to the total number of ephippia counted in the season.

Discussion S2.1

Environmental and ecological variables in the Aegelsee.

We observe cyclical changes in different environmental variables. Every year, the *Daphnia magna* population emerges when water temperature reaches about 12 °C (Supplementary Fig. S2.1A). Temperature then increases to about 25 °C in summer, occasionally reaching peaks of 30 °C. In October, the warm ammoniacal condensation water is released in the pond, bringing temperature to 35−50 °C (Supplementary Fig. S2.1A). The main increase in parasite prevalence occurs when water temperature rises above 15 °C (Supplementary Fig. S2.1A). Water level in the Aegelsee is managed to make room for inflow of the condensation water in Fall. Therefore, every year the water level is lowered by about two meters over the course of the season. At its lowest level in late September, more than 80% of the pond sediments are exposed and the maximum water level is about one meter (Supplementary Fig. S2.1B). *Daphnia* density shows irregular dynamics with a first peak typically in early summer, but further peaks may follow later. In most years, *D. magna* increases in relative frequency among all *Daphnia* species (Supplementary Fig. S2.1C). We observe one or two peaks of *D. magna* male density during the season (Supplementary Fig. S2.1D). We did not estimate the number of sexual females in the population, we instead collected resting stages in the sediment traps. Sexual egg counts cannot directly be compared with the frequencies of males, as they are time-shifted.

We observe a correlation between temperature cycles and *Pasteuria ramosa* epidemics in the *D. magna* Aegelsee population. Animals are observed to be infected by the bacteria as temperature rises above 15 °C every year in late April. We infer that epidemics are possibly influenced by water temperature, although the phenology of many other environmental factors may play a role. For example, longer day length, increased *Daphnia* density and lower water level (Supplementary Fig. S2.1). It has been suggested that parasite-mediated selection in the *D. magna*−*P. ramosa* system is strongest at 20−25 °C (Mitchell et al. 2005; Vale et al. 2008). Given climate change model predictions of pond warming and longer seasons with temperatures above 15 °C, selection for resistance can thus be expected to intensify in our study population. Warming could also affect the evolution of stress tolerance, as exposure to the pathogen disrupts the host's ability to cope with thermal stress in this system (Hector et al. 2019). Environmental factors may also change the mode of selection: it has been shown that, under some temperature and food availability conditions, hosts in this system become more tolerant, thus potentially increasing parasite prevalence and slowing down coevolution (Vale et al. 2011). Parasite fitness may also be influenced by the interaction of genotype and environmental factors such as temperature and food availability (Vale and Little (2009), in a plant-parasite system: Laine 2007). Thus, while natural selection on resistance is precipitated on a high specificity of host−parasite interactions in the *D. magna*−*P. ramosa* system, it may also be linked to environmental conditions.

In the *D. magna*−*P. ramosa* system, host-parasite specificity is high, and spore attachment is not known to be influenced by environmental factors (Duneau et al. 2011; Luijckx et al. 2011). However, other host and parasite traits are influenced by the environment and there is intra-specific variability in how different genotypes respond to different environmental conditions (reviewed in Ebert et al. 2016). Temperature was found to influence infectivity and spore production in the parasite in the present system (Vale et al. 2008; Vale and Little 2009) and in the *D. dentifera*−*P. ramosa* system (Duffy and Hunsberger 2019). In the host, temperature was found to influence virulence in the present system (Mitchell et al. 2005) and filtering rate and parasite prevalence in a *D. laevis*−fungal host−pathogen system (Dallas and Drake 2016; Kirk et al. 2018; Kirk et al. 2019). Temperature also increased epidemic size in two mesocosm experiments, in the present system (Auld and Brand 2017) and in a *D. dentifera*−fungal parasite system (Shocket, Strauss, et al. 2018). This was explained in the latter *Daphnia*–fungus system by an increase of the transmission rate, composed of infectivity and foraging rate (Shocket, Vergara, et al. 2018). Nutrient availability increased tolerance of *D. magna* to *P. ramosa*, and increased spore production in the parasite, irrespective of temperature variations (Vale et al. 2011). Nutrient availability has also been shown to have a differential impact on fecundity and survival in distinct *D. magna* genotypes, leading to differential consequences of infection by a viral parasite (Reyserhove et al. 2017). Epidemiological variables such as prevalence, virulence, transmission rate and infection rate are thereby shaped by environmental variables (Hite and Cressler 2018).

Selection and sexual reproduction

Figures S2.2 to S2.4

The *Daphnia magna* overwintering resting stages in the Aegelsee. The *Daphnia magna* population in the Aegelsee goes through a cyclical pattern of resistotype (resistance phenotype) frequency. Resistant phenotypes increase in frequency over the course of the epidemics but resistotype diversity is created anew each spring via the hatching of the resting stages overwintering population. We collected and hatched ephippia laid in the water column by the planktonic population of *D. magna* throughout the active season in 2014, 2015, 2017 and 2018 using sediment traps (Supplementary Fig. S2.2). We subsequently collected and hatched ephippia from surface sediment in winter 2014 as a representative sample of the spring *D. magna* cohort (Supplementary Fig. S2.3). Supplementary Figure S2.4 represents planktonic, ephippia and hatchling data together as a timeseries.

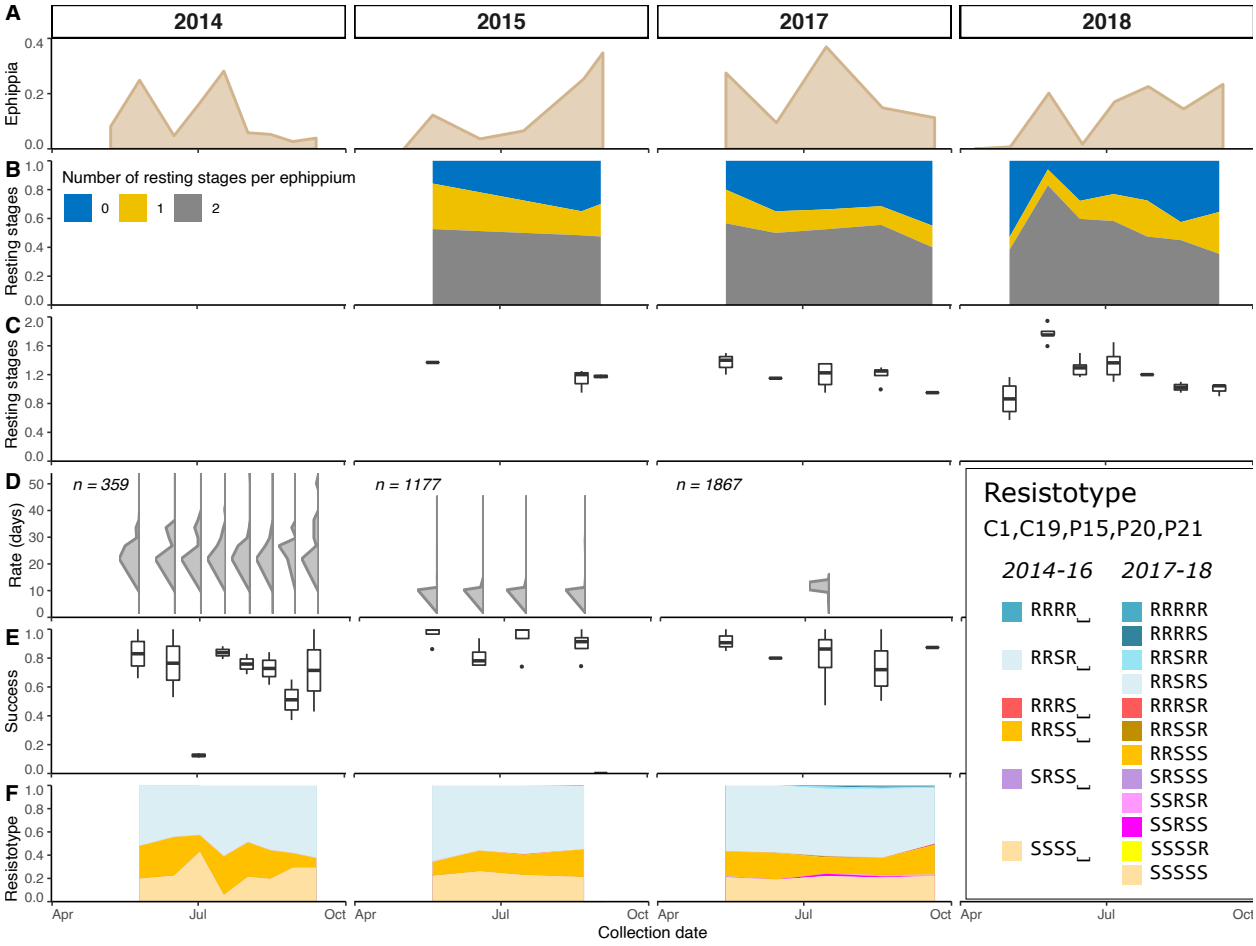

Figure S2.2

Hatching of the *Daphnia magna* overwintering resting stages in the Aegelsee. Ephippia were collected in 2014, 2015, 2017 and 2018 during the active season. We used five to nine sediment traps at each collection date. Ephippia were subsequently stored at 4 °C to mimic the resting period and hatching was induced the following spring by placing the ephippia in outside containers. In 2014, the first ephippia sample was lost. In 2015, no ephippia hatched from the last sample because of exposure to the warm ammoniacal condensation water released into the pond at the end of the season. **A**: relative proportion of ephippia laid in the water column during the active season of *D. magna*. **B and C**: Number of resting stages per ephippium. On a subset of ephippia not used in the hatching experiment, we counted the number of resting stages present in the ephippial case. In ephippia collected in 2014, egg number was counted after the hatching experiment. This is why we do not plot it here, but we did use the values to infer hatching success (see E below). We checked ten to 20 ephippia for a minimum of two repeats at each collection date. **B**: Number of resting stages per ephippium, as the proportion of ephippia containing zero, one or two resting stages. **C**: Number of resting stages per ephippium, as the mean number of resting stages in the ephippial case. **D**: Hatching rate and pattern of collected ephippia. We induced hatching of the collected resting stages by putting 20 to 100 ephippia; depending on how many were collected; of each repeat of each collection date in outside containers. Resting stages collected in 2014, 2015 and 2017 were induced on 18 March 2015, 11 April 2016 and 29 March 2018, respectively. Hatching was monitored every second day. Vertical graphs represent the relative proportion of hatchlings over time after hatching induction. Each vertical graph represents ephippia from each collection date during the season. The different repeats for each collection date are pooled in one vertical graph. The y-axis (x-axis of the vertical graphs) is the number of days since hatching induction. In 2017, the total proportion of hatchlings across repeats and collection dates is presented. Resting stages collected on the last collection date of 2015 did not hatch because the warm ammoniacal condensation water had been released before our sampling. Variation across years might be due to the different hatching induction dates in the different years. **E**: Hatching success. We calculated hatching rate for each repeat for each collection date. We used the total number of hatchlings and the total number of resting stages induced, inferred from the subset of ephippia opened (B & C). For resting stages collected in 2014, only the number of remaining resting stages after hatching induction was counted. We inferred the total number of induced resting stages by adding the number of remaining resting stages to the total number of hatchlings. **F**: Resistotype (resistance phenotype) of hatched animals. Hatchlings were cloned in the laboratory to assess their resistotype. We tested 20 *D. magna* clonal lines (clones) for each repeat for each collection date, resulting in about 100 clones for each collection date.

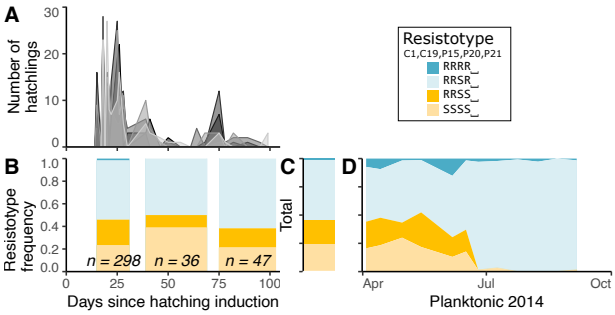

Figure S2.3

Daphnia magna overwintering resting stages in the Aegelsee, collected in the sediment in winter 2014. The overwintering resting stages in winter 2014 were laid in the active season in 2013 and reflects the spring 2014 *D. magna* cohort. We collected five replicates of surface sediment in the pond in February 2014, before onset of the natural hatching season. A hundred ephippia from each replicate were placed in outdoor containers in late February 2014 and hatching was monitored every second day. **A**: Number of hatchlings over time after hatching induction. The five replicates are represented in different shades of grey. A total of 608 hatchlings were recorded. **B**: Resistotype (resistance phenotype) distribution of hatchlings over time after hatching induction. Hatchlings were put separately in jars to produce clonal lines. We measured resistotype on a subset of 381 randomly chosen clones. We represent resistotype frequency of hatched animals in three date intervals because of low sample sizes at some dates. The x-axis in A and B spans from day 0, the 20 February 2014 to day 103, the 3 June 2014. **C**: total resistotype proportions resulting from all 381 hatchlings. **D**: resistotype frequency of sampled *D. magna* in 2014.

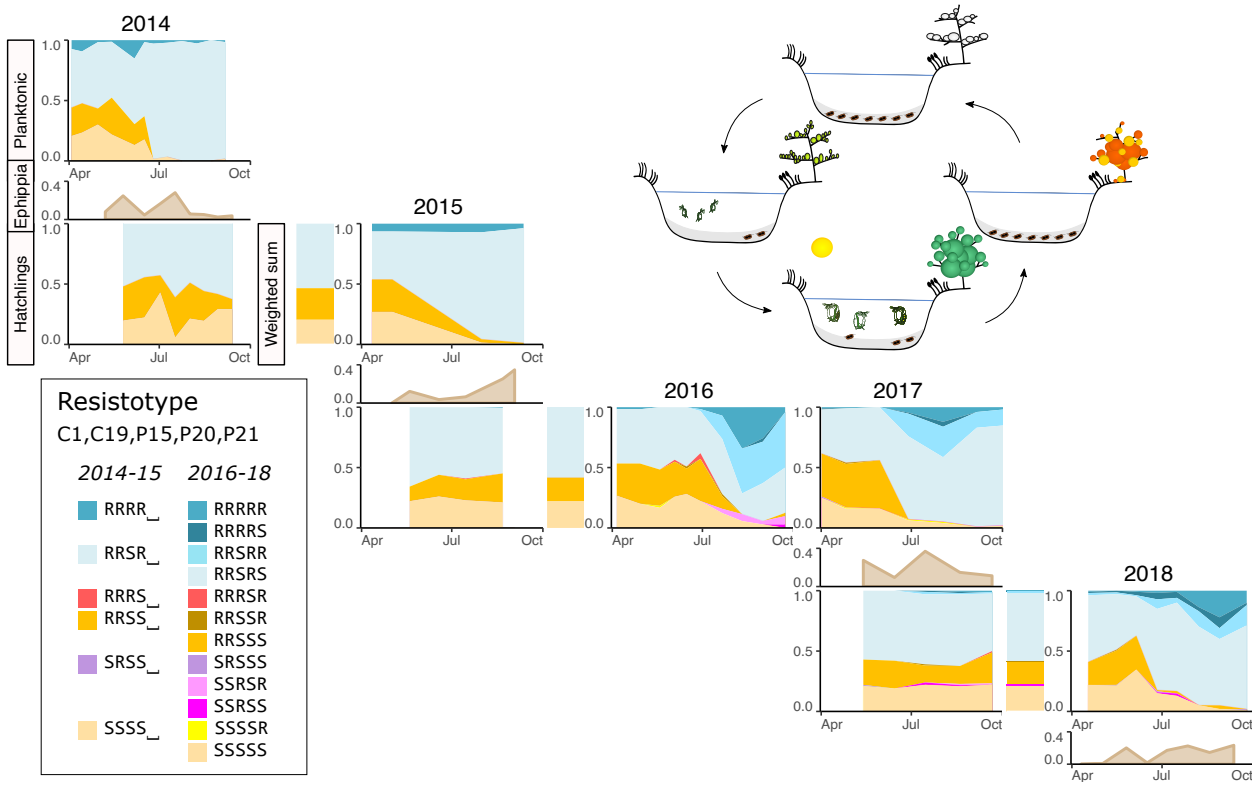

Figure S2.4

Daphnia magna overwintering resting stages in the Aegelsee, collected in the water column throughout the active season. The spring *D. magna* cohort hatches from the resting stages present in the pond sediment. Throughout the active season (from early April to early October), *D. magna* reproduce asexually (clonal eggs) and sexually (fertilized resting stages). The resting stages create the overwintering population. In early October, warm condensation ammoniacal water is released in the pond, killing all plankton but not the resting stages. In winter, no ephippia hatch. **Planktonic**: Resistotype frequency in the *D. magna* population from 2014 to 2018. A large batch of animals was collected from early April to early October every 2−4 weeks to clone about 60 to 100 females. The resistotype is the full resistance phenotype to five *Pasteuria ramosa* isolates: C1, C19, P15, P20 and P21. Resistance and susceptibility are denoted as R and S, respectively. Note that in different years, different numbers of *P. ramosa* isolates were tested. We use the placeholder "_" in the resistotype when a bacterial isolate was not tested. Resistance to P20 is highlighted because of its importance in the evolution of the host population (Ameline et al. 2021). **Ephippia**: relative number of *D. magna* ephippia laid in the pond. Five to nine ephippia traps were set up in 2014, 2015, 2017 and 2018 and collected every 2−4 weeks from early April to early October. We plot the mean number of ephippia per trap at each timepoint divided by the total mean number of ephippia laid during the whole year. Time on the x-axis represents the middle point between setup and collection of the traps. **Hatching**: *D. magna* resting stages collected in 2014, 2015 and 2017 were hatched in outside containers the following spring, after a resting period at 4 °C. In each container, 20 to 100 ephippia per trap per timepoint were placed, depending on how many were collected. Hatched animals were cloned in the laboratory. In *Daphnia*, hatchlings from resting stages are female, which allows to clone them. We measured the resistance phenotype (resistotype) of 20 clones per trap per timepoint, resulting in 100 clones per timepoint. **Weighted sum**: weighted sum of *D. magna* resistotype frequency from hatched ephippia. Total *D. magna* resistotype frequency from hatched ephippia weighted by the relative number of ephippia laid at each timepoint. The weighted sum of resistotype frequency represents the overwintering resting stages. In 2014, the first ephippia sample was lost. In 2015, no ephippia hatched from the last sample because of exposure to the warm ammoniacal condensation water released into the pond at the end of the season.

Calculation of expected resistotype frequencies in resting stages

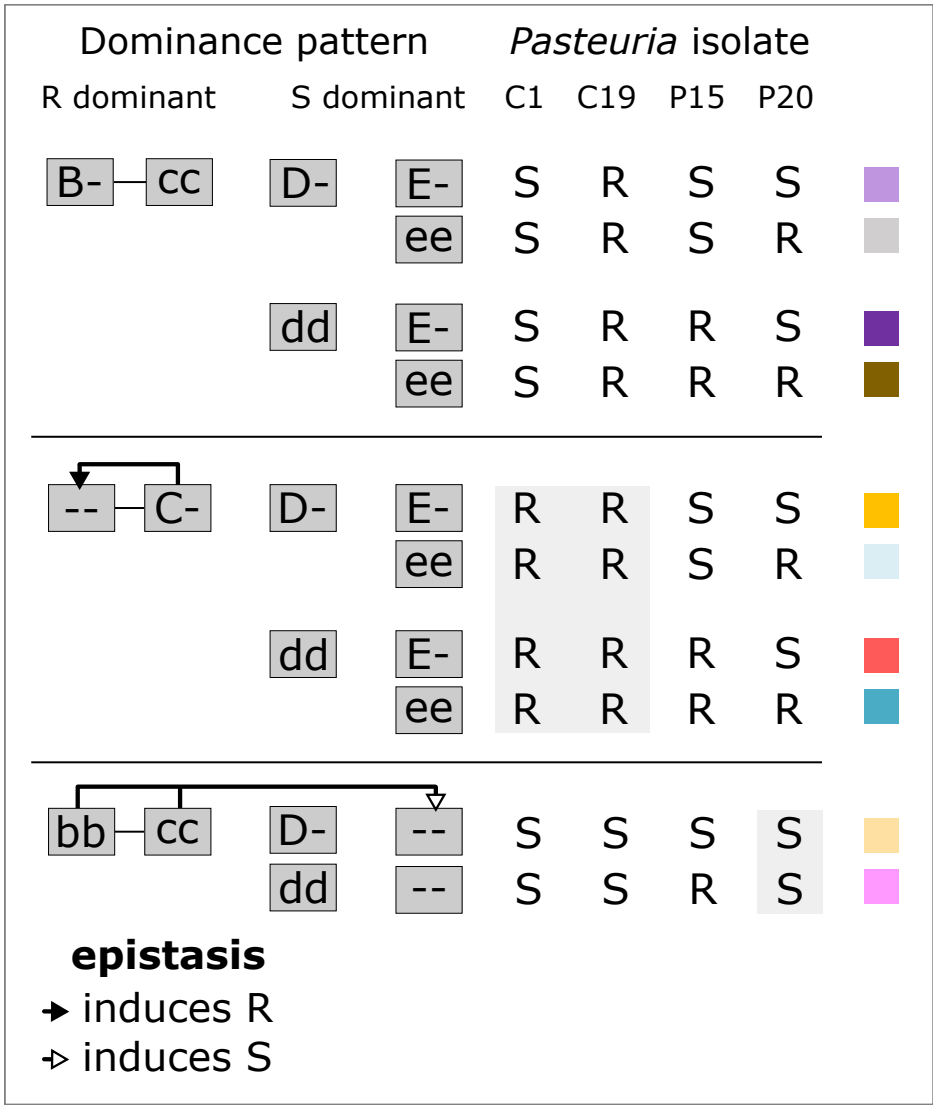

Figure S2.5

Genetic model of resistance in the Aegelsee. The model includes resistotypes to C1, C19, P15 and P20 *Pasteuria ramosa* isolates. Resistance to C1 and C19 determined by the ABC cluster was described in Metzger et al. (2016). The dominant allele at the B locus induces resistance (R) to C19 and susceptibility (S) to C1. The dominant allele at the C locus confers resistance to both C1 and C19 *P. ramosa* isolates, regardless of the genotype at the B locus. Variation at the A locus is not considered here as the recessive allele at this locus is believed to be fixed in the population (Ameline et al. 2021). The D-locus determines resistance to P15 (Bento et al. 2020). The E locus determines resistance to P20 (Ameline et al. 2021). Resistance is dominant at the B and C loci (resistance to C1 and C19) whereas resistance is recessive at the D and E loci (resistance to P15 and P20, respectively). Recessive homozygosity at the B and C loci induces susceptibility to P20, regardless of the genotype at the E locus (Ameline et al. 2021). Hence the epistasis can only be observed phenotypically in "bbccee" (SS_S) offspring. If the epistatic relationship is not present in this case, the observed phenotype would be SS_R. Such SS_R individuals were never observed in the population. Resistotypes determined by the "B-" and the "dd" genotype, regardless of the genotype at other loci, are very rare or do not occur in the *D. magna* population. We assume the B and the d alleles are rare in the population and might induce poor fitness. We implement this genetic model of resistance in the *D. magna*–*P. ramosa* system in the "peas" R package (Supplementary Doc. S2.1). We subsequently test the model using resting stages hatching data (Supplementary Figs. S2.6 and S2.7, Tables S2.1 and S2.2).

Figs. S2.6 and S2.7, Tables S2.1 and S2.2

Predicted resistotype frequency resulting from resting stages hatching in the Aegelsee.

Using the genetic model of resistance inheritance in the *Daphnia magna−Pasteuria ramosa* system, we calculate predicted resistotype frequency resulting from hatching of *D. magna* resting stages, or ephippia, produced throughout the active season. We compare this expected resistotype frequency to the observed resistotype frequency obtained from hatching of field-collected resting stages. The genetic model and calculations are described in Supplementary Fig. S2.5, Doc. S2.1, Doc. S2.2 and Fig. S2.8. In short, we use three input datasets: (i) the longitudinally observed resistotype frequency, from the F0 generation performing sexual reproduction during the active season, (ii) the predicted F1 resistotype segregation given by the genetic model and (iii) the genotype distribution within resistotypes in the *D. magna* population, the F0 generation, described here. Because we use phenotype distribution data, we input genotype distribution within each phenotype. **Figs. S2.6 and S2.7**: observed vs. expected resistotype frequency resulting from resting stages hatching. We calculate expected resistotype frequency according to different allele frequency scenarios in the *D. magna* population. **Tables S2.1 and S2.2**: Allele frequency scenarios in the *D. magna* population. We use the list of possible genotypes and their corresponding resistotypes given by the genetic model of resistance in the system. In each scenario, we fix an allele at one or several loci and we equally distribute genotype proportions among the other loci. In resistotypes where it is not possible to fix the allele, we equally distribute genotype proportions among heterozygous genotypes or among homozygous genotypes for the alternative allele when this is the only possible genotype determining the resistotype. **Table S2.2** presents the "bbDD" scenario, additionally implemented with observed allele frequency at the C and E loci. Observed C and E loci allele frequency were measured in spring sample (Ameline et al. 2021).

- **scenario "bbDD"**: the "bb" and "DD" genotypes are fixed in all possible resistotypes.
- **scenario "bb"**: the "bb" genotype is fixed in all possible resistotypes.
- **scenario "BB"**: the "BB" genotype is fixed in all possible resistotypes.
- **scenario "CC"**: the "CC" genotype is fixed in all possible resistotypes.
- **scenario "DD"**: the "DD" genotype is fixed in all possible resistotypes.
- **scenario "ee"**: the "ee" genotype is fixed in all possible resistotypes.
- **scenario "EE"**: the "EE" genotype is fixed in all possible resistotypes.
- **scenario "hetero"**: all loci show heterozygous genotype in all possible resistotypes.

Note: we use four-letter resistotype because the genetic model of resistance includes resistance to the four *P. ramosa* isolates C1, C19, P15 and P20.

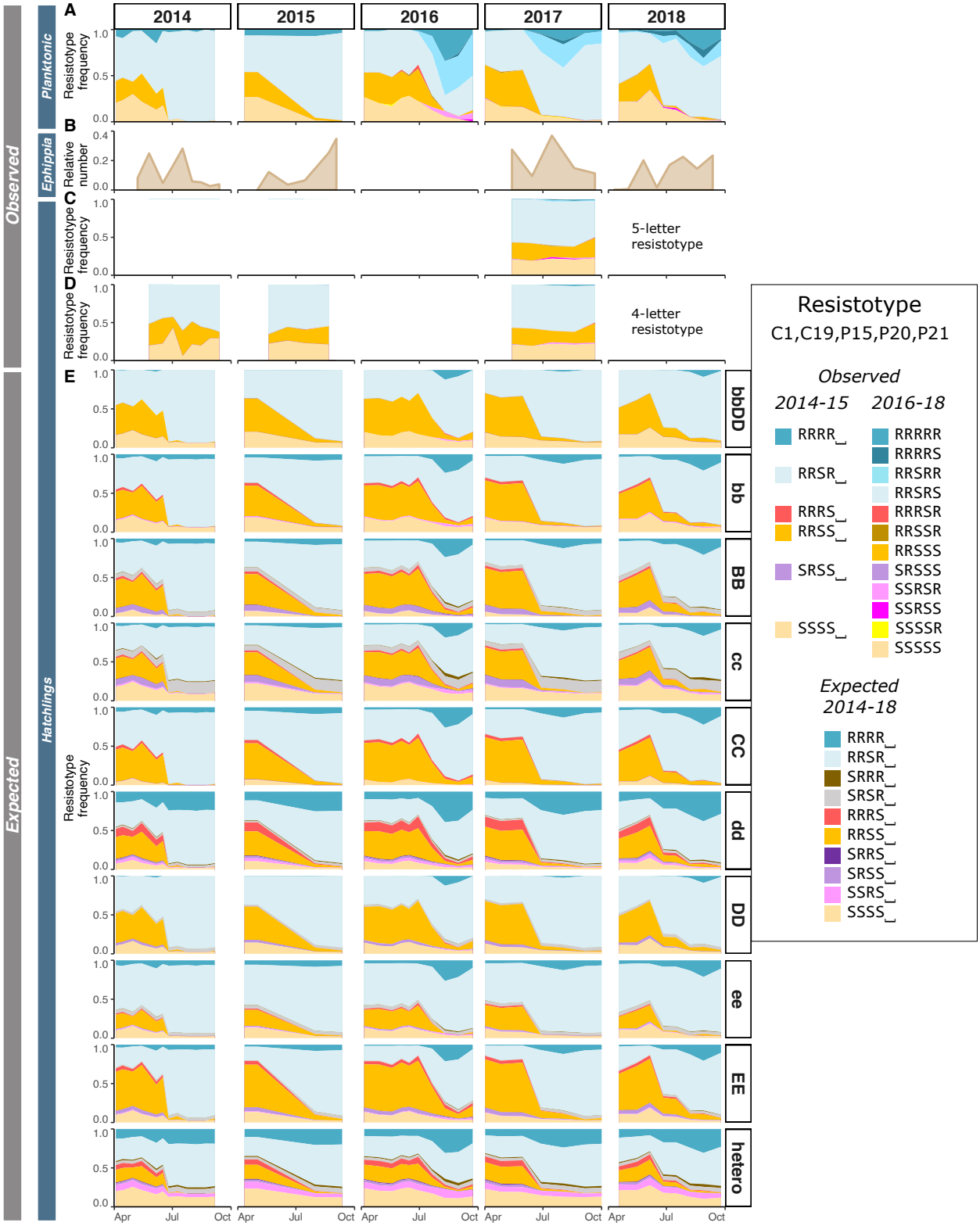

Figure S2.6

Expected resistotype frequency resulting from resting stages, or ephippia, laid throughout the active season of *Daphnia magna*. We use the genetic model of resistance inheritance in the *Daphnia magna*−*Pasteuria ramosa* system, presented in Supplementary Fig. S2.5. Allele frequency scenarios are detailed in Supplementary Table S2.1.

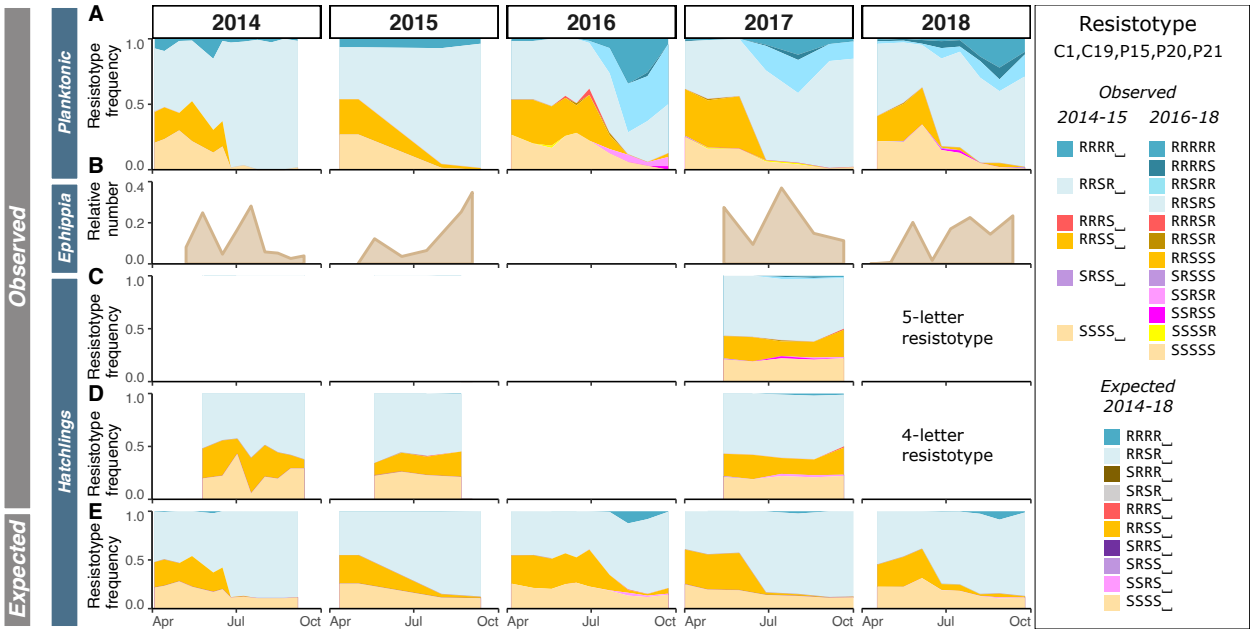

Figure S2.7

Expected resistotype frequency resulting from resting stages produced throughout the active season of *Daphnia magna*. We use the genetic model of resistance inheritance in the *Daphnia magna*–*Pasteuria ramosa* system, presented in Supplementary Fig. S2.5. This allele frequency scenario produces an expected resistotype distribution that fits best the observed one. The scenario is detailed in Supplementary Table S2.2.

Table S2.1

Genotype distribution scenarios in the Aegelsee *Daphnia magna* population. In each scenario we fix an allele at one or two loci and we equally distribute proportions in the remaining possible genotypes, within each resistotype. In resistotypes where it is not possible to fix the allele, we equally distribute genotype proportions among heterozygous genotypes or among homozygous genotypes for the alternative allele when this is the only possible genotype determining the resistotype. The genetic model described in Supplementary Fig. S2.5 provided the list of possible genotypes and their corresponding resistotypes. The different scenarios are described above. This table corresponds to the "freq" table described in Supplementary Doc. S2.2 and Fig. S2.8.

Phenotype	Genotype	Scenarios of genotype distribution within resistotypes									
		bbDD	bb	BB	cc	CC	dd	DD	ee	EE	hetero
RRRR	bb~Cc | dd | ee	1/2	1/2		1/3		1/6	1/6	1/6	1/6	
RRRR	Bb~Cc | dd | ee				1/3		1/6	1/6	1/6	1/6	1
RRRR	BB~Cc | dd | ee			1/2	1/3		1/6	1/6	1/6	1/6	
RRRR	bb~CC | dd | ee	1/2	1/2			1/3	1/6	1/6	1/6	1/6	
RRRR	Bb~CC | dd | ee					1/3	1/6	1/6	1/6	1/6	
RRRR	BB~CC | dd | ee			1/2		1/3	1/6	1/6	1/6	1/6	
RRSR	bb~Cc | Dd | ee		1/4		1/6		1/6		1/12	1/12	
RRSR	Bb~Cc | Dd | ee				1/6		1/6		1/12	1/12	1
RRSR	BB~Cc | Dd | ee			1/4	1/6		1/6		1/12	1/12	
RRSR	bb~CC | Dd | ee		1/4			1/6	1/6		1/12	1/12	
RRSR	Bb~CC | Dd | ee					1/6	1/6		1/12	1/12	
RRSR	BB~CC | Dd | ee			1/4		1/6	1/6		1/12	1/12	
RRSR	bb~Cc | DD | ee	1/2	1/4		1/6			1/6	1/12	1/12	
RRSR	Bb~Cc | DD | ee				1/6			1/6	1/12	1/12	
RRSR	BB~Cc | DD | ee			1/4	1/6			1/6	1/12	1/12	
RRSR	bb~CC | DD | ee	1/2	1/4			1/6		1/6	1/12	1/12	
RRSR	Bb~CC | DD | ee					1/6		1/6	1/12	1/12	
RRSR	BB~CC | DD | ee			1/4		1/6		1/6	1/12	1/12	
SRRR	Bb~cc | dd | ee	1	1		1/2	1/2	1/2	1/2	1/2	1/2	1
SRRR	BB~cc | dd | ee			1	1/2	1/2	1/2	1/2	1/2	1/2	
SRSR	Bb~cc | Dd | ee		1/2		1/4	1/4	1/2		1/4	1/4	1
SRSR	BB~cc | Dd | ee			1/2	1/4	1/4	1/2		1/4	1/4	
SRSR	Bb~cc | DD | ee	1	1/2		1/4	1/4		1/2	1/4	1/4	
SRSR	BB~cc | DD | ee			1/2	1/4	1/4		1/2	1/4	1/4	
RRRS	bb~Cc | dd | Ee	1/4	1/4		1/6		1/12	1/12	1/6		
RRRS	Bb~Cc | dd | Ee				1/6		1/12	1/12	1/6		1
RRRS	BB~Cc | dd | Ee			1/4	1/6		1/12	1/12	1/6		
RRRS	bb~CC | dd | Ee	1/4	1/4			1/6	1/12	1/12	1/6		
RRRS	Bb~CC | dd | Ee					1/6	1/12	1/12	1/6		
RRRS	BB~CC | dd | Ee			1/4		1/6	1/12	1/12	1/6		
RRRS	bb~Cc | dd | EE	1/4	1/4		1/6		1/12	1/12		1/6	
RRRS	Bb~Cc | dd | EE				1/6		1/12	1/12		1/6	
RRRS	BB~Cc | dd | EE			1/4	1/6		1/12	1/12		1/6	
RRRS	bb~CC | dd | EE	1/4	1/4			1/6	1/12	1/12		1/6	
RRRS	Bb~CC | dd | EE					1/6	1/12	1/12		1/6	
RRRS	BB~CC | dd | EE			1/4		1/6	1/12	1/12		1/6	
RRSS	bb~Cc | Dd | Ee		1/8		1/12		1/12		1/12		
RRSS	Bb~Cc | Dd | Ee				1/12		1/12		1/12		1
RRSS	BB~Cc | Dd | Ee			1/8	1/12		1/12		1/12		
RRSS	bb~CC | Dd | Ee		1/8			1/12	1/12		1/12		
RRSS	Bb~CC | Dd | Ee					1/12	1/12		1/12		
RRSS	BB~CC | Dd | Ee			1/8		1/12	1/12		1/12		
RRSS	bb~Cc | DD | Ee	1/4	1/8		1/12			1/12	1/12		
RRSS	Bb~Cc | DD | Ee				1/12			1/12	1/12		
RRSS	BB~Cc | DD | Ee			1/8	1/12			1/12	1/12		
RRSS	bb~CC | DD | Ee	1/4	1/8			1/12		1/12	1/12		
RRSS	Bb~CC | DD | Ee					1/12		1/12	1/12		
RRSS	BB~CC | DD | Ee			1/8		1/12		1/12	1/12		
RRSS	bb~Cc | Dd | EE		1/8		1/12		1/12			1/12	
RRSS	Bb~Cc | Dd | EE				1/12		1/12			1/12	
RRSS	BB~Cc | Dd | EE			1/8	1/12		1/12			1/12	
RRSS	bb~CC | Dd | EE		1/8			1/12	1/12			1/12	
RRSS	Bb~CC | Dd | EE					1/12	1/12			1/12	
RRSS	BB~CC | Dd | EE			1/8		1/12	1/12			1/12	
RRSS	bb~Cc | DD | EE	1/4	1/8		1/12			1/12		1/12	
RRSS	Bb~Cc | DD | EE				1/12			1/12		1/12	
RRSS	BB~Cc | DD | EE			1/8	1/12			1/12		1/12	
RRSS	bb~CC | DD | EE	1/4	1/8			1/12		1/12		1/12	
RRSS	Bb~CC | DD | EE					1/12		1/12		1/12	
RRSS	BB~CC | DD | EE			1/8		1/12		1/12		1/12	
SRRS	Bb~cc | dd | Ee	1/2	1/2		1/4	1/4	1/4	1/4	1/2		1
SRRS	BB~cc | dd | Ee			1/2	1/4	1/4	1/4	1/4	1/2		
SRRS	Bb~cc | dd | EE	1/2	1/2		1/4	1/4	1/4	1/4		1/2	
SRRS	BB~cc | dd | EE			1/2	1/4	1/4	1/4	1/4		1/2	
SRSS	Bb~cc | Dd | Ee		1/4		1/8	1/8	1/4		1/4		1
SRSS	BB~cc | Dd | Ee			1/4	1/8	1/8	1/4		1/4		
SRSS	Bb~cc | DD | Ee	1/2	1/4		1/8	1/8		1/4	1/4		
SRSS	BB~cc | DD | Ee			1/4	1/8	1/8		1/4	1/4		
SRSS	Bb~cc | Dd | EE		1/4		1/8	1/8	1/4			1/4	
SRSS	BB~cc | Dd | EE			1/4	1/8	1/8	1/4			1/4	
SRSS	Bb~cc | DD | EE	1/2	1/4		1/8	1/8		1/4		1/4	
SRSS	BB~cc | DD | EE			1/4	1/8	1/8		1/4		1/4	
SSRS	bb~cc | dd | ee	1/3	1/3	1/3	1/3	1/3	1/3	1/3	1		
SSRS	bb~cc | dd | Ee	1/3	1/3	1/3	1/3	1/3	1/3	1/3			1
SSRS	bb~cc | dd | EE	1/3	1/3	1/3	1/3	1/3	1/3	1/3		1	
SSSS	bb~cc | Dd | ee		1/6	1/6	1/6	1/6	1/3		1/2		
SSSS	bb~cc | DD | ee	1/3	1/6	1/6	1/6	1/6		1/3	1/2		
SSSS	bb~cc | Dd | Ee		1/6	1/6	1/6	1/6	1/3				1
SSSS	bb~cc | DD | Ee	1/3	1/6	1/6	1/6	1/6		1/3			
SSSS	bb~cc | Dd | EE		1/6	1/6	1/6	1/6	1/3			1/2	
SSSS	bb~cc | DD | EE	1/3	1/6	1/6	1/6	1/6		1/3		1/2	

Table S2.2

Resistance genotype distribution scenario in the Aegelsee *Daphnia magna* population, producing an expected resistotype distribution that fits best the observed one. We fix the "b" and the "D" alleles, and we distribute proportions in the remaining possible genotypes, within each resistotype, using C- and E-loci allele frequency observed in spring 2015. In resistotypes where it is not possible to fix the allele, we equally distribute genotype proportions among heterozygous genotypes or among homozygous genotypes for the alternative allele when this is the only possible genotype determining the resistotype. The genetic model described in Supplementary Fig. S2.5 provided the list of possible genotypes and their corresponding resistotypes. This table corresponds to the "freq" table described in Supplementary Doc. S2.2 and Fig. S2.8.

Phenotype	Genotype	Genotype distribution within resistotypes	
			bbDD scenario and C- and E-loci allele frequency inferred
RRRR	bb~Cc | dd | ee	x	fRRRR(Cc)=f(Cc)/(f(Cc)+f(CC))=0.65
RRRR	Bb~Cc | dd | ee		
RRRR	BB~Cc | dd | ee		
RRRR	bb~CC | dd | ee	x	fRRRR(CC)=f(CC)/(f(Cc)+f(CC))=0.35
RRRR	Bb~CC | dd | ee		
RRRR	BB~CC | dd | ee		
RRSR	bb~Cc | Dd | ee		
RRSR	Bb~Cc | Dd | ee		
RRSR	BB~Cc | Dd | ee		
RRSR	bb~CC | Dd | ee		
RRSR	Bb~CC | Dd | ee		
RRSR	BB~CC | Dd | ee		
RRSR	bb~Cc | DD | ee	x	fRRSR(Cc)=f(Cc)/(f(Cc)+f(CC))=0.65
RRSR	Bb~Cc | DD | ee		
RRSR	BB~Cc | DD | ee		
RRSR	bb~CC | DD | ee	x	fRRSR(CC)=f(CC)/(f(Cc)+f(CC))=0.35
RRSR	Bb~CC | DD | ee		
RRSR	BB~CC | DD | ee		
SRRR	Bb~cc | dd | ee	x	fSRRR=1
SRRR	BB~cc | dd | ee		
SRSR	Bb~cc | Dd | ee		
SRSR	BB~cc | Dd | ee		
SRSR	Bb~cc | DD | ee	x	fSRSR=1
SRSR	BB~cc | DD | ee		
RRRS	bb~Cc | dd | Ee	x	fRRRS(Cc__Ee)=(f(Cc)*f(Ee))/((f(Cc)+f(CC))*(f(Ee)+f(EE)))=0.557
RRRS	Bb~Cc | dd | Ee		
RRRS	BB~Cc | dd | Ee		
RRRS	bb~CC | dd | Ee	x	fRRRS(CC__Ee)=(f(CC)*f(Ee))/((f(Cc)+f(CC))*(f(Ee)+f(EE)))=0.294
RRRS	Bb~CC | dd | Ee		
RRRS	BB~CC | dd | Ee		
RRRS	bb~Cc | dd | EE	x	fRRRS(Cc__EE)=(f(Cc)*f(EE))/((f(Cc)+f(CC))*(f(Ee)+f(EE)))=0.097
RRRS	Bb~Cc | dd | EE		
RRRS	BB~Cc | dd | EE		
RRRS	bb~CC | dd | EE	x	fRRRS(CC__EE)=(f(CC)*f(EE))/((f(Cc)+f(CC))*(f(Ee)+f(EE)))=0.052
RRRS	Bb~CC | dd | EE		
RRRS	BB~CC | dd | EE		
RRSS	bb~Cc | Dd | Ee		
RRSS	Bb~Cc | Dd | Ee		
RRSS	BB~Cc | Dd | Ee		
RRSS	bb~CC | Dd | Ee		
RRSS	Bb~CC | Dd | Ee		
RRSS	BB~CC | Dd | Ee		
RRSS	bb~Cc | DD | Ee	x	fRRSS(Cc__Ee)=(f(Cc)*f(Ee))/((f(Cc)+f(CC))*(f(Ee)+f(EE)))=0.557
RRSS	Bb~Cc | DD | Ee		
RRSS	BB~Cc | DD | Ee		
RRSS	bb~CC | DD | Ee	x	fRRSS(CC__Ee)=(f(CC)*f(Ee))/((f(Cc)+f(CC))*(f(Ee)+f(EE)))=0.294
RRSS	Bb~CC | DD | Ee		
RRSS	BB~CC | DD | Ee		
RRSS	bb~Cc | Dd | EE		
RRSS	Bb~Cc | Dd | EE		
RRSS	BB~Cc | Dd | EE		
RRSS	bb~CC | Dd | EE		
RRSS	Bb~CC | Dd | EE		
RRSS	BB~CC | Dd | EE		
RRSS	bb~Cc | DD | EE	x	fRRSS(Cc__EE)=(f(Cc)*f(EE))/((f(Cc)+f(CC))*(f(Ee)+f(EE)))=0.097
RRSS	Bb~Cc | DD | EE		
RRSS	BB~Cc | DD | EE		
RRSS	bb~CC | DD | EE	x	fRRSS(CC__EE)=(f(CC)*f(EE))/((f(Cc)+f(CC))*(f(Ee)+f(EE)))=0.052
RRSS	Bb~CC | DD | EE		
RRSS	BB~CC | DD | EE		
SRRS	Bb~cc | dd | Ee	x	fSRRS(Ee)=f(Ee)/(f(Ee)+f(EE))=0.85
SRRS	BB~cc | dd | Ee		
SRRS	Bb~cc | dd | EE	x	fSRRS(EE)=f(EE)/(f(Ee)+f(EE))=0.15
SRRS	BB~cc | dd | EE		
SRSS	Bb~cc | Dd | Ee		
SRSS	BB~cc | Dd | Ee		
SRSS	Bb~cc | DD | Ee	x	fSRSS(Ee)=f(Ee)/(f(Ee)+f(EE))=0.85
SRSS	BB~cc | DD | Ee		
SRSS	Bb~cc | Dd | EE		
SRSS	BB~cc | Dd | EE		
SRSS	Bb~cc | DD | EE	x	fSRSS(EE)=f(EE)/(f(Ee)+f(EE))=0.15
SRSS	BB~cc | DD | EE		
SSRS	bb~cc | dd | ee	x	fSSRS(ee)=f(ee)=0.55
SSRS	bb~cc | dd | Ee	x	fSSRS(Ee)=f(Ee)=0.38
SSRS	bb~cc | dd | EE	x	fSSRS(EE)=f(EE)=0.07
SSSS	bb~cc | Dd | ee		
SSSS	bb~cc | DD | ee	x	fSSSS(ee)=f(ee)=0.55
SSSS	bb~cc | Dd | Ee		
SSSS	bb~cc | DD | Ee	x	fSSSS(Ee)=f(Ee)=0.38
SSSS	bb~cc | Dd | EE		
SSSS	bb~cc | DD | EE	x	fSSSS(EE)=f(EE)=0.07

Figure S2.8

Participation of the different resistotypes to sexual reproduction in the host population. To assess whether sexual reproduction was biased towards some resistotypes, we collected in August 2020 *Daphnia magna* samples and quantified the resistotype distribution of females carrying resting stages, of males and of a random sample of females. Since males cannot be cloned, we cannot produce replicates to assess their resistotype, resulting in higher uncertainty of their resistotypes, in particular for the less easy scorable P15 and P21 *Pasteuria ramosa* isolates.

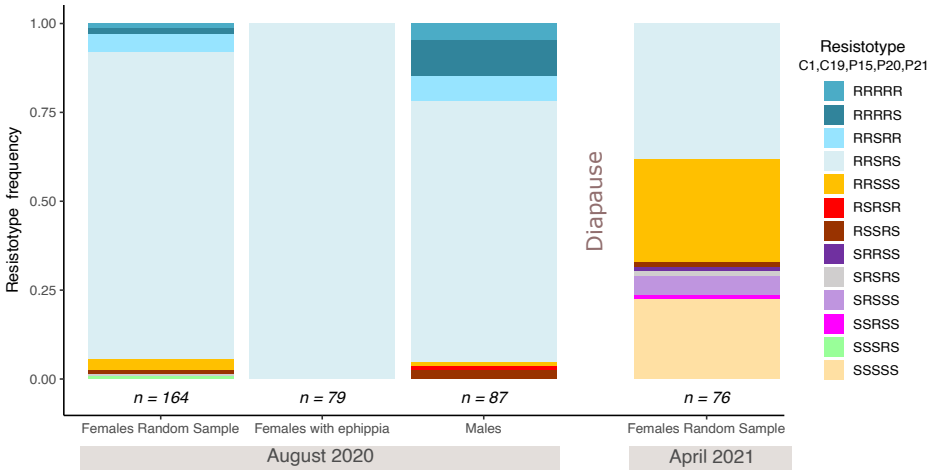

Materials and methods

Hatching modelling

Document S2.1

Peas implementation of the genetic model of resistance in the *Daphnia magna–Pasteuria ramosa* system.

Genetic model for resistance in the Aegelsee

implemented in peas R package

BCDE genetic model

1. Install the package

```
#install.packages("devtools")
#devtools::install_github("JanEngelstaedter/peas", build_vignettes = TRUE)

library(peas)
```

2. Set up the genetic model

2.1 Defining the genetic system

```
r2<-(1-exp(-2*23.1/100))/2 ## recombination rate between the B and C loci (Metzger et al. 2016)

# 4 loci with 2 alleles each, BC clustered togheter (Metzger et al. 2016).
BCDE <- newGenopheno(nloci = 2,
                     alleleNames = list(c("b", "B"), c("c", "C")),
                     rec = r2)
BCDE <- addLinkageGroup(BCDE, alleleNames = list(c("d", "D")))
BCDE <- addLinkageGroup(BCDE, alleleNames = list(c("e", "E")))
```

2.2 Set genotypes and their corresponding phenotypes : THE GENETIC MODEL

```
BCDE <- setPhenotypes(BCDE, "S/R", "__~__ | __ | __","SSRR") # default all recevice --> SSRR
# (we don't take the epistasis relation into account, this will be the last line of the model)

BCDE <- setPhenotypes(BCDE, "S/R", "B_~__ | __ | __","SRRR") # B --> R to C19

BCDE <- setPhenotypes(BCDE, "S/R", "B_~__ | D_ | __","SRSR") # D --> S to P15

# (Bento et al. 2020)
BCDE <- setPhenotypes(BCDE, "S/R", "B_~__ | __ | E_","SRRS") # E --> S to P20

BCDE <- setPhenotypes(BCDE, "S/R", "B_~__ | D_ | E_","SRSS") #

BCDE <- setPhenotypes(BCDE, "S/R", "__~C_ | __ | __","RRRR") # C hides B and --> R to C1 and C19

BCDE <- setPhenotypes(BCDE, "S/R", "__~C_ | D_ | __","RRSR") #
```

```
BCDE <- setPhenotypes(BCDE, "S/R", "__~C_ | __ | E_","RRRS") #
BCDE <- setPhenotypes(BCDE, "S/R", "__~C_ | D_ | E_","RRSS") #

# b/c-E epistasis #
# "bbcc" genotype induces S to P20, regardless of genotype at E-locus

BCDE <- setPhenotypes(BCDE, "S/R", "bb~cc | D_ | __","SSSS") #
BCDE <- setPhenotypes(BCDE, "S/R", "bb~cc | dd | __","SSRS") #
```

Summary of model

```
BCDE

## Genetic system comprising 3 linkage groups:
##   Linkage group 1: autosomal, 2 loci with recombination rate
0.1849888
##     Alleles at locus 1: b, B
##     Alleles at locus 2: c, C
##   Linkage group 2: autosomal, 1 locus
##     Alleles at locus 1: d, D
##   Linkage group 3: autosomal, 1 locus
##     Alleles at locus 1: e, E
## Phenotypes defined for the following traits:
##   S/R (trait values: SSRS, SRRR, RRRR, SSSS, SRSR, RRSR, SRRS,
RRRS, SRSS, RRSS)
```

List of all possible genotype combinations and corresponding phenotypes

```
BCDEallgeno<-getPhenotypes(BCDE)
nrow(BCDEallgeno) # 81 possible genotypes
## [1] 81
nrow(unique(BCDEallgeno)) # 10 possible resistotypes
## [1] 10
BCDEallgeno$geno<-row.names(BCDEallgeno) # add "geno"
column
BCDEallgeno<-BCDEallgeno[order(BCDEallgeno$`S/R`),] # sort
resistotypes
# rename "S/R" column as "pheno"
library(tidyverse)
BCDEallgeno<-rename(BCDEallgeno, pheno=`S/R`)
# export in xl file
library(xlsx)
write.xlsx(BCDEallgeno,"BCDEallgeno.xlsx")
```

3. Predict crosses

```
# all possible genotype crossings and their
# expected F1 genotype and phenotype segregation

cross<-matrix(list(), nrow=nrow(BCDEallgeno),
        ncol=nrow(BCDEallgeno), byrow=T)

for (i in 1:nrow(BCDEallgeno)) {
 for (j in 1:nrow(BCDEallgeno)) {
  cross[[i,j]]<-predictCross(BCDE,
BCDEallgeno$geno[i],BCDEallgeno$geno[j])
   # we add the corresponding resistotypes to the genotype output
  cross[[i,j]]$genotypes$SRtrait <- getPhenotypes(BCDE,
equivalent = "none")[row.names(cross[[i,j]]$genotypes), ]
 }
}

# large matrix of 81*81=6561 elements
# example: cross between genotype#1 and genotype#2
BCDEallgeno[1,]

##              pheno         geno
## bb~Cc | dd | ee  RRRR bb~Cc | dd | ee
BCDEallgeno[2,]

##              pheno         geno
## Bb~Cc | dd | ee  RRRR Bb~Cc | dd | ee
cross[[1,2]]

## $genotypes
##                fraction SRtrait
## bB~CC | dd | ee 0.20375279    RRRR
## bb~CC | dd | ee 0.04624721    RRRR
## bB~Cc | dd | ee 0.25000000    RRRR
## bb~Cc | dd | ee 0.25000000    RRRR
## bB~cc | dd | ee 0.04624721    SRRR
## bb~cc | dd | ee 0.20375279    SSRS
##
## $phenotypes
##    S/R  fraction
## 1 RRRR 0.75000000
## 2 SRRR 0.04624721
## 3 SSRS 0.20375279

# find a genotype
match("Bb~cc | dd | EE", BCDEallgeno$geno) # position 59
## [1] 59
```

Doc. S2.2 and Fig. S2.9

Theoretical resistotype frequency resulting from ephippia hatching in the Aegelsee. Using the genetic model of resistance in the *Daphnia magna−Pasteuria ramosa* system, we calculate theoretical resistotype (resistance phenotype) frequency resulting from hatching of *D. magna* resting stages laid throughout the active season.

Note: we use four-letter resistotype because the genetic model of resistance includes resistance to the four *P. ramosa* isolates C1, C19, P15 and P20.

Document S2.2

Calculations of the theoretical resistance phenotype frequency resulting from ephippia hatching in the Aegelsee.

prop data frame: observed resistotype proportion in the study population at each sampling date.

prop

	pheno-1 (RRRR)	…	pheno-k	…	pheno-n (SSSS)
date-1	$p_{1,1}$	…	$p_{1,k}$	…	$p_{1,n}$
date-2	$p_{2,1}$	…	$p_{2,k}$	…	$p_{2,n}$
date-3	$p_{3,1}$	…	$p_{3,k}$	…	$p_{3,n}$
…	…	…	…	…	…
date-i	$p_{i,1}$	…	$p_{i,k}$	…	$p_{i,n}$
…	…	…	…	…	…
date-d	$p_{d,1}$	…	$p_{d,k}$	…	$p_{d,n}$

freq data frame: fraction of each possible genotype within each phenotype. We use the list of possible genotypes and their corresponding phenotypes given by the genetic model of resistance implemented in the "peas" R-package. This list is given by the "getPhenotypes" function in the "peas" R-package (Supplementary Doc. S2.1). The fraction of each possible genotype within each phenotype (fq) is implemented by the user. In Supplementary Figs. S2.6 and S2.7, Tables S2.1 and S2.2 we test different scenarios of genotype distribution within the resistotypes.

freq

pheno	geno	fq
pheno-1 (RRRR)	geno-1	$f_{1,1}$
pheno-1 (RRRR)	geno-2	$f_{2,1}$
pheno-1 (RRRR)	geno-3	$f_{3,1}$
pheno-2	geno-4	$f_{4,2}$
pheno-2	geno-5	$f_{5,2}$
pheno-2	geno-6	$f_{6,2}$
…	…	…
pheno-k	…	…
pheno-k	…	…
pheno-k	…	…
pheno-k	geno-j	$f_{j,k}$
…	…	…
pheno-n (SSSS)	geno-g	$f_{g,n}$

We then calculate the proportion of each genotype at each sampling date:

$$d_{j,i} = f_{j,k} * p_{i,k}$$

with

$\mathbf{d}_{j,i}$: proportion of the j-genotype at the i-date.

$\mathbf{f}_{j,k}$ from the **freq** data frame: proportion of the j-genotype within the k-phenotype. This is implemented by the user.

$\mathbf{p}_{i,k}$ from the **prop** data frame: proportion of the k-phenotype at the i-date. Input from sampled data in the study population.

freq

pheno	geno	fq	date-1	date-2	…	date-**i**	…	date-d
pheno-1	geno-1	$f_{1,1}$	$d_{1,1}$	$d_{1,2}$	…	$d_{1,i}$	…	$d_{1,d}$
pheno-1	geno-2	$f_{2,1}$	$d_{2,1}$	$d_{2,2}$	…	$d_{2,i}$	…	$d_{2,d}$
pheno-1	geno-3	$f_{3,1}$	$d_{3,1}$	$d_{3,2}$	…	$d_{3,i}$	…	$d_{3,d}$
pheno-2	geno-4	$f_{4,2}$	$d_{4,1}$	$d_{4,2}$	…	$d_{4,i}$	…	$d_{4,d}$
pheno-2	geno-5	$f_{5,2}$	$d_{5,1}$	$d_{5,2}$	…	$d_{5,i}$	…	$d_{5,d}$
pheno-2	geno-6	$f_{6,2}$	$d_{6,1}$	$d_{6,2}$	…	$d_{6,i}$	…	$d_{6,d}$
…	…	…	…	…	…	…	…	…
pheno-**k**	…	…	…	…	…	…	…	…
pheno-**k**	…	…	…	…	…	…	…	…
pheno-**k**	…	…	…	…	…	…	…	…
pheno-**k**	geno-**j**	$f_{j,k}$	$d_{j,1}$	$d_{j,2}$	…	$\mathbf{d}_{j,i}$	…	$d_{j,d}$
…	…	…	…	…	…	…	…	…
pheno-n	geno-g	$f_{g,n}$	$d_{g,1}$	$d_{g,2}$	…	$d_{g,i}$	…	$d_{g,d}$

di matrix: fraction of all possible genotype crossings at the i-date considering random mating and equal contribution of all individuals to sexual reproduction.

$$di = \begin{pmatrix} d_{1,i} \\ d_{2,i} \\ \vdots \\ d_{j,i} \\ \vdots \\ d_{g,i} \end{pmatrix} * t \begin{pmatrix} d_{1,i} \\ d_{2,i} \\ \vdots \\ d_{j,i} \\ \vdots \\ d_{g,i} \end{pmatrix} = \begin{pmatrix} di_{1,1} & di_{1,2} & \cdots & di_{1,m} & \cdots & di_{1,g} \\ di_{2,1} & di_{2,2} & \cdots & di_{2,m} & \cdots & di_{2,g} \\ \vdots & \vdots & \ddots & \vdots & \ddots & \vdots \\ di_{l,1} & di_{l,2} & \cdots & di_{l,m} & \cdots & di_{l,g} \\ \vdots & \vdots & \ddots & \vdots & \ddots & \vdots \\ di_{g,1} & di_{g,2} & \cdots & di_{g,m} & \cdots & di_{g,g} \end{pmatrix}$$

with

di$_{l,m}$: proportion of mating events between the l-genotype and m-genotype at the i-date.

The sum of the elements of the di matrix is equal to 1.

cross matrix

$$\begin{pmatrix} c_{1,1} & c_{1,2} & \cdots & c_{1,m} & \cdots & c_{1,g} \\ c_{2,1} & c_{2,2} & \cdots & c_{2,m} & \cdots & c_{2,g} \\ \vdots & \vdots & \ddots & \vdots & \ddots & \vdots \\ c_{l,1} & c_{l,2} & \cdots & c_{l,m} & \cdots & c_{l,g} \\ \vdots & \vdots & \ddots & \vdots & \ddots & \vdots \\ c_{g,1} & c_{g,2} & \cdots & c_{g,m} & \cdots & c_{g,g} \end{pmatrix}$$

c$_{l,m}$: data frame containing predicted genotypic and phenotypic crossing results between the l- and the m-genotype. This was calculated using the "predictCross" function in the "peas" R-package. See implementation of the genetic model of resistance in Supplementary Doc. S2.1.

Example:

c$_{1,2}$: crossing result between genotype #1 and genotype #2

```
BCDEallgeno[1,]

##              pheno          geno
## bb~Cc | dd | ee  RRRR bb~Cc | dd | ee

BCDEallgeno[2,]

##              pheno          geno
## Bb~Cc | dd | ee  RRRR Bb~Cc | dd | ee

cross[[1,2]]

## $genotypes
##                 fraction SRtrait
## bB~CC | dd | ee 0.20375279    RRRR
## bb~CC | dd | ee 0.04624721    RRRR
## bB~Cc | dd | ee 0.25000000    RRRR
## bb~Cc | dd | ee 0.25000000    RRRR
## bB~cc | dd | ee 0.04624721    SRRR
## bb~cc | dd | ee 0.20375279    SSRS
##
## $phenotypes
##    S/R  fraction
## 1 RRRR 0.75000000
## 2 SRRR 0.04624721
## 3 SSRS 0.20375279
```

c$_{l,m}$**$genotypes**

	fraction	SRtrait
geno-a	α_a	pheno-a
geno-b	α_b	pheno-a
geno-c	α_c	pheno-b
…	…	…
geno-x	α_x	pheno-y

With y ≤ x as there can be several genotypes underlying one phenotype (see example above)

c$_{l,m}$**$phenotypes**

	S/R	fraction
1	pheno-a	β_a
2	pheno-b	β_b
…	…	…
z	pheno-y	β_y

prophatch data frame: final data frame with expected resistotype proportions at each sampling date.

prophatch

	pheno-1 (RRRR)	…	pheno-**k**	…	pheno-n (SSSS)
date-1	$h_{1,1}$	…	$h_{1,k}$	…	$h_{1,n}$
date-2	$h_{2,1}$	…	$h_{2,k}$	…	$h_{2,n}$
date-3	$h_{3,1}$	…	$h_{3,k}$	…	$h_{3,n}$
…	…	…	…	…	…
date-**i**	$h_{i,1}$	…	$\mathbf{h}_{i,k}$	…	$h_{i,n}$
…	…	…	…	…	…
date-d	$h_{d,1}$	…	$h_{d,k}$	…	$h_{d,n}$

$\mathbf{h}_{i,k}$: expected frequency of the k-resistotype at the i-date.

$$h_{i,k} = \sum_{m=0}^{j} \sum_{l=0}^{j} c_{l,m}\$phenotypes\$\beta_k * di_{l,m}$$

The same calculation can be done with the genotypes fractions (α) instead of the phenotypes fractions (β).

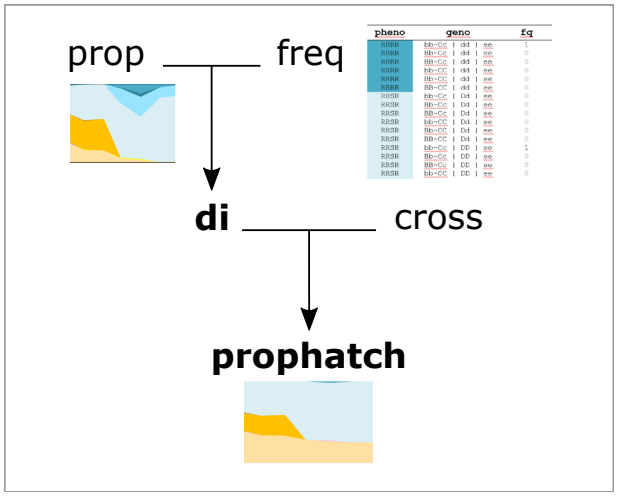

Figure S2.9

Summary illustration of Supplementary Doc. S2.2: calculation of theoretical resistotype (resistance phenotype) frequency resulting from resting stages hatching in the Aegelsee *Daphnia magna* population. The theoretical resistotype frequency over time is calculated using the genetic model of resistance in the *D. magna*–*Pasteuria ramosa* system and the observed resistotype frequency over time in the *D. magna* population. Input elements are written in regular font style, output elements are written in bold. **Prop** data frame: observed resistotype proportion in the study population at each sampling date. **Freq** data frame: fraction of each possible genotype within each phenotype. We use the list of possible genotypes and their corresponding phenotypes given by the genetic model of resistance implemented in the "peas" R-package. **Di** matrix: calculated from "prop" and "freq": fraction of all possible genotype crossings at the i-date considering random mating in the *D. magna* population. **Cross** matrix: predicted genotypic and phenotypic crossing results from all possible genotype crossings. Each element of the matrix is a data frame containing predicted genotypic and phenotypic crossing results of one genotype crossing. **Prophatch** data frame: calculated from "di" and "cross": final data frame with expected resistotype proportions resulting from sexual reproduction at each sampling date.

Document S2.3

Statistical software.

Unless otherwise stated, all statistical analyses and graphics were performed in the R software version 3.6.1 (R Core Team 2021). Graphics were edited in Inkscape v. 1.0.1 (https://inkscape.org/). Mean values are presented with standard error: mean ± se (Package RVAideMemoire v. 09-45-2: Hervé 2015). Packages used in R for package installation, data manipulation and graphics are the following: package development, documentation and installation: devtools v. 2.2.1 (Wickham, Hester, et al. 2019) and roxygen2 v. 6.1.1 (Wickham et al. 2018), data manipulation: dplyr v. 0.8.3 (Wickham, François, et al. 2019), tidyr v. 1.0.0 (Wickham and Henry 2019), tidyquant v. 0.5.8 (Dancho and Vaughan 2019), tidyverse v. 1.2.1 (Wickham 2017), xlsx v. 0.6.1 (Dragulescu and Arendt 2018), graphics: ggplot2 v. 3.3.0 (Wickham 2016), extrafont v. 0.17 (Chang 2014), scales v. 1.0.0 (Wickham 2018), cowplot v. 1.0.0 (Wilke 2019), gridExtra v. 2.3 (Auguie 2017), ggpubr v. 0.2.3 (Kassambara 2019), ggplotify v. 0.0.4 (Yu 2019), magick v. 2.2 (Ooms 2019), egg v. 0.4.5 (Auguie 2019), ggsci v. 2.9 (Xiao 2018) and png v. 0.1-7 (Urbanek 2013).

References

Ameline C, Bourgeois Y, Vögtli F, Savola E, Andras J, Engelstädter J, Ebert D. 2021. A two-locus system with strong epistasis underlies rapid parasite-mediated evolution of host resistance. *Molecular Biology and Evolution* **38**:1512–1528.

Auguie B. 2017. gridExtra: Miscellaneous functions for "Grid" graphics. Available from: https://CRAN.R-project.org/package=gridExtra

Auguie B. 2019. egg: Extensions for "ggplot2": Custom geom, custom themes, plot alignment, labelled panels, symmetric scales, and fixed panel size. Available from: https://CRAN.R-project.org/package=egg

Auld SKJR, Brand J. 2017. Simulated climate change, epidemic size, and host evolution across host-parasite populations. *Global Change Biology* **23**:5045–5053.

Bento G, Fields PD, Duneau D, Ebert D. 2020. An alternative route of bacterial infection associated with a novel resistance locus in the *Daphnia–Pasteuria* host–parasite system. *Heredity* **125**:173–183.

Chang W. 2014. extrafont: Tools for using fonts. Available from: https://CRAN.R-project.org/package=extrafont

Dallas T, Drake JM. 2016. Fluctuating temperatures alter environmental pathogen transmission in a *Daphnia* -pathogen system. *Ecology and Evolution* **6**:7931–7938.

Dancho M, Vaughan D. 2019. tidyquant: Tidy quantitative financial analysis. Available from: https://CRAN.R-project.org/package=tidyquant

Dragulescu AA, Arendt C. 2018. xlsx: Read, write, format Excel 2007 and Excel 97/2000/XP/2003 files. Available from: https://CRAN.R-project.org/package=xlsx

Duffy MA, Hunsberger KK. 2019. Infectivity is influenced by parasite spore age and exposure to freezing: do shallow waters provide *Daphnia* a refuge from some parasites? *Journal of Plankton Research* **41**:12–16.

Duneau D, Luijckx P, Ben-Ami F, Laforsch C, Ebert D. 2011. Resolving the infection process reveals striking differences in the contribution of environment, genetics and phylogeny to host–parasite interactions. *BMC biology* **9**:1–11.

Ebert D, Duneau D, Hall MD, Luijckx P, Andras JP, Du Pasquier L, Ben-Ami F. 2016. A population biology perspective on the stepwise infection process of the bacterial pathogen *Pasteuria ramosa* in *Daphnia*. *Advances in Parasitology* **91**:265–310.

Hector TE, Sgrò CM, Hall MD. 2019. Pathogen exposure disrupts an organism's ability to cope with thermal stress. *Global Change Biology* **25**:3893–3905.

Hervé M. 2015. RVAideMemoire: Diverse basic statistical and graphical functions. Available from: http://CRAN.R-project.org/package=RVAideMemoire

Hite JL, Cressler CE. 2018. Resource-driven changes to host population stability alter the evolution of virulence and transmission. *Philosophical Transactions of the Royal Society B: Biological Sciences* **373**:20170087.

Kassambara A. 2019. ggpubr: "ggplot2" based publication ready plots. Available from: https://CRAN.R-project.org/package=ggpubr

Kirk D, Jones N, Peacock S, Phillips J, Molnár PK, Krkošek M, Luijckx P. 2018. Empirical evidence that metabolic theory describes the temperature dependency of within-host parasite dynamics.Pawar S, editor. *PLOS Biology* **16**:e2004608.

Kirk D, Luijckx P, Stanic A, Krkošek M. 2019. Predicting the thermal and allometric dependencies of disease transmission via the metabolic theory of ecology. *The American Naturalist* **193**:661–676.

Laine A-L. 2007. Pathogen fitness components and genotypes differ in their sensitivity to nutrient and temperature variation in a wild plant–pathogen association. *Journal of Evolutionary Biology* **20**:2371–2378.

Luijckx P, Ben-Ami F, Mouton L, Du Pasquier L, Ebert D. 2011. Cloning of the unculturable parasite *Pasteuria ramosa* and its *Daphnia* host reveals extreme genotype–genotype interactions. *Ecology Letters* **14**:125–131.

Metzger CMJA, Luijckx P, Bento G, Mariadassou M, Ebert D. 2016. The Red Queen lives: Epistasis between linked resistance loci. *Evolution* **70**:480–487.

Mitchell SE, Rogers ES, Little TJ, Read AF. 2005. Host-parasite and genotype-by-environment interactions: temperature modifies potential for selection by a sterilizing pathogen. *Evolution* **59**:70–80.

Ooms J. 2019. magick: Advanced graphics and image-processing in R. Available from: https://CRAN.R-project.org/package=magick

R Core Team. 2021. R: A language and environment for statistical computing. R Foundation for Statistical Computing, Vienna, Austria. Available from: http://www.R-project.org

Reyserhove L, Samaey G, Muylaert K, Coppé V, Van Colen W, Decaestecker E. 2017. A historical perspective of nutrient change impact on an infectious disease in *Daphnia*. *Ecology* **98**:2784–2798.

Shocket MS, Strauss AT, Hite JL, Šljivar M, Civitello DJ, Duffy MA, Cáceres CE, Hall SR. 2018. Temperature drives epidemics in a zooplankton-fungus disease system: A trait-driven approach points to transmission via host foraging. *The American Naturalist* **191**:435–451.

Shocket MS, Vergara D, Sickbert AJ, Walsman JM, Strauss AT, Hite JL, Duffy MA, Cáceres CE, Hall SR. 2018. Parasite rearing and infection temperatures jointly influence disease transmission and shape seasonality of epidemics. *Ecology* **99**:1975–1987.

Urbanek S. 2013. png: Read and write PNG images. Available from: https://CRAN.R-project.org/package=png

Vale PF, Little TJ. 2009. Measuring parasite fitness under genetic and thermal variation. *Heredity* **103**:102–109.

Vale PF, Stjernman M, Little TJ. 2008. Temperature-dependent costs of parasitism and maintenance of polymorphism under genotype-by-environment interactions. *Journal of Evolutionary Biology* **21**:1418–1427.

Vale PF, Wilson AJ, Best A, Boots M, Little TJ. 2011. Epidemiological, evolutionary, and coevolutionary implications of context-dependent parasitism. *The American Naturalist* **177**:510–521.

Wickham H. 2016. ggplot2: Elegant graphics for data analysis. New York: Springer-Verlag

Wickham H. 2017. tidyverse: Easily install and load the "Tidyverse." Available from: https://CRAN.R-project.org/package=tidyverse

Wickham H. 2018. scales: Scale functions for visualization. Available from: https://CRAN.R-project.org/package=scales

Wickham H, Danenberg P, Eugster D. 2018. roxygen2: In-line documentation for R. Available from: https://CRAN.R-project.org/package=roxygen2

Wickham H, François R, Henry L, Müller K. 2019. dplyr: A grammar of data manipulation. Available from: https://CRAN.R-project.org/package=dplyr

Wickham H, Henry L. 2019. tidyr: Tidy messy data. Available from: https://CRAN.R-project.org/package=tidyr

Wickham H, Hester J, Chang W. 2019. devtools: Tools to make developing R packages easier. Available from: https://CRAN.R-project.org/package=devtools

Wilke CO. 2019. cowplot: Streamlined plot theme and plot annotations for "ggplot2." Available from: https://CRAN.R-project.org/package=cowplot

Xiao N. 2018. ggsci: Scientific journal and sci-fi themed color palettes for "ggplot2." Available from: https://CRAN.R-project.org/package=ggsci

Yu G. 2019. ggplotify: Convert plot to "grob" or "ggplot" object. Available from: https://CRAN.R-project.org/package=ggplotify

Supplementary Material Chapter 3

Overview

Section in main manuscript	Element	Description	Page
Materials and methods			
Genetic crosses			
	Table S3.1	Parent clones	p. 140
Poolseq association study			
	Fig. S3.1	Coverage	p. 140
Results			
Genetic model and resistance diversity			
	Table S3.2	History of the genetic model	p. 141
	Figs. S3.2 to S3.8	Genetic models	p. 142–145
Genetic crosses			
	Tables S3.3 to S3.13	Selfing results	p. 146–150
	Table S3.14	Statistical tests results	p. 150
References			p. 151

Materials and methods

Genetic crosses

Table S3.1

Overview of the F0 *Daphnia magna* parent clones used to produce selfed F1 offspring sorted by their inferred genotypes. These genetic crosses are presented in Chapter 1, with the difference that we consider here two additional *Pasteuria ramosa* isolates, P15 and P21. The resistotype corresponds to the resistance phenotype to the five *Pasteuria ramosa* isolates used in this study: C1, C19, P15, P20 and P21, in that order. The inferred genotype at the C and E loci is the result of genetic markers analysis of the parent clone (Chapter 1). Two exceptions (marked with an asterisk "*") are cases where the marker genotype at the E locus was "EE", although segregation in the selfed F1 offspring revealed a "Ee" genotype. Genotype at the other loci, the A, B, D and F loci, is inferred from segregation in the selfed F1, evidence from the PoolSeq association study and previous studies (Luijckx et al. 2012; Luijckx et al. 2013; Metzger et al. 2016; Bento et al. 2020; Fredericksen et al. in prep). The C- and E-loci genotype of the two "SRSSS" parents was inferred using only the segregation pattern of their selfed offspring. The markers were designed to map resistance to C1, C19 and P20 in the Aegelsee population, using the three main resistotypes only: RR_S_, RR_R_ and SS_S_, and were consequently not linked to the genotype in SR____ individuals. F0 parents correspond to females caught from plankton (clone name starting with "CH") or hatched from resting eggs (clone name starting with "t") collected from the Aegelsee natural population between 2011 and 2016 and subsequently clone in the laboratory.

Resistotype	Inferred genotype	Repeat name	Parent clone name	n (offspring) total n = 1266		Selfing results
Common variation						
C- and E-loci variation						
RRSSS	aabbCCDDEEff	a	t3_12.3_1i_12	43	Table 3.1 main manuscript	Table S3.3
		b	t3_12.3_1i_21	37		
RRSSS	aabbCCDDEeff	a	CH-2015-36	89		Table S3.4
		b	t3_12.3_1	31		
		c	CH-H-2015-49	79	*	
RRSRS	aabbCCDDeeff	a	CH-H-434-inb2-1	39		Table S3.5
RRSSS	aabbCcDDEEff	a	t2_17.3_4i_12	19		Table S3.6
RRSSS	aabbCcDDEeff	a	t3_14.3_1	48		Table S3.7
		b	t2_17.3_1	64		
		c	CH-H-2015-59	65	*	
RRSRS	aabbCcDDeeff	a	t1_10.3_4	36		Table S3.8
		b	t5_10.3_3	49		
		c	CH-H-434-inb2-2	22		
SSSSS	aabbccDDEEff	a	CH-H-2015-97	87		Table S3.9
SSSSS	aabbccDDEeff	a	CH-H-2015-113	84		Table S3.10
		b	t4_10.3_16	65		
SSSSS	aabbccDDeeff	a	t4_13.3_2	74		Table S3.11
Additional rare variation						
B-locus variation						
SRSSS	aaBbccDDEEff		t0_9.3_7	37	Table 3.2 main	Table S3.12
SRSSS	aaBbccDDEeff		t0_28.2_43	38		Table S3.13
D-locus variation						
RRSRS	aabbCCDDeeff		CH-H-2015-16	70	1	Table 3.8
RRSSS	aabbCcDdEeff		t2_17.3_4	34	2	Table S3.3
RRRRR	aabbCCddeeFF		t1_10.3_2	42	3	Table 3.9
D- and F-loci variation *used in PoolSeq association*						
RRRRR	aabbCCDdeeFf		CH-H-2016-b-70	79	4	Tables 3.4 and 3.5
SSSSS	aabbccDdeeFf		CH-H-2015-86	35	5	Tables 3.6 and 3.7

* E-locus genetic marker not linked, gives "EE" genotype

1 Little P15-resistotype segregation

2 P15 and P21 resistotypes segregate and are coupled

3 Little P21-resistotype segregation

4 P15 and P21 resistotypes segregate, evidence for D-locus variation from PoolSeq association

5 P21 resistotype segregates, evidence for D-locus variation from PoolSeq association

Poolseq association study

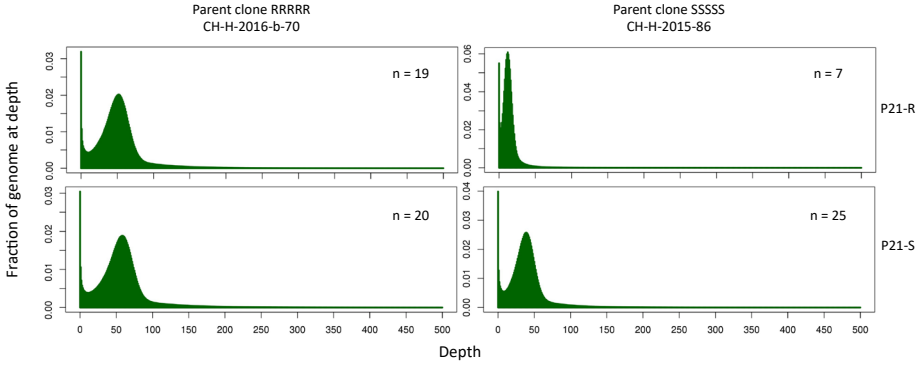

Figure S3.1

Coverage of the PoolSeq subgroups.

Results

Genetic model and resistance diversity

Table S3.2

A chronological history of the investigation of the genetic model of resistance to *Pasteuria ramosa* in *Daphnia magna*.

Publication	Method	*D. magna*		*P. ramosa*		Findings	Genetic model	Genetic map
		No of clones	Origin	No of clones or isolates	Origin			
Luijckx et al. 2011	Genetic crosses in the host Infection trials Cloning of the parasite by limited dilution and single-spore infection	14 + 4	Europe + Laboratory crosses between the European clones	8 clones	5 European isolates	High specificity in the system is unveiled using clones of the parasite.		
Luijckx et al. 2012	Genetic crosses in the host Infection trials Attachment test	284 F1 and F2 clones	Finland	1 clone: C1 (produced in Luijckx et al. 2011)	Russian isolate	Resistance to the parasite shows Mendelian inheritance with dominance.	Fig. S3.2	A locus
Luijckx et al. 2013	same as Luijckx et al. 2012			2 clones: C1 and C19 (Luijckx et al. 2011)	Russian and German isolates	Using an additional bacterial clone, a Matching-Allele Model for resistance is revealed	Fig. S3.3	A and B loci
Routtu and Ebert 2015	QTL analysis Attachment test	195 F2 clones	QTL panel with parents originating from Germany and Finland	1 clone: C19	German isolate	A QTL analysis for resistance reveals a single strong QTL which explains 50 % of the observed variation		Later called ABC cluster, or PR locus
Metzger et al. 2016	Genetic crosses in the host Attachment test	> 7000 clones from 3 crosses of F0, 13 F1 clones, each of which produce an F2 panel by selfing	4 Finnish clones	2 clones: C1 and C19	Russian and German isolates	Genetic crossings in the host yield a three-loci model with epistatic interactions	Fig. S3.4	A, B and C loci
Bourgeois et al. 2017	A GWAS and a naïve genome scan for signatures of selection performed in parallel Attachment test	97	13 populations in Switzerland, Germany and Finland	2 clones: C1 and C19	Russian and German isolates	A GWAS and a naïve genome scan for signatures of selection performed in parallel reveal two regions associated with resistance and under selection. The first is the QTL found by Routtu and Ebert (2015) and the second is a new region.		ABC cluster, new regions
Bento et al. 2017	Fine mapping of the QTL region found in Routtu and Ebert (2015)	NA	NA	NA	NA	The region is thereafter called the PR-locus (*Pasteuria* resistance locus) and contains the ABC-cluster described in Metzger et al. (2016).		
Bento et al. 2020	QTL analysis of resistance to a parasite which attaches to a different part of the *Daphnia* gut Attachment test	208 core panel and 169 extended panel F2 clones 174 clones	QTL panel with parents originating from Germany and Finland Diversity panel: the whole distribution of *D. magna*, i.e. the holarctic	3 clones and isolates: C1, C19 and P15	P15 is a Belgian isolate that has been passaged several times in a susceptible host	A new genomic region responsible for resistance to P15 is found, the dominance pattern and a weak epistatic interaction are described	Fig. S3.5	D locus
Ameline et al. 2021 (Ch 1)	GWAS Genetic crosses in the host Attachment test Genetic crosses in the host Attachment test	37 clones 1274 clones from 24 selfed F1 groups	Switzerland, the Aegelsee population Switzerland, the Aegelsee population	3 clones and isolates: C1, C19 and P20	P20 isolated from the Aegelsee, passaged several times	A new genomic region responsible for resistance to P20 is desribed, the E-locus, dominance and epistasis are found	Fig. S3.6	E locus P15 used but not considered for the genetic model
Ameline et al. preprint (Ch 2)	Collection and hatching of overwintering resting sexual eggs Attachment test Modelling of the output of recombination using the genetic model of resistance in the host (Fig. 2.5)	1495 NA	Resting eggs collected in the Aegelsee population NA	4 clones and isolates: C1, C19, P15 and P20 NA	Russia, Germany, Belgium and Switzerland NA	This study tests and partly supports the genetic model of resistance inheritance (Fig. 2.5) using modelling of the *Daphnia* overwintering eggs hatching		P21 used but not considered for the genetic model
Fredericksen et al. in prep	QTL analysis Genetic crosses in the host Attachment test	208 core panel and 169 extended panel F2 clones	QTL panel with parents originating from Germany and Finland Diversity panel: the whole distribution of *D. magna*, i.e. the holarctic	5 clones and isolates: C1, C19, P15, P20 and P21	P21 isolated from the Aegelsee, passaged several times	New genomic region responsible for resistance to P21, the F locus, with dominance, close to the ABC cluster	Fig. S3.7	F locus
Gattis 2018	Genetic crosses in the host Attachment test	34 selfed F1 groups 13 F1 clones	Produced in Metzger et al. 2016	5 clones and isolates: C1, C19, P15, P20 and P21	Russia, Germany, Belgium and Switzerland	Mostly confirms the genetic model in a wide geographic distribution, describes two new resistance loci and epistatic interactions	Fig. S3.8	G and H loci
The present study	Genetic crosses in the host Attachment test PoolSeq association study Attachment test	same as in Ameline et al. 2021 (Ch 1) 2 selfed F1 groups	from Ameline et al. 2021 (Ch1)	5 clones and isolates: C1, C19, P15, P20 and P21	Russia, Germany, Belgium and Switzerland	Describes new epistatic interactions	Fig. 3.1 main manuscript	

Figures S3.2 to S3.8

Models of resistance to *Pasteuria ramosa* in *Daphnia magna*. The left panel represents resistance loci as grey boxes and their interactions. The right panel depicts the resistance phenotypes, i.e. resistotype to the five *P. ramosa* isolates. The placeholder indicates that an isolate is not considered. Color boxes represent resistotypes that were found in the Aegelsee population.

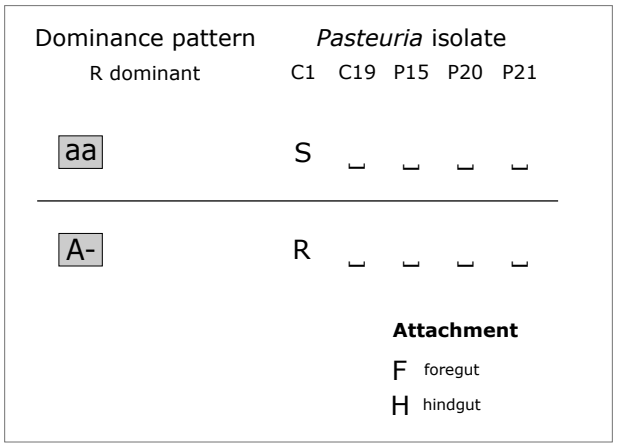

Figure S3.2

Model of resistance to *Pasteuria ramosa* C1 in *Daphnia magna*.

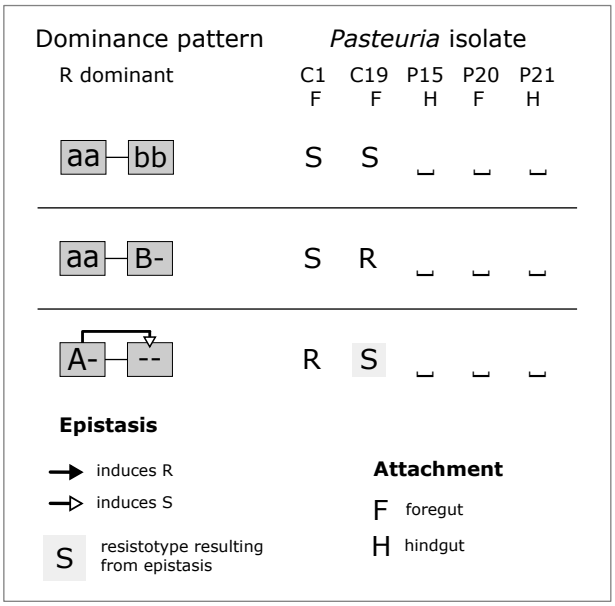

Figure S3.3

Model of resistance to *Pasteuria ramosa* C1 and C19 in *Daphnia magna*, including the A and the B loci.

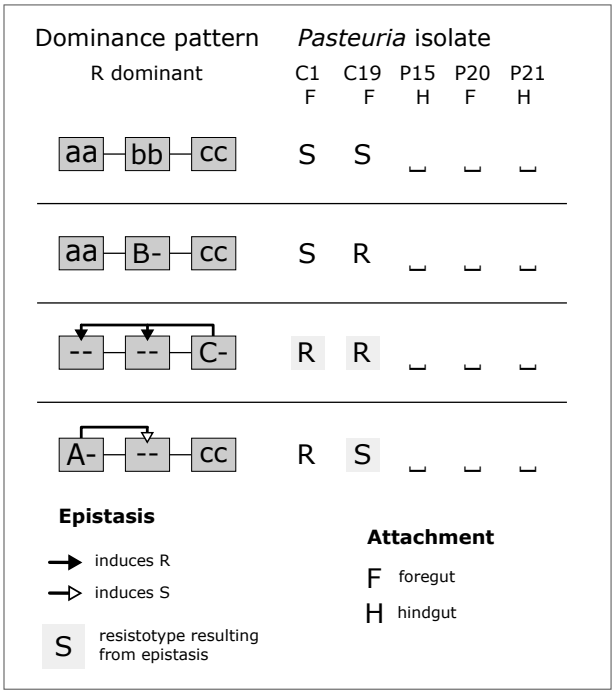

Figure S3.4

Model of resistance to *Pasteuria ramosa* C1 and C19 in *Daphnia magna*, including the A, B and C loci.

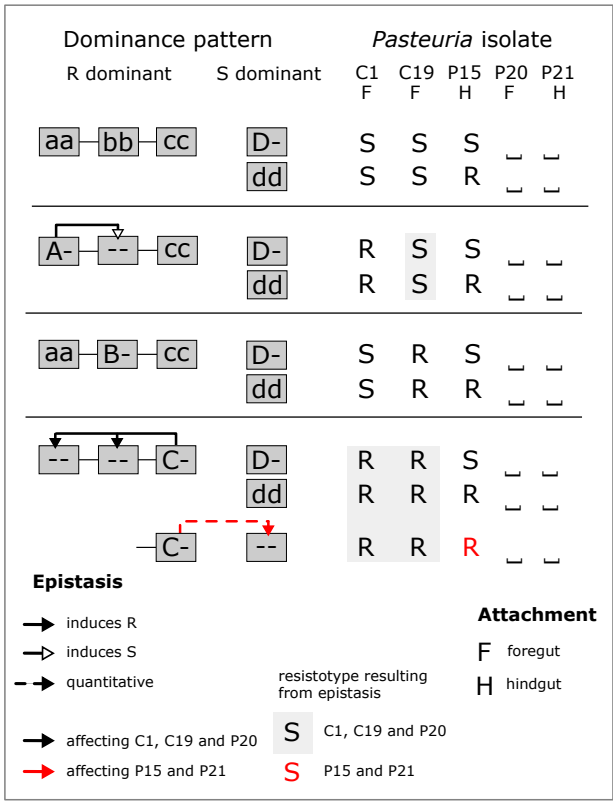

Figure S3.5

Model of resistance to *Pasteuria ramosa* C1, C19 and P15 in *Daphnia magna*.

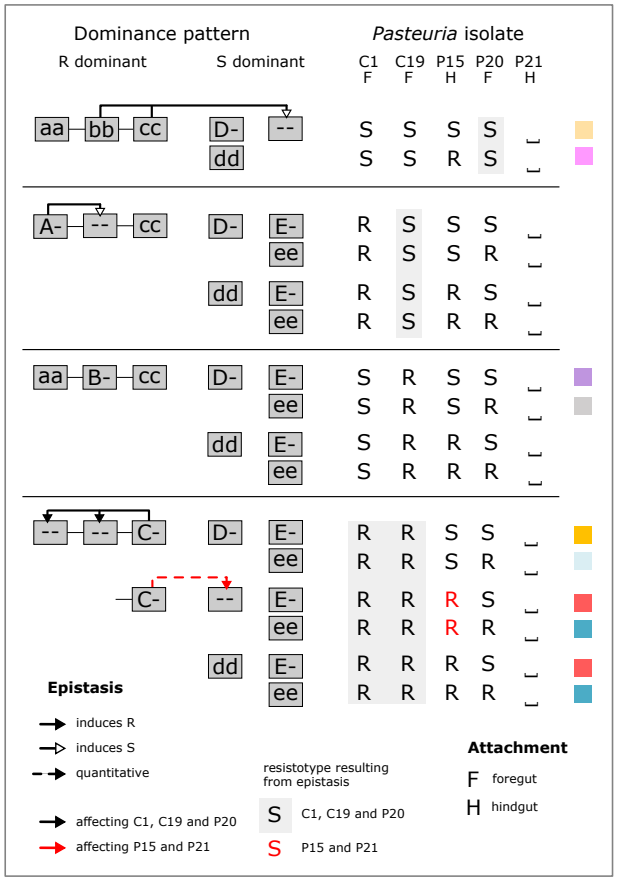

Figure S3.6

Model of resistance to *Pasteuria ramosa* C1, C19, P15 and P20 in *Daphnia magna*.

Figure S3.7

Model of resistance to *Pasteuria ramosa* C1, C19, P15, P20 and P21 in *Daphnia magna*. No epistatic interactions are considered among the F locus and other loci.

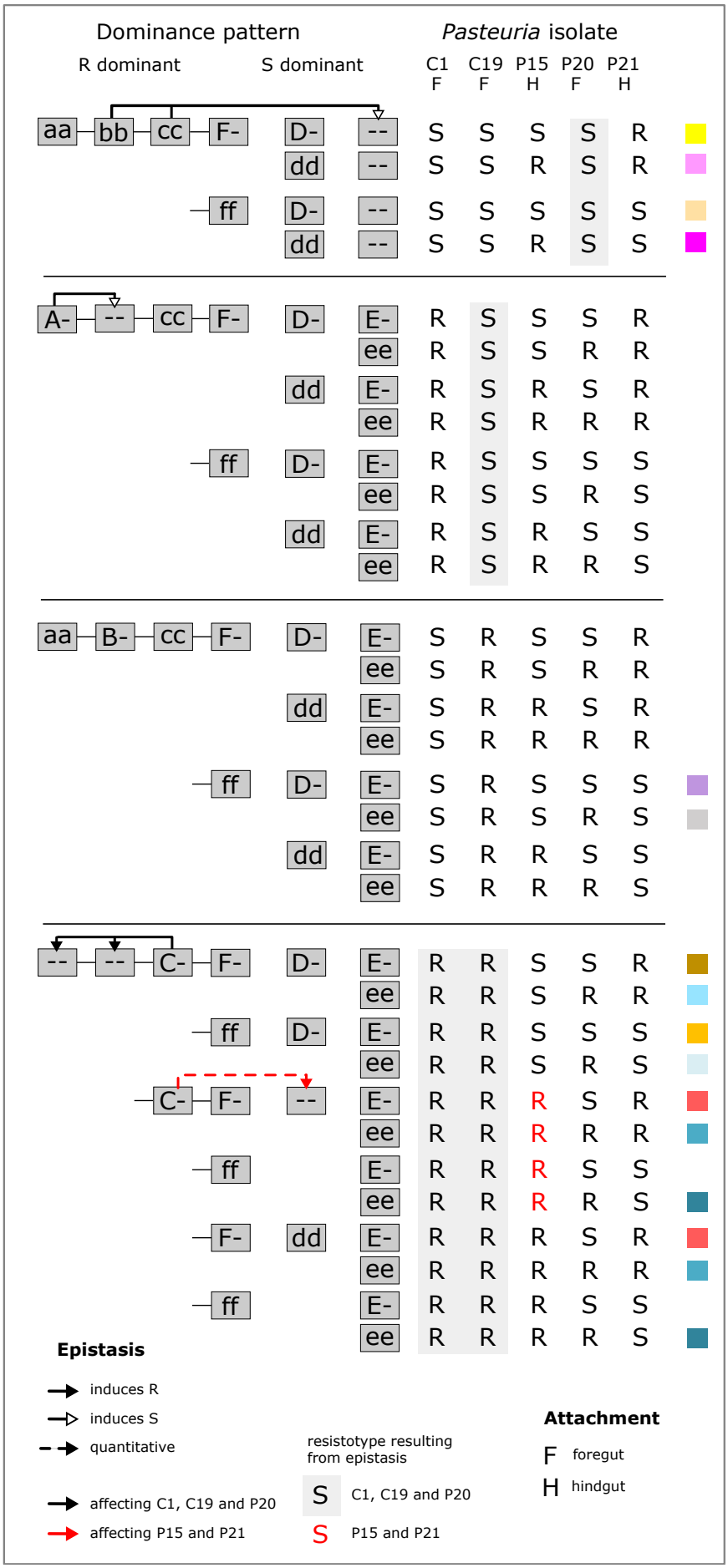

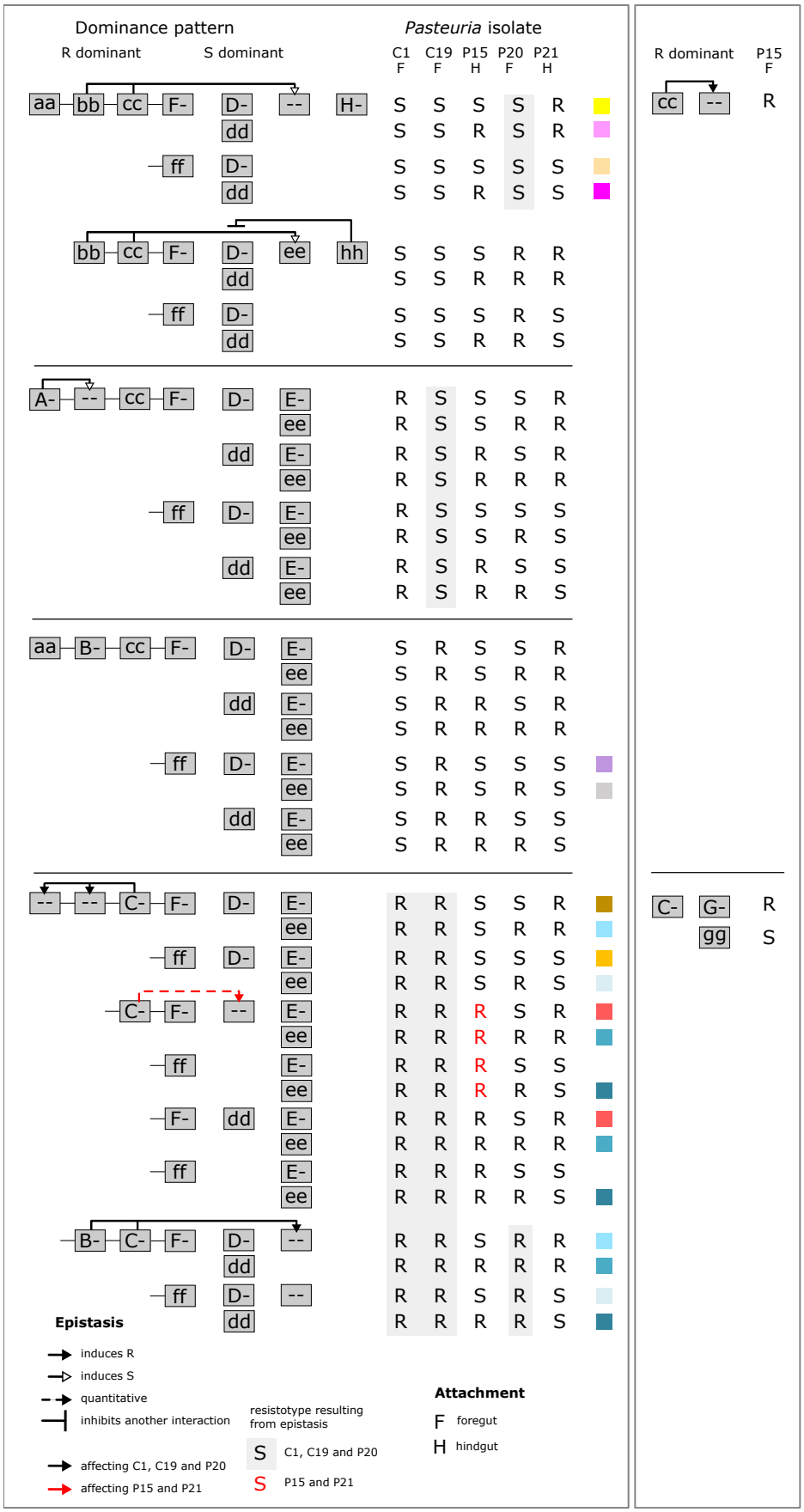

Figure S3.8

Model of resistance to *Pasteuria ramosa* C1, C19, P15, P20 and P21 in *Daphnia magna*. Adapted from (Gattis 2018).

Genetic crosses

Tables S3.3 to S3.13

This data corresponds to genetic crosses presented in Chapter 1, where we consider resistance phenotypes, a.k.a. resistotypes, to *Pasteuria ramosa* isolates C1, C19, and P20. In the present chapter we additionally consider variation at the P15 and P21 resistotypes. The overall resistotype describes resistance (R) and susceptibility (S) to C1, C19, P15, P20 and P21, in that order, e.g. a host clone with a SSSSS resistotype shows susceptibility to all bacterial isolates. In the Aegelsee *D. magna* population, resistance to C1 and C19 is determined by variation at the B and C loci, while resistance to P20 is determined by variation at the B, C and E loci (Chapter 1, Fig 1.5). We inferred from the observed phenotypic variation that the a-allele was fixed in the population and that the B allele was rare (Chapter 1, results section). Variation at the P15 and P21 resistotypes is rare and mostly coupled, i.e. the resistotype is the same for the two isolates. Resistance to P15 is mostly determined by variation at the D locus, at which resistance is recessive (Bento et al. 2020), see also Chapter 2 Supplementary Model Fig. S2.1). Resistance to P21 is mostly determined by variation at the F locus, where resistance is dominant (Fredericksen et al. in prep). We inferred from phenotypic variation in the Aegelsee population that the d and the F alleles are rare in the Aegelsee *D. magna* population. The "DDff" genotype is consequently common, and all F1 offspring groups described here possess this genotype. Resistance genotype is inferred from phenotypic segregation in the F1 offspring groups. Text in red denotes genotypes and their corresponding phenotypes where the epistatic relationship between the B, C and the E loci is expected to be revealed in the phenotype (see Chapter 1 Fig. 1.5). **A.** Expected Punnett square for the selfed genotype according to the genetic model. **B.** Expected vs. observed phenotypes of selfed F1 offspring. Expected phenotypic segregation was calculated from the Punnett square. We compared expected vs. observed resistotype segregation in the F1 groups using the Cochran–Mantel–Haenszel (C-M-H) test for repeated tests of independence. When there was only one repeat (Supplementary Table S3.6), we used the Fisher test. In cases where there was only one category of expected and observed phenotype, no test was run (Supplementary Tables S3.3, S3.5, S3.9, S3.10 and S3.11). In these cases, expectation and observation show a perfect match. Following each C-M-H test, assumption of homogeneity of the odds ratio across repeats was confirmed using a Breslow-Day test (R package DescTools: Signorell et al., 2018). However, this test can only be operated in 2x2 tables (Supplementary Tables S3.4 and S3.8). We then ran a Fisher test of independence for each comparison (expected vs. observed for each repeat, Bonferroni corrected) to detect possible significant differences in opposite directions across repeats, which would result in a non-significant C-M-H test. We did not detect such differences in direction (see Supplementary Table S3.14 below for all detailed results of statistical analyses). Tests were run on counts, although we present here segregation of offspring as fractions.

Tables S3.3 to S3.11

Expected and observed resistotypes of F1 offspring groups resulting from the selfing of F0 parents where variation at the C and E loci was observed (see Supplementary Table S3.1 for parent clones details).

Tables S3.12 and S3.13

Expected and observed phenotypes of F1 offspring resulting from the selfing of F0 parents where variation at the B and E loci was observed (see Supplementary Table S3.1 for parent clones details).

Table S3.3

Selfed genotype aabbCCDDEEff. F0 parents: **a**: t3_12.3_1i_12, **b**: t3_12.3_1i_21.

A	**RRSSS** aabbCCDDEEff	abCDEf
	abCDEf	RRSSS

B

F0 parent		F1 offspring						
Inferred genotype	Resistotype	Inferred genotype	Resistotype	Proportion				C-M-H test on counts
				Expected	Observed			
					Repeat			
					a	b		
					n = 43	*n* = 37		
aabbCCDDEEff	RRSSS	aabbCCDDEEff	RRSSS	1	1	1		NA

Table S3.4

Selfed genotype aabbCCDDEeff. F0 parents: **a**: CH-2015-36, **b**: t3_12.3_1, **c**: CH-H-2015-49.

A	**RRSSS** aabbCCDDEeff	abCDEf	abCDef
	abCDEf	RRSSS	RRSSS
	abCDef	RRSSS	RRSRS

B

F0 parent		F1 offspring							
Inferred genotype	Resistotype	Inferred genotype	Resistotype	Proportion					C-M-H test on counts
				Expected	Observed				
					Repeat				
					a	b	c		
					n = 89	*n* = 31	*n* = 79		
aabbCCDDEeff	RRSSS	aabbCCDDE-ff	RRSSS	0,75	0,79	0,74	0,84		X^2=0.85, *df*=1, *p*=0.36
		aabbCCDDeeff	RRSRS	0,25	0,21	0,26	0,16		

Table S3.5

Selfed genotype aabbCCDDeeff. F0 parents: **a**: CH-H-434-inb2-1.

A	**RRSRS** aabbCCDDeeff	abCDef
	abCDef	RRSRS

B

F0 parent		F1 offspring						
Inferred genotype	Resistotype	Inferred genotype	Resistotype	Proportion				C-M-H test on counts
				Expected	Observed			
					Repeat			
					a			
					n = 39			
aabbCCDDeeff	RRSRS	aabbCCDDeeff	RRSRS	1	1			NA

Table S3.6

Selfed genotype aabbCcDDEEff. F0 parent: **a**: t2_17.3_4i_12.

A

RRSSS aabbCcDDEEff	abCDEf	abcDEf
abCDEf	RRSSS	RRSSS
abcDEf	RRSSS	SSSSS

B

F0 parent		F1 offspring					
				Proportion			
					Observed		
				Expected	Repeat		C-M-H test on counts
Inferred genotype	Resistotype	Inferred genotype	Resistotype		a		
					n = 19		*Fisher test on counts*
aabbCcDDEEff	RRSSS	aabbC-DDEEff	RRSSS	0,75	0,74		
		aabbccDDEEff	SSSSS	0,25	0,26		*p*=1

Table S3.7

Selfed genotype aabbCcDDEeff. F0 parents: **a**: t3_14.3_1, **b**: t2_17.3_1, **c**: CH-H-2015-59.

A

RRSSS aabbCcDDEeff	abCDEf	abCDef	abcDEf	abcDef
abCDEf	RRSSS	RRSSS	RRSSS	RRSSS
abCDef	RRSSS	RRSRS	RRSSS	RRSRS
abcDEf	RRSSS	RRSSS	SSSSS	SSSSS
abcDef	RRSSS	RRSRS	SSSSS	SSSSS

B

F0 parent		F1 offspring						
				Proportion				
					Observed			
				Expected	Repeat			C-M-H test on counts
Inferred genotype	Resistotype	Inferred genotype	Resistotype		a	b	c	
					n = 48	*n* = 64	*n* = 65	
aabbCcDDEeff	RRSSS	aabbC-DDE-ff	RRSSS	0,56	0,48	0,64	0,52	M^2=1.9, *df*=2,
		aabbccDD--ff	SSSSS	0,25	0,29	0,14	0,22	*p*=0.39
		aabbC-DDeeff	RRSRS	0,19	0,23	0,22	0,26	

Table S3.8

Selfed genotype aabbCcDDeeff. F0 parents: **a**: t1_10.3_4, **b**: t5_10.3_3, **c**: CH-H-434-inb2-2.

A

RRSRS aabbCcDDeeff	abCDef	abcDef
abCDef	RRSRS	RRSRS
abcDef	RRSRS	SSSSS

B

F0 parent		F1 offspring						
				Proportion				
					Observed			
				Expected	Repeat			C-M-H test on counts
Inferred genotype	Resistotype	Inferred genotype	Resistotype		a	b	c	
					n = 36	*n* = 49	*n*= 22	
aabbCcDDeeff	RRSRS	aabbC-DDeeff	RRSRS	0,75	0,75	0,80	0,64	X^2=0.0062,
		aabbccDDeeff	SSSSS	0,25	0,25	0,20	0,36	*df*=1, *p*=0.94

Table S3.9

Selfed genotype aabbccDDEEff. F0 parent: **a**: CH-H-2015-97.

A		
	SSSSS aabbccDDEEff	abcDEf
	abcDEf	SSSSS

B	F0 parent		F1 offspring					
	Inferred genotype	Resistotype	Inferred genotype	Resistotype	Proportion			C-M-H test on counts
					Expected	Observed		
						Repeat		
						a		
						n = 87		
	aabbccDDEEff	SSSSS	aabbccDDEEff	SSSSS	1	1		NA

Table S3.10

Selfed genotype aabbccDDEeff. F0 parents: **a**: CH-H-2015-113, **b**: t4_10.3_16.

A			
	SSSSS aabbccDDEeff	abcDEf	abcDef
	abcDEf	SSSSS	SSSSS
	abcDef	SSSSS	SSSSS

B	F0 parent		F1 offspring						
	Inferred genotype	Resistotype	Inferred genotype	Resistotype	Proportion				C-M-H test on counts
					Expected	Observed			
						Repeat			
						a	b		
						n = 84	*n* = 65		
	aabbccDDEeff	SSSSS	aabbccDDE-ff	SSSSS	1	1	1		NA

Table S3.11

Selfed genotype aabbccDDeeff. F0 parents: **a**: t4_13.3_2.

A		
	SSSSS aabbccDDeeff	abcDef
	abcDef	SSSSS

B	F0 parent		F1 offspring					
	Inferred genotype	Resistotype	Inferred genotype	Resistotype	Proportion			C-M-H test on counts
					Expected	Observed		
						Repeat		
						a		
						n = 74		
	aabbccDDeeff	SSSSS	aabbccDDeeff	SSSSS	1	1		NA

Table S3.12

Selfed genotype aaBbccDDEEff. F0 parent: t0_9.3_7.

A

SRSSS aaBbccDDEEff	aBcDEf	abcDEf
aBcDEf	SRSSS	SRSSS
abcDEf	SRSSS	SSSSS

B

F0 parent		F1 offspring				
				Proportion		
Inferred genotype	Resistotype	Inferred genotype	Resistotype	Expected	Observed	Fisher test on counts
					n = 37	
aaBbccDDEEff	SRSSS	aaB-ccDDEEff	SRSSS	0,75	0,76	
		aabbccDDEEff	SSSSS	0,25	0,22	*p*=1
		aaB-ccDDeeff	SRSRS	0,00	0,03	

Table S3.13

Selfed genotype aaBbccDDEeff. F0 parent: t0_28.2_43.

A

SRSSS aaBbccDDEeff	aBcDEf	aBcDef	abcDEf	abcDef
aBcDEf	SRSSS	SRSSS	SRSSS	SRSSS
aBcDef	SRSSS	SRSRS	SRSSS	SRSRS
abcDEf	SRSSS	SRSSS	SSSSS	SSSSS
abcDef	SRSSS	SRSRS	SSSSS	SSSSS

B

F0 parent		F1 offspring				
				Proportion		
Inferred genotype	Resistotype	Inferred genotype	Resistotype	Expected	Observed	Fisher test on counts
					n = 38	
aaBbccDDEeff	SRSSS	aaB-ccDDE-ff	SRSSS	0,56	0,55	
		aabbccDDE-ff	SSSSS	0,25	0,32	*p*=0.58
		aaB-ccDDeeff	SRSRS	0,19	0,13	

Table S3.14

Detailed results of statistical analyses applied to F1 offspring groups. Analyses are described in tables legends above.

	CMH test				BD test			Fisher test					
								repeat a		repeat b		repeat c	
	M2	*df*	*p*		X^2	*df*	*p*	*p*	*p + Bonf.*	*p*	*p + Bonf.*	*p*	*p + Bonf.*
Table S3.3	NA	NA	NA	NA	NA	NA	NA	NA	NA	NA	NA	NA	NA
Table S3.4	X^2 = 0.85	1	0,36	CI = (0.49, 1.25), estimate = 0.78, null value = 1	0,83	2	0,66	0,86	1	1	1	0,24	0,72
Table S3.5	NA	NA	NA	NA	NA	NA	NA	NA	NA	NA	NA	NA	NA
Table S3.6	NA	NA	NA	NA	NA	NA	NA	1	NA	NA	NA	NA	NA
Table S3.7	1,9	2	0,39	NA	NA	NA	NA	0,76	1	0,29	1	0,49	1
Table S3.8	X^2 = 0.0062	1	0,94	CI = (0.55, 1.9), estimate = 1.03, null value = 1	1,12	2	0,57	1	1	0,81	1	0,51	1
Table S3.9	NA	NA	NA	NA	NA	NA	NA	NA	NA	NA	NA	NA	NA
Table S3.10	NA	NA	NA	NA	NA	NA	NA	NA	NA	NA	NA	NA	NA
Table S3.11	NA	NA	NA	NA	NA	NA	NA	NA	NA	NA	NA	NA	NA
Table S3.12	NA	NA	NA	NA	NA	NA	NA	1	NA	NA	NA	NA	NA
Table S3.13	NA	NA	NA	NA	NA	NA	NA	0,58	NA	NA	NA	NA	NA

References

Ameline C, Vögtli F, Andras JP, Dexter E, Engelstädter J, Ebert D. preprint. Genetic slippage after sex maintains diversity for parasite resistance in a natural host population. *bioRxiv*.

Ameline C, Vögtli F, Savola E, Bourgeois Y, Andras JP, Engelstädter J, Ebert D. in prep. A two-locus system with strong epistasis underlies rapid parasite-mediated evolution of host resistance.

Bento G, Fields PD, Duneau D, Ebert D. 2020. An alternative route of bacterial infection associated with a novel resistance locus in the *Daphnia–Pasteuria* host–parasite system. *Heredity* **125**:173–183.

Bento G, Routtu J, Fields PD, Bourgeois Y, Du Pasquier L, Ebert D. 2017. The genetic basis of resistance and matching-allele interactions of a host–parasite system: The *Daphnia magna–Pasteuria ramosa* model. *PLOS Genetics* **13**:e1006596.

Bourgeois Y, Roulin AC, Müller K, Ebert D. 2017. Parasitism drives host genome evolution: Insights from the *Pasteuria ramosa–Daphnia magna* system. *Evolution* **71**:1106–1113.

Fredericksen M, Fields PD, Bento G, Ebert D. in prep. QTL and fine mapping parasite resistance in *Daphnia magna*.

Gattis S. 2018. Segregation of resistance to the parasite *Pasteuria ramosa* in the freshwater crustacean *Daphnia magna*.

Luijckx P, Ben-Ami F, Mouton L, Du Pasquier L, Ebert D. 2011. Cloning of the unculturable parasite *Pasteuria ramosa* and its *Daphnia* host reveals extreme genotype–genotype interactions. *Ecology Letters* **14**:125–131.

Luijckx P, Fienberg H, Duneau D, Ebert D. 2012. Resistance to a bacterial parasite in the crustacean *Daphnia magna* shows Mendelian segregation with dominance. *Heredity* **108**:547–551.

Luijckx P, Fienberg H, Duneau D, Ebert D. 2013. A matching-allele model explains host resistance to parasites. *Current Biology* **23**:1085–1088.

Metzger CMJA, Luijckx P, Bento G, Mariadassou M, Ebert D. 2016. The Red Queen lives: Epistasis between linked resistance loci. *Evolution* **70**:480–487.

Routtu J, Ebert D. 2015. Genetic architecture of resistance in *Daphnia* hosts against two species of host-specific parasites. *Heredity* **114**:241–248.

Signorell A et al. 2018. DescTools: Tools for descriptive statistics. R package version 0.99.26.

SUPPLEMENTARY MATERIAL CHAPTER 4

Overview

Section in main manuscript	Element	Description	Page
Materials and methods			
Host and parasite genotypes			
	Table S4.1	Host clones “L4” and “LA” attachment	p. 154
Attachment pictures			
	Table S4.2	Host clones for attachment pictures	p. 155

Materials and methods

Host and parasite genotypes

Table S4.1

Selfed inbred F1 groups where the new attachment sites trunk limb 4 “L4” and all trunk limbs “LA” were observed.

Parent genotype	n selfed F1 group	Resistotype parent	Attachment sites observed in S genotypes in the selfed F1 group		
			P15	P20	P21
CH-H-2015-97	87	SSSSS	D	FLA	D, L4
t2_17.3_4i_12	19	RRSSS	D	FLA	D, L4
CH-H-2015-59	65	RRSSS	D	FLA	D, L4 variable
t3_12.3_1i_12	43	RRSSS	D, L4 variable	FLA	D, L4
t3_12.3_1i_21	37	RRSSS	D, L4	FLA	D, L4
CH-H-2015-36	89	RRSSS	D, L4 variable	FLA	D, L4

Attachment pictures

Table S4.2

Details about the *Daphnia magna–Pasteuria ramosa* genotypes used in the pictures of this chapter. Attachment is described as a string of letters containing all sites where attachment was observed in one host individual. Credits: CA: Camille Ameline, BH: Benjamin Hüssy, MF: Maridel Fredericksen.

Picture	*D. magna* clone	*P. ramosa* isolate	Resistotype	Attachment site	n spores	Dilution	Comment	Credits
Fig. 4.1B	CH-H-2015-36	P20	NA	NA	500	1:100	Picture used to show the anatomy. Trial picture to set the number of spores to use, too few spores were used to observe attachment.	CA
Fig. 4.1C	t1_10.3_2i_2	C1	R	F	500	1:100	**Host clone used to isolate P38**. Negative control, same as Fig. 4.2B.	CA
Fig. 4.1D	CH-H-2015-35	P38	S	E	500	1:100	Attachment not expected in the foregut, picture taken to show the anatomy of the foregut	CA
Fig. 4.2B	t1_10.3_2i_6	P39	S	A	1000	1;100	**Host clone used to isolate P40**. Too few spores to observe sufficient attachment, picture used to show anatomy	CA
Fig. 4.2C			S	E	4000	1:100	Few spores visible on the external postabdomen, too few spores used, picture used to show anatomy	CA
Fig. 4.2D	t1_10.3_2i_2	P38	S	A	500	1;100	Too few spores to observe attachment, picture used to show anatomy of the postabdominal opening	CA
Fig. 4.3B	CH-H-2015-9	P20	S	F	500	1:10	The *Daphnia* was slightly crushed, which is why spores are observed below the mouth	BH
Fig. 4.3C	CH-H-2015-35	C1	S	F	2000	1;100	NA	CA
Fig. 4.3D	CH-H-2015-36	P20	S	F	1000	1:100	NA	CA
Fig. 4.4B	CH-H-2015-35	P21	S	D	500	1:10	NA	BH
Fig. 4.4C	CH-H-2015-35	P21	S	D	500	1:10	NA	BH
Fig. 4.4D	CH-H-2015-35	P41	S	DE	500	1:10	NA	BH
Fig. 4.4E	NA	NA	S	RDE	10000	1:10	NA	MF
Fig. 4.4F	NA	NA	S	RDE	10000	1:10	NA	MF
Fig. 4.4G	NA	NA	S	DE	10000	1:10	NA	MF
Fig. 4.4H	CH-H-2015-9	P20	NA	NA	10000	1:10	Rare pattern, not in the hindgut, migth be an artefact	BH
Fig. 4.5B	CH-H-2015-20	P41	S	RE	1000	1:10	NA	BH
Fig. 4.5C	CH-H-2015-35	P21	S	DRE	1000	1:10	NA	BH
Fig. 4.5D	t1_10.3_2i_2	C1	NA	NA	1000	1;100	Possible artefact that looks like R attachment	CA
Fig. 4.6B	t1_10.3_2i_6	P39	S	AD	4000	1;100	NA	CA
Fig. 4.6C	t1_10.3_2i_6	P40	S	A	4000	1;100	NA	CA
Fig. 4.6D	t1_10.3_2i_2	C1	S	DA	4000	1:100	NA	CA
Fig. 4.6E	CH-H-2015-42	P39	S	AE	4000	1;100	NA	CA
Fig. 4.6F	t1_10.3_2i_2	P41	S	RAE	10000	1:10	Picture taken of a moving *Daphnia* with a camera through the ocular in a standard attachment test	CA
Fig. 4.7B	t1_10.3_2i_6	P42	S	E	4000	1;100	NA	CA
Fig. 4.7C	CH-H-2015-9	C19	S	RDAE	4000	1;10	NA	BH
Fig. 4.7D	NA	NA	S	RDAE	4000	1:10	NA	BH
Fig. 4.8B	RU-BOL-1	4048	S	L5	10000	1;10	Picture taken of a moving *Daphnia* with a camera through the ocular in a standard attachment test	MF
Fig. 4.8C	RU-BOL-1	4048	S	L5	4000	1;100	NA	CA
Fig. 4.8D	CH-H-2015-97i-6	P21	S	DL5	10000	1:100	NA	CA
Fig. 4.9B	t2_17.3_4	P21	S	DL4	10000	1:100	NA	CA
Fig. 4.9C	CH-H-2015-97i-6	P21	S	DL4	10000	1:100	NA	CA
Fig. 4.9D	CH-H-2015-36	P15	S	DRL4	10000	1:10	NA	CA
Fig. 4.10B	t2_17.3_4i_12i_10	P20	S	FLA	10000	1:10	Picture taken of a moving *Daphnia* with a camera through the ocular in a standard attachment test	CA
Fig. 4.10C	CH-H-2015-97i-6	P20	S	FLA	10000	1:100	NA	CA
Fig. 4.10D	t2_17.3_4	P20	S	FLA	10000	1:100	NA	CA
Fig. 4.11A	CH-H-2015_97	P20	S	F	1000	1:100	Moult	CA
Fig. 4.11B	NA	NA	S	DE	10000	1:10	Picture taken of a moving *Daphnia* with a camera through the ocular in a standard attachment test	CA
Fig. 4.11C	NA	NA	NA	NA	NA	NA	Moult, picture taken through the ocular of a stereomicroscope with normal light	MF
Fig. 4.11D	NA	NA	NA	NA	NA	NA	Moult, picture taken through the ocular of a stereomicroscope with normal light	MF

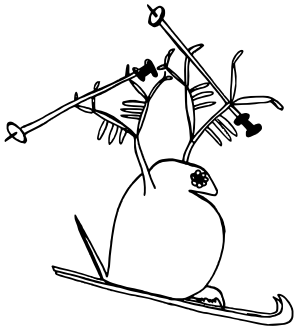

Concluding remarks

Parasites are believed to be one of the main drivers of the evolution and maintenance of diversity and sexual reproduction (Jaenike 1978; Bell and Smith 1987; Jeffery and Bangham 2000; Sommer 2005; Radwan et al. 2020). In this context, many models of the dynamics and the genetics of resistance have been proposed (Agrawal and Lively 2002; Dybdahl et al. 2014; Thrall et al. 2016). Chief among them is the Red Queen theory for the maintenance of sex, which assumes high specificity between hosts and their parasites, matching-allele models of infection and fluctuating allele frequencies created by the advantage of rare alleles (Lively 2010; Brockhurst et al. 2014; Lighten et al. 2017). In contrast with the large amount of theory that has been proposed about the dynamics and genetics of resistance, few studies have directly investigated them in natural systems (Samson et al. 1996; Magalhães and Sucena 2016; Gibson et al. 2018; Alves et al. 2019).

In this thesis, I investigated the evolution of resistance in a population of the cyclic parthenogen *Daphnia magna* that undergoes strong epidemics of the bacteria *Pasteuria ramosa*. I witnessed a highly repeatable pattern of rapid increase in resistance throughout the planktonic season of the host. I show that this increase is adaptive by measuring resistance to the local parasite in field and laboratory experiments. Further, I resolve the underlying genetics of resistance in this population, using a combination of genome-wide association study and genetic crosses in the host. The knowledge of the dynamics of resistance and its underlying genetic architecture allowed me to infer the dynamics of resistance allele frequency in the population, therefore providing the link between observed natural selection and its underlying genetics. By characterizing the genomic region under selection in the host population, I further provide for future studies the opportunity to directly monitor dynamics of resistance allele frequency in response to parasite-mediated selection.

I use the remarkable capacity of cyclic parthenogens to alternate between clonal and sexual reproduction to distinguish between the effect of natural selection and recombination on the evolution of resistance in the host. I find that, during the planktonic season of the host, mean resistance increases, while variance decreases through parasite-mediated selection. Sexual reproduction results in the decrease in mean resistance, but an increase of resistance diversity in the population. These findings provide empirical evidence for genetic slippage in response to sex in a cyclical parthenogen (Lynch and Deng 1994; Decaestecker et al. 2009).

When reviewing previous evidence and investigating further the genetic model of resistance in the host, I find that resistance in the host is determined by several loci with distinct patterns of dominance and linked with epistatic interactions. I also find that, depending on the allelic diversity in a focal population, the overall complexity of the genetic model might not be relevant. I bring functional support for the importance of epistatic interactions in shaping host–parasite interactions (Wilfert and Schmid-Hempel

2008; Kouyos et al. 2009; Jones et al. 2014).

A key aspect of host–parasite interactions is a high specificity between host and parasite genotypes (Otto and Nuismer 2004; Martinů et al. 2018; Liu et al. 2019). In the last chapter I describe new sites and patterns of attachment of the bacterial spores on the host cuticle, an infection step that has been shown to be highly specific in the *D. magna–P. ramosa* system (Duneau et al. 2011; Luijckx et al. 2011). The increasing complexity of the attachment step I describe could have implications in the degree of genotype–genotype specificity in the system.

Using the long-term monitoring of a natural *D. magna* population, I gained functional knowledge about the evolution of resistance and the mechanisms underlying it in the host population. This knowledge can be used in direct measurement of resistance allele frequency, in genomic characterization of the impact of selection on the host, or in studies monitoring combined host and parasite dynamics, which would allow us to better understand the interplay between the host and the parasite.

References

Agrawal A, Lively CM. 2002. Infection genetics: gene-for-gene versus matching-alleles models and all points in between. *Evolutionary Ecology Research* 4:79–90.

Alves JM, Carneiro M, Cheng JY, Lemos de Matos A, Rahman MM, Loog L, Campos PF, Wales N, Eriksson A, Manica A, et al. 2019. Parallel adaptation of rabbit populations to myxoma virus. *Science* 363:1319–1326.

Bell G, Smith JM. 1987. Short-term selection for recombination among mutually antagonistic species. *Nature* 328:66–68.

Brockhurst MA, Chapman T, King KC, Mank JE, Paterson S, Hurst GDD. 2014. Running with the Red Queen: the role of biotic conflicts in evolution. *Proceedings of the Royal Society B: Biological Sciences* 281:1–8.

Decaestecker E, De Meester L, Mergeay J. 2009. Cyclical parthenogenesis in *Daphnia*: sexual versus asexual reproduction. In: Schön I, Martens K, Dijk P, editors. Lost Sex. Dordrecht: Springer Netherlands. p. 295–316.

Duneau D, Luijckx P, Ben-Ami F, Laforsch C, Ebert D. 2011. Resolving the infection process reveals striking differences in the contribution of environment, genetics and phylogeny to host–parasite interactions. *BMC biology* 9:1–11.

Dybdahl MF, Jenkins CE, Nuismer SL. 2014. Identifying the molecular basis of host-parasite coevolution: merging models and mechanisms. *The American Naturalist* 184:1–13.

Gibson AK, Delph LF, Vergara D, Lively CM. 2018. Periodic, parasite-mediated selection for and against sex. *The American Naturalist* 192:537–551.

Jaenike J. 1978. An hypothesis to account for the maintenance of sex within populations. *Evolutionary Theory* 3:191–194.

Jeffery KJM, Bangham CRM. 2000. Do infectious diseases drive MHC diversity? *Microbes and Infection* 2:1335–1341.

Jones AG, Bürger R, Arnold SJ. 2014. Epistasis and natural selection shape the mutational architecture of complex traits. *Nature Communications* 5:1–10.

Kouyos RD, Salathé M, Otto SP, Bonhoeffer S. 2009. The role of epistasis on the evolution of recombination in host–parasite coevolution. *Theoretical Population Biology* 75:1–13.

Lighten J, Papadopulos AST, Mohammed RS, Ward BJ, G. Paterson I, Baillie L, Bradbury IR, Hendry AP, Bentzen P, van Oosterhout C. 2017. Evolutionary genetics of immunological supertypes reveals two faces of the Red Queen. *Nature Communications* 8:1294.

Liu C, Gibson AK, Timper P, Morran LT, Tubbs RS. 2019. Rapid change in host specificity in a field population of the biological control organism *Pasteuria penetrans*. *Evolutionary Applications* 12:744–756.

Lively CM. 2010. A review of Red Queen models for the persistence of obligate sexual reproduction. *Journal of Heredity* 101:S13–S20.

Luijckx P, Ben-Ami F, Mouton L, Du Pasquier L, Ebert D. 2011. Cloning of the unculturable parasite *Pasteuria ramosa* and its *Daphnia* host reveals extreme genotype–genotype interactions. *Ecology Letters* 14:125–131.

Lynch M, Deng H-W. 1994. Genetic slippage in response to sex. *The American Naturalist* 144:242–261.

Magalhães S, Sucena É. 2016. Genetics of host–parasite interactions: towards a comprehensive dissection of *Drosophila* resistance to viral infection. *Molecular Ecology* 25:4981–4983.

Martinů J, Hypša V, Štefka J. 2018. Host specificity driving genetic structure and diversity in ectoparasite populations: Coevolutionary patterns in *Apodemus* mice and their lice. *Ecology and Evolution* 8:10008–10022.

Otto SP, Nuismer SL. 2004. Species interactions and the evolution of sex. *Science* 304:1018–1020.

Radwan J, Babik W, Kaufman J, Lenz TL, Winternitz J. 2020. Advances in the evolutionary understanding of MHC polymorphism. *Trends in Genetics* 36:298–311.

Samson M, Libert F, Doranz BJ, Rucker J, Liesnard C, Farber C-M, Saragosti S, Lapouméroulie C, Cognaux J, Forceille C, et al. 1996. Resistance to HIV-1 infection in Caucasian individuals bearing mutant alleles of the CCR-5 chemokine receptor gene. *Nature* 382:722–725.

Sommer S. 2005. The importance of immune gene variability (MHC) in evolutionary ecology and conservation. *Frontiers in Zoology* 2:16.

Thrall PH, Barrett LG, Dodds PN, Burdon JJ. 2016. Epidemiological and evolutionary outcomes in gene-for-gene and matching allele models. *Frontiers in Plant Science* 6:1–12.

Wilfert L, Schmid-Hempel P. 2008. The genetic architecture of susceptibility to parasites. *BMC Evolutionary Biology* 8:187.